CERN, December 2005

RD50 Status Report 2005

Radiation hard semiconductor devices for very high luminosity colliders

Centro Nacional de Microelectrónica (IMB-CNM, CSIC), Barcelona, Spain
Francesca Campabadal, Celeste Fleta, Manuel Lozano, Giulio Pellegrini, Joan Marc Rafí, Miguel Ullán

Dipartimento Interateneo di Fisica & INFN - Bari, Italy
Marianna Ambrico, Donato Creanza, Mauro De Palma, Teresa Ligonzo, Norman Manna, Valeria Radicci, Luigi Schiavulli

Institut für Kristallzüchtung, Berlin, Germany
Klaus Irmscher, Günter Wagner

Brookhaven National Laboratory, Upton, NY, USA
Jim Kierstead, Zheng Li

Department of Physics, University of Bologna, Bologna, Italy
Anna Cavallini

National Institute for Materials Physics, Bucharest - Magurele, Romania
Manuela Buda, Sorina Lazanu, Lucian Pintilie, Ioana Pintilie, Andreia-Ioana Popa

University of Bucharest, Faculty of Physics
Ionel Lazanu

CERN, Geneva, Switzerland
Paula Collins, Karl Aaron Gill, Maurice Glaser, Christian Joram, Herbert Hödlmoser, Michael Moll[♣]

Universitaet Dortmund, Lehrstuhl Experimentelle Physik IV, Dortmund, Germany
Claus Goessling, Jonas Klaiber-Lodewigs, Reiner Klingenberg, Olaf Krasel, Jens Weber, Renate Wunstorf

---

[♣] *Co-spokesperson*

CiS Institut für Mikrosensorik gGmbH, Erfurt, Germany
Ralf Roeder, Dieter Stolze, Hartmut Uebersee

University of Exeter, Department of Physics, Exeter, United Kingdom
James Adey, A. Blumenau, J. Coutinho, T. Eberlein, C. Fall, J. Goss, B. Hourahine, Robert Jones, N. Pinho

Fermilab, USA
Rita Coluccia, Simon Kwan, Greg Sellberg

INFN Florence – Department of Energetics, University of Florence, Italy
Emilio Borchi, Mara Bruzzi♦, Ettore Focardi, Stefano Lagomarsino, Anna Macchiolo, David Menichelli, Stefania Miglio, Monica Scaringella, Silvio Sciortino, Carlo Tosi

University of Freiburg, Germany
Simon Eckert, Thies Ehrich, Susanne Kuehn, Ulrich Parzefall

Dept. of Physics & Astronomy, Glasgow University, Glasgow, UK
Richard Bates, Andrew Blue, Peter Bussey, Craig Buttar, William Cunningham, Alison G Bates, Lina Haddad, Grant James, Keith Mathieson, J. Melone, Val OShea, Chris Parkes, David Pennicard, Aldo Saavedra

Institute for Experimental Physics, University of Hamburg, Germany
Peter Buhmann, Devis Contarato, Eckhart Fretwurst, Frank Hönniger, Gunnar Lindström, Uwe Pein, Jörg Stahl

Helsinki Institute of Physics, Helsinki, Finland
Jaakko Härkönen, Katri Lassila-Perini, Panja Luukka, Jukka Nysten, Eija Tuominen, Esa Tuovinen

Ioffe Phisico-Technical Institute of Russian Academy of Sciences, St. Petersburg, Russia
Vladimir Eremin, Igor Ilyashenko, Alexandr Ivanov, Evgenia Kalinina, Alexander Lebedev, Nikita Strokan, Elena Verbitskaya

Institute of Physics PAS and Institute of Electronics Technology, Warsaw, Poland
Adam Barcz

Institute of Electronic Materials Technology, Warszawa, Poland
Andrzej Brzozowski, Pawel Kaminski, Roman Kozlowski, Michal Kozubal, Zygmunt Luczynski, Elzbieta Nossarzewska-Orlowska, Barbara Surma, Piotr Zabierowski

University of Karlsruhe, Institut fuer Experimentelle Kernphysik, Karlsruhe, Germany
Wim de Boer, Alex Furgeri, Frank Hartmann, Florian Hauler, Valery Zhukov

Institute for Nuclear Research of the Academy of Sciences of Ukraine, Radiation PhysicDepartments
L. Barabash, A. Dolgolenko, A. Groza, A. Karpenko, V. Khivrich, V. Lastovetsky, P. Litovchenko, L. Polivtsev

♦ Co-s*pokesperson*

Department of Physics, Lancaster University, Lancaster, United Kingdom
Timothy John Brodbeck, Duncan Campbell, Alexandre Chilingarov, Gareth Hughes, Brian Keith Jones, Terence Sloan

Lappeenranta University of Technology, Department of Electrical Engineering, Lappeenranta, Finland
Miia Koski, Kari Leinonen, Tanja Palviainen, Tuure Tuuva

Department of Physics, University of Liverpool, United Kingdom
Phillip Allport, Stephen Biagi, Themis Bowcock, Gianluigi Casse, Jaap Velthuis

Jožef Stefan Institute and Department of Physics, University of Ljubljana, Ljubljana, Slovenia
Vladimir Cindro, Irena Dolenc, Gregor Kramberger, Igor Mandić, Marko Mikuž, Marko Zavrtanik

Université catholique de Louvain, Institut de Physique Nucléaire, Louvain-la-Neuve, Belgium
Samia Assouak, Eric Forton, Ghislain Grégoire, Vincent Lemaitre

Belarusian State University, Minsk
Nikolai Kazuchits, Leonid Makarenko

Groupe de la Physique des Particules, Université de Montreal, Canada
Sébastien Charron, Marie-Helene Genest, Alain Houdayer, Celine Lebel, Claude Leroy

State Scientific Center of Russian Federation, Institute for Theoretical and Experimental Physics, Moscow, Russia
Gleb Bondarenko, Victor Golovine, Eugene Grigoriev, Aleksey Karpov, Sergey Kazakov, Sergey Rogozhkin, Alexandre Zaluzhny

University of New Mexico, USA
Igor Gorelov, Martin Hoeferkamp, Giuseppe Latino, Dmitri Naoumov, Sally Seidel

University of Oslo, Physics Department/Physical Electronics, Oslo, Norway
Giovanni Alfieri, Klaus M H Johansen, Andrej Kuznetsov, Edouard Monakhov, Bengt G. Svensson

Dipartimento di Fisica and INFN Sezione di Padova, Padova, Italy
Dario Bisello, Andrea Candelori, Vladimir Khomenkov, Alexei Litovchenko, Devis Pantano, Riccardo Rando

I.N.F.N. and Università di Perugia - Italy
Gian Mario Bilei, Francesco Moscatelli, Daniele Passeri, Marco Petasecca, Giorgio Umberto Pignatel, Andrea Scorzoni

Universita` di Pisa and INFN sez. di Pisa, Italy
Laura Borrello, Alberto Messineo, Gabriele Segneri, Daniel Sentenac

Institute of Physics, Academy of Sciences of the Czech Republic, Praha, Czech Republic
Jiri Popule, Petr Sicho, Michal Tomasek, Vaclav Vrba

Czech Technical University in Prague, Czech Republic
Dominik Chren, Tomas Horazdovsky, Zdenek Kohout, Vladimir Linhart, Stanislav Pospisil, Michael Solar, Vít Sopko, Bruno Sopko, Josef Uher

Charles University Prague, Czech Republic
Jan Broz, Zdenek Dolezal, Peter Kodys, Alexej Tsvetkov, Ivan Wilhelm

Paul Scherrer Institut, Laboratory for Particle Physics, Villigen, Switzerland
Roland Horisberger, Tilman Rohe

Purdue University, USA
Gino Bolla, Daniela Bortoletto, Kim Giolo, Jun Miyamoto, Carsten Rott, Amitava Roy, Ian Shipsey, SeungHee Son

University of Rochester
Veronique Boisvert, Regina Demina, Sergey Korjenevski, Paul Tipton

Santa Cruz Institute for Particle Physics, USA
Alexander Grillo, Jessica Metcalfe, Hartmut Sadrozinski, Bruce Schumm, Abraham Seiden, Ned Spencer

Dept of Physics and Astronomy, University of Sheffield, Sheffield, U.K.
Ian Dawson, Paul Dervan

SINTEF ICT, Blindern - Oslo, Norway
Andreas Werner

Department of Physics, University of Surrey, Guildford, United Kingdom
Paul Sellin

Experimental Particle Physics Group, Syracuse University, Syracuse, USA
Marina Artuso

Tel Aviv University, Israel
J. Guskov, Sergey Marunko, Arie Ruzin, Tamir Tylchin

Experimental Physics Department, University of Torino, Italy
Floriana Fasolo, Franco Fizzotti, Yiuri Garino, Alessandro Lo Giudice, Claudio Manfredotti, Paolo Olivero, Chiara Paolini

ITC-IRST, Microsystems Division, Povo, Trento, Italy
Maurizio Boscardin, Gian - Franco Dalla Betta, Paolo Gregori, Claudio Piemonte, Alberto Pozza, Sabina Ronchin, Mario Zen, Nicola Zorzi

IFIC, joint research institute of CSIC and Universitat de Valencia-Estudi General, Valencia, Spain
Carlos Escobar, Carmen Garcia, Sergio González Sevilla, Salvador Marti i Garcia

Institute of Materials Science and Applied Research, Vilnius University, Vilnius, Lithuania
Eugenijus Gaubas, Kestutis Jarasiunas, Vida Kazlauskiene, Vaidotas Kazukauskas, Stanislavas Sakalauskas, Jurgis Storasta, Markas Sudzius, Juozas Vidmantis Vaitkus

Contents

1. Introduction

The objective of the CERN RD50 Collaboration is the development of radiation hard semiconductor detectors for very high luminosity colliders, particularly to face the requirements of a possible upgrade scenario of the LHC to a luminosity of $10^{35}cm^{-2}s^{-1}$, corresponding to expected total fluences of fast hadrons above $10^{16}cm^{-2}$ and reduced bunch-crossing interval of ~10 ns [1,2]. This document reports the status of research and main results obtained after the third year of activity of the collaboration.

Presently, RD50 counts a total of 258 members with 51 participating institutes, from 16 different countries in West and East Europe, 8 from North America (USA, Canada), one from middle east (Israel). During the third year of activity two workshops and collaboration board meetings have been held to discuss the recent results and co-ordinate the research activities of RD50: June 2-4 in Helsinki, Finland and November 14-16, 2005 at CERN. Each workshop has registered a quite high rate of participation, counting an average of 75 participants with about 30 talks. More details can be found at the collaboration web-site [1].

Review papers describing the common research activities of the RD50 collaboration have been published in 2003 [1], 2004 [1,2] and 2005 [1-3]. As in the previous years, the research activity of RD50 has been presented in form of invited oral contributions at several international conferences and workshops [1]:

- **ATLAS upgrade workshop, February**, "Progress on Detector Materials and RD50 Programme", Workshop on ATLAS Upgrades for High Luminosity, CERN, Geneva, 13-14.2.2005 [11].
- **IFAE, April**, "RD50 - Sviluppo di rivelatori a semiconduttore resistenti alla radiazione", IFAE Incontri di Fisica delle Alte energie – Catania 30 Marzo - 1 Aprile 2005 [12].
- **ATLAS Tracker upgrade workshop, June**, "Middle/Outer Radii: R&D plan in Europe", ATLAS Tracker Upgrade Workshop, Genova, July 18-20, 2005 [13].
- **NSREC 2005, July**, "Semiconductor materials and detectors for future very high luminosity colliders", Nuclear and Space Radiatian Effects Conference (NSREC), 11th-15th July 2005 [14].
- **Pixel 2005, September**, "Radiation Tolerant Sensors for Pixel Detectors", PIXEL 2005 international workshop, September 5-8, Bonn, Germany [15].
- **RD05, October**, "Development of Radiation Tolerant Silicon Detectors for the SLHC", 7th International Conference on Large Scale Applications and Radiation Hardness of Semiconductor Detectors, Florence, Italy, 5-7 October 2005 [16].
- **TIME05, October**, "Radiation Tolerant Semiconductor Sensors for Tracking Detectors", Workshop on Tracking In high Multiplicity Environments October 3-7, Zürich, Switzerland [17].
- **VERTEX 2005, November**, "Recent Results from RD50", Vertex 2005 November 7 - 11, 2005 Chuzenji Lake, Nikko, Japan [18].

The scientific organization of RD50 is organised in two major lines, Material Engineering and Device Engineering, each of the two lines are subdivided into three projects as shown in Table 1-1. The management of the projects is assigned to members of RD50 of proven relevant experience (conveners). In the framework of the research activity of each project, working groups are active with specific tasks. Each working group is composed of few institutes, which are directly involved in the research program and co-ordinated by an RD50 member. During this year one additional working

group has been assessed in the FDS project, focussed on the development of radiation-hard electronics. The coordinators of this working group is Hartmut Sadrozinski from the Santa Cruz University. Table 1-1 lists working groups and common activities within each project, with the corresponding co-ordinator.
Besides working groups, common activities have been started on subjects of common interest. Some of these activities are partially supported with the RD50 common fund.
In the next section our scientific work is reviewed in an executive summary. This section is followed by six sections describing the status of the research activities of each individual research line. Finally a work plan, milestones and an overview about the needed resources for 2006 are given.

[1] R&D Proposal - DEVELOPMENT OF RADIATION HARD SEMICONDUCTORDEVICES FOR VERY HIGH LUMINOSITY COLLIDERS, LHCC 2002-003 / P6, 15.2.2002.
[2] RD50 Status Report 2004 – Radiation hard semiconductor devices for very high luminosity colliders, CERN-LHCC-2004-031 and LHCC-RD-005, January 2005
[3] RD50 collaboration web site: http://www.cern.ch/rd50/.
[4] Michael Moll on behalf of the CERN RD50 collaboration, “Development of radiation hard sensors for very high luminosity colliders - CERN - RD50 project – “Nucl. Instr. & Meth. in Phys. Res. A 511 (2003) 97-105.
[5] Mara Bruzzi on behalf of the CERN RD50 Collaboration, “Material Engineering for the Development of Ultra-Radiation Hard Semiconductor Detectors”, Nucl. Instrum. & Meth. A 518, 1-2, 2004, 336-337.
[6] Panja Luukka on behalf of the CERN RD50 Collaboratin “Status of Defect Engineering Activity of the RD50 Collaboration” Nucl. Instrum. & Meth. A 530, 1-2, 2004, 152-157.
[7] M.Moll et al. (RD50 Collaboration), "Development of radiation tolerant semiconductor detectors for the Super-LHC", NIMA 546 , 99-107 (2005).
[8] M. Bruzzi et al. (RD50 Collaboration); "Radiation-hard semiconductor detectors for SuperLHC"; NIMA, 541, 189-201 (2005).
[9] F.Fretwurst et al. (RD50 Collaboration), "Recent advancements in the development of radiation hard semiconductor detectors for S-LHC"; NIMA 552, 7-19 (2005).
[10] Electronic versions of the talks are available on the RD50 www-page under http://www.cern.ch/rd50/doc/
[11] Michael Moll, CERN, on behalf of the CERN RD50 Collaboration
[12] Anna Macchiolo, Università degli Studi di Firenze e INFN Firenze, on behalf of the CERN RD50 Collaboration
[13] Gianluigi Casse, Liverpool University, on behalf of the CERN RD50 Collaboration
[14] Andrea Candelori, Padua University/INFN, on behalf of the CERN RD50 Collaboration
[15] Michael Moll, CERN, on behalf of the CERN RD50 Collaboration
[16] Maurizio Boscardin, IRST, Italy, on behalf of the CERN RD50 Collaboration
[17] Michael Moll, CERN, on behalf of the CERN RD50 Collaboration
[18] Daniela Bortoletto, Purdue University, on behalf of the CERN RD50 Collaboration

	Line	Project Convener	Main Research Activity	Working groups and common acitivities
Spokespersons♣ Mara Bruzzi (INFN and Uni. of Florence) and Michael Moll (CERN)	Material Engineering	**Defect/Material Characterisation** Bengt G. Svensson Univ. Oslo, Norway	Characterisation of the microscopic properties of standard-, defect engineered and new materials, pre- and post-irradiation.	
		Defect Engineering Eckhart Fretwurst Univ. of Hamburg, Germany	Development and testing of defect engineered silicon: Oxygen enriched FZ (DOFZ), High res. Cz, Epitaxial, Si enriched with Oxygen dimmers	(1) Oxygen Dimer (M. Moll)
		New Materials Elena Verbitskaya Ioffe, St.Petersburg, Russia	Development of new materials with promising radiation hard properties: bulk and epitaxial SiC, GaN	(1) SiC (I. Pintilie) (2) GaN (J. Vaitkus)
	Device Engineering	**Pad Detector Characterisation** Jaakko Harkonen Helsinki Inst. Physics, Finland	Characterisation of macroscopic properties of heavily irradiated single pad detectors in different operational conditions.	(1) Standardisation of macroscopic measurements (A.Chilingarov) (2) Technotest (V.Eremin)
		New Structures Richard Bates Univ. of Glasgow, UK	Development of 3D, semi-3D and thin detectors and study of their pre- and post-irradiation performance.	(1) 3D (M.Boscardin) (2) Semi-3D (Z.Li)
		Full Detector Systems Gianluigi Casse Univ. of Liverpool, UK	- Systematic characterisation of segmented (microstrips, pixels) LHC-like detectors. - Links with LHC experiments	(1) Pixel detectors (D.Bortoletto- T.Rohe) (2) Radhard electronics (H.Sadrozinski, SCIPP)

Table 1-1.: Organisation structure of the research activity in RD50.

♣ In November 2005 the RD50 Collaboration Board elected M.Bruzzi and M.Moll as Co-spokespersons of the RD50 project. Until November 2005 M.Bruzzi was the Spokesperson while M.Moll was the Deputy Spokesperson.

2. Executive Summary

2.1. Defect and Material Characterization (DMC)

- *Epitaxial silicon;* systematic studies of irradiation-induced shallow donor formation in n-type epi-Si have been conducted. These donors contribute to suppressing type inversion at high doses and are found to be stable after long-term post-irradiation annealing. The donor generation exhibits a linear dose dependence for 24 GeV/c protons and evidence is presented for oxygen dimer involvement in the donor generation. Further, high-resolution photoinduced transient spectroscopy studies show that the epi-layers contain a significant amount of hydrogen, which may not be too surprising since they are grown in a hydrogen ambient.

- *DOFZ silicon;* Admittance spectroscopy and capacitance voltage measurements, performed over a wide range of frequencies and temperatures, of p+-n--n+ detectors reveal that for proton doses below the inversion point, charge carrier trapping is dominated by a level situated ~0.43 eV below the conduction band edge. This trap is primarily associated with divacancy centers. For doses above the inversion point, charge carrier trapping is dominated by a deep acceptor state close to mid-gap and presumably related to high-order vacancy clusters.

- *X-centers;* The one-to-one transformation from divacancy centers to X-centers during annealing at temperatures between 200 and 300 °C is found to exhibit first-order kinetics with an activation energy of 1.30 eV.

- *MCz silicon;* the reason(s) for an increased radiation hardness of MCz-Si has been investigated in detail. In particular, a shallow radiation-induced donor with substantial concentration is observed. This donor partially compensates the irradiation-induced deep acceptors, suppressing space charge sign inversion. Moreover, the generation of the vacancy-oxygen center is at least three times higher in MCz-Si than in ordinary FZ-Si, reducing the generation of deep acceptors like, e.g., the so-called I-center.

- *MCz, carrier lifetime;* lifetime measurements on highly irradiated MCz-Si samples show a substantial decrease of the carrier lifetime at low temperatures with large variations over a small temperature interval. Such a behavior cannot be explained by 'ordinary' defects in silicon and suggests that intercenter recombination plays an important role.

2.2. Defect Engineering (DE)

- *Standard and Oxygen enriched FZ silicon (DOFZ)*: Both material types have been studied mainly for comparison with the other type of materials under investigation of the RD50 collaboration.

- *High resistivity Cz silicon*: The radiation hardness of n- and p-type MCz silicon grown by Okmetic has been investigated by several irradiation campaigns. TSC (Themally Stimulated Current) studies have proven that in Cz material the formation of shallow donors by irradiation play a major role in the macroscopic behavior of the devices. But is has to be noted that this shallow donor is not related to the well known Thermal Donors ($TD^{0/+}$ and/or $TD^{+/++}$), which are observed when the diodes are heat treated at temperatures of 430°C. As a special variant p-type MCz material was thermally treated at 430°C introducing thermal donors. By

this method the full depletion voltage could be tailored or an inversion to n-type material could be achieved which was demonstrated by TCT measurements.

- *Epitaxial silicon*: In continuation of the research plan 50 Ω·cm n-type epitaxial layers with a thickness of 25 μm and 75 μm were grown by ITME and processed by CiS in order to investigate possible changes in the defect kinetics due to the different growth time needed for the different layers and different oxygen content introduced during the high temperature treatments involved in the device processing. Depth profiles of the oxygen concentration have been measured by the SIMS-method showing that oxygen is out-diffusing from the Cz substrate mainly during the high temperature diode process steps as verified by comparison of SIMS results with process simulations. It could be demonstrated that the introduction rate of shallow donors is maximal for the 25 μm epi-layer and decreases with increasing layer thickness. This trend correlates with the evolution of the effective doping concentration as function of fluence observed for the different epi-layers. In conclusion it is very likely that the shallow donor, found in epi-silicon after irradiation, is indeed responsible for the dominating positive space charge build up in these devices and that this donor is generated via an enhanced concentration of oxygen dimers (O_2) out-diffusing from the Cz substrate.

- *Defect engineering by treatments at elevated temperatures*: A new approach, called DRIVE (Detector Recovery/Improvement Via Elevated Temperature Annealing), was proposed by the Ioffe Physico-Technical Institute, Brookhaven National Laboratory and the Helsinki Institute of Physics. The basic idea behind this approach is that in oxygen-rich (oxygenated FZ Si and MCZ Si) detectors thermal treatments at temperatures in the range between 400°C and 500°C lead to an introduction of shallow thermal donors and that some of the radiation induced deep defect centers anneal out or form new defects which are less harmful. With the DRIVE method it is anticipated that oxygen-rich Si detectors can be recovered through ETA with respect to the following properties: 1) decrease of the detector leakage current; 2) decrease of the net space charge concentration and, therefore, the full depletion voltage; and 3) increase of the charge collection efficiency (CCE). Systematic studies on high resistivity n- and p- type MCz silicon detectors have proven, that after annealing at 450°C for a specific duration, which depends on the accumulated fluence, the radiation induced negative space charge can be compensated or even over-compensated and a recovery of the reverse current to its initial value before irradiation could be achieved.

- *Defect engineering by pre-irradiation treatments*: Radiation hardening studies by preliminary neutron irradiation of silicon, which is expected to create gettering sites in the silicon bulk, have been carried on. Preliminary irradiation of silicon by fast neutrons and the subsequent annealing lead to the formation of sinks for primary radiation defects. These sinks are complexes of radiation-induced defects with neutral impurities, such as C and O, being always present in the silicon wafers. Detectors manufactured by IRST from standard n-type float zone silicon (FZ), as a reference, and from pre-irradiated and annealed FZ silicon were investigated after irradiation with reactor neutrons. It could be demonstrated that the introduction rate of deep acceptors β of the pre-irradiated FZ devices is lower than that observed for the FZ reference detector. Furthermore, TSCAP measurements on irradiated standard and pre-irradiated FZ devices have shown that the radiation induced reduction of the free charge carrier concentration in pre-irradiated samples is much less pronounced in the investigated temperature range (20 K – 300 K) in comparison to the standard FZ material. These results have lad to the conclusion that pre-irradiated FZ silicon is more radiation hard than standard FZ material especially after neutron damage which was so far not observed for oxygen enriched FZ devices.

- *Hydrogen in silicon*: Detailed studies on hydrogen in FZ silicon have shown that all silicon detectors under investigation contain hydrogen which remains in these structures after fabrication. The devices were manufactured by three different companies (CiS, ST Microelectronics and ELMA). Hydrogen was detected via the formation of the VOH defect

complex after electron irradiation and subsequent isochronal annealing up to 350 °C. From depth profile DLTS-measurements and correlated depth profiles of the free charge carrier concentration extracted from C-V measurements it could be concluded that hydrogen is most likely found near to the p^+ and n^+ contacts or the SiO_2-Si interface. Further, it is shown that the annealing of divacancies is different for the devices manufactured by the different producers. These observations can be explained by the interaction of divacancies with hydrogen diffusing from near surface regions into the bulk.

2.3. Pad Detector Characterization (PDC)

The research of the PDC group in 2005 has been focused to the two most promising material candidates for the SLHC tracker, MCz and epitaxial silicon detectors. The properties of p^+-n type detectors from both were studied and for MCz also n^+-p detector structures were studied. Fabrication of MCz detectors with variable N_{eff} through processing of both n and p types was developed and first devices were already produced. Effect of detector processing on its macroscopic properties was also investigated.

2.4. New Materials (NM)

Two types of detectors were manufactured on n-type 4H-SiC epitaxial layers grown earlier at the Institute of Crystal Growth of Berlin and on CREE epilayers. The diodes were processed in the framework of two sub-projects: 1) Schottky diodes, produced by Alenia Marconi, Rome and 2) p^+-n junction diodes produced by Perugia University jointly with CNR-IMM, Bologna. The charge collection efficiency to MIPs has been investigated by a ^{90}Sr β source. The highest thickness of SiC epilayer tested is 50μm. The pulse height spectrum giving the charge response measured by the SiC detectors when exposed to ^{90}Sr β source was measured as a function of the reverse voltage before irradiation and 100% charge collection efficiency was measured. The collected charge stays high up to few 10^{14} n/cm^2 and decreases sharply after a fluence of 10^{15} n/cm^2 (1MeV neutron irradiation at Ljubljana). After irradiation by $1 \cdot 10^{16}$ n/cm^2 the collected charge is only 130 e^-. This result shows that SiC detectors do not show enhanced radiation hardness in comparison to Si detectors.

2.5. New Structures (NS)

The major advances in the area of new structure developments over the past year have been in thin detectors and 3D detector fabrication. Better understanding of the charge collection properties of thin silicon detectors has been achieved with the use of Schokley-Read-Hall based models; while the first 3D detectors fabricated at ITC-irst have been realised and tested. The majority of work in the area of 3D detectors over the past year has been to develop a fabrication effort in 3D detectors in a non-university institute. For this aim ITC-irst and CNM have worked together to produce their first 3D detectors. At present these are not full 3D devices as a simpler design was chosen for the first fabrication run to maximise yield. The University of Glasgow has developed a process to allow both n and p type doping of etched pores; however fabrication of significant numbers of devices was not possible to date due to the refurbishment of their engineering facilities.

Preliminary results from the detectors electrical characterization show the evidence of the very good yield obtained with this process and demonstrate the feasibility of this technological approach. A thorough analysis of device C-V characteristics with the aid of TCAD simulations is under way to gain deep insight into the depletion mechanisms characterizing these detectors. Devices from these wafers have been distributed to the Glasgow, Freiburg, SCIPP and Florence groups for further electrical and change collection characterization. A new wafer run will be performed with deeper holes (230um) and thinner wafers (250um) so that the pores almost penetrate the full thickness of the device. These devices will be fully studied at collaborating institutes within the RD50 collaboration in the next year.

2.6. Full detector Systems (FDS)

In 2005 the p-type microstrip silicon detectors irradiated in 2004 were tested to study their performance after reverse annealing. They are capacitively coupled, polysilicon biased, 1 cm long, 80μm pitch micro-strip detector processed on 280 μm thick, 2.8 kΩcm p-type FZ and Diffusion Oxygenated FZ silicon wafers by the Centro Nacional de Microelectronica (Barcelona). The strip insulation method was p-spray. The measurements were performed at low temperature (-20^{o}C) and using the LHC-speed analogue SCT128a chipbased ^{106}Ru test-stand at Liverpool.

The annealing studies were performed after irradiation to 1.1, 3.5 and 7.5×10^{15} p cm^{-2}, and they were performed according the *standard* procedures: the detectors were submitted to several annealing steps of ~1 hour at +80^{o}C. Their charge collection properties were measured after each step. For annealing equivalent to up to three years of working at SuperLHC, no difference of the charge collection efficiency before and after annealing for the different fluences tested. The charge collected at 300V after the lower dose shows a sensitive (30% loss) degradation only after 4 y_{EQ}, while at higher voltages the collected charge remains about constant up to the maximum time investigated. First MCz p-type silicon microstrip detectors have been produced by IRST-Trento. They have been tested and first results after irradiation are promising. Their characterization is still in progress.

3. Defect and Material Characterization

3.1 Epitaxial silicon; donor generation by 24 GeV/c protons

3.1.1 Introduction

Previous irradiation experiments on Epi-diodes (50 μm epitaxial silicon grown on low resistivity Cz substrate) have shown that, despite the low oxygen concentration (≈ 10^{17} cm^{-3}), these devices are highly superior to any standard or oxygenated float zone silicon devices and that contrary to those and similar to Cz material the Epi diodes do not get "type inverted" [1, 2]. These investigations suggested that the beneficial effect of oxygen may not only be connected with the concentration of oxygen interstitial O_i, which influences the generation of deep acceptors (like the I defect [3]), but also with the concentration of oxygen dimers O_{2i}, which may determine the generation of shallow bistable donors (BDs) in the material [4, 5]. These first investigations concerning the proposed defect models call for more systematic studies of the defect formation. Thus, more studies were done to establish the thermal stability of the BD centers, the BD introduction rates in Epi diodes of different thicknesses, the BD connection with the presence of oxygen dimers and their influence on the device performance. 25, 50 and 75 μm thick epitaxial n-type layers with a nominal resistivity of 50 Ωcm were produced by ITME, using highly doped Cz-silicon substrates (0.01 Ωcm) and pad diodes (5 x 5 mm² active area) were processed by CiS. Depth profiles of oxygen concentration are displayed in Fig.3-1. Oxygen is out-diffusing from the Cz substrate mainly during the high temperature diode process steps as verified by comparison of SIMS results with process simulations [6].

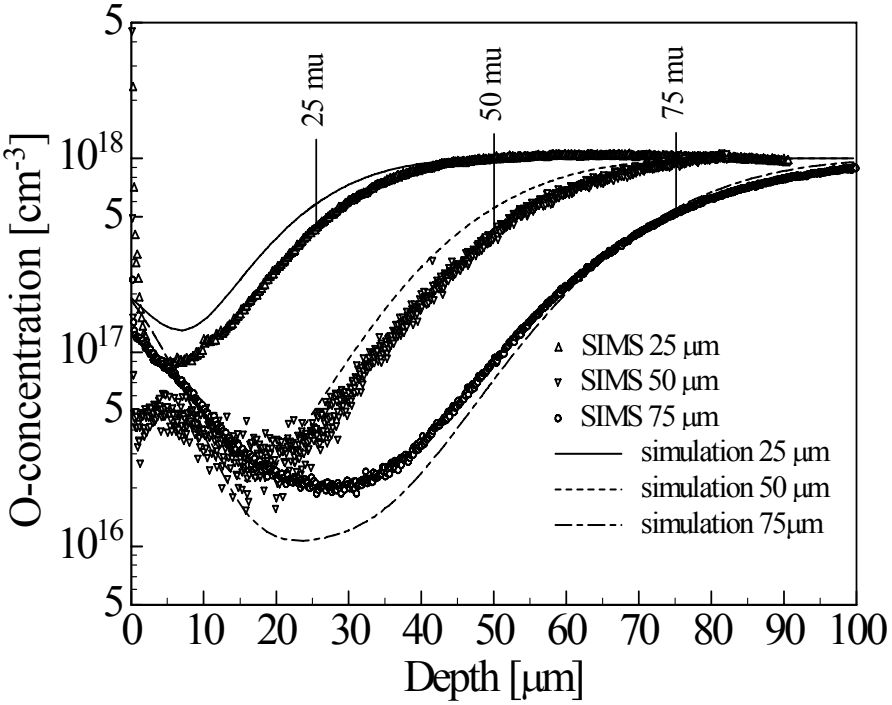

Fig.3-1 Oxygen concentration versus depth profiles measured with SIMS (symbols) in comparison with process simulation results (lines) in the n-type epi-diodes under test.

3.1.2 BD center – thermal stability [7]

Fig.3-2 shows TSC spectra obtained from a 50 μm thick Epi diode irradiated with an equivalent fluence of 3.05x10^{14} cm^{-2} for three annealing conditions. As can be seen the concentration of the BD remains unchanged during the very long time annealing at moderate temperatures. Thus, the generation of BD represents a stable modification after irradiation with 24 GeV/c protons.

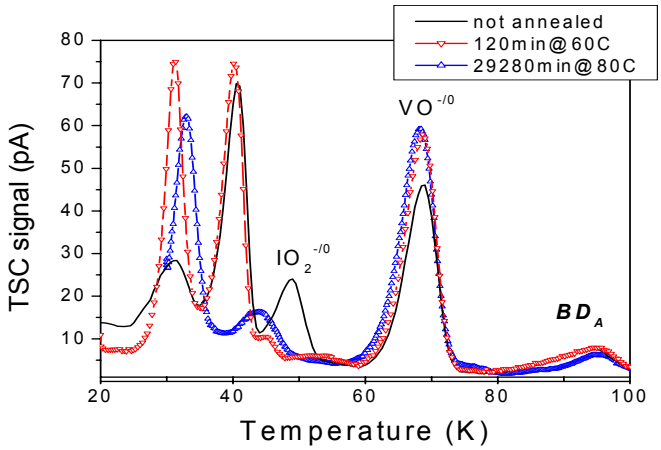

Fig.3-2. TSC spectra after irradiation with 24 GeV/c protons with an equivalent fluence of $3.05x10^{14}$ cm^{-2} recorded on 50 μm thick Epi material after different annealing conditions.

3.1.3 BD center – fluence dependence [7]

Fig. 3-3 shows TSC spectra obtained from 50 μm thick Epi diodes irradiated with equivalent fluences of $1.24x10^{14}$ cm^{-2}, $3.05x10^{14}$ cm^{-2} and $3.73x10^{14}$ cm^{-2} after 120 minutes annealing at 60 °C. The corresponding BD concentration in these Epi diodes are evaluated to be $1.3x10^{12}$ cm^{-3}, $3.0x10^{12}$ cm^{-3} and $3.8x10^{12}$ cm^{-3} indicating a linear dose dependence of the BD generation with an introduction rate of about $1x10^{-2}$ cm^{-1}.

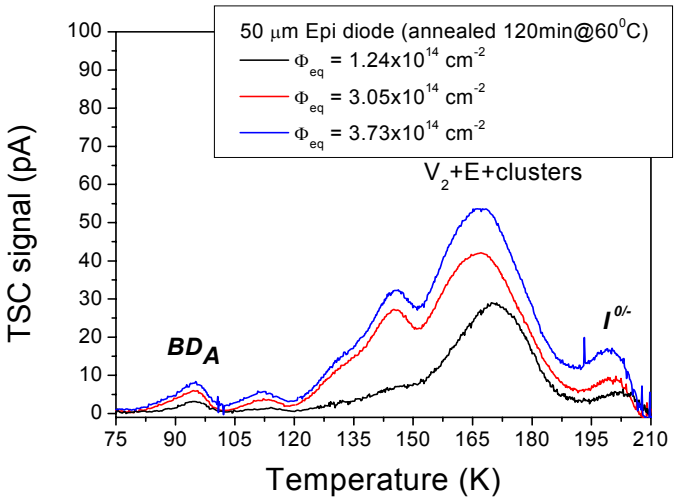

Fig.3-3 TSC spectra recorded on 50 μm thick Epi diodes after irradiation with 24 GeV/c protons with equivalent fluences of $1.24x10^{14}$ cm^{-2}, $3.05x10^{14}$ cm^{-2} and $3.73x10^{14}$ cm^{-2} and after 120 minutes annealing at 60 °C. The diodes were kept 2 days in dark at RT prior to TSC measurement. Forward injection was performed at 15 K for filling the traps.

3.1.4 Evidence for oxygen dimer involvement in BD generation [7]

The strong similarity of the BD complex to earlier stage thermal double donors and the well known fact that oxygen dimers O_{2i} are precursors for the formation of thermal donors leads to the assumption that dimers are involved in the damage produced BD defects. A first and relative estimation of the dimer concentration in Epi diodes compared with Cz ones was done via the detection of the IO_{2i} center presuming that the sum of all interstitials related defects in the two materials is the same. We had considered the following reactions for the capture of interstitials during irradiation:

$$I + O_{2i} \rightarrow IO_{2i} \quad (1)$$
$$I + C_s \rightarrow C_i \quad (2)$$
$$I + Y \rightarrow IY \quad (3)$$

The first two account for the detection of IO_{2i} and C_i, respectively while the latter reaction is considered for the capture of interstitials during irradiation in unknown traps (IY) which release the interstitials during annealing as it is resulting from Table 3-1. It can be seen that the sum of all interstitial related defect concentrations immediately after irradiation is almost 40% smaller in Epi with respect to Cz diodes. This suggests an unknown trap for interstitials (Y), which might be electrically inactive, with the largest concentration in Epi diodes or the disappearance of interstitials at the surface or in the substrate. However, after 860 min. annealing at 80 ^{0}C the differences in the sum of the introduction rates for interstitials in the investigated materials decrease significantly. This effect supports the assumption of unknown traps for interstitials (Y – not electrically active) in Epi diodes which release the interstitials during the annealing.

	Cz	**Epi**
Σ I (1/cm) after proton irradiation	**2.8**	**1.7**
Σ I (1/cm) after annealing for 860 min at 80^{0}C	**2.6**	**2.5**

Table 3-1. The sum of the introduction rates of the interstitial related defects in Cz and Epi diodes.

The introduction rate of IO_{2i}, prior to the annealing treatment, was evaluated to be 1.9 cm^{-1} and 0.7 cm^{-1} in Cz and Epi materials respectively. These values can be used to estimate the relative dimer concentration in the two materials (the $[O_{2i}]^{Cz}/[O_{2i}]^{Epi}$ ratio). Considering the similar carbon concentrations in the Silicon epi-layer and in Cz material (see Fig.3-4) and the similar introduction rates for C_i related defects in the two materials (including the C_iO_i complex - see Ref.[7]), it results that the introduction rate of IO_{2i} in Cz material should balance the sum of the IO_{2i} and IY introduction rates in Epi-samples. Thus, the introduction rate of IY defect result to be of about 1.2 cm^{-1} and the $[O_{2i}]^{Cz}/[O_{2i}]^{Epi}$ ratio can be determined as:

$$\frac{[O_{2i}]^{Cz}}{[O_{2i}]^{Epi}} = 1 + \frac{R(I,Y)}{R(I,O_{2i})} \cdot \frac{[Y]^{Epi}}{[O_{2i}]^{Epi}} = 1 + \frac{[IY]^{Epi}}{[IO_{2i}]^{Epi}} \sim 2.7 \qquad (4)$$

where: R(I,Y) is the probability for reaction I+Y $\rightarrow$ IY (the capture radius for I at Y).

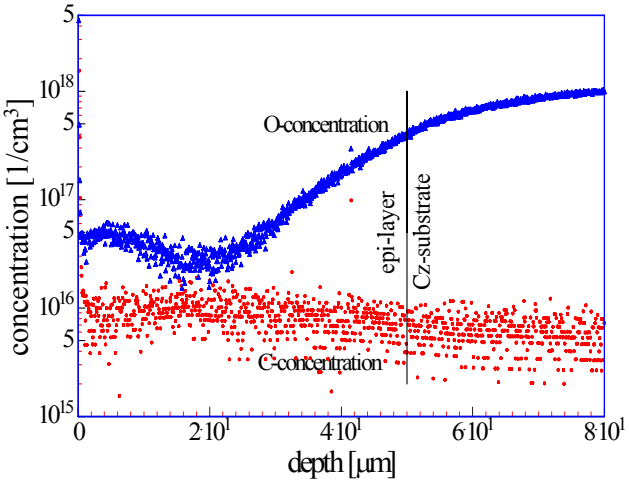

Fig.3-4 SIMS concentration profiles in 50 μm epitaxial Si deposited on 300 μm Cz substrate.

Considering the average O-concentrations as measured by SIMS (8x10^{17} in Cz and 1x10^{17} cm^{-3} in Epi) the $[O_{2i}]^{Cz}/[O_{2i}]^{Epi}$ ratio is expected to be 64 (the $[O_{2i}] \sim [O_i]^2$, see ref.[8]) which is much larger than the 2.7 value resulted from our experiments. In our opinion, the presence of such a large dimer concentration in Epi is due to the diode structure (epi-layer grown on Cz substrate). Both the oxygen

dimers (O_{2i}) and interstitials (O_i) can migrate into the epitaxial layer during the high temperature process steps via out-diffusion from the Cz-substrate. However, as the diffusion constant of dimers is known to be much larger than that of the oxygen interstitials, the $[O_{2i}]/[O_i]$ ratio can be higher in the epilayer than in Cz substrate. The IO_{2i} defect was not detected in any float zone silicon based structures (STFZ or DOFZ) after low irradiation fluences indicating a much lower concentration of oxygen dimers in these materials.

By taking into account the donor removal and the generation of the I-center, the change of N_{eff} at 293 K in 50 μm Epi diodes can be explained with an accuracy of about 10% of the N_{eff} value attributed to negative space charge mainly determined by irradiation-induced clusters. In the case of Cz material it was not possible to determine the full concentration of BD-centers from TSC experiments. However, an estimation of the BD concentration, considering a 2.7 higher concentration of oxygen dimers in Cz compared with the Epi material, has led to similar values in the two materials for the concentration of negative space charge introduced by irradiation-induced clusters at RT after the same annealing time (~2.2×10^{-2} cm^{-1} after 120 min. at 60 ^{0}C) giving thus a further indication for dimers involvement in the formation of BD centers.

3.1.5 Dependence of BD generation rate on Epi-layer thickness [6]

To verify that the formation of BD is indeed due to the out-diffusion of oxygen from Cz substrate, studies regarding the BD introduction rate were carried out on Epi diodes with different thicknesses of the silicon epitaxial layer. Fig. 3-5 shows results of TSC-spectra for 3 n-type epi diodes with thicknesses of 25, 50 and 75 μm, all grown on 300 μm thick low resistivity Cz substrate. While the well known point defects like e.g. C_iO_i, the divacancy (V_2) as well as the peak at 115 K, known from previous work in FZ diodes [9] are measured with concentrations independent of the diode type and hence independent of the O-concentration, the TSC signal due to the shallow donor BD has a strong dependence on the epi-layer thickness as the oxygen concentration diffusing in from the Cz substrate varies significantly (see Fig.3-1). The BD introduction rates were determined via TSC experiments to be of about 2.2×10^{-2} cm^{-1}, 1.0×10^{-2} cm^{-1} and 0.6×10^{-2} cm^{-1} for 25, 50 and 75 μm epi-layer thickness, respectively. Thus, a proper design of radiation detectors based on epitaxial silicon should take into account that for processing the diodes in the standard way the diode thickness largely influence the BD introduction rate and thus the desired beneficial effect on the device characteristics.

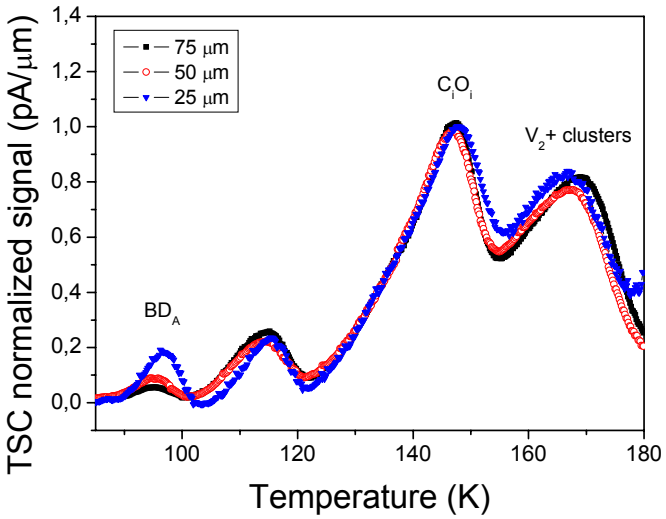

Fig.3-5 TSC spectra for 25, 50 and 75 μm n-type Epi diodes after 24 GeV/c proton irradiation with $\Phi_{eq} = 1.24\times10^{14}$ cm^{-2} and 120 min annealing at 60 ^{o}C.

3.2 Epi silicon; defect evolution versus 24 GeV/c proton fluence

High-Resolution Photoinduced Transient Spectroscopy (HRPITS) [10] has been used to investigate defect centres in n-type epitaxial silicon after 24 GeV/c proton irradiation with fluences of 3×10^{14} (samples A) and 9×10^{14} cm^{-2} (samples B) followed by a long-term annealing at 80 ^{o}C. The test diodes used for studies of defect centres were $p^+/n/n^+$ epitaxial silicon detectors. The epitaxial layer

was deposited on <111> orientated n^+ monocrystalline Czochralski substrates with a resistivity of about 0.01 Ωcm, doped with Sb. The epitaxial process was carried out in a vertical type, RF heated reactor at atmospheric pressure with a flow of hydrogen with $SiCl_4$ as silicon source and PH_3 as dopant. The oxygen concentration in the reaction gas was below 0.1 ppm in volume. Deposition was performed at 1100 ^{0}C with a growth rate of 1 μm/min. The epi-layer thickness was 50 μm and the phosphorus concentration about $7x10^{13}$ cm^{-3}. As a result of the oxygen diffusion from the Cz-Si substrate into the growing epitaxial layer, the average oxygen concentration in the epitaxial layer is around $9x10^{16}$ cm^{-3} and is higher than that in FZ silicon. The carbon concentration in the layers was found to be around $5x10^{15}$ cm^{-3}. The epitaxial detectors investigated in this work were fabricated by the company CiS in Erfurt (Germany).

The parameters of defect centres obtained from the HRPITS measurements are summarised in Table 3-2. The results presented in Table 3-2 show that as a result of the high-energy proton irradiation and subsequent long-term annealing, 9 defect centres with activation energies ranging from 5 to 460 meV are formed in the both samples. They include shallow donors PT1 (5 meV) and PT2 (25 meV), oxygen related complexes PT4 (165 meV), PT5 (190 meV), PT7 (320 meV) and PT9 (460 meV) as well as divacancies in different charge states PT6 (230 meV) and PT8 (420 meV). In particular, two remarks can be made: First, in the material irradiated with the lower fluence the concentration of the E_c-0.46 eV level is approximately 4 times lower than that of divacancies $V_2^{-/0}$. The irradiation with the higher fluence changes the material defect structure and the concentration of the E_c-0.46 eV level is around 6 times higher compared to that of divacancies $V_2^{-/0}$. This non-linear fluence dependence supports the identification of the two associated levels at E_c-0.46 and E_c-0.19 eV with a higher-order defect. Second, The centre PT7 (320 meV) is related to the acceptor level of $VOH^{-/0}$ complex [11]. The presence of hydrogen in the epitaxial layers is very likely because they are grown in a hydrogen ambience. It may be noted that this centre has also been observed by DLTS technique in DOFZ material [12].

Table 3-2. Parameters of defect centres detected by means of the HRPITS method in high-energy proton irradiated epitaxial silicon. Sample A - proton fluence $3x10^{14}$ cm^{-2}; Sample B - proton fluence $9x10^{14}$cm^{-2}.

Label	T_e [a] [K] e_T=3000 s^{-1}	E_a [b] (meV)	A [b] (s^{-1}K^{-2})	σ_a [c] (cm^2)	Sample	Tentative identification
PT1	17	5	$3x10^2$	$3x10^{-19}$	A, B	shallow donor
PT2	41	25	$2x10^3$	$2x10^{-18}$	A, B	shallow donor
PT3	97	120	$5x10^5$	$5x10^{-16}$	A, B	$C_iC_s(B)^{-/0}$
PT4	110	165	$1x10^7$	$1x10^{-14}$	A, B	$VO^{-/0}$
PT5	115	190	$6x10^7$	$5x10^{-14}$	A, B	$V_2O^{--/-}$ or $X^{--/-}$
PT6	160	230	$2x10^6$	$2x10^{-15}$	A, B	$V_2^{--/-}$
PT7	208	320	$4x10^6$	$4x10^{-15}$	A, B	$VOH^{-/0}$
PT8	252	420	$1x10^7$	$1x10^{-14}$	A, B	$V_2^{-/0}$
PT9	241.5	460	$4x10^8$	$4x10^{-13}$	A, B	$V_2O^{-/0}$ or $X^{-/0}$

a) T_e - the temperature at which the thermal emission rate e_T is 3000 s^{-1};

b) E_a and A - the activation energy and pre-exponential factor in the Arrhenius formula $e_T = AT^2 exp(-E_a/kT)$, respectively;

c) The values of the apparent capture cross-section refer to electron traps according to the identification given in the last column.

3.3 DOFZ; defect clusters related to space charge sign inversion

P^+-n^--n^+ detectors fabricated by SINTEF using DOFZ-Si have been irradiated with 24 GeV/c protons to doses between $7.5x10^{12}$ and $6.5x10^{14}$ cm^{-2} and analysed by admittance spectroscopy (AS)

and capacitance-voltage (CV) measurements. The analysis was performed at frequencies from 1 kHz to 1 MHz and in the temperature range of 100 to 350 K. Fig.3-6 shows the carrier concentration as obtained by CV (1 kHz, 300 K) versus proton dose. The point of expected type inversion is included and the data indicate that type inversion has occurred for the two highest doses used ($9x10^{13}$ cm^{-2} and $6.5x10^{14}$ cm^{-2}) but not for the lower ones.

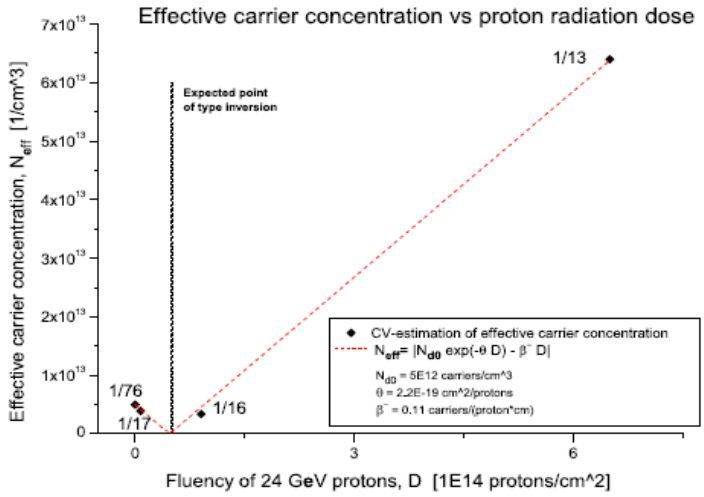

Fig.3-6 Carrier concentration, as deduced by CV measurements (1 kHz, 300 K), versus proton dose.

In Fig.3-7, AS and CV results are depicted for the sample irradiated with $7.5x10^{12}$ p/cm^2 (below inversion) and carrier freeze out takes place at an energy level located ~0.43 eV below E_c. This level can predominantly be associated with the single negative acceptor acceptor state of the divacancy center with some possible contributions from the vacancy-phosphorus center and higher order defect clusters (possibly of vacancy-type)[13]. For doses above the inversion point, AS and CV spectra are dominated by a level situated ~0.55 eV above E_V, as illustrated in Fig.8 for a detector irradiated with $6.5x10^{14}$ p/cm^2. The spectrum in Fig.3-8 suggests clearly that the type inversion is not dominated by a shallow acceptor state but rather by a deep acceptor state close to mid-gap. The origin of the 0.55 eV level is not known but one possible candidate is the so-called I center[14].

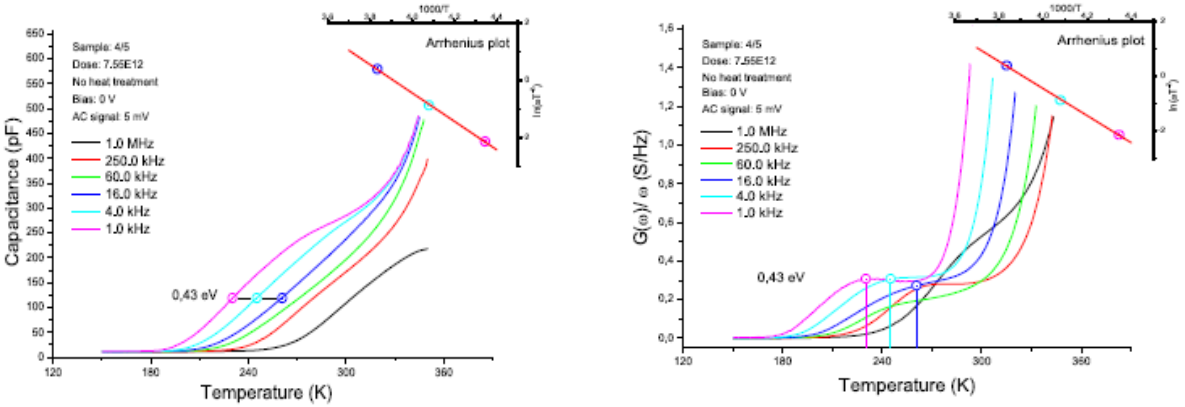

Fig.3-7 Capacitance and conductance as a function of temperature for a detector irradiated with $7.5x10^{12}$ p/cm^2. The insets show Arrhenius plots corresponding to trap activation enthalpy.

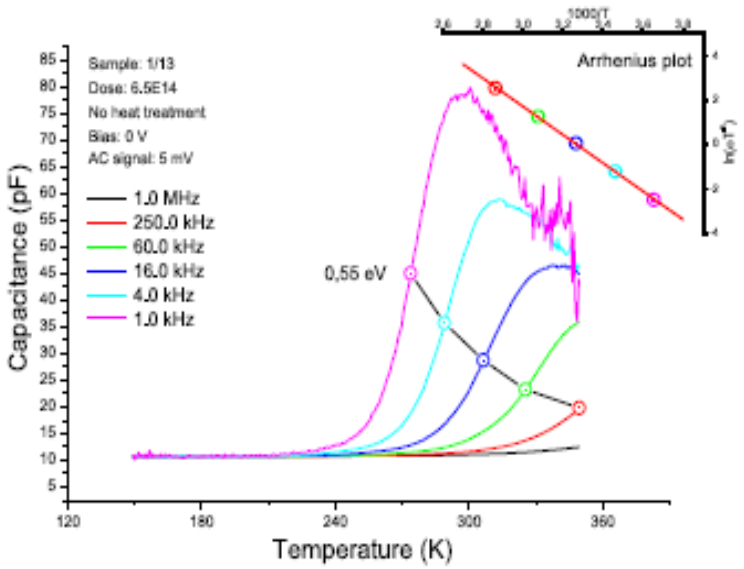

Fig.3-8 Capacitance as a function of temperature for a detector irradiated with 6.5×10^{14} p/cm^2. The inset shows an Arrhenius plot corresponding to the trap activation enthalpy.

3.4 DOFZ Si; kinetics of V_2 annealing and X formation [15]

P^+-n^--n^+ detectors fabricated by SINTEF using DOFZ-Si have been irradiated with 15 MeV electrons to doses in the 10^{12} cm^{-2} range and analysed by deep level transient spectroscopy (DLTS). In particular, the thermal kinetics of the transformation from the V_2 to the X-center has been studied in detail for temperatures from 205 to 285 °C and activation energies are deduced. As illustrated by the isothermal data in Fig.3-9, the annealing of V_2 exhibits first-order kinetics and is accompanied by a one-to-one growth of the X-center, Fig.3-10. A small deviation (≤10 %) occurs for the single negative charge sate of X because of formation of a minor level overlapping with the position of X(-/0) [15].

The corresponding Arrhenius plot is displayed in Fig.11 and the transformation process takes place with an activation energy (E_a) of 1.30 eV and a pre-factor of 4×10^8 s^{-1}. The E_a value is identical with that reported for migration of V_2 [16] and if O_i is assumed to be the main trap, a V_2 diffusivity pre-exponential-factor of $3 \pm 1.5 \times 10^{-3}$ cm^2/s is extracted from the experiments. This value is in excellent agreement with that predicted by a first-order theoretical model of V_2 diffusion in Si [15].

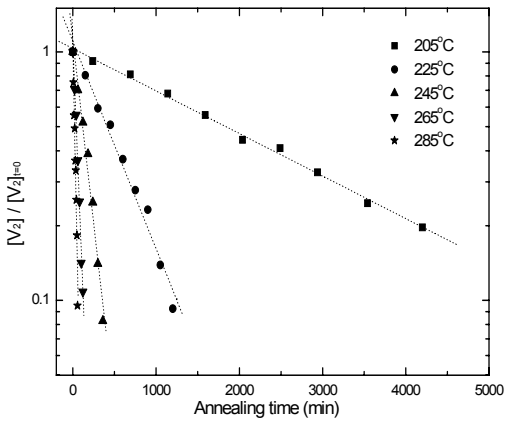

Fig.3-9 Intensity of V_2 during isothermal annealing in the temperature range 205 to 285 °C. The intensity is normalized to that in as-irradiated samples.

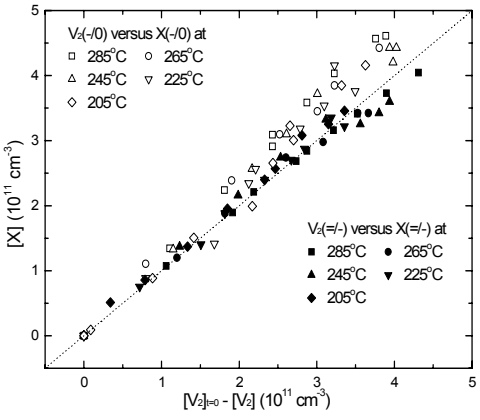

Fig.3-10 Growth in X versus loss in V_2. The dotted line represents a one-to-one proportionality.

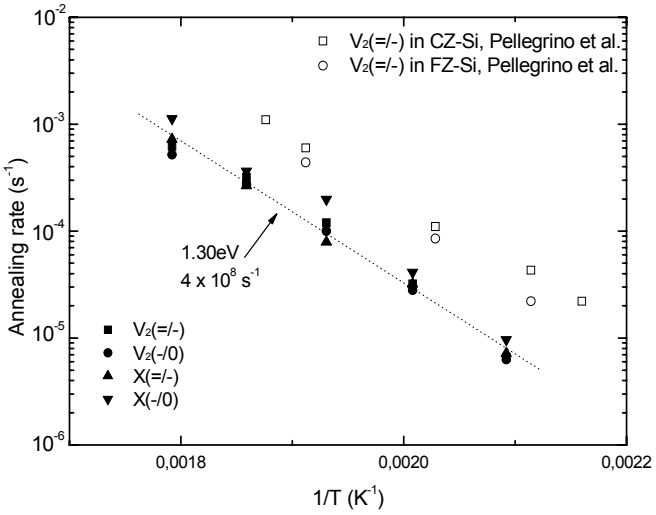

Fig.3-11 Arrhenius plot for the rates of annealing and formation of V_2 and X, respectively. Included are also data from Pellegrino et al., Phys. Rev. B 64, 195211 (2001).

3.5 MCz-Si; mechanism for increased radiation hardness

One objective in 2005 has been to investigate the radiation-induced defects responsible of the increased radiation hardness of high resistivity magnetic Czochralski (MCz) Si. Thermally Stimulated Currents (TSC) measurements have been carried out on n-type MCz and Fz Si detectors, processed by ITC-IRST, Trento on Okmetic, Finland wafers. Fig.3-12 shows the TSC spectrum in the low-temperature range after irradiation with 24GeV/c p up to $4x10^{14}p/cm^2$ and an annealing treatment of 1260min at 60°C [17].

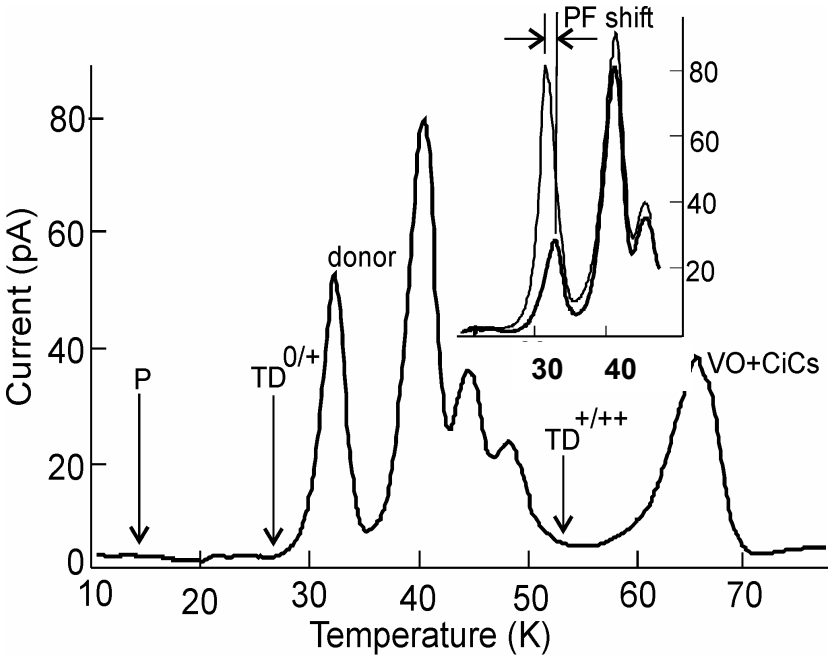

Fig.3-12 TSC spectrum at low temperatures after irradiation with 24 GeV/c protons and a dose of $4x10^{14}$ cm^{-2} followed by annealing at 60 °C for 1260 min.

In particular, the TSC peak visible at 30K has been related to a shallow charged defect: the inset shows the occurrence of the Poole Frenkel effect (evidenced by the characteristic shift of the peak temperature as the applied reverse voltage is changed) indicating that the radiation-induced defect should be charged, possibly donor-like. We note that the peaks related to Thermal Donors emissions ($TD^{0/+}$ and $TD^{+/++}$), observed when the diodes are heated at temperatures of 430°C [18], are not present after irradiation. Similarly, the shallow energy level due to phosphorous is not observed, probably as a consequence of the formation of the phosphorous-vacancy complex. The same peak, which is related to a defect with energy around 80meV [19] has been observed also in p-type MCz Si after similar irradiation and annealing [20]. For comparison TSC measurements have been also carried out in n-type standard Fz Si after the same irradiation fluence. In FZ, this radiation-induced energy level was found with a concentration at least five times lower than in MCz Si [19]. Moreover, in agreement with expectations, the VO concentration has been observed to be at least three times lower in FZ Si than in n-type MCz Si [19]. The higher concentrations observed for the VO complex and for the shallow donor at 30K are in agreement with the higher radiation hardness of MCz Si observed after proton irradiation with respect of standard Fz Si. We suggest that the shallow defect, as a donor, is partially compensating the radiation-induced deep acceptors (I defect at 0.54eV), while the enhanced formation of the VO complex should be related to a partially suppressed I defect formation: the macroscopic effect is to suppress space charge sign inversion, or eventually shift it to higher fluences. To study the space charge sign inversion on similarly irradiated n-type MCz Si samples, Transient Current technique (TCT) analysis have been carried out by the Ioffe group in St. Petersburg. The TCT spectra have been corrected by the effect of trapping and a fit has been carried out to evidence the shape of the electric field. Preliminary measurements show indeed that the dominant junction is still on the front electrode even after an irradiation up to $1x10^{15}$ cm^{-2} with 24GeV protons [19] providing evidence for no space charge sign inversion. Details of these measurements are reported in the PDC charter.

3.6 MCz-Si; charge carrier recombination versus γ-ray dose

The decay of photoconductivity and carrier lifetime variations were measured at different temperatures in γ-ray irradiated MCz silicon samples. The n- and p-type MCz silicon samples were irradiated with Co-60 γ-rays doses ranged from 50 Mrad to 370 Mrad. The lifetime measurements were based on the decay of photoconductivity after excitation by a short light pulse, monitored by the absorption of the microwave signal (MWA), which depends on the sample conductivity.

A survey of the investigated samples is given in Table 3-3. As illustrated in Fig.3-13, a nearly linear increase of the inverse recombination lifetime with respect to the irradiation dose confirms point defect formation in the MCz samples. The determined charge carrier capture cross-sections of these defects indicate mainly the role of single charged repulsive centers. It can be noted that the inverse recombination lifetime values obtained in FZ Si (a star in Fig.3-13), irradiated with 400 Mrad dose, deviate significantly from the fitted average values for MCz in the range of the largest irradiation doses. Thus, the photoconductivity decay components at T = 300 K are shorter in MCz Si than that in FZ Si, irradiated at similar values of dose. As the initial resistivity of the MCz and FZ Si materials was in the same range, differences in recombination lifetimes for the post-irradiated samples can be attributed to enhanced formation of irradiation-induced and oxygen related complexes in MCz Si.

Table 3-3. Survey of the investigated samples

Type Sample Processing	MCZ p-Si		MCZ n-Si		FZ n-Si
	A1, A2	A3, A4	B1, B2	B3, B4	
	TD	no TD	TD	no TD	
γ-ray irradiation dose (Mrad)	50-370	50	50-370	50	400

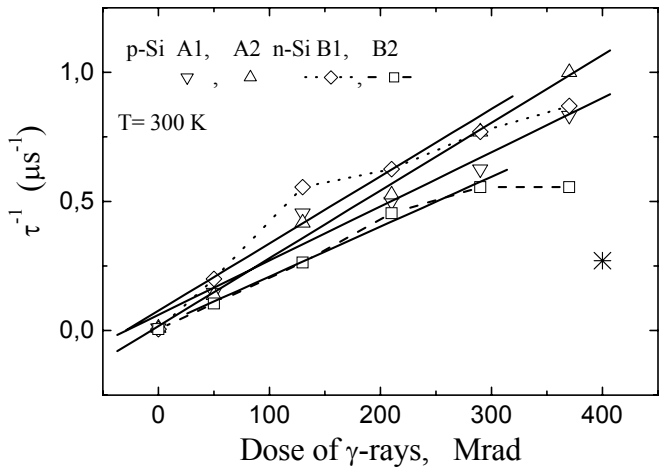

Fig.3-13 Inverse initial instantaneous lifetime versus γ-ray dose for different MCz-Si samples of n- and p-type.

Moreover, an interesting and intriguing result is a substantial decrease of the lifetime at low temperature with large variations in rather small temperature intervals, Fig.14. The 'ordinary' centers in the silicon cannot explain such features and therefore it could be proposed that inter-center recombination [21] plays an important role in highly irradiated material at low temperatures. Hence, in a comprehensive analysis of the charge carrier recombination the influence of defect clusters and their configurational multi-stability should be taken into account (especially at low temperatures).

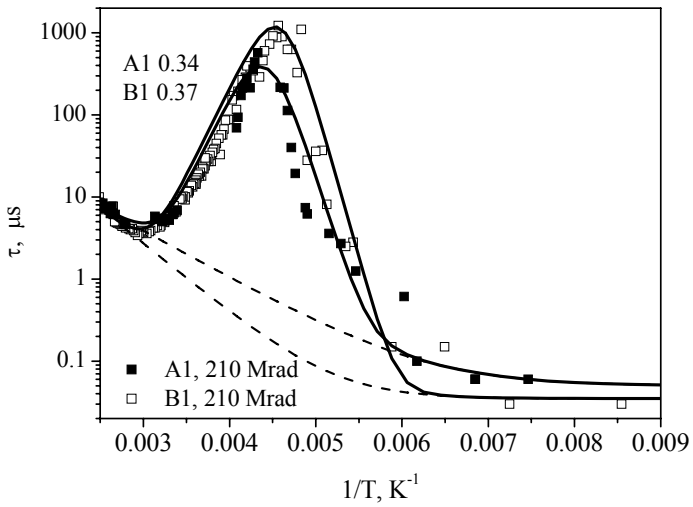

Fig.3-14 Carrier lifetime as a function of the inverse absolute temperature for 210 Mrad irradiated MCz-Si samples of n- and p-type. Identical excitation conditions were used.

3.7 Modeling of defect reactions in irradiated silicon

In 2002, using state of the art plane wave density functional theory, Goedecker et al.[22] predicted the existence of a new type of primary defect: Si_{FFCD} (**F**our**f**olded **C**oordinated silicon **D**efect) that is a pseudo-vacancy. It is obtained by moving atoms from the initial positions, but this displacement does not break the bonds with the neighbours. The bond lengths are between 2.25÷2.47 Å and angles vary in the 97÷116° range. So, the bond length and angle do not deviate significantly from their bulk values. The formation energy is 2.45 eV (for p-type silicon), 2.42 eV (intrinsic), 2.39 eV (n-type), i.e. lower than the energy of formation of both vacancies and interstitials.

Assuming the following characteristics for the Si_{FFCD} defect

- It represents about 10% from all vacancies generated per act of interaction,
- Has an energy level in the band gap between $E_c - (0.46 \div 0.48)$ eV,
- Has a capture cross section between $(5 \cdot \div 10) \times 10^{-15}$ cm^2

- Ratio $\sigma_p/\sigma_n = 1 \div 5$.

the experimentally observed evolution as a function of dose and post-irradiation time of the leakage current and effective carrier concentration can be reproduced by simulations employing rate equations and 'ordinary' defect reactions. This holds, in particular, for hadron irradiation, which is, indeed, a new and encouraging accomplishment [23]. On the other hand, the assumed properties for the Si_{FFCD} defect are in direct contradiction to experimental results, reported by numerous groups, regarding defect generation in irradiated silicon, i.e., there is no experimental evidence for the existence of a defect with such prominent characteristics as those assigned to Si_{FFCD}. Further work is being pursued to resolve this intriguing issue.

3.8 References

1. G. Lindström, E. Fretwurst, G. Kramberger, I. Pintilie , Journal of Optoelectronic and Advanced Materials, **6**, 23-38 (2004)
2. G.Kramberger et al., Nucl. Instr. & Meth. in Phys. Res. A **515**, 655 (2003)
3. I. Pintilie, E. Fretwurst, G. Lindström and J. Stahl, Appl. Phys. Lett. **82**, 2169 (2003)
4. I. Pintilie et al., Nucl. Instr. & Meth. A **514** 18 (2003)
5. J. Stahl, E. Fretwurst, G. Lindström and I. Pintilie, Physica B: Condensed Matter **340-342**, 705 (2003)
6. Gunnar Lindström et al., Epitaxial Silicon Detectors for Particle Tracking-Radiation Tolerance at Extreme Hadron Fluences- submitted for publication to Nucl. Instr. and Meth. A
7. I. Pintilie, M. Buda, E. Fretwurst, G. Lindström, J. Stahl; Stable radiation induced donor generation and its influence on the radiation tolerance of silicon diodes; submitted for publication to Nucl. Instr. and Meth. A
8. L. I. Murin, T. Hallber, V. P. Markevich and J. L. Lindström, Phys. Rev. Lett. **80**, 93 (1998)
9. M. Moll. PhD thesis. University of Hamburg 1999; DESY-THESIS -1999-040, December 1999
10. P. Kaminski, R. Kozlowski, E. Nossarzewska-Orlowska, Nucl. Instr. and Meth. B **186**, 152-156 (2002)
11. O. Andersen, L. Dobaczewski, A.R. Peaker, K. Nielsen Bonde, B. Hourahine, R. Jones, P.R. Briddon and S. Öberg, Physica B **308-310,** 139-142 (2001)
12. M. Mikelsen, *et al*., "Annealing behaviour of defects in irradiated MCZ- and DOFZ-Si detector materials", presented on the 4th RD50 Workshop, 5-7 May 2004, CERN, Geneva, Switzerland
13. B.G. Svensson, EMIS Data Review No. **20** "Properties of Crystalline Silicon", 763 (1999)
14. I. Pintilie, E. Fretwurst, G. Lindstrøm and J. Stahl, Appl. Phys. Lett. **82**, 2169 (2003)
15. M. Mikelsen, E.V. Monakhov, G. Alfieri, B.S. Avset and B.G. Svensson, Phys. Rev. B, accepted (2005)
16. G.D. Watkins and J.W. Corbett, Phys. Rev. **138**, A543 (1965)
17. M. Bruzzi et al. , Nucl. Instrum. Meth. A **552**, 20-26 (2005)
18. M. Bruzzi, D. Menichelli, M. Scaringella, J. Härkönen, E. Tuovinen, Z. Li, Thermal Donors Formation via Isochronal Annealing in Magnetic Czochralski High Resistivity Silicon, submitted to J. App. Phys. (2005)
19. M. Scaringella et al., "Localized energy levels generated in magnetic Czochralski silicon by proton irradiation and their influence on the sign of the space charge density", 7th International Conference on Large Scale Applications and Radiation Hardness of Semiconductor Detectors Florence, Italy, 4-7 October 2005. To be submitted to Nucl. Instrum. Meth. A.
20. D. Menichelli et al., "Shallow donors in MCz-Si n- and p-type Detectors at different process temperature, irradiation and thermal treatments", 6th RD50 Workshop, Helsinki June 2-4 2005 http://rd50.web.cern.ch/rd50/6th-workshop/
21. W.M. Cheng, B. Monemar and E. Janzén, Phys. Rev. Lett. **61**, 1914 (1991)
22. S. Goedecker, Th. Deutsch, L. Billard, Phys. Rev. Lett. **88**, 235501 (2002)
23. S. Lazanu and I. Lazanu, "The role of primary point defects in the degradation of silicon detectors due to hadron and lepton irradiation", submitted to Nucl. Instr. Meth. B (2005)

4. Defect Engineering

4.1. Standard and DOFZ silicon

Both standard and DOFZ silicon are mainly investigated for comparison with high resistivity Cz or Magnetic Czochralski silicon (MCz), epitaxial material (EPI) or pre-irradiated FZ and MCz silicon. Investigations of a possible defect engineering by hydrogenation of silicon is until now concentrated on standard and oxygen enriched silicon only.

4.2. High resistivity Czochralski silicon

Silicon crystals grown by the Czochralski (Cz) or the Magnetic Czochralski (MCz) method have a much higher oxygen concentration ([O] ≈ 4-10·10^{17} cm^{-3}) compared to any oxygen enriched DOFZ material ([O] ≈ 1-3·10^{17} cm^{-3}) due to the growth technology itself.

It has been demonstrated by recent studies that such high concentration of oxygen will strongly influence the radiation induced creation of oxygen related defects and the defect kinetics resulting in an improved radiation hardness beyond the level observed so far in DOFZ silicon. Furthermore, it is well known that in Cz material different thermal donors can be formed or annihilated by specific heat treatments. This also leads to a further possibility to influence the radiation tolerance of this material. The radiation hardness of n- and p-type MCz devices has been studied by different groups and recent results on the radiation induced change of the macroscopic properties will be presented in Section 5 (PDC). Microscopic studies are included in Section 3 (DMC). In particular, TSC measurements on irradiated samples have evidenced the introduction of shallow donors. But is has to be noted that the peaks related to Thermal Donors emissions (TD0/+ and TD+/++), observed when the diodes are heated at temperatures of 430°C, are not present after irradiation.

7.3.1 Thermal donor generation in Czochralski silicon particle detectors

Introduction

High resistivity Cz-Si detectors have been fabricated and tested as part of various irradiation campaigns within the framework of CERN RD50 collaboration [1,2,3]. The n on p and p on n Cz-Si devices require both about 300 V reverse bias for full depletion. Heat treatment of Cz-Si wafers between 400 – 600°C leads to the aggregation of interstitial oxygen atoms resulting in electrically active shallow levels in the silicon's band gap. This process is known as the TD formation and it depends on the temperature, the oxygen concentration in the silicon material and the presence of hydrogen in device manufacturing process [4,5,6]. An interesting feature of Cz-Si is the formation of thermal donors (TD) at certain temperatures. When the TDs are generated in boron doped Cz-Si, the p-type bulk will be compensated and if necessary, eventually turn to n-type. With this method, it is possible to fabricate, without increasing the process complexity, high oxygen concentration p on n or n on p detectors that can be depleted with voltages less than 100V [7,8].

Samples

All samples used in this study have been processed on p-type magnetic Czochralski silicon wafers (MCz-Si). The starting material of the detectors was 4" double-side-polished 300±2 μm-thick <100> Cz-Si wafers. The nominal resistivity, measured by the four point probe method, of the boron-doped wafers is 1800 Ωcm, which corresponds to a boron concentration of 4.38·10^{12} cm^{-3}. The oxygen concentration of these wafers was measured by the Fourier Transformation Infrared (FTIR) spectroscopy. The measurements were done on a thick reference wafer at the Institute of Electronic Materials Technology (ITME), Warszawa, Poland. Four measurements showed the following oxygen

concentrations: $4.95 \cdot 10^{17}$ cm^{-3} (center), $4.89 \cdot 10^{17}$ cm^{-3} (right), $4.93 \cdot 10^{17}$ cm^{-3} (left) and $4.93 \cdot 10^{17}$ cm^{-3} (bottom).

Two types of pad detectors were processed at the Microelectronics Center of the Helsinki University of Technology. The active pad implanted area of the diodes is 5mm × 5mm. It is surrounded by one wide guard ring (100μm) and 16 small guard-rings (each 16μm wide). The distance between the active area implant and the first guard ring is 10μm. A 1 mm diameter round opening in the front metallization was left for TCT (Transient Current Technique) measurements.

The first set of samples were $p^+/p^-/n^+$ pin-diode structures, i.e. the pad has been implanted by boron and the back-plane by phosphorous. The second set of samples with $n^+/p^-/p^+$ structures was processed with a different mask set. An additional mask level and boron ion implantation was required because of the electron accumulation layer at the SiO_2/Si interface. The surface inversion was terminated by boron implanted guard rings. One 100μm wide and eight 16μm wide guard rings between the n^+ rings. No boron field implantation (often referred as p-spray) was done for these samples. All samples were passivated by an approximately 60nm thick silicon nitride (Si_3N_4) film grown by Plasma Enhanced Chemical Vapor Deposition (PECVD) method. The deposition temperature of PECVD Si_3N_4 is 300°C.

The last process step of these detectors was the aluminum sintering. In order to study the thermal donor generation, the detector wafers were sintered at 430°C for different durations at the peak temperature: 35, 45, 60, 70 and 80 minutes. The thermal profile of sintering is 2 minutes "push-in" followed by 10 minutes stabilization while the furnace settles again at the peak temperature (the furnace door is open during the push-in). After heating at the peak temperature the wafers were "pulled-out" in 2 minutes. A $n^+/p^-/p^+$ reference wafer was processed and sintered at 370°C.

After the processing the wafers containing 80 pad detectors were diced. The diodes were characterized at the probe station by capacitance-voltage (CV) and current-voltage (IV) measurements. In order to study the effect of a possible radial dispersion in the oxygen concentration on the TD formation, ten diodes along the diameter of each wafer were chosen for CV and IV measurements. Further, it was observed that the introduction of TD's does not influence the leakage current of the devices.

Measurements

The Fig 4-1. shows the effective doping concentration with respect of heating time at 430^0 C. The compensation of the boron doping, i.e. type inversion, occurs after about 55-60 minutes heating.

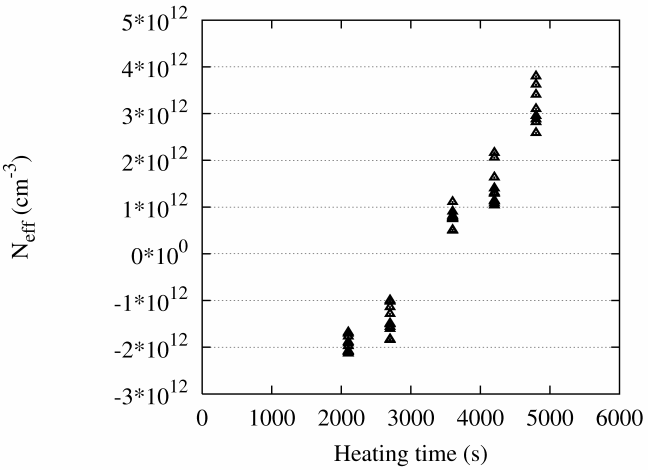

Figure 4-1. Effective doping concentration Neff versus heating time at 430°C. The heating time data points correspond 10 diodes picked along the wafer diameter.

The TD induced Space Charge Sign Inversion (SCSI) in p+/p/n+ devices was further studied by the Transient Current Technique (TCT) method. After sufficient TD generation, the bulk is compensated and inverted to n-type, switching the junction to the front side (p^+-side). Figure 2 shows a TCT transient of the hole current of a detector that has been heat treated for 35 minutes at 430^0C.

A decreasing induced current with time can be seen in Fig. 2, thus indicating holes drift from the high electric field (n^+-side) to the low field (p^+-side). The junction, as expected, is on the backside (n^+-side). Figure 3 shows a TCT transient of hole current of a similar detector as in Figure 2 that has been heat treated 75 minutes at 430^0C.

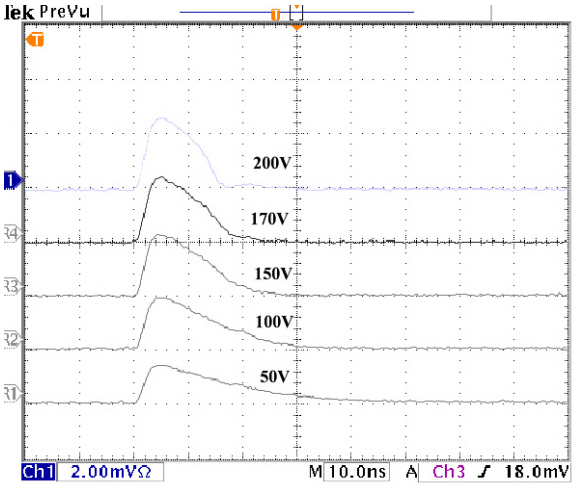

Figure 4-2. Current transients with different reverse bias voltages of p+/p/n+ detector. In this sample thermal donors have been generated at 430°C for 35 minutes. The detector has been illuminated from the backside (n^+-side).

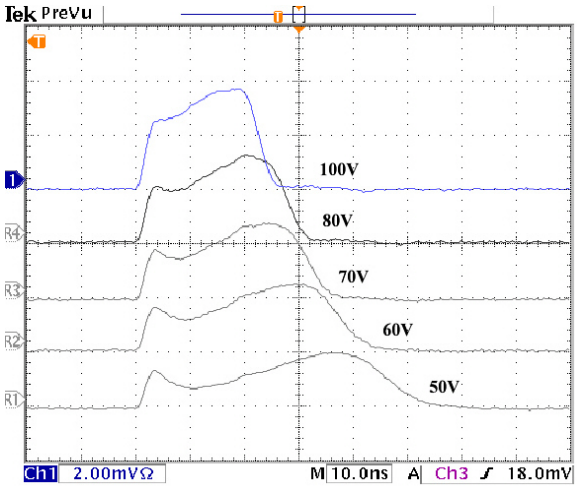

Figure 4-3. Current transients with different reverse bias voltages of p+/p/n+ detector. In this sample thermal donors have been generated at 430°C for 75 minutes. The detector has been illuminated from the backside (n^+-side).

It is clear that the hole current shapes shown in Figure 4-3 are drastically different from those shown in Figure 4-2: the hole current transients increase with time, indicating holes drifting from low electric field (n^+-side) to high electric field (p^+-side). Now the junction is switched from the backside (n^+-side) to front side (p^+-side). The SCSI has taken place from negative to positive, and the bulk is type-inverted to n^- type. The device structure is therefore transformed from the original $p^+/p^-/n^+$ to the intended $p^+/n^-/n^+$.

Summary

The thermal donor formation is a feature of Czochralski silicon. It cannot be observed in standard detector materials such as Fz-Si or diffusion oxygenated Fz-Si, because the concentration of interstitial oxygen is too low in these materials The TDs are shallow donor levels, within 0.01 eV –0.2 eV below the conduction band. The formation of TDs is strongly depended on temperature and oxygen concentration in the silicon material. Heat treatment between 400 – 600^0C lead to TD formation.

The detector processing was carried out using the common procedure to produce $n^+/p^-/p^+$ or $p^+/n^-/n^+$ detector structures. During the last process step, i.e. sintering of aluminum electrode, the p-type bulk was turned to n-type through generation of Thermal Donors (TD). The full depletion voltage of detectors could be tailored in a wide range from 30 V up to close 1000 V by changing the duration of the heat treatment at 400^0C – 450^0C from 20 to 80 minutes. The Space Charge Sign Inversion (SCSI) in the TD generated devices (from p+/p-/n+ to p^+/n^-(inverted)$/n^+$) has been verified by Transient Current Technique (TCT) measurements.

Recently, p-type silicon materials have gained a growing interest among the scientific community aiming to improve radiation hardness of silicon devices. The benefit of p-type materials is the absence of SCSI, thus the collecting junction remains on the front side (n^+) of the detector and the main part of the signal is due to electron collection allowing a higher charge collection than in $p^+/n^-/n^+$ devices. If p-type MCz-Si wafers are used for the production of $n^+/p^-/p^+$ devices, the TD formation can be utilized in order to tailor the V_{fd}.

References

[1] J. Härkönen et al., ” Processing microstrip detectors on Czochralski grown high resistivity silicon”, Nucl. Instr. And Meth, A485 (2002), 159-165.

[2] E. Tuominen et al., ” Radiation Hardness of Czochralski Silicon studied by 10 MeV and 20 MeV protons”, IEEE Trans. Nucl. Sci. 50 (2003).

[3] P. Luukka et al., " Results of Proton Irradiations of Large Area Strip Detectors made on High-Resistivity Czochralski Silicon" , Nuclear Instruments and Methods in Physics Research A530 (2004) 117-121.
[4] G.S. Oehrlein, "Silicon–oxygen complexes containing three oxygen atoms as the dominant thermal donor species in heat-treated oxygen-containing silicon", J. Appl. Phys. 54 (1983) 5453.
[5] K. Wada, ""Unified model for formation kinetics of oxygen thermal donors in silicon", Phys. Rev. B, 10 (1984) 5884.
[6] A. Simoen et al, "Hydrogen plasma-enhanced thermal donor formation in n-type oxygendoped high-resistivity float-zone silicon", Appl. Phys. Lett. 81 (10) (2002) 1842.
[7] J. Härkönen et al., "p+/n-/n+ Cz-Si detectors processed on boron doped substrates with thermal donor induced space charge sign inversion", IEEE Transactions on Nuclear Science, (in press).
[8] J. Härkönen et al., " Proton irradiation results of p+/n-/n+ Cz-Si detectors processed on boron doped substrates with thermal donor induced space charge sign inversion", Nuclear Instruments and Methods in Physics Research A (in press).

4.3. Thin epitaxial silicon layers

The very promising first results on the radiation tolerance of 50 μm thick and highly doped n-type epitaxial silicon layers ([P] = 7 10^{13} cm^{-3}) up to a 24 GeV/c proton fluence of 2 10^{15} cm^{-2} had been extended to 1.2 10^{16} cm^{-2} . It could be demonstrated that the devices do not undergo type inversion in the overall range, that the full depletion voltage after the maximal accumulated fluence of 1.2 10^{16} cm^{-2} increases to 250 V (two times the value before irradiation) and that a storage of these devices at room temperature for a prolonged period of 250 days (beam off period of LHC) will even reduce the full depletion voltage. More details and references are presented in section 5 (PDC).

In continuation of the research plan 50 Ω·cm n-type epitaxial layers with a thickness of 25 μm and 75 μm were grown by ITME and processed by CiS in order to investigate possible changes in the defect kinetics due to the different growth time needed for the different layers and different oxygen depth profiles introduced during the high temperature treatments involved in the device processing.

Depth profiles of the resistivity and oxygen concentration are displayed in Fig. 4-4 and Fig. 4-5 respectively. Oxygen is out-diffusing from the Cz substrate mainly during the high temperature diode process steps as verified by comparison of SIMS results with process simulations [1, 2].

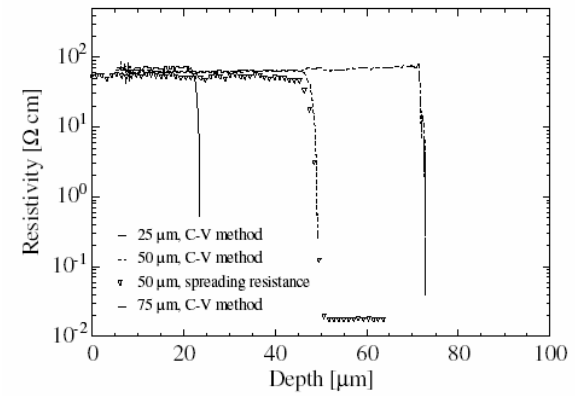

Fig. 4-4 Resistivity depth profiles as measured by spreading resistance (symbols) and C/V methods (lines) for 25, 50 and 75 μm n-type epi diodes.

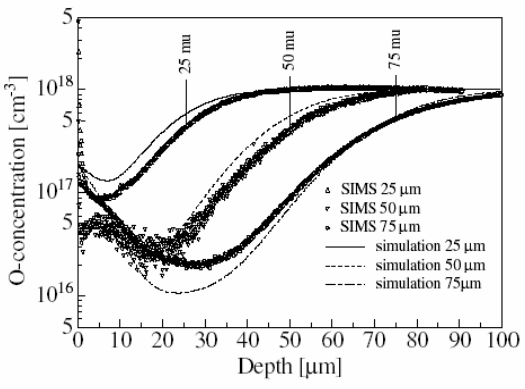

Fig. 4-5 Oxygen concentration profiles measured with SIMS symbols) in comparison with process simulation results (lines) in the n-type epi-diodes under test.

From investigations of the change of the effective doping concentration N_{eff} due to irradiation with different particles (see section PDC) three main effects attribute to the stable damage. The donor removal reduces the positive space charge by formation of E-centers (vacancy-phosphorus complex). This component, responsible for the first part of the fluence dependence, is exponentially saturating due to the exhaustion of available P-donors. A large value of the doping concentration, as possible in thin diodes, will delay this exhaustion. For larger fluences in epi-diodes the possible creation of acceptors is obviously always overcompensated by donors causing the almost linear increase of N_{eff} in the high fluence range ($\Phi_{eq} > 10^{15}$ cm^{-2}, see Fig. 4-6).

It is however striking that the effect of stable donor generation is largely depending on the thickness of the device. Indeed the differences in $N_{eff}(\Phi_{eq})$ seen in Fig. 4-6 between 25 µm (large increase) and 75 µm diodes (only small increase) are obviously correlated with the oxygen concentration profiles displayed in Fig. 4-5. A direct correlation has to be excluded, because a similar effect was not observed in oxygen enriched silicon (DOFZ) diodes with the same average O-concentration. A first understanding was provided by defect spectroscopy investigations, revealing a shallow donor at E_C-0.23 eV, which is not detectable in FZ diodes [3, 4, 5]. Fig. 4-7 shows results of TSC-spectra for all 3 n-type epi diodes. While the well known point defects like e.g. C_iO_i, the double vacancy as well as the peak at 115 K, known from previous work in FZ diodes [6] are measured with concentrations independent on the diode type and hence independent of the O-concentration, the TSC signal due to the shallow donor (denoted BD) has a very similar dependence on the material as the average O-concentration (Fig. 4-5) and the stable damage generation (Fig. 4-6).

The following tentative explanation for the generation of the BD donor and hence the superior radiation tolerance of n-type epi diodes had been proposed in Ref. [3, 4]. A strong similarity of the BD complex to thermal double donors and the well known fact that oxygen dimers O_{2i} are precursors for the formation of thermal donors (see [7]) leads to the assumption that dimers are involved in the damage produced BD defects. It is also known that oxygen dimers have a much larger diffusion constant than oxygen interstitials. Thus it can be expected that they out-diffuse from the Cz substrate predominantly after the last high temperature process step thus leading to a relatively larger dimer concentration in the epi diodes than could be expected from the oxygen concentration alone. And indeed by monitoring the oxygen dimers with measurements of the IO_{2i} concentration an appreciable enhancement of the relative dimer ratio in n-type epi diodes with respect to that found in n-type Cz silicon by at least a factor of 2 was shown. In standard and oxygen enriched n-type FZ diodes no IO_{2i} defect was found supporting the general picture [8].

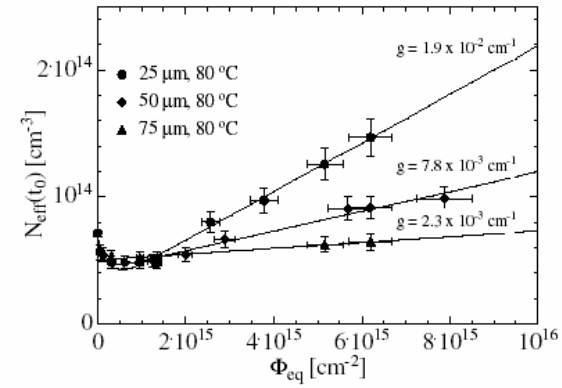

Fig. 4-6 Effective doping concentration, as measured after the end of beneficial annealing as function of fluence after 24 GeV/c proton irradiation. Solid lines represent fits according to a model description [9], slope values assigned to the curves represent the donor generation rates.

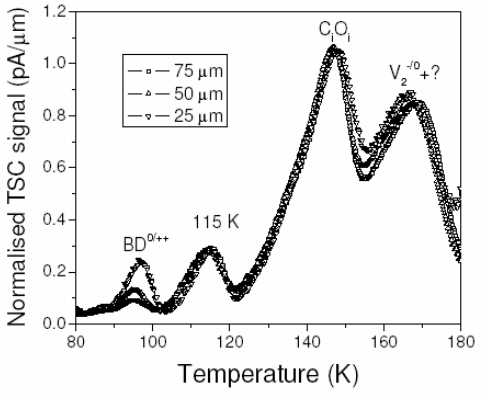

Fig. 4-7 TSC spectra for 25, 50 and 75 µm n-type epi diodes after 24 GeV/c proton irradiation with Φ_{eq} = $1.8 \cdot 10^{14}$ cm^{-2} and 120 min annealing at 60°C (top curve: 25 µm, bottom one: 75 µm).

In conclusion it is therefore very likely that the shallow donor (the BD complex), found in epi-silicon after irradiation, is indeed responsible for the dominating positive space charge build up in these devices and that this donor is generated via the enhanced concentration of oxygen dimmers out-diffusing from the Cz substrate.

References for Section 4.3

[1] A. Barcz, SIMS laboratory, Institute of Phhysics, Warsaw; private communication
[2] Li Long, Institute for Micro Sensors CiS, Erfurt, private communication
[3] I. Pintilie, M. Buda, E. Fretwurst, G. Lindström, J. Stahl; Stable radiation induced donor generation and its influence on the radiation tolerance of silicon diodes; submitted for publication to Nucl. Instr. and Meth. A

[4] I. Pintilie, E. Fretwurst, F. Hönniger, G. Lindström. J. Stahl; Radiation induced donor generation in epitaxial and Cz diodes; Nucl. Instr. and Meth. A, in press
[5] J. Stahl, E. Fretwurst, G. Lindström. I. Pintilie; Physica B 340-342 (2003) 705-709
[6] M. Moll. PhD thesis. University of Hamburg 1999; DESYTHESIS -1999-040, December 1999
[7] Y.L. Lee, J. von Boehm, M. Pesola. R.M. Nieminen; Phys. Rev. B 65 ((2202) 085205
[8] J. Stahl, PhD thesis, University of Hamburg 2004, DESYTHESIS-2004-028, July 2004
[9] G. Lindström, E. Fretwurst, F. Hönniger, G. Kramberger, M. Möller-Ivens, I. Pintilie. A. Schramm; Radiation tolerance of epitaxial silicon detectors at very large proton fluences; submitted for publication to Nucl. Instr. and Meth. A

4.4. Defect engineering by treatments at elevated temperatures

A new approach for the recovery or improvement of detector properties after irradiation by thermal treatments is proposed by the Ioffe Physico-Technical Institute, Brookhaven National Laboratory and the Helsinki Institute of Physics.

Detector Recovery/Improvement Via Elevated-temperature-annealing (DRIVE)

One of the possible methods of removing the radiation damage is annealing of radiation induced defects. This universal procedure is routinely applied e.g. in processing of homogeneous neutron transmutation doped Si in which even defect clusters can be annealed at temperature T of about 800-900°C. However, elevated temperature annealing of Si detectors irradiated by neutrons and charged particles leads to the so called reverse annealing, which causes even more increase in negative space charge and, therefore, further increase of the detector full depletion voltage [1, 2]. Recent studies in oxygen-rich (oxygenated FZ Si and MCZ Si) detectors have revealed that annealing of these silicon detectors at medium temperatures (400-500°C) leads to the introduction of shallow thermal donors [3]. This effect is favorable for the purpose of annealing heavily irradiated Si at medium temperatures since the negative space charge due to reverse annealing can be over-compensated by positive space charge due to the thermal donor generation. The manipulation of the space charge sign using medium temperature annealing was demonstrated recently for detectors processed from p-type CZ Si in which an introduction of thermal donors resulted in a space charge sign inversion (SCSI) from negative to positive [4-5]. A new approach, called DRIVE (Detector Recovery/Improvement Via ETA), was proposed at the 5th CERN RD50 Collaboration Workshop [6]. With the DRIVE approach, it is anticipated that oxygen-rich Si detectors can be recovered through ETA as the following: 1) decrease in detector leakage current; 2) decrease in the net space charge concentration and therefore the detector full depletion voltage; and 3) increase of the charge collection efficiency (CCE).

The goal of the study is the development of the experimental method to prove the DRIVE concept and to find out the optimal annealing temperature and time for different radiations and radiation fluences.

Experimental

All investigated detectors were processed at the Helsinki Institute of Physics. The detectors are subdivided into two groups:

- group 1 (five detectors ## P352-…) is manufactured as p^+-p-n^+ pad structures with multiple guard rings (GRs) from p-type MCZ Si with a resistivity of about 3 kΩ·cm and a wafer thickness of 300 μm;

- group 2 (## C1-3 and D2-3) is manufactured as p^+-n-n^+ pad structures with multiple GRs from n-type MCZ Si with a resistivity of about 1 kΩ·cm and a wafer thickness of 380 μm.

Table 1. Detectors and radiation fluence.

E_p	**Protons 24 GeV/c**			**Protons 20 MeV**	
Si type	**p-type**			**n-type**	
#	P352-18	P352-59	P352-48	C1-3	D2-3
F_p (cm^{-2})	$9 \cdot 10^{13}$	$3.6 \cdot 10^{14}$	$5 \cdot 10^{14}$	$5.9 \cdot 10^{13}$	$1.2 \cdot 10^{14}$
annealing steps	8	12	13	8	10
T (°C)	150-450	300-450	450	430-450	430-450
initial space charge sign before ETA	- (minus)	-	-	-	-
space charge sign after final ETA step	+	+	+	+	+

Detectors of groups 1 and 2 were irradiated with high (24 GeV/c, CERN PS) and medium (20 MeV, HIP) energy protons, respectively, and with fluence values in the range $5.9 \cdot 10^{13}$-$5 \cdot 10^{14}$ cm^{-2}. Beneficial annealing was carried out at 80°C. The annealing was performed at BNL as a multi-step process with a variable time. Heat treatment was made in the nitrogen flow and terminated in fast cooling (~10 min) of the samples. In Table 1 the investigated detectors and radiation and annealing parameters are presented. Annealing cycles for three annealed detectors from group 1 and detector # D2-3 from group 2 are shown in Fig. 1. For most annealing steps, the annealing temperature was 450°C for the introduction of thermal donors and the annealing time t_{ann} varied from 10 min to 2 h. For two samples, ## P352-18 and P352-59, preliminary annealing steps in the range 150-400°C, each step with a duration of 10 min, were performed to stimulate the N_{eff} reverse annealing. The annealing cycle of detector # C1-3 was similar to that of detector # D2-3 but had a shorter annealing time.

Before ETA and after each annealing step, all detectors were characterized by measurements of I-V and C-V characteristics in the bias voltage range up to 500 V and current pulse response in the bias voltage range up to 1000 V. The Transient Current Technique (TCT) with a red laser (660 nm) pulse generation of non-equilibrium carriers was applied for the pulse response measurements. Spectra of deep levels were measured at the Ioffe Institute by C-DLTS after the final detector annealing.

Experimental results

Three stages of the changes of detector characteristics were observed for all detectors irrespective to the energy and fluence of the protons:

1) reverse annealing at which the negative N_{eff} increases significantly so that the full depletion voltage V_{fd} can exceed 1 kV (the limit of the TCT setup) and the current pulse response from the detector p^+ side disappears (T < 430 ºC);
2) significant decrease of the reverse current and recovery of the signal from the p^+ side and (T ≥ 430 ºC, and t_{ann} > 1 hour);
3) SCSI (T ≥ 450 ºC, and t_{ann} > 2 hour).

The changes of detector characteristics are shown in the diagrams of detector annealing cycles (Fig. 1).

Recovery of detector reverse current

The I-V characteristics of two detectors irradiated by 24 GeV/c protons with different fluences are presented in Fig. 2. The I-V characteristics of as-processed detectors show a standard behavior with a saturation of the current at full depletion. The difference between the changes of I-V characteristic of two detectors is related to specific fluences and features of heat treatments. For detector # P352-18 short successive annealing (10 min each) at T ranging from 150 to 300°C did not change the

saturating behavior of the I-V curve (Fig. 2, a). It led however to the increase of the saturated current and the voltage corresponding to its saturation from 30 V for as-irradiated sample up to 250 V for detector annealed at 300°C. The same behavior was observed also in the C-V dependences (Fig. 3) in which the saturated capacitance was the evidence of detector full depletion. Saturation of C-V curves was observed for as-irradiated detector and after the two first steps of preliminary annealing at 150°C and 200°C. Starting from T = 300°C C-V curves did not show saturation. The temperature of 270°C corresponds to the annealing of one of the major radiation induced defects - divacancy [1, 7]. However the dominating reverse annealing implies that mid-gap defects responsible for the negative N_{eff} increase are annealed in. After annealing at 450°C a further increase of the reverse current and lack of the saturation of I-V and C-V curves was observed. The recovery of the current (a decrease down to 1 nA that is far less than the current of as-irradiated detector) arose after the total annealing time of 150 min at T = 450°C (seventh annealing step). Reversal to the saturated capacitance occurred simultaneously with the reverse current recovery. After the final annealing step the C-V curve shows no saturation that implies the increase of N_{eff}.

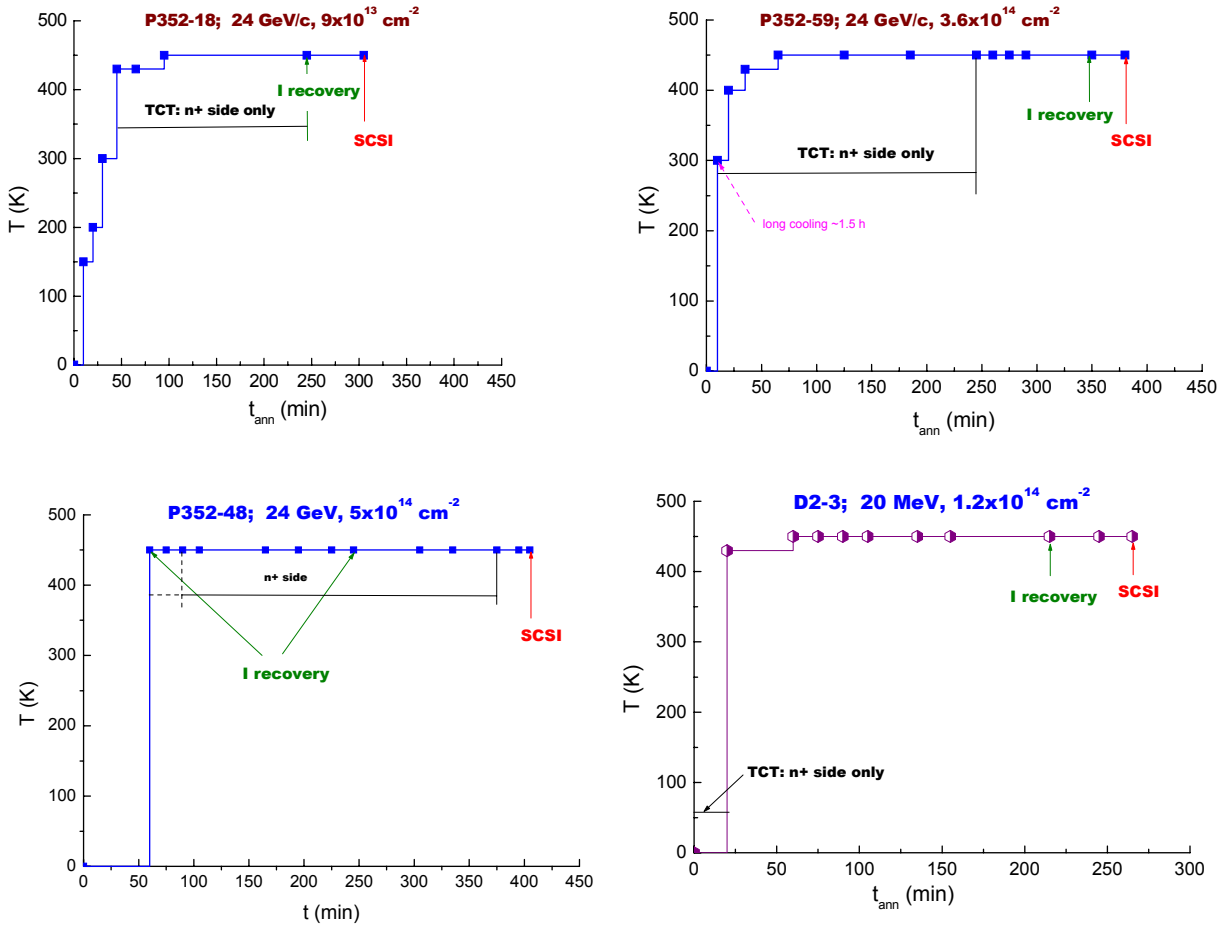

Fig. 1. Diagrams of the annealing cycles and behavior of detectors irradiated with 24 GeV/c protons

All heat treatments of the detector # P352-48 irradiated at larger fluence ($5 \cdot 10^{14}$ cm^{-2}) were carried out at 450°C exclusively. The reverse current showed successive recovery at any annealing step and finally decreased down to 10-20 nA (Fig. 2, b).

The reverse current recovery of detectors from group 2 resulted in the reduction of the current down to few nA. Still, after the final annealing steps the current had a leakage at voltages beyond 200 V.

For all detectors an essential reduction of the current occurred if the duration of the annealing step was in the range 1-2 hours.

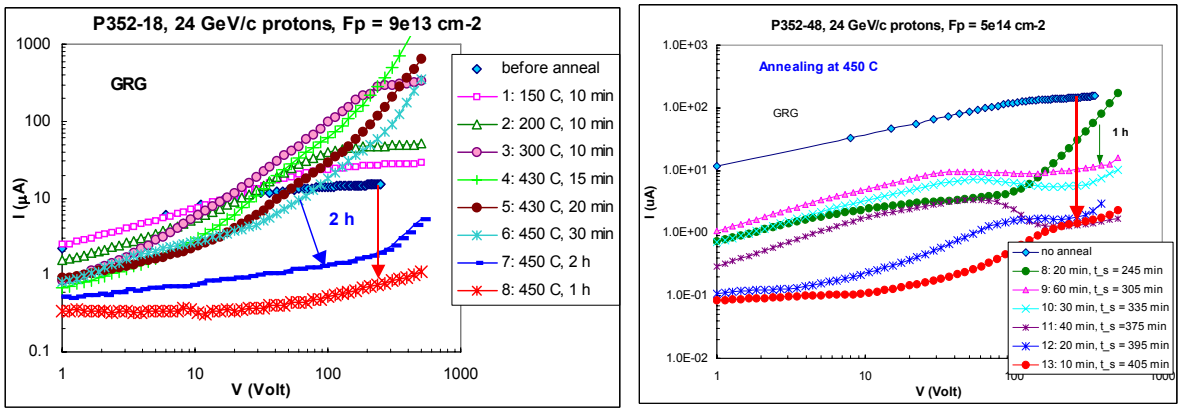

Fig. 2. Annealing of reverse current of two p-type MCZ detectors irradiated by 24 GeV/c protons

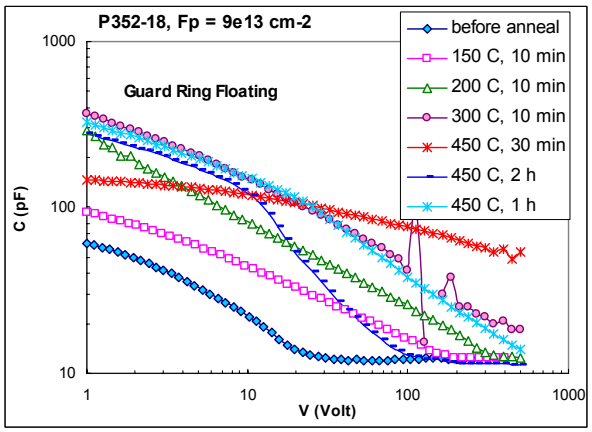

Fig. 3. Changes of C-V characteristics under ETA of p-type MCZ detector # P352-18 irradiated by 24 GeV/c protons

Behavior of current pulse response under ETA

Specific features of degradation and recovery of the detector pulse response is that the changes of the signal from the p^+ side depend on the thermal treatment. Therefore below we describe the changes of the pulse response separately for each detector.

a) Detector # P352-18 with preliminary heat treatment in the interval 150-300°C

Before annealing the shape of the current pulse response is typical for a detector with a negative space charge (Fig. 4). At any step of preliminary annealing the shape corresponds to a negative N_{eff} with increasing value of the voltage at which the signal starts to develop from the p^+ side. This value reaches 600 V at T = 300°C. Then, the signal from the p^+ side of this detector vanishes just after ETA at 430°C. The signal from the detector n^+ side has an abnormal shape with a peak and extended time decay of about 100 ns (Fig. 5) until the total annealing time at T = 450°C reaches 150 min. At this stage the recovery of the signal from the p^+ side occurs and the shapes of the signals from both detector sides are still typical for the negative N_{eff}. After the final annealing step SCSI to the positive N_{eff} is observed in the shapes of TCT signals (Fig. 6).

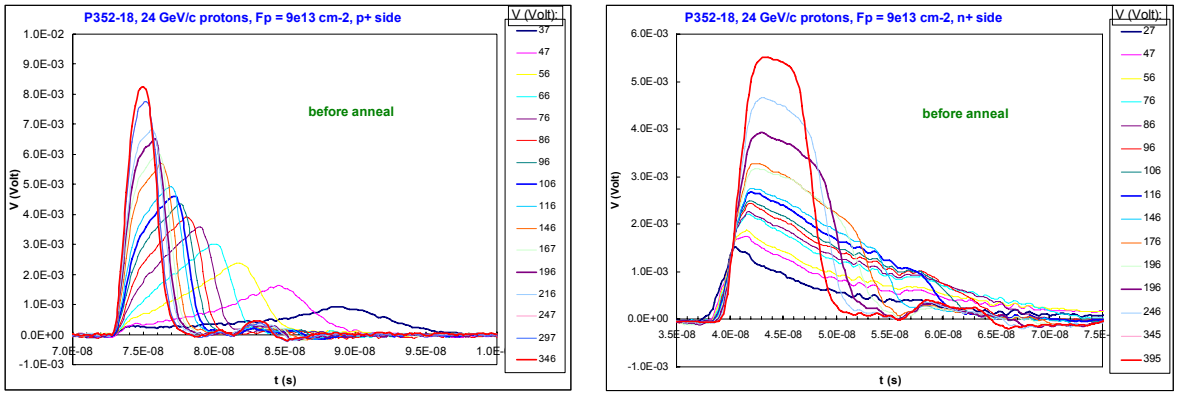

Fig. 4. Current pulse response of detector # P352-18 irradiated by 24 GeV/c protons before annealing.

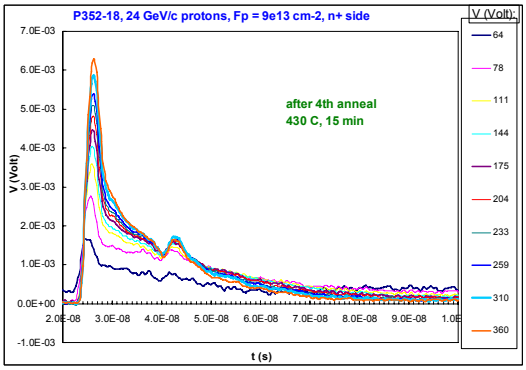

Fig. 5. Current pulse response with extended pulse decay recorded from the n^+ side of detector # P352-18 irradiated by 24 GeV/c protons after annealing at 430°C

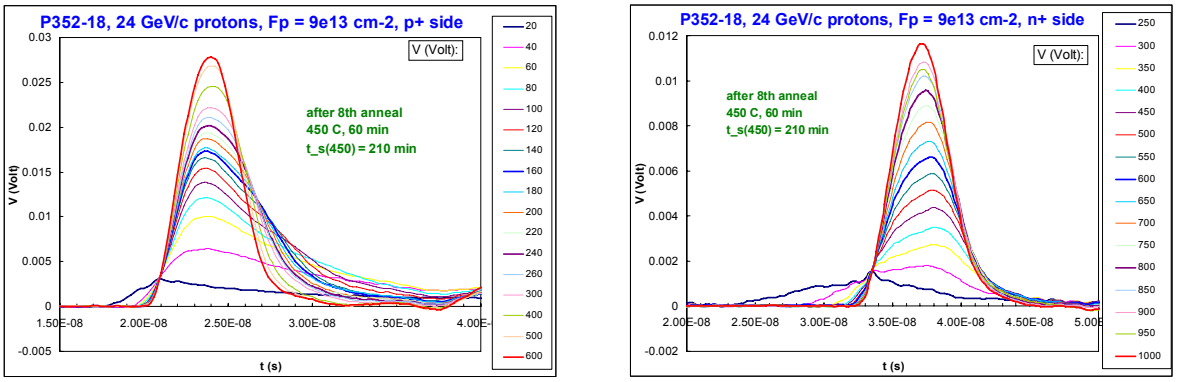

Fig. 6. Current pulse shapes of detector # P352-18 after final annealing step (total annealing time of 210 min at 450°C) demonstrating SCSI to a positive N_{eff} (left: p^+ side, right: n^+ side illumination).

b) Detector # P352-59 with preliminary heat treatment at 300°C and 400°C

Before annealing the current pulse response from the p^+ side has a double peak (DP) shape that implies that the electric field has two peaks near the detector contacts. Just after annealing at 300°C the signal from the p^+ side disappears while the signal from the n^+ side has an abnormal shape similar to that of detector # P352-18. Due to a higher radiation fluence of this detector, recovery of the signal from the p^+ side occurs at a larger annealing time (210 min). At t_{ann} = 315 min the shape of the current pulse response has practically flat top that implies that the space charge significantly drops down. Finally, at t_{ann} = 345 min the signal from the n^+ side has an ascending slope and starts to develop only at V = 410 V that shows that SCSI to a positive N_{eff} has occurred.

c) Detector # P352-48

Before annealing the current pulse response has a double peak (DP) shape from both sides of the detector (Fig. 7) that implies that the electric field distribution is non-uniform. All heat treatments of this detector irradiated at the largest fluence were carried out at 450°C exclusively. Specific feature is that at $t_{ann} \leq 150$ min the current pulse response has an abnormal shape with extended time decay from both detectors sides and then the signal from the p^+ side vanishes. Recovery of the signal from the p^+ side occurs after annealing of about 6 hours and the shape just after recovery also reveals extended time decay. After a final annealing step (total t_{ann} of 405 min) SCSI occurs. The current pulse responses from the n^+ side of detectors ## P352-59 and P352-48 are compared in Fig. 8. The signals have an ascending slope that shows that N_{eff} is positive.

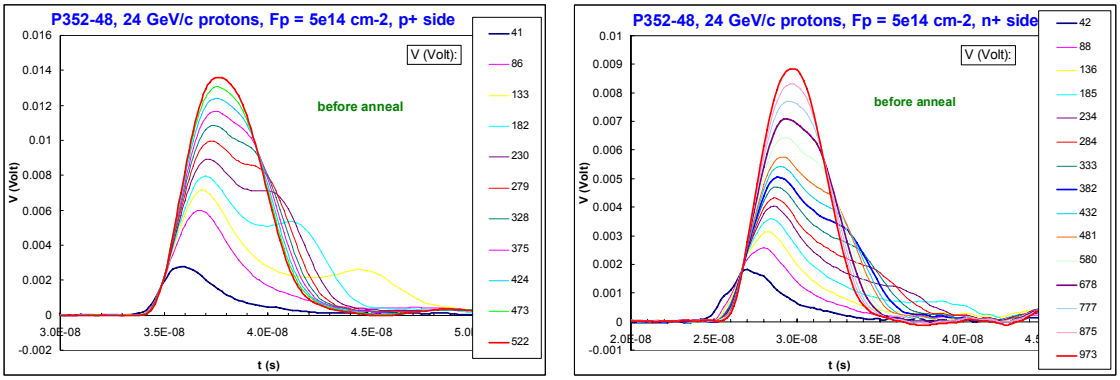

Fig. 7. Current pulse shapes of detector # P352-48 irradiated by 24 GeV/c protons before annealing

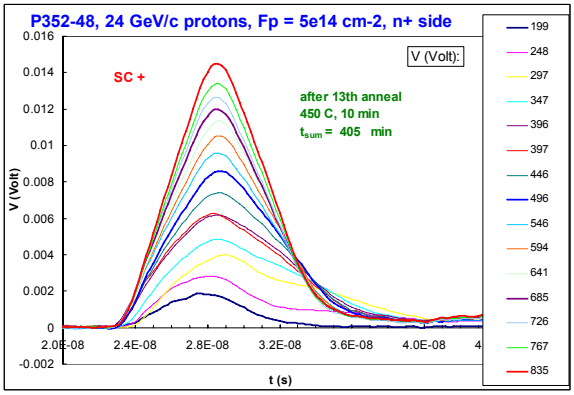

Fig. 8. Current pulse responses from the n^+ side of detectors ## P352-59 and P352-48

d) Detectors ## C1-3 and D2-3 irradiated by 20 MeV protons

For these detectors the initial annealing step was performed at 430°C for 20 min. Thereafter the detectors were kept in the fridge for six months to prevent reverse annealing at room temperature. Before the second anneal the current pulse response was observed only from the n^+ side and had an abnormal shape described above.

Successive annealing started as the second step and all following heat treatments were done at 450°C. The second step with a duration of 1 h resulted in the recovery of the signal from the p^+ side while the signal from the n^+ side had an extended decay. Thus, for both detectors irradiated by 20 MeV protons the annealing time required for a recovery of the signal from the p^+ side was shorter than that for detectors irradiated by 24 GeV/c protons. The reasonable explanation of this difference is the influence of defect clusters introduced into the silicon bulk by high-energy protons that stimulates essential reverse annealing and inhibits the detector characteristic recovery. A comparison of the pulse responses from the n^+ side of detector # D2-3 at the two last annealing steps (Fig. 9) shows the change of the pulse top slopes from descending at the 9^{th} step to ascending at the 10^{th} step that corresponds to the inversion from negative to positive space charge.

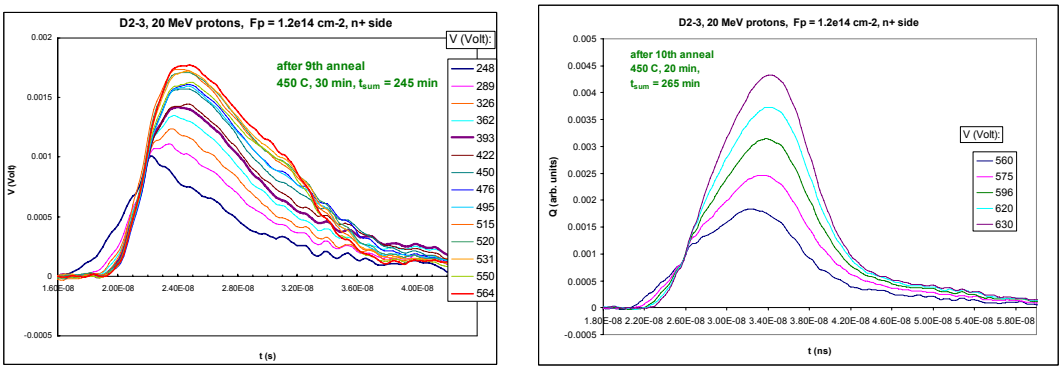

Fig. 9. Current pulse responses from the n^+ side of detector # D2-3 irradiated by 20 MeV protons with a fluence of $1.2 \cdot 10^{14}$ cm^{-2} just before and after SCSI.

Microscopic defect spectra after SCSI

Spectra of microscopic defects in the bulk of three detectors were measured using C-DLTS technique in the temperature interval 77 K to 300 K after final steps of annealing when SCSI occurred. In Fig. 10 C-DLTS spectra of radiation induced defects in a reference detector # P204-I-A-3-7 irradiated by 24 GeV/c protons with a fluence of $1.5 \cdot 10^{11}$ cm^{-2} are compared to the spectra of three detectors studied here and annealed beyond SCSI. Typical radiation induced defects, namely, three electron traps and a hole trap, are clearly observed in the spectra of a reference detector. At the same time continuous spectra of defects are specific for annealed detectors with major features which are similar for both proton energies. Considering the peaks that are visualized in the defect spectra, we made a fit to the experimental spectra of detector # P352-18. The fitting curves and electron and hole traps that can be resolved in spectra are shown in Fig. 11 and the corresponding parameters of deep levels are presented in Table 2.

Table 2. Parameters of deep levels in detector #P352-18 after final annealing.

Electron traps:

DL	E1	E2	E3	E4	E5	E6	E7	E8
E (eV)	$E_c - 0.18$	$E_c - 0.196$	$E_c - 0.26$	$E_c - 0.25$	$E_c - 0.37$	$E_c - 0.41$	$E_c - 0.515$	$E_c - 0.6$
σ (cm^2)	$3.0 \cdot 10^{-15}$	$7.0 \cdot 10^{-16}$	$2.0 \cdot 10^{-15}$	$3.0 \cdot 10^{-17}$	$3.0 \cdot 10^{-15}$	$1.0 \cdot 10^{-15}$	$5.0 \cdot 10^{-15}$	$2.0 \cdot 10^{-15}$
N (cm^3)	$1.0 \cdot 10^{12}$	$4.5 \cdot 10^{11}$	$2.0 \cdot 10^{11}$	$2.8 \cdot 10^{11}$	$6.9 \cdot 10^{11}$	$7.2 \cdot 10^{11}$	$4.5 \cdot 10^{11}$	$2.6 \cdot 10^{11}$

Hole traps:

DL	H1	H2	H3	H4	H5
E (eV)	$E_v + 0.203$	$E_v + 0.28$	$E_v + 0.3$	$E_v + 0.37$	$E_v + 0.545$
σ (cm^2)	$1.0 \cdot 10^{-16}$	$1.0 \cdot 10^{-15}$	$3.0 \cdot 10^{-16}$	$4.0 \cdot 10^{-16}$	$1.0 \cdot 10^{-15}$
N (cm^3)	$1.5 \cdot 10^{12}$	$1.6 \cdot 10^{12}$	$7.0 \cdot 10^{11}$	$5.4 \cdot 10^{12}$	$1.3 \cdot 10^{12}$

The parameters are different from those of known radiation induced defects. Therefore we assume that deep levels detected after annealing arise as products of the decay under annealing of defect complexes induced by radiation. The final defect concentrations are within 10% of as-induced radiation defect concentration and decrease with the increase of the annealing time. These concentrations are in the range of a few 10^{11} cm^{-3} in detector P352-48 for which t_{ann} is maximal.

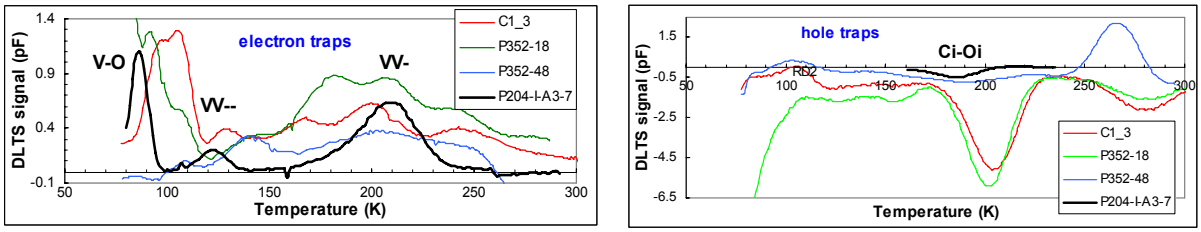

Fig. 10. C-DLTS spectra of microscopic defects in a reference detector irradiated by 24 GeV/c protons with a fluence of $1.5 \cdot 10^{11}$ cm^{-2} and three detectors studied here after SCSI

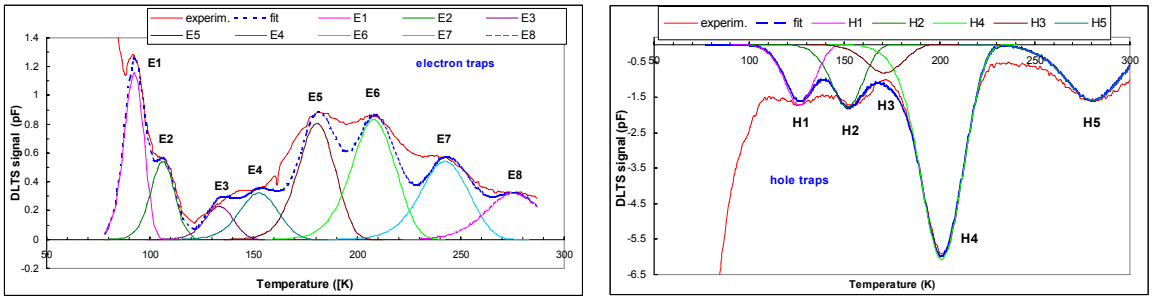

Fig. 11. Experimental and fitted C-DLTS spectra of detector #P352-18 after a final annealing.

The resulting spectra are different from those presented in Ref. 4 (Chapter 3, pp. 3-9 - 3-11). This difference may be related to the difference in the type of radiation: electrons in [4] and medium and high energy protons in this study.

Evolution of the space charge concentration

Space charge concentrations in the bulk of annealed detectors were estimated from the values of full depletion voltage V_{fd} derived from TCT measurements. The full depletion voltage was defined as a voltage at which the decay of the current pulse from the low field region became sharp.

A special procedure was developed for the calculation of N_{eff} from signals with an extended decay time. As an example for such a shape, the current pulse response from the n^+ side of detector # P352-18 after 4th anneal is presented in Fig. 12, a. The current pulse has a peak and a long-term decay extending up to 100 ns. The peak is related to the charge transfer within the space charge region near the n^+ contact. The decay time constant depends on the bias voltage (Fig. 5) and at the same bias voltage varies at different annealing steps (Fig. 12, b).

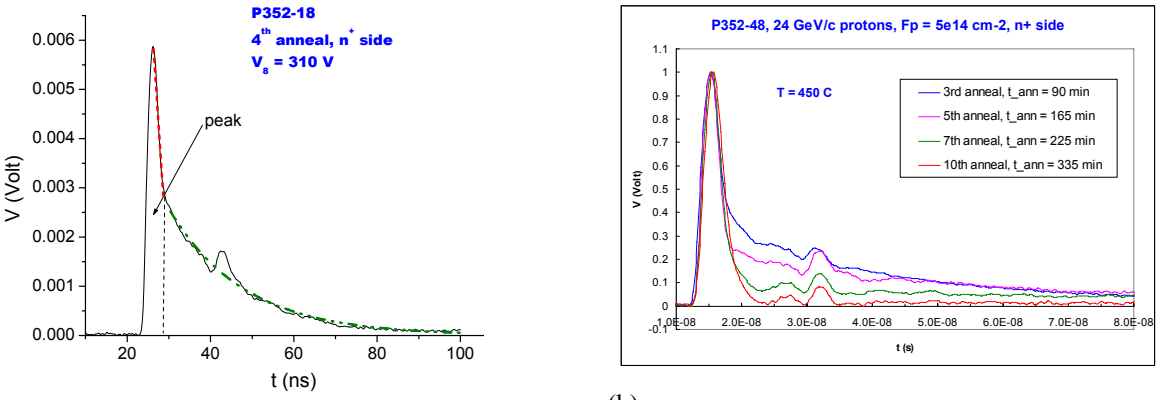

(a) (b)

Fig. 12. Current pulse response with an extended decay time: a) detector #P352-18 after 4th annealing operating at the bias voltage of 310 V; b) changes of the decay time constant under annealing for detector # P352-48 at the bias voltage of (350±20) V.

The ratio of the charge Q_{peak} collected within the space charge region W near the n^+ contact to the total collected charge Q_{col} is proportional to the ratio W/d, where d is the detector thickness. At the n^+ contact:

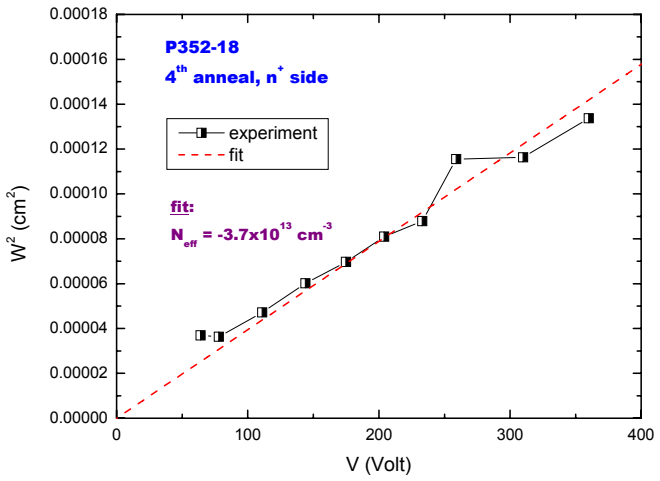

Fig. 13. W^2 versus V dependence illustrating the calculation of N_{eff} from the current pulse response with long-term decay.

$$W \sim \sqrt{V / N_{eff}}$$

By integrating the current pulses we can obtain Q_{peak}/Q_{col} and N_{eff} can be derived from the slope of the linear $W^2(V)$ dependence (Fig. 13).

A 3D-plot, illustrating the evolution of the space charge concentration versus T and annealing time in detector # P352-18, is presented in Fig. 14. The evolution of N_{eff} in p-type MCZ Si detectors irradiated with 24 GeV/c protons in the temperature range corresponding to reverse annealing, and at T = 450°C corresponding to the thermal donor introduction are shown in Fig. 15, a and b, respectively.

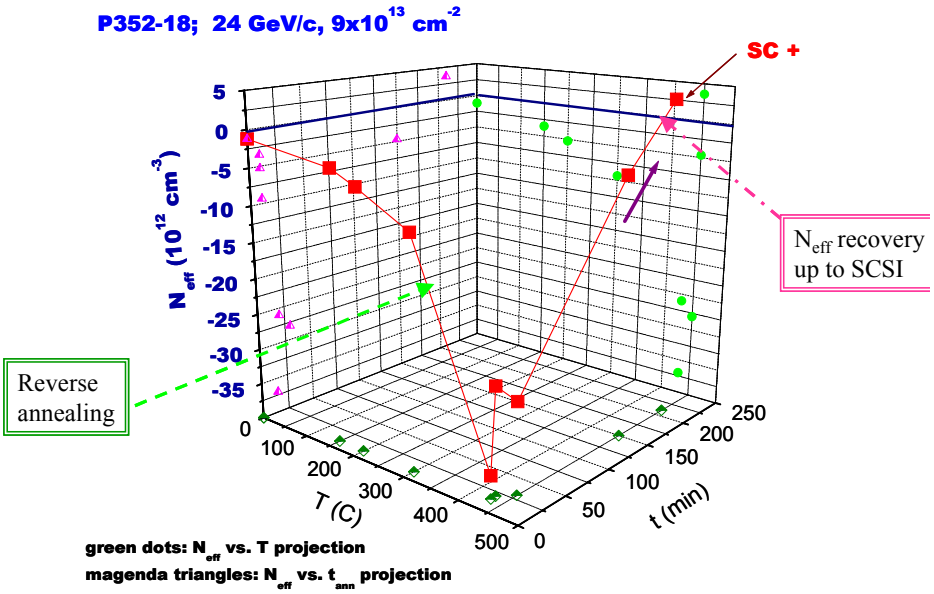

Fig. 14. Evolution of space charge concentration versus T and annealing time in detector # P352-18.

Finally, the dependence of the annealing time at T = 450°C required for SCSI in the bulk of detectors irradiated by protons is presented in Fig. 16. SCSI to a positive Neff was achieved for all detectors regardless of the original type of silicon, the proton energy and fluence, and the procedure of the heat treatment. The linear dependence obtained for the detectors irradiated with 24 GeV/c protons is optimistic for practical application of the DRIVE approach in the experiments, especially with a limited amount of detectors. Still, at the final stage of heat treatments a fine tuning of the annealing time is required for a precise manipulation of the introduction of thermal donors and resulting Neff, which obviously needs further studies and experience.

In practical aspects, the ETA in the DRIVE approach can be various for detectors in a real experiment, such as that: 1) localized laser anneal; 2) localized anneal using a lamp; 3) annealing using pre-built-in external heating resistors; and 4) annealing using leakage current of the detector itself. The annealing methods 3) and 4) can be easily realized by turning on and of an electric switch, and 4) is the easiest and most practical method.

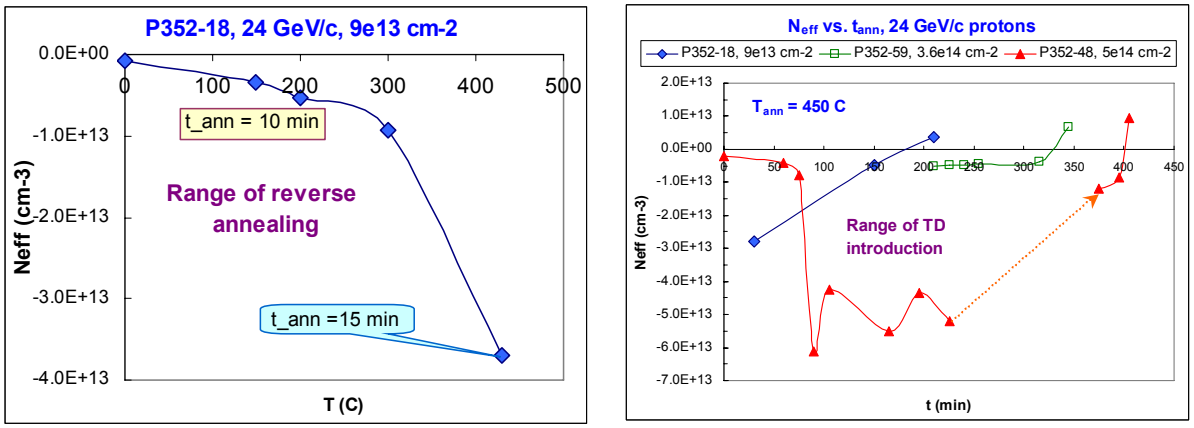

(a) **(b)**

Fig. 15. Evolution of the space charge concentration in p-type MCZ Si detectors irradiated by 24 GeV/c protons in the temperature range corresponding to reverse annealing (a), and at T = 450°C corresponding to the thermal donor introduction (b)

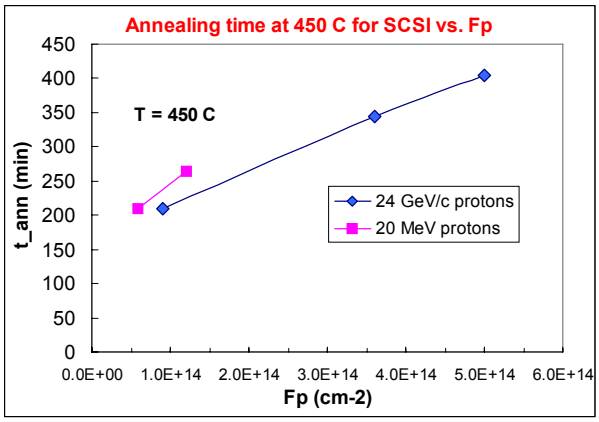

Fig. 16. Annealing time at T = 450°C required for SCSI

Conclusions

1. Over-compensation of the negative space charge in proton irradiated oxygen-rich silicon detectors and recovery of the initial positive space charge and detector reverse current are realized by ETA at 450°C.
2. The dependence of the annealing time at T = 450°C required for SCSI through thermal donor introduction on the fluence of 24 GeV/c protons is linear irrespective to the thermal pre-history before thermal donor introduction.

References for Section 4.4.

[1] Z. Li, IEEE Trans. Nucl. Sci., Vol. 42, No. 4, 224 (1995)
[2] M. Moll, Ph.D. Thesis, University of Hamburg, 1999, DESY THESIS-1999-040, ISSN-1435-80859.
[3] B. Dezillie et al, IEEE Trans. Nucl. Sci., Vol. 47, No. 6, 1892-1897 (2000)
[4] CERN-LHCC-2004-031 and LHCC-RD-005, RD50 Status Report 2004
[5] M. Bruzzi, Z. Li, J. Härkönen, E. Tuovinen, P. Luukka, D. Menichelli, "N_{eff} tuning in MCz-Si detectors by isothermal annealing", presented at 5th CERN RD50 Workshop, Florence, Oct 14-16, 2004, http://rd50.web.cern.ch/rd50/5th-workshop/
[6] Z. Li and J. Harkonen, presented at 5th CERN RD50 Workshop, Florence, Italy, October 14-16, 2004 http://rd50.web.cern.ch/rd50/5th-workshop/
[7] V. S. Vavilov, V. F. Kiselev, B. N. Mukashev, "Defects in silicon and at its surface", Moscow, Nauka, 1990 (in russian).

4.5. Defect engineering by pre-irradiation treatments

In the frame of the RD50 research project, the INFN in Padova, the Institute of Nuclear Research (KINR) in Kiev and IRST have investigated radiation hardening by preliminary neutron irradiation of silicon, which is expected to create gettering sites in the silicon bulk. Preliminary irradiation of silicon by fast neutrons and the subsequent annealing lead to the formation of sinks for primary radiation defects. These sinks are complexes of radiation-induced defects with neutral impurities, such as C and O, always present in the silicon wafers. Preliminary irradiation can increase the radiation hardness of silicon and the best effect is achieved in each particular case by optimizing the sink concentration. At the previous 9th European Symposium on Semiconductor Detectors preliminary results on the radiation hardening of pre-irradiated silicon were reported by the authors [1]. In this study we have investigated reactor fast neutron irradiation of diodes manufactured by IRST from standard float zone silicon (FZ), as a reference, and from silicon pre-irradiated by fast neutrons.

The starting materials for tested diodes are n-type float zone silicon wafers from Topsil with the following characteristics: <111>, carrier concentration $3.4 \cdot 10^{11}$ cm^{-3}, 370 μm thick and life time of minority carriers (τ) about 300 μsec. Tested devices are p^+-n silicon diodes processed by IRST on standard high purity n-Si and pre-irradiated silicon wafers. The active area of each diode is surrounded on the junction side by guard-rings. The diodes manufactured from standard n-Si are considered reference devices. The pre-irradiations [2] were performed in the nuclear research reactor of KINR by fast neutrons up to a fluence of about 10^{16} neutrons/cm^2. After preliminary irradiation the samples were thermally treated in order to anneal all electrically active radiation defects [3]. The highest temperature during the thermal treatment is 850 °C. After pre-irradiation changes in the electrical characteristics are negligibly small [2].

As an example, Fig. 1 shows that the deep acceptor introduction rate β of the FZ pre-irradiated devices is lower than for the FZ reference diode. These experimental results remark the positive effect of silicon pre-irradiation in order to limit the V_{dep} increase after SCSI when the detectors are exposed to fast neutrons: a result which, on the contrary, has not been observed so far for FZ, DOFZ [4], CZ and MCZ [5] Si.

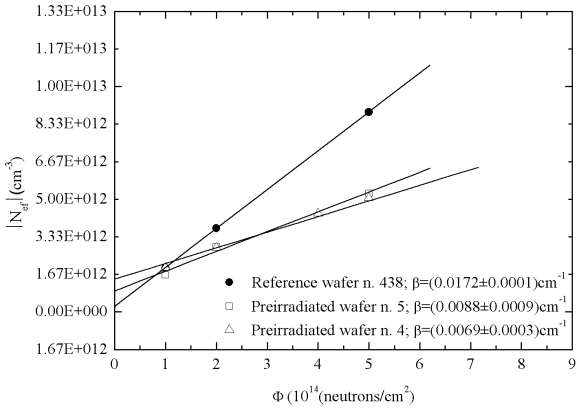

Fig. 1. Effective substrate doping concentration as a function of the 1 MeV neutron equivalent fluences for standard (reference) (close symbols) and pre-irradiated (open symbols) devices. The thin lines are linear fits of the experimental data. The introduction rates *β*, i.e. the slopes of the linear fits, are also reported.

Thermally stimulated capacitance (TSCAP) measurements were performed at the Oslo University in a temperature range of 20-300 K using an Agilent capacitance meter with probing frequencies from 1 kHz to 1 MHz.

Sample *A* – reference based on high purity n-Si and sample *B* – processed on pre-irradiated substrate were studied. Figures 2 and 3 show TSCAP spectra measured at a frequency of 60 kHz for un-irradiated samples and for samples after reactor neutron irradiation with fluences of $5 \cdot 10^{12}$ and $3 \cdot 10^{13}$ neutrons/cm^2. No significant amount of electrically active centers is observed in un-irradiated samples *A* (Fig. 2) and *B* (Fig. 3). Both show carrier freeze-out at ~20 K, which is expected for phosphorus (P) doped Si.

Irradiation with fluence of $5 \cdot 10^{12}$ neutrons/cm^2 results in the formation of a considerable amount of electrically active defects that are observed in the TSCAP spectra as step-like decreases of the capacitance with decreasing temperature. However, a substantial difference in the formation kinetics of different defects occurs for sample *A* and *B*. For the reference sample (*A*) a significant increase in capacitance at 300 K is observed, indicating an increased carrier concentration. However, as the temperature decreases, a complete carrier freeze-out caused by trapping of the carriers at deep levels

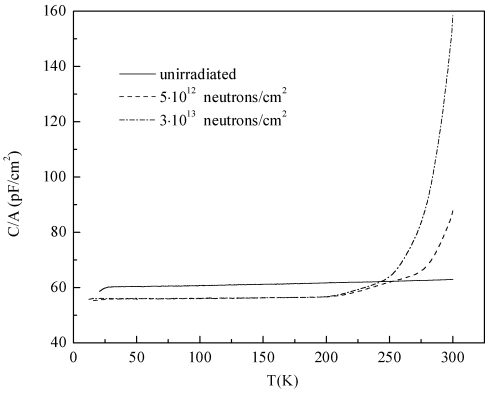

Fig2. TSCAP spectra of reference diodes measured at a frequency of 60 kHz for unirradiated samples and for samples after reactor neutron irradiation (fluences $5{\cdot}10^{12}$ and $3{\cdot}10^{13}$ neutrons/cm^2).

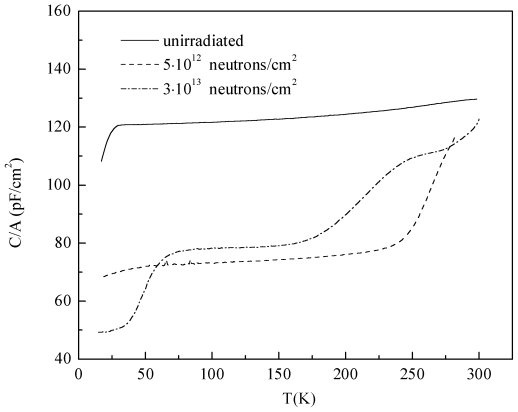

Fig3. TSCAP spectra of pre-irradiated diodes measured at a frequency of 60 kHz for un-irradiated samples and for samples after reactor neutron irradiation (fluences $5{\cdot}10^{12}$ and $3{\cdot}10^{13}$ neutrons/cm^2).

takes place at ~200 K. The TSCAP spectrum indicates the presence of at least two electron traps that become active at ~300 K and 225 K. On the contrary, no considerable change in capacitance at 300 K is observed for sample B after irradiation with a fluence of $5{\cdot}10^{12}$ neutrons/cm^2 (Fig. 3). Moreover, although a dominant electron trap at ~250 K is present in the sample, the TSCAP spectrum indicates the presence of free carriers at lower temperatures down to ~20 K, where the carrier freeze-out is observed.

After irradiation with a higher fluence, $3{\cdot}10^{13}$ neutrons/cm^2, the capacitance of sample *A* at 300 K increases further (Fig. 2). Similarly to what happens in the case of the lower fluence irradiation, two major levels are observed at ~300 K and 225 K, leading to a complete carrier freeze-out at ~200 K. For sample *B*, however, the capacitance at 300 K does not exhibit a considerable change (Fig. 3). Two levels are detected in the TSCAP spectrum which become active at ~200 K and ~50 K. It should be noted that despite the high irradiation fluence, free carriers are present in sample *B* at temperatures down to ~50 K.

The data show that the effect of radiation on the carrier concentration in sample *B* is significantly less pronounced as compared to that in the reference sample (sample *A*). This suggests an increased radiation hardness of sample *B*.

More details can be found in the full paper [6].

References for Section 4.5.

[1] P. G. Litovchenko, A. Candelori, A. P. Litovchenko, A. Kaminski, A. A. Groza, A. P. Dolgolenko, et al., Radiation hardening of silicon detectors by preliminary irradiation, 9th European Symposium on Semiconductor Detectors, Schloss Elmau, Germany, (2002), 23-27 June.

[2] P.G. Litovchenko, D. Bisello, A. Candelori, A.P. Litovchenko, A.A. Groza, et al., Radiation hardening of silicon for detectors by preliminary irradiation, Solid State Phen., vol.95-96 (2004), pp. 399-404.

[3] A. K. Semenuk, Radiation effects in polivalley semiconductors Luzk, Nastiria (2001).

[4] A. Candelori, D. Bisello, R. Rando, A. Kaminski, J. Wyss, A. Litovchenko, *et al.*, "Radiation hardness of silicon detectors for High Energy Physics applications," *IEEE Trans. Nucl. Sci.*, vol. 50, no. 4, pp. 1121-1128, August 2003.

[5] Z. Li, J. Harkonen, W. Chen, J. Kierstaed, P. Luukka, E. Tuominen, *et al.*, "Radiation hardness of high resistivity Magnetic Czochralski silicon detector after gamma, neutron and proton radiations," *IEEE Trans. Nucl. Sci.,* vol. 51, no. 5, pp. 1901-1908, August 2004.

[6] P.G. Litovchenko, A.A. Groza, V.F. Lastovetsky, L.I. Barabash, M.I. Starchik et al., Radiation hardness of silicon detectors based on pre-irradiated silicon, submitted for publication to Nucl. Instr. and Meth. A

4.6. Hydrogen in high purity FZ silicon

Introduction

It is well-known that hydrogen can easily penetrate into silicon crystals at various stages of manufacturing p-n structures [1, 2]. Therefore, most likely all silicon particle detectors contain hydrogen which remains in these structures after fabrication and there are some indications on the interaction of residual hydrogen with defects in irradiated Si detectors [3-5]. An increase of the hydrogen content might lead to an increase of the radiation tolerance of devices, may be due to hydrogen passivation of radiation defects [1, 2, 6] and acceleration of oxygen diffusion by promoting the formation of oxygen dimers O_2 [7-9].

Both, the high mobility and the reaction ability of hydrogen, result in its redistribution during subsequent technological processes occurring even at rather low temperatures of 200-400 C. Therefore, one expects that the concentration of hydrogen in various areas of detectors will depend substantially on the sequence of technological steps of the manufacturing process. Presently there is not enough information on hydrogen in fully processed detector structures. It is the aim of this work to get experimental data on the hydrogen content and distribution in p^+-n-n^+ structures made of detector grade high resistivity float zone (FZ) silicon and influence of hydrogen on the elimination of electrically-active radiation induced defects.

Experimental

Detector structures were manufactured from standard n-type Wacker Si by the following producers: 1) CiS Institute for Microsensors, Erfurt, Germany (CA-diodes); 2) ST Microelectronics, Catania, Italy (W336-diodes); 3) ELMA, Zelenograd, Russia (Z-diodes). Simple p^+-n-n^+ structures with at least one guard ring were employed. The area of the p^+ region was 5×5 mm^2. The wafer thickness of CA- and W-samples was in the range of about 285 μm and 290 μm. The thickness of Z samples was 330 μm. Initial material resistivity for CA- and Z-samples was 4 kΩ·cm and 2 kΩ·cm for W-samples. Irradiation with electrons (E_e=3.5 MeV or 6 MeV) was performed using the accelerators at the Institute of Solid State and Semiconductor Physics (Minsk). The irradiated samples were subjected to 30 min isochronal annealing in the temperature range of 50-350 °C with temperature increments of 50 °C.

Table 1. Parameters of dominant traps formed in silicon detector structures after electron irradiation and annealing at different temperatures

Peak Label	T_{max}, K [c]	A[a], $s^{-1}K^{-2}$	σ_A[b] cm^2	E_A[a], eV	Peak origin
E1	94	$3.9\ 10^7$	$6\ 10^{-15}$	0.174	VO+CiCs
E2	133	$1.9\ 10^7$	$3.1\ 10^{-15}$	0.246	$VV^=$
E3	~192	$\sim1.3\ 10^7$	$\sim2\ 10^{-15}$	~0.358	Stable up to100-150 °C
E4a	230	$7.5\ 10^6$	$1.1\ 10^{-15}$	0.423	VV^-
E5	174	$9.6\ 10^6$	$1.5\ 10^{-15}$	0.314	VOH
E6	111	$1.9\ 10^5$	$2.9\ 10^{-17}$	0.163	Formed during annealing at T≥300 °C, possibly observed in [14,18]
E7	146	$\sim8.2\ 10^5$	$\sim1.2\ 10^{-16}$	~0.238	—
E8	198	$5.9\ 10^6$	$0.9\ 10^{-15}$	0.356	Formed during annealing at T≥300 °C, observed in [10,18-20]
E9	186	$\sim9.1\ 10^4$	$\sim1.4\ 10^{-17}$	~0.269	—
E10	276	$\sim3.8\ 10^5$	$\sim6.1\ 10^{-17}$	~0.51	—

[a] Parameters A and E_A determine the electron emission rate for traps as: $e_n(T)=AT^2\exp(E_A/kT)$.

[b] The apparent capture cross section σ_A is related to the pre-exponential factor A as: $\sigma_A=A/(v_{th}(300)N_c(300)\cdot9\cdot10^4)$, where $v_{th}(300)$ is the thermal velocity and $N_c(300)$·is the effective density of states in conduction band at T=300 K

[c] For $e_w=190\ s^{-1}$

Traps formed during irradiation and annealing at high temperatures

Our interpretation of defect reactions with impurities is based on the identification of traps observed by DLTS. The trap parameters and the conditions of the appearance of the traps have been taken into account. The parameters of all traps observed after irradiation and annealing are presented in Table 1.

Some of the observed traps are well known and their origins have been investigated in great detail while others have been observed frequently but not identified yet.

Immediately after irradiations 4 peaks (E1 to E4) were observed in the DLTS spectra (Fig. 1). These peaks are caused by the formation of 6 traps.

The E1 peak is due to electron emission by vacancy-oxygen (VO) and interstitial carbon – substitutional carbon (C_iC_s) complexes. The increase in the amplitude of E1 peak after annealing at 150 °C is caused by additional formation of C_iC_s complexes.

The E2 peak is due to electron emission from the second acceptor level of the divacancy $V_2^{(=/-)}$ with a level at about E_c-0.23 eV (activation energy of electron emission is the sum of ionization enthalpy $\Delta H \approx 0.230$ eV and electron capture barrier $E_\sigma \approx 0.017$ eV [10]). Electron emission from the lower acceptor level of the divacancy ($E_t(V^{(-/0)}) \approx E_c$-0.42 eV) results in the appearance of the peak E4 to which another trap is contributing as well. We shall label them as E4a and E4b, accordingly. The trap E4b is less stable and completely disappears after annealing at 150 °C. The E3 trap has a similar thermal stability. The nature of these traps (E3 and E4b) is unclear yet.

Another trap, labeled as E5, with a peak near T=174 K appears immediately after irradiation only in Z-structures. It is unambiguously established [6, 11-16] that atomic hydrogen is a constituent of this trap. Moreover it is generally accepted that the E5 trap is the vacancy-oxygen-hydrogen complex (VOH). This complex has an acceptor level $E_t(VOH^{(-/0)}) \approx E_c$-0.32 eV and a donor level $E_t(VOH^{(0/+)}) \approx E_v$+0.27 eV [5,11,17]. Thus, the E5 peak can be used as an indicator of the availability of hydrogen in the irradiated structures.

The formation of VOH complexes is observed in the other structures only after annealing at high temperatures. Thus, the VOH complex is generated in W336 and CA structures after the heat

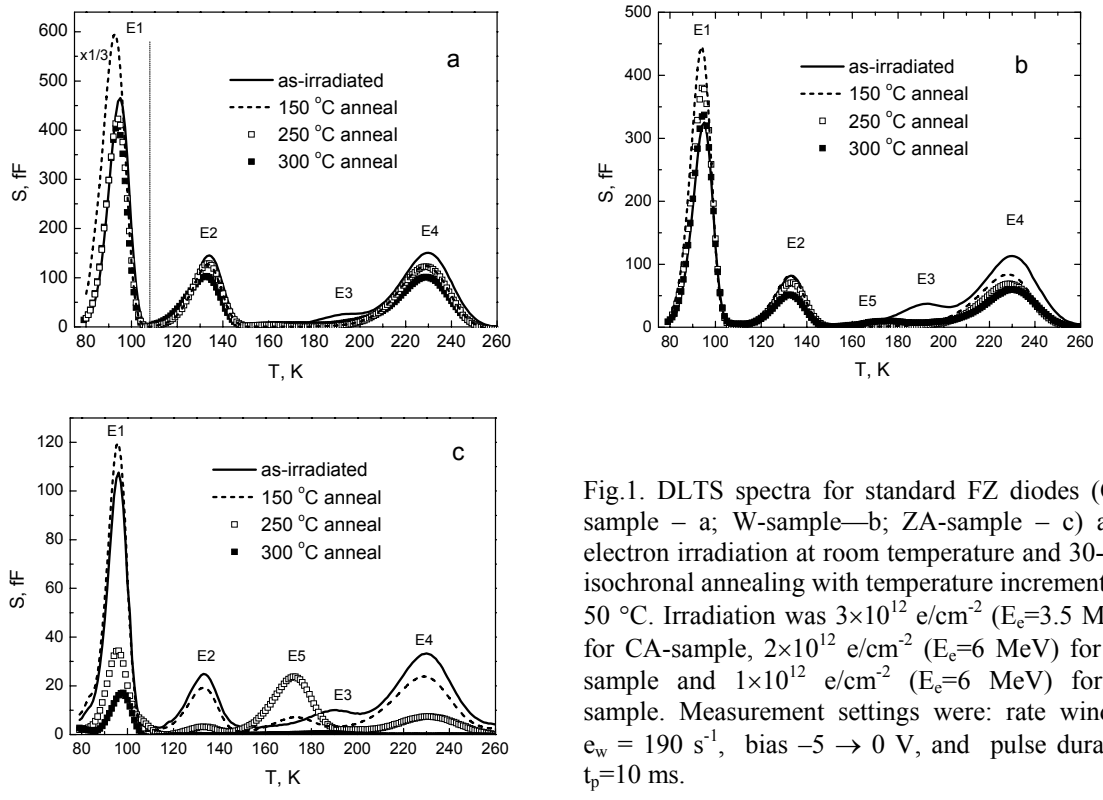

Fig.1. DLTS spectra for standard FZ diodes (CA-sample – a; W-sample—b; ZA-sample – c) after electron irradiation at room temperature and 30-min isochronal annealing with temperature increments of 50 °C. Irradiation was 3×10^{12} e/cm^{-2} (E_e=3.5 MeV) for CA-sample, 2×10^{12} e/cm^{-2} (E_e=6 MeV) for W-sample and 1×10^{12} e/cm^{-2} (E_e=6 MeV) for Z-sample. Measurement settings were: rate window e_w = 190 s^{-1}, bias –5 → 0 V, and pulse duration t_p=10 ms.

treatment at 300 °C (Fig.1b) and 350 °C (Fig.2, solid line), respectively. It is necessary to note, that

the annealing at 350 °C has led to the most essential changes of the DLTS-spectra in all types of diodes. The two divacancy peaks (E2 and E4a) have disappeared in all investigated diodes. The amplitude of peak E1 has essentially decreased in CA-and W336-diodes and new peaks, E6-E8, have appeared. While the E1 peak is totally vanished in Z-diodes.

From the dependence of the peak amplitudes on filling pulse duration (Fig.3) it follows that the E6, E7, E8 and E10 traps have rather low capture cross sections.

DLTS-peaks which may be similar to the E6 peak were observed earlier in [14,18]. However, as follows from Fig. 3, two traps are contributing to this peak, which are labeled E6a and E6b. From the available data it is difficult to identify which of the E6-centers was observed in the earlier publications. As follows from our data, E6a may be formed from the VO complex.

After annealing at T≥300 °C more often was previously observed in DLTS-spectra a trap with an activation energy of E_A ≈0.36 eV (E8, according to our designations) [6,10,18-20]. However, it seems that not always these traps are related to the same defect. In [19] a trap with ionization energy E_A ≈0.36 eV was identified as an iron related complex. However, the E8 trap detected here has an electron capture cross-section about five times smaller than the trap reported in [19] indicating that it is not the same type of iron related defect. In addition, the iron contamination of all our samples is very unlikely. The electron emission rate of the E8 trap is practically the same with the one reported in [10] for a defect with the same activation energy (0.36eV). However, there is not enough information to speculate on the origin of this center. Similar is the case for the traps E7, E9 and E10, for which there are not enough data, neither in the literature nor in the present study to allow an identification of these centers.

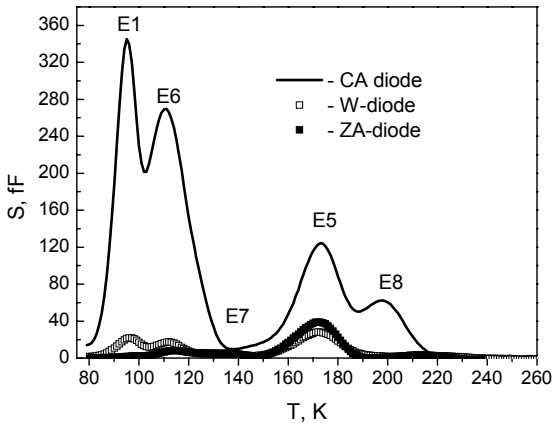

Fig. 2. DLTS spectra for different diodes made of standard FZ silicon after isochronal annealing at temperature 350 °C during 30 min. Measurement settings were: e_w = 190 s^{-1}, bias –5 → 0 V, and pulse duration (t_p) – 10 ms.

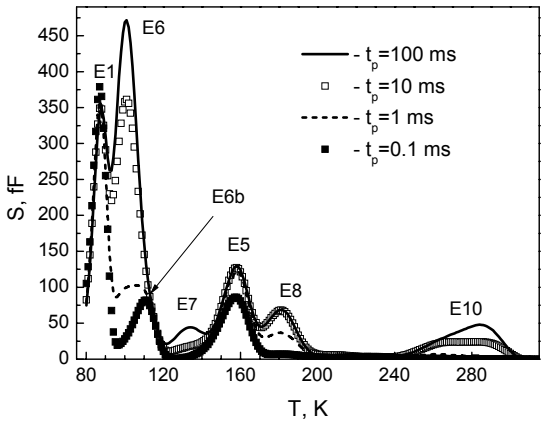

Fig.3. DLTS spectra for standard FZ diode (CA-sample) after isochronal annealing at temperature 350 °C. Measurement settings were e_w = 19 s^{-1}, bias –5 → 0 V, and pulse duration (tp): 100 ms , 10 ms, 1 ms, 0.1 ms.

Influence of p^+ and n^+ regions on the annealing of radiation induced defects

A different behavior of the divacancy elimination in the three types of diodes is observed (Fig. 4). In Z-diodes the annealing of the divacancy begins at rather low temperatures and proceeds gradually in a wide temperature interval. For W336-and CA-structures typically a sharp decrease of the divacancy concentration is observed at T_{ann}=300 °C and T_{ann}=350 °C, respectively.

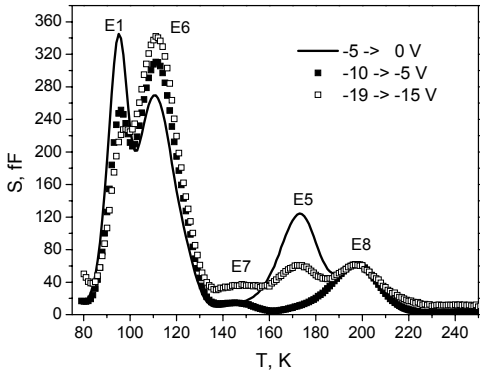

Fig.5. DLTS spectra for standard FZ diode (CA-sample) after irradiation with 3.5 MeV electrons at room temperature and upon 30-min annealing at 350 °C. Dose of irradiation was 3×10^{12} cm^{-2}. Measurement settings were: rate window of 190 s^{-1}, pulse duration of 10 ms, bias: a) -5 → 0 V, b) −10→ −5 V and c) −19→ −15 V. The peak amplitudes are normalized assuming constant concentration of E8 trap (see text).

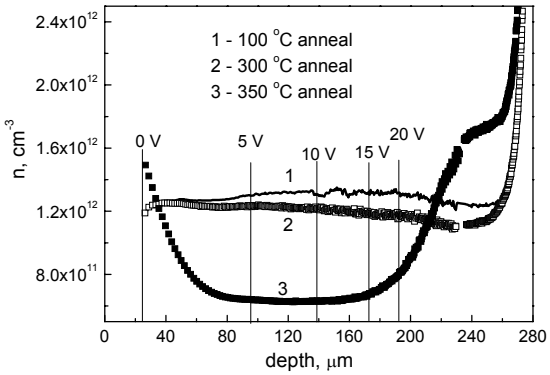

Fig.6. Carrier depth profile for a CA sample determined from C-V characteristics. Vertical lines mark inverse voltage which is necessary to obtain corresponded width of depletion region at room temperature for the 3rd curve.

A possible explanation for the disappearance of the divacancy in W336-and CA-samples is its interaction with impurities diffusing from near surface regions of the structures under study. To check this hypothesis we performed a uniformity test for the depth distribution of the deep centers in the bulk of the diodes. It turned out, that practically all defects are distributed non-uniformly (Fig. 5). The strongest non-uniformity is observed for the VOH complex (trap E5). At small reverse bias voltages its concentration is comparable with the concentration of other traps; increasing the voltage leads first to the disappearance of the center and then to its reappearance. For comparing the spectra corresponding to various depths, we assumed that the concentration of the E8 trap remains constant over large distances from the p^+-contact. This assumption is supported by the experimental data presented in Ref. [20]. Thus, the spectra presented in Fig. 5 are normalized to the heights of the E8 peak.

The C-V measurements, presented in Fig.6, reveal that in the base of the detector structures annealed at 350 °C there is a non-uniform depth distribution of charge carriers *n(x)* too. Thus, in the middle region, from ~80 up to ~170 microns, a strong decrease of the carrier concentration as compared to the one after T_{ann}=300 °C, is observed. This fact can be explained by the formation of deep acceptors in this middle region. On the other hand, the rising dependence of *n(x)* in the near surface regions can be related to the formation of thermal donors. These risings are also correlated with the VOH distribution which can be deduced from Fig.5. After annealing at 350 °C the VOH complex is generated in the same regions where thermal donors have been formed. The DLTS-measurements presented here reveal that these donors do not have energy levels with E_A=0,14÷0,15 eV and thus they are not related to oxygen thermal donors. In addition, considering that their formation depth corresponds to diffusion of hydrogen (monitored via the VOH complex) it is possible to draw the conclusion that the observed thermal donors are formed due to hydrogen.

Hence, the differences observed in CA-, W336-and Z-structures regarding the annealing of the radiation induced defects, as well as the formation of other defects during the high temperature treatments, may be connected with the absence of hydrogen in the bulk of the first two types of diodes and with presence of hydrogen in the bulk of the last type of diodes. In CA-and W336-structures hydrogen is present in significant concentrations only in near the surface regions or at the Si-SiO_2 boundary.

References for Section 4.6

[1] S.J. Pearton, J.W. Corbett, T.S. Shi, Appl. Phys., A43 (1987) 153
[2] S.J. Pearton, J.W. Corbett, and M. Stavola, Hydrogen in Crystalline Semiconductors, Springer-Verlag, Berlin, 1992
[3] M. Bruzzi, Nucl. Instr. and Meth. A 352 (1995) 618
[4] C. Da Via and S. J. Watts, Nucl. Instr. and Meth. B 186 (2002) 111
[5] L. F. Makarenko, F. P. Korshunov, S. B. Lastovski., N. I. Zamyatin, Semiconductors. 37 (2003) 611 (Translated from Fizika i Tekhnika Poluprovodnikov, Vol. 37, No. 5, 2003, pp. 629–)33)
[6] O.V. Feklisova, N. Yarykin. Semicond. Sci. Techn., 12 (1997) 742
[7] R. C. Newman, J. H. Tucker, A. R. Brown, and S. A. McQuaid. J. Appl. Phys. 70 (1991) 3061
[8] V. P. Markevich, L. I. Murin, J. L. Lindström and M. Suezawa. Semiconductors 34 (2000) 998
[9] R C Newman J. Phys.: Condens. Matter 12 (2000) R335
[10] S.D. Brotherton, P.J. Bradley,. J. Appl. Phys., **53** (1982) 5720
[11] K. Irmscher,H. Klose,KJ.Maas, J. Phys.C, **17** (1984) 6317
[12] Y. Tokuda and T. Seki, Semicond. Sci. Technol., **15** (2000) 126
[13] K. Bonde Nielsen et al., Physica B, **273-274** (1999) 167
[14] M.W. Hüppi, J. Appl. Phys. 68 (1990) 2072-2707
[15] A. Hallen, N. Keskitalo, F. Masszi, V. Nagl. J. Appl. Phys. **79** (1996) 3906
[16] R. Peaker, J. H. Evans-Freeman, L. Rubaldo, I. D. Hawkins, K. Vernon-Parry, and L.Dobaczewski, Physica B **273–274** (1999) 243
[17] O.V. Feklisova, N. Yarykin., T.B. Yakimov, J. Weber. Physica B **308–310** (2001) 210
[18] O.O. Awadwlkarim, H.Weman, B.G. Svensson, J.L. Lindström, J. Appl. Phys. 60 (1986) 1074.
[19] Z.-P. You, M. Gong, J.-Y. Chen, J.W. Corbett, J. Appl. Phys., **63** (1988) 324.
[20] B.G. Svensson, K.-H. Rydén, B.M.S. Lewerentz, J. Appl. Phys. 66, (1989) 1699.

5. Pad Detector Characterization

The research of the PDC group in 2005 has been focused to the two most promising material candidates for the SLHC tracker, MCz and epitaxial silicon detectors. The properties of p^+-n type detectors from both were studied and for MCz also the use of n^+-p detector structures. Fabrication of MCz detectors with variable N_{eff} through processing of both n and p types was developed and first devices were already produced. Effect of detector processing on its macroscopic properties was also investigated in the framework of a Technotest subproject.

5.1. RD50 PDC subproject "Technotest"

This sub-project, headed by Vladimir Eremin (Ioffe Physico-Technical Institute), is carried out as collaborative work of several institutions: Ioffe Physico-Technical Institute (PTI), Research Institute of Material Science and Technology (RIMST), Brookhaven National Laboratory (BNL), Helsinki Institute of Physics (HIP), Josef Stefan Institute, Glasgow University and ITEP (Moscow). The work in 2005 was mostly performed by PTI, BNL and HIP.

The main objective of the subproject is to investigate the influence of the detector processing, performed at different processing facilities, on the radiation tolerance of detectors. The influence of the processing might depend on the type of the used high resistivity Si material as well as on the type of irradiation. The difference between neutron irradiated detectors processed from different types of Si was studied in 2004 and the results are described in [1]. The goal for 2005 was investigation of the influence of technology on characteristics of detectors manufactured from n-type CZ Si irradiated by 24 GeV/c protons.

Experimental

The wafers of MCZ silicon manufactured by Okmetic Oij were distributed between PTI, BNL and HIP and then the test pad detectors were processed. The photo masks and technology procedures were used as they are developed in each institution (see Table 1.). A more detailed description of difference in processing can be found in [1]. Heat treatment applied in detector processing did not include any special thermal-donor (TID) introduction. The concentration of TID is therefore for all three processes much lower than that of initial donors.

	BNL	**HIP**	**PTI**
Oxidation	1100ºC/6 h	done after implantation	1100ºC/6 h
p^+ - Implant	45 keV/$2\cdot10^{14}$ cm^{-2}	20 keV/$1\cdot10^{15}$ cm^{-2}	50 keV/$3\cdot10^{14}$ cm^{-2}
n^+ - Implant	80 keV/$6\cdot10^{14}$ cm^{-2}	70 keV/$1\cdot10^{15}$ cm^{-2}	80 keV/$9\cdot10^{14}$ cm^{-2}
annealing	700ºC/30 min	1100ºC/4 h	700ºC/40 min
Al sintering	430ºC/5 min (low concentr. Of TD)	370ºC/40 min (no TD)	430ºC/7 min

Table 2: Processing properties for detectors used in TECHNOTEST.

Pad p^+-n-n^+ detectors were irradiated by 24 GeV/c protons at CERN PS to the fluences Φ_p of $1\cdot10^{14}$ cm^{-2} and $1\cdot10^{15}$ cm^{-2}. Beneficial annealing was carried out by keeping detectors at 80°C for 4 minutes. Then, detectors were investigated at PTI using TCT. The main objectives of these measurements were:

- estimation of possible influence of technology on V_{fd} after irradiation
- effects of long term annealing on differences in V_{fd} between different detectors
- investigation of electric field distribution using the approach for electric field reconstruction developed for heavily irradiated detectors with double peak (DP) current pulse response shape [2, 3].

In TCT measurements the laser with a wavelength of 870 nm was used for non-equilibrium carrier generation. All measurements were done with a laser illuminating the p^+ side of the detector. The current pulse shapes were recorded by LeCroy oscilloscope with time resolution of 0.9 ns. The measurements were performed at 24°C in the range from 0 to 500 V. The total accumulated annealing time of 1075 min at 80°C was reached in seven steps. After each annealing step the samples were kept at 24°C during 24 hours for stabilization of characteristics.

To define V_{fd}, the charge Q collected during 35 ns dependence on bias voltage was plotted and according to the procedure described in [4], the inclination point at which the Q dependence on V shows a tendency to saturation was treated as V_{fd}. This value was compared with the bias voltage at which the induced current exhibits a distinctive decrease (abrupt drop) in the tail, which is an evidence of full depletion. All points in the plots presented in the report satisfied to both criteria of full depletion.

Detectors irradiated to proton fluence of $1 \cdot 10^{14}$ cm^{-2}

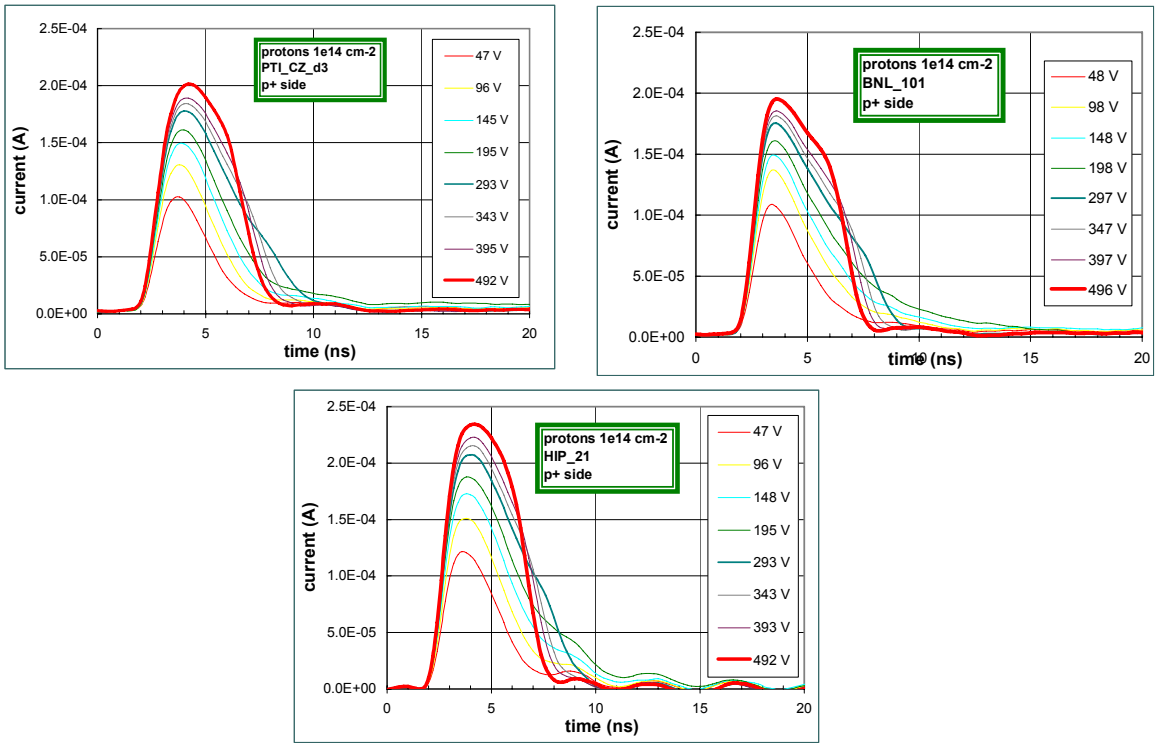

Figure 1: Current pulse responses of n-type CZ Si detectors irradiated by 24 GeV/c protons with a fluence of $1 \cdot 10^{14}$ cm^{-2} before long term annealing.

The current pulse responses from the p^+ side (electron collection) of detectors processed by PTI, BNL and HIP and irradiated by Φ_p of $1 \cdot 10^{14}$ cm^{-2} are shown in Fig. 1. All curves and their changes with increasing bias are similar and confirm the positive space charge. The collected charge Q was calculated as current integral in given time window. Dependence of Q on V for different integration times is shown in Fig. 2. The minimal integration time of 10 ns corresponds approximately to the shaping time of electronics at SLHC.

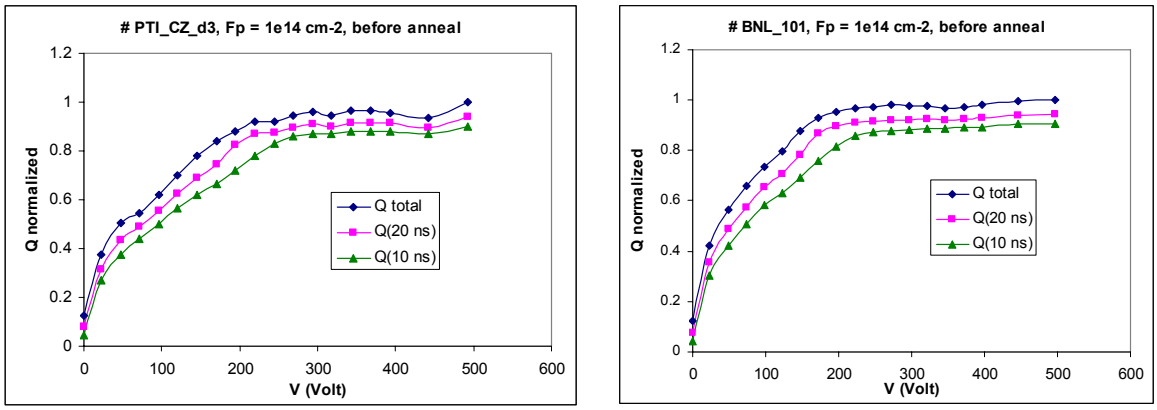

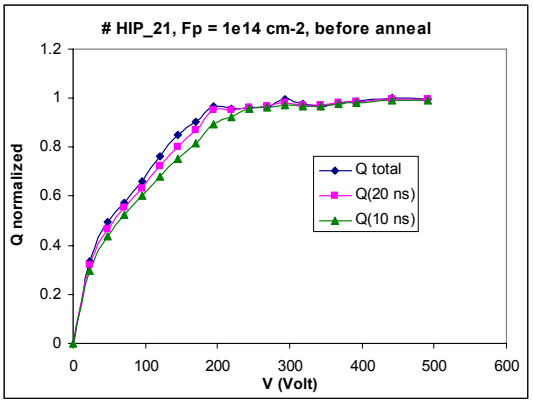

Figure 2: Collected charge vs. bias voltage for the same detectors as in Fig. 1 obtained by integrating the current pulse response over 35 ns (total), 20 ns and 10 ns.

For detector comparison the values of the collected charges in all curves of any individual detector were normalized to its maximal total collected charge. It can be seen that only insignificant reduction (within 10%) of the collected charge at collection time of 10 ns occurs in detectors of PTI and BNL while the charge collected in HIP detector is independent on the integration time of electronics.

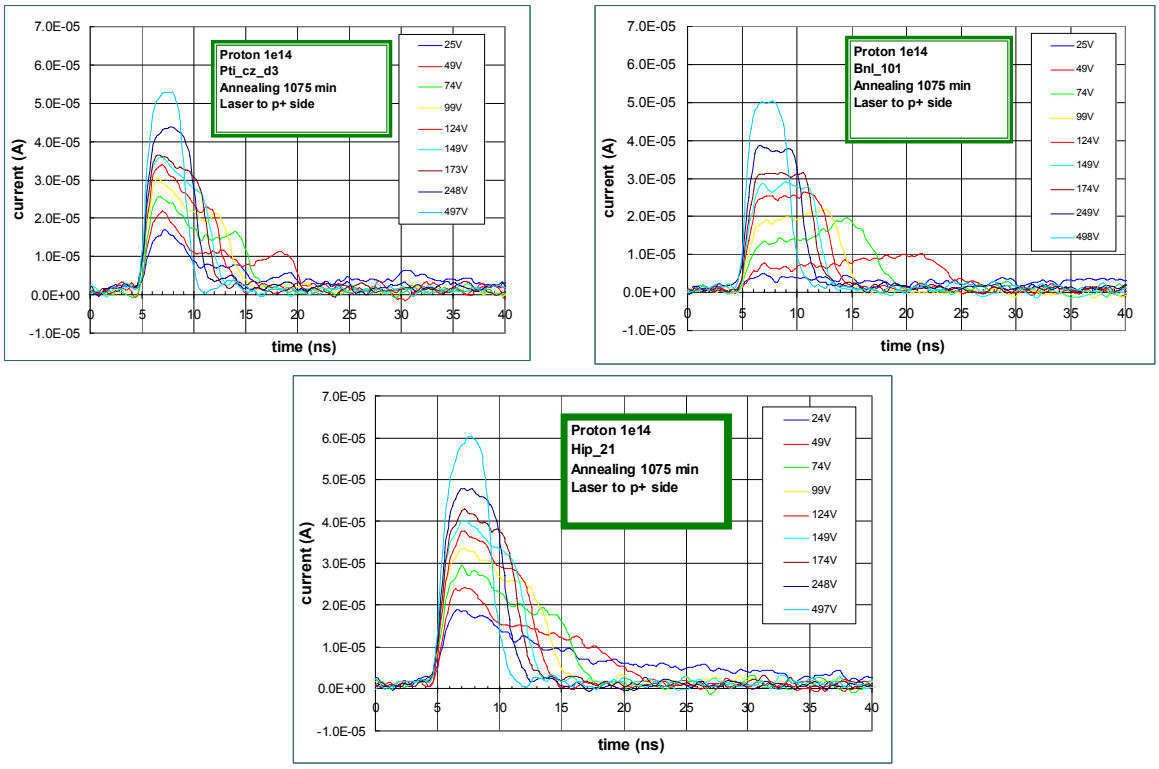

Figure 3: Current pulse responses of the same detectors as in Fig. 1, after final annealing at 80°C, accumulated time is 1075 min

Full depletion voltage (as defined above) of around 200 V is practically the same for the three detectors. The same measurements were made at each annealing step. The difference between the pulse shapes of different samples becomes detectable at the second step of the annealing (total t_{ann} of 35 min) and very evident after final annealing step (accumulated time of 1075 min) as shown in Fig. 3. The difference in responses for PTI and HIP detectors is well observed however it is small enough. The response of PTI detector has a "double peak" shape at lower V that is the evidence of a non-uniform distribution of the space charge density in the detector bulk. The concentration of effective donors is higher at the p^+-contact and of effective acceptors is higher at the n^+ contact. The detector processed at HIP facility has a uniformly distributed positive space charge. Different to this, the pulses of detector BNL have slightly ascending slope of the pulse at lower V and practically flat top at higher V that shows that the space charge concentration N_{eff} is negative and detector is just beyond SCSI.

Using the values of full depletion voltage at different annealing steps, the curves of V_{fd} vs. elapsed annealing time t_{ann} were plotted for three detectors (Fig. 4). The curves started at the same depletion voltage of 200 V for all detectors that shows that the influence of technology on the initial defect formation is small.

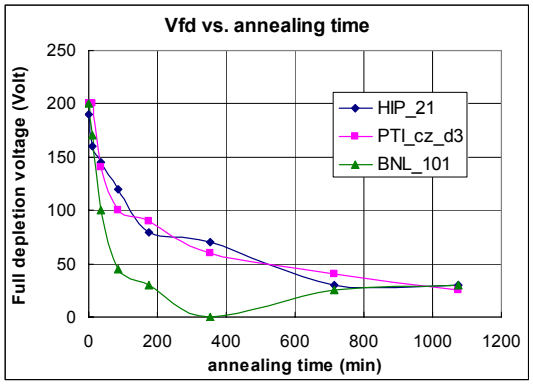

Figure 4: V_{fd} vs. annealing time in n-type CZ Si detectors irradiated by 24 GeV/c protons with a fluence of $1 \cdot 10^{14}$ cm^{-2}.

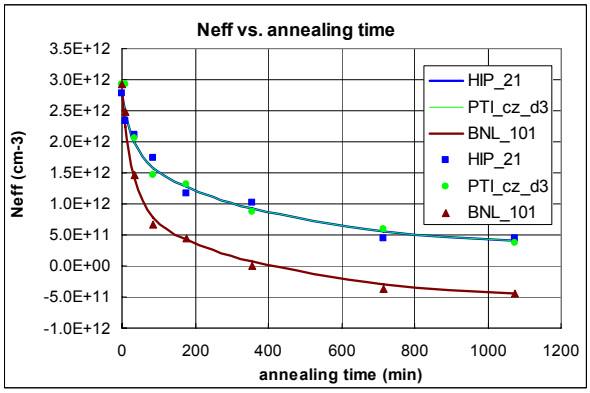

Figure 5: Dependences of space charge concentration on annealing time in n-type CZ Si detectors irradiated by 24 GeV/c protons with a fluence of $1 \cdot 10^{14}$ cm^{-2}: symbols – experiment, lines – fit according to Eq. (1)

The corresponding N_{eff} is of about $3 \cdot 10^{12}$ cm^{-3} (see Fig. 5). During annealing the V_{fd} decreases, which can be explained by effective creation of acceptors (reverse annealing) compensating the positive space charge. The reduction of full depletion voltage is larger for detector processed at BNL than for those processed by PTI and HIP. The BNL detector undergoes SCSI from positive space charge to negative after around 350 min at 80°C.

The long term annealing curves of N_{eff} vs. t_{ann} were fitted with the double exponential model, where $Neff_0$ is the effective dopant concentration after irradiation and g_1, g_2 are the introduction rates of effective acceptors.

$$N_{eff} = N_{eff\,0} - g_1\Phi\left[1-\exp\left(-t/\tau_1\right)\right] - g_2\Phi\left[1-\exp\left(-t/\tau_2\right)\right] \qquad (1)$$

This description considers fast and slow processes that control the reverse annealing. Fitting the model to the data shown in Fig. 5 yields the values of parameters as listed in Table 1. It can be concluded that the only difference between three detectors is in the introduction rate of effective acceptors (g_1) responsible for the fast component of reverse annealing. It is about twice as large for BNL detector when compared to PTI and HIP ones. It seems that only the short term component is affected by the fabrication process.

Detector #	HIP_21	PTI_cz_d3	BNL_101
N_{eff0} (cm^{-3})	$2.8 \cdot 10^{12}$	$2.8 \cdot 10^{12}$	$2.8 \cdot 10^{12}$
g_1 (cm^{-1})	0.01	0.01	0.0185
τ_1 (min)	30	30	30
g_2 (cm^{-1})	0.015	0.015	0.015
τ_2 (min)	400	400	400

Table 3: Parameters of N_{eff} annealing for detectors from n-type CZ Si irradiated by 24 GeV/c protons at Φ_p of $1 \cdot 10^{14}$ cm^{-2}.

Detectors irradiated to proton fluence of $1 \cdot 10^{15}$ cm^{-2}

The current pulse responses after the p^+ side illumination of detectors processed by PTI, BNL and HIP and irradiated with Φ_p of $1 \cdot 10^{15}$ cm^{-2} are shown in Fig. 6. The "double peak" shape is evident in the full range of applied bias voltages up to 400 V, a limit set by large reverse current. There is only small difference between the pulse shapes (ratio of both peaks) of PTI and BNL detectors and somewhat larger difference between them and BNL detector. It is clear that the electric field distributions are different.

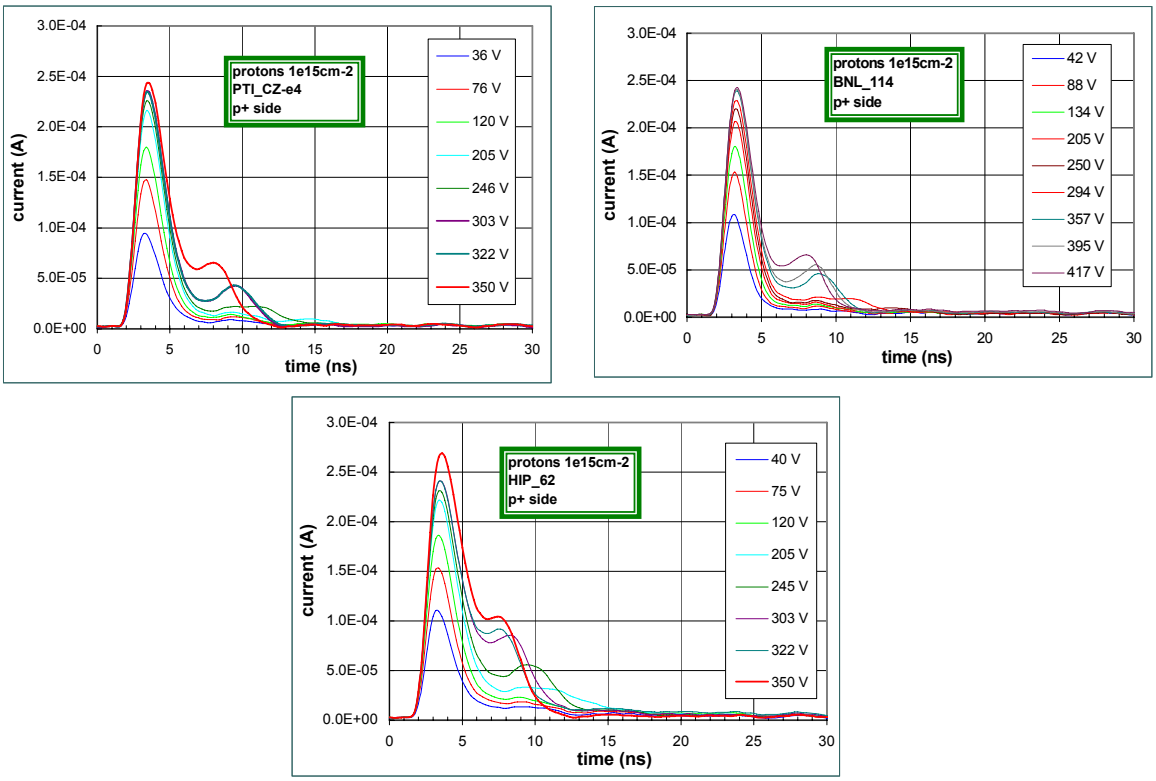

Figure 6: Current pulse responses of n-type CZ Si detectors irradiated by 24 GeV/c protons with a fluence of $1 \cdot 10^{15}$ cm^{-2} before annealing.

The dependences of the collected charge on bias voltage at different shaping (collection) time do not show saturation, differently from detectors irradiated by a fluence of $1 \cdot 10^{14}$ cm^{-2}. This can be explained by significantly shorter trapping times for higher irradiation fluence and hence larger reduction of the collected charge (see Fig. 7.).

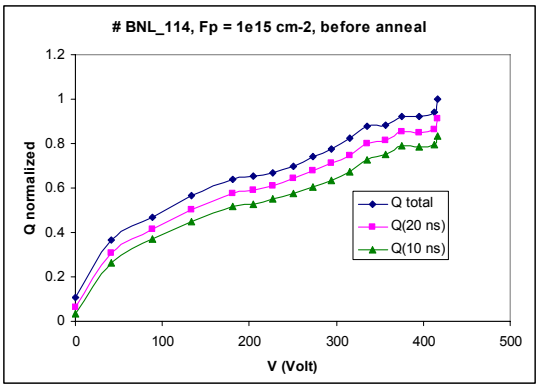

Figure 7: Collected charge vs. bias voltage dependences for detector BNL_114 irradiated by a fluence of $1 \cdot 10^{15}$ cm^{-2} obtained by integrating the current pulse response over the total time range and in the intervals of 20 ns and 10 ns.

The influence of technological procedure becomes more pronounced with detector annealing. Fig. 8 presents the current pulse response shapes after final annealing in the range of bias voltages up to 450 V. The DP shape is evidently dominating for all

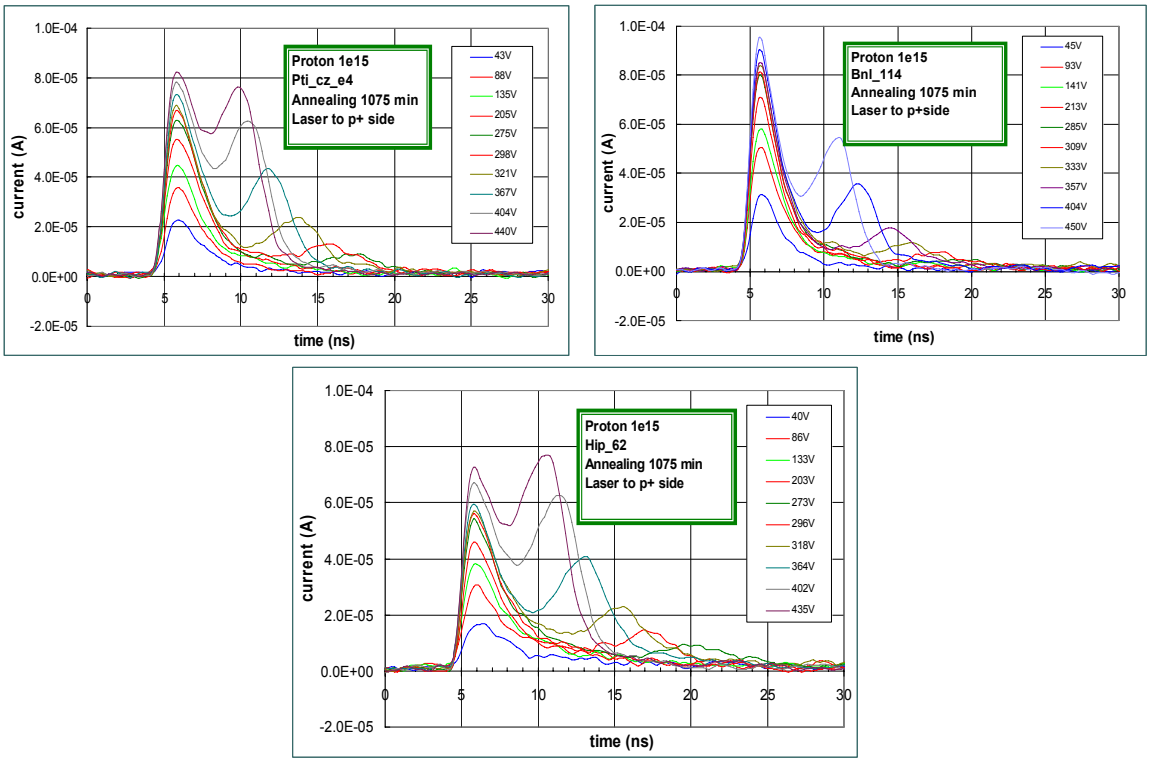

Figure 8: Current pulse responses of the same detectors as in Fig. 6, after final annealing at 80°C, accumulated time is 1075 min.

detectors. Similar behavior is observed for detectors of PTI and HIP. With increasing bias voltage the height of the second peak increases and the heights of the peaks become close at V of about 400-450 V. Meanwhile, in detector of BNL the first peak dominates at any bias voltage.

These peculiarities in the response shape give indication on the different electric field distribution that is affected by technological procedure. Since the first peak in the induced current arises from the charge collected near the p^+ contact, implies that an essential fraction of the detector bulk has positive space charge [3]. The DP shape is the evidence that the electric field and N_{eff} distributions are non-uniform and have maxima at both detector contacts [2, 3]. In the investigated detectors irradiated by a fluence of $1 \cdot 10^{15}$ cm^{-2} evolution of the second peak starts at the bias voltage of about 200 V and 250 V before and after final annealing, respectively. The appearance of the second peak in the signal is the evidence that at these voltages the electric field is distributed over the whole detector bulk, though its distribution is vastly non-uniform. The increase of the second peak that is especially pronounced in the detectors after annealing indicates the increase of the negative space charge concentration with the annealing time. However, the quantitative interpretation and/or parameterization of the annealing effect in detectors with severe radiation damage need special data treatment and development of a new approach for the estimation of detector properties. Therefore, the complete interpretation of the responses needs reconstruction of the electric field and N_{eff} distributions. This study will be included in the future plans of the sub-project.

Conclusion of the TECHNOTEST sub-project

1. Experimental results show the influence of technology on radiation hardness of detectors from n-type CZ silicon irradiated by 24 GeV/c protons up to a fluence of $1 \cdot 10^{15}$ cm^{-2}.
2. The shapes of the induced current pulses of the investigated detectors show that the fluence corresponding to SCSI is significantly larger ($\geq 1 \cdot 10^{14}$ cm^{-2}) in detectors from n-type CZ Si as compared to that for FZ and DOFZ Si.
3. At fluence of $1 \cdot 10^{15}$ cm^{-2} the electric field is distributed over the total bulk of CZ detectors starting from the bias voltage of about 200 V that is advantageous for fast and effective charge collection.
4. The DP current pulse shape is very pronounced in detectors irradiated up to $1 \cdot 10^{15}$ cm^{-2}.
5. The task for the future investigations arisen in the sub-project is to give the answer how the observed peculiarities are linked to the technology plans and how to optimize the plans to reach higher radiation hardness.

References

[1] CERN-LHCC-2004-031 and LHCC-RD-005, RD50 Status Report 2004
[2] V. Eremin, E. Verbitskaya, Z. Li. "The Origin of Double Peak Electric Field Distribution in Heavily Irradiated Silicon Detectors", NIM A 476 (2002) 556.
[3] E. Verbitskaya et al., "Operation of heavily irradiated silicon detectors in non-depletion mode", pres. at 5 RESMDD, Florence, Oct 10-13, 2004 (NIM, in press).
[4] V.Eremin, N.Strokan, E.Verbitskaya, Z.Li, "The development of transient current and charge techniques for the measurement of effective impurity concentration in the space charge region of p-n junction detectors". Nucl. Instr.& Meth. A 373 (1996) pp. 388-398.

5.2. Thermal donor generation in Czochralski silicon particle detectors

High resistivity Cz-Si detectors have been fabricated and tested as part of various irradiation campaigns within the framework of CERN RD50 collaboration [1,2,3]. The fabricated n-on-p and p-on-n Cz-Si devices require both about 300 V reverse bias for full depletion. Heat treatment of Cz-Si wafers between 400 – 600^{0}C leads to the aggregation of interstitial oxygen atoms resulting in electrically active shallow levels in the silicon's band gap. This process is known as the "Thermal Donor" (TD) formation and it depends on the temperature, the oxygen concentration in the silicon material and the presence of hydrogen in device manufacturing process [4,5,6]. An interesting feature of Cz-Si is the formation of thermal donors (TD) at certain temperatures. When the TDs are generated in boron doped Cz-Si, the p-type bulk will be compensated and if necessary, eventually turned to n-type. With this method, it is possible to fabricate, without increasing the process complexity, high oxygen concentration p-on-n or n-on-p detectors that can be depleted with voltages less than 100V [7,8].

Samples

All samples used in this study have been processed on p-type magnetic Czochralski silicon wafers (MCz-Si). The starting material of the detectors was 4" double-side-polished 300±2 μm-thick <100> Cz-Si wafers. The nominal resistivity, measured by the four point probe method, of the boron-doped wafers is 1800 Ωcm, which corresponds to a boron concentration of $4.38 \cdot 10^{12}$ cm^{-3}. The oxygen concentration of these wafers was measured by the Fourier Transformation Infrared (FTIR) spectroscopy. The measurements were done on a thick reference wafer at the Institute of Electronic Materials Technology (ITME), Warszawa, Poland. Four measurements showed following oxygen concentrations; $4.95 \cdot 10^{17}$ cm^{-3} (center), $4.89 \cdot 10^{17}$ cm^{-3} (right), $4.93 \cdot 10^{17}$ cm^{-3} (left) and $4.93 \cdot 10^{17}$ cm^{-3} (bottom).

Two types of pad detectors were processed at the Microelectronics Center of Helsinki University of Technology. The active pad implanted area of the diodes is 5 mm×5mm. It is surrounded by one wide guard ring (100 μm) and 16 small guard-rings (each 16 μm wide). The distance between the active area implant and the first guard ring is 10 μm. A 1 mm diameter round opening in the front metallization was left for TCT (Transient Current Technique) measurements.

The first set of samples were p^+-p^--n^+ pin-diode structures, i.e. the pad has been implanted by the boron and backplane by the phosphorous. The second set of samples was n^+-p^--p^+ structures processed with a different mask set. An additional mask level and boron ion implantation was required because of the electron accumulation at the SiO_2/Si surface. The surface inversion was terminated by boron implanted guard rings. One 100 μm wide and eight 16 μm wide guard rings between the n^+ rings. No boron field implantation (often referred as p-spray) was done for these samples. All samples were passivated by approximately 60 nm thick silicon nitride (Si_3N_4) film grown by Plasma Enhanced Chemical Vapor Deposition (PECVD) method. The deposition temperature of PECVD Si_3N_4 is 300°C.

The last process step of these detectors was the aluminum sintering. In order to study the thermal donor generation, the detector wafers were sintered at 430°C for different durations at the peak temperature; 35, 45, 60, 70 and 80 minutes. The thermal profile of sintering is "push-in" 2 minutes followed by 10 minutes stabilization while the furnace settles again at the peak temperature (the furnace door is open during the push-in). After heating at the peak temperature the wafers were "pulled-out" in 2 minutes. A $n^+/p^-/p^+$ reference wafer was processed and sintered at 370°C.

After the processing the wafers containing 80 pad detectors were diced. The diodes were characterized at the probe station by the capacitance-voltage (CV) and current-voltage (IV) measurements. In order to study the effect of oxygen concentration distribution on the TD formation, ten diodes along the diameter of each wafer

were chosen for the CV measurements. The introduction of TDs was observed not to influence the leakage current of devices.

Measurements

The Fig. 9 shows the effective doping concentration with respect of heating time at 430^0 C. The compensation of the boron doping, i.e. type inversion, occurs after about 55-60 minutes heating.

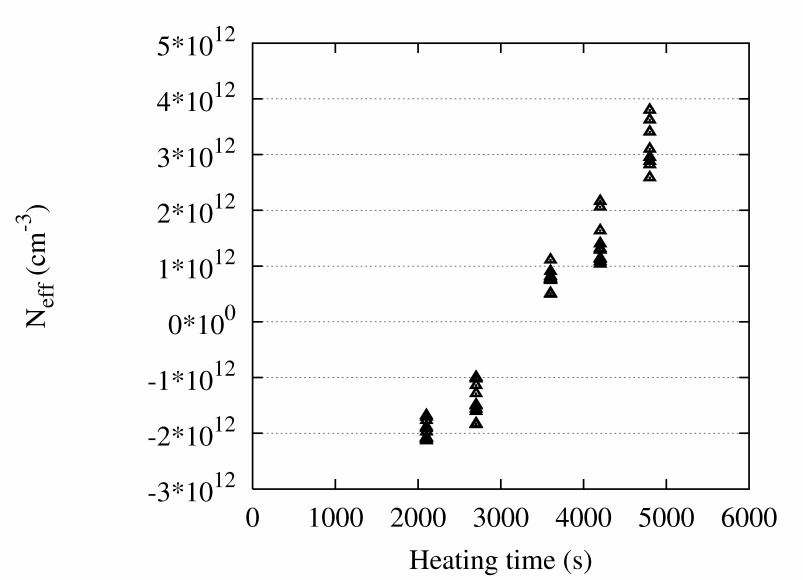

Figure 9: . Effective doping concentration N_{eff} versus heating time at 430°C. The data points at given heating time correspond to 10 diodes picked along the wafer diameter.

The compensation of the boron doping, i.e. type inversion, occurs after about 55-60 minutes heating. The TD induced Space Charge Sign Inversion (SCSI) in p^+-p-n^+ devices were further studied by the Transient Current Technique (TCT) method. After sufficient TD generation, the bulk is compensated and inverted to n-type, switching the junction to the front side (p^+-side). Fig. 10a shows a TCT transient of hole current of a detector that has been heat treated 35 minutes at 430^0C. A decreasing induced current with time can be seen observed, indicating drift of holes from the high electric field (n^+-side) to the low field (p^+-side). The junction, as expected, is on the backside (n^+-side). Induced hole current in a similar detector as shown in Fig. 10a, which has been heat treated for 75 minutes at 430^0C is shown in Fig. 10b.

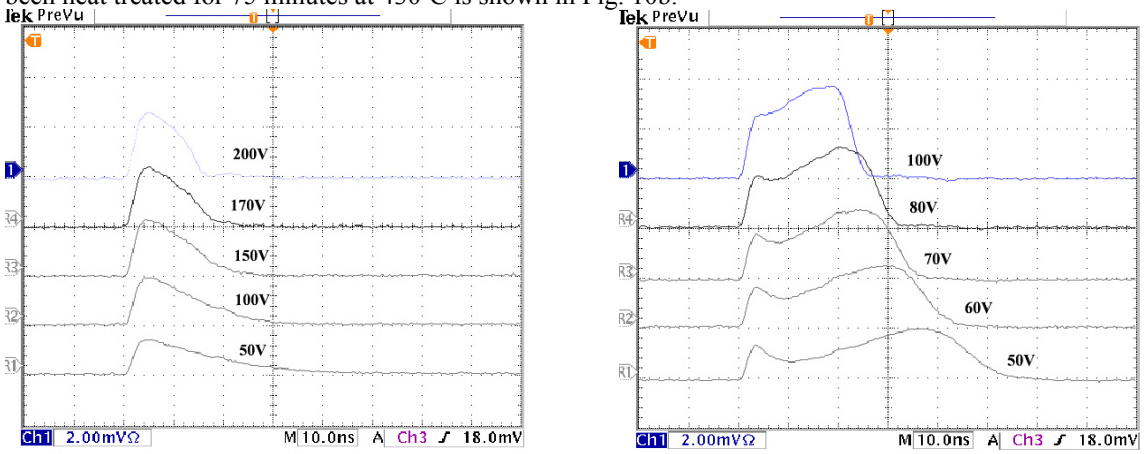

(a) (b)

Figure 10: Current transients with different reverse bias voltages of p+/p/n+ detector. Thermal donors have been generated at 430^0C for 35 minutes (a) and 70 min (b). The detector has been illuminated from the backside (n^+-side).

It is clear that the hole current shapes shown in Fig. 10b are drastically different from those shown in Fig. 10a: the hole current transients increase with time, indicating holes drifting from low electric field (n^+-side) to high electric field (p^+-side). Now the junction is switched from the backside (n^+-side) to front side (p^+-side). The

SCSI has taken place from negative to positive, and the bulk is type-inverted to n^- type. The device structure is therefore transformed from the original $p^+/p^-/n^+$ to the intended $p^+/n^-/n^+$.

Summary

The thermal donor formation is a feature of Czochralski silicon. It cannot be observed in standard detector materials such as Fz-Si or diffusion oxygenated Fz-Si, because the concentration of interstitial oxygen is too low in these materials The TDs are shallow donor levels, between 0.01 eV and 0.2 eV below the conduction band. The formation of TDs is strongly depended on temperature and oxygen concentration in the silicon. Heat treatment between 400 – 600^{0}C lead to TD formation.

The detector processing was carried out using the common procedure to produce n^+-p^--p^+ or p^+-n^--n^+ detector structures. During the last process step, i.e. sintering of aluminum electrode, the p-type bulk was turned to n-type through generation of Thermal Donors (TD). The full depletion voltage of detectors could be tailored in wide range from 30 V up to close 1000 V by changing heat treatment at 400^{0}C – 450^{0}C duration from 20 to 80 minutes. The Space Charge Sign Inversion (SCSI) in the TD generated devices (from p^+-p^--n^+ to p^+-n^-(inverted)-n^+) has been verified by Transient Current Technique (TCT) measurements.
Recently, p-type silicon materials have gained a growing interest among the scientific community aiming to improve radiation hardness of silicon devices. The benefit of p-type materials is the absence of SCSI, thus the collecting junction remains on the front side of the detector and the majority of the signal comes from electrons allowing a higher charge collection than in $p^+/n^-/n^+$ devices. If p-type MCz-Si wafers are used for the production of $n^+/p^-/p^+$ devices, the TD formation can be utilized in order to tailor the V_{fd}.

References

[1] J. Härkönen et al., ” Processing microstrip detectors on Czochralski grown high resistivity silicon”, Nucl. Instr. And Meth, A485 (2002), 159-165.
[2] E. Tuominen et al., ” Radiation Hardness of Czochralski Silicon studied by 10 MeV and 20 MeV protons”, IEEE Trans. Nucl. Sci. 50 (2003).
[3] P. Luukka et al., “ Results of Proton Irradiations of Large Area Strip Detectors made on High-Resistivity Czochralski Silicon” , Nuclear Instruments and Methods in Physics Research A530 (2004) 117-121.
[4] G.S. Oehrlein, “Silicon–oxygen complexes containing three oxygen atoms as the dominant thermal donor species in heat-treated oxygen-containing silicon”, J. Appl. Phys. 54 (1983) 5453.
[5] K. Wada, “"Unified model for formation kinetics of oxygen thermal donors in silicon", Phys. Rev. B, 10 (1984) 5884.
[6] A. Simoen et al, “Hydrogen plasma-enhanced thermal donor formation in n-type oxygendoped high-resistivity float-zone silicon”, Appl. Phys. Lett. 81 (10) (2002) 1842.
[7] J. Härkönen et al., “p+/n-/n+ Cz-Si detectors processed on boron doped substrates with thermal donor induced space charge sign inversion”, IEEE Transactions on Nuclear Science, (in press).
[8] J. Härkönen et al., “ Proton irradiation results of p+/n-/n+ Cz-Si detectors processed on boron doped substrates with thermal donor induced space charge sign inversion”, Nuclear Instruments and Methods in Physics Research A (in press).

5.3. SMART project

The research activity of the SMART project, a collaboration funded by I.N.F.N. of Italian research institutes members of RD50, has been focused in year 2005 on the electrical characterization of pad and micro-strip devices made on n- and p-type 4” silicon wafers, grown with Standard Float Zone (SFZ), high resistivity Magnetic Czochralski (MCz) and epitaxial (EPI) techniques. Single pad detectors, microstrip sensors and other test structures have been manufactured [1,2], irradiated and tested before and after irradiation at very high fluences with 24 GeV/c and 26 MeV protons (up to ~ 5 10^{15} cm^{-2} 1 MeV neutrons eq. (n_{eq}/cm^2)) and with reactor neutrons (up to ~ 8 10^{15} n_{eq}/cm^2). A photograph of one of he processed wafers is given in Fig. 11. Preliminary results before and after irradiation are discussed here. In particular, this section describes the most important results on single pad structures, while main results on microstrip detectors are reported in the Full Detector Systems chapter.

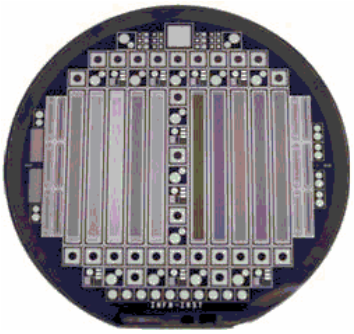

Figure: 11 Photograph of a processed wafer [1].

Materials, processing and irradiation

Bare wafer materials with both n- and p-type bulk doping used in this study belong to the common RD50 procurement.

MCz 4'' wafers were produced by Okmetic Ltd (Vantaa, Finland), few n-type epitaxial wafers (ρ = 50 Ωcm, EPI layer thickness = 50μm) grown at ITME, (Varsaw, Poland) have been also used. SFZ silicon wafers were also processed for performance comparison.

Wafer layout includes 66 test structures and 10 micro-strip sensors of different geometries. Processing has been performed by ITC-IRST (Trento, Italy) in two successive runs. First run for n-type (RUN-I) and second one for p-type (RUN-II) materials have been processed with the same mask-set designed to be used with all the different silicon materials. For RUN-II the uniform p-spray technique has been used to increase n^+ implants isolation with two different implantation doses, namely $3x10^{12}$ cm^{-2} (low p-spray) or $5x10^{12}$ cm^{-2} (high p-spray). Further details can be found in references [3,4].

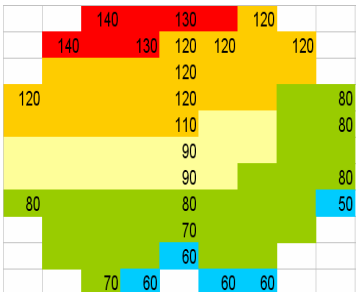

Figure 12: Spread of full depletion voltage values (Volt) in a MCz Si p-type wafer after processing [5,6].

Devices irradiation has been done with different particle beams. A first proton irradiation campaign was carried out at the CERN-SPS proton beam facility with 24 GeV/c protons with fluences up to 3×10^{15} n_{eq}/cm^2. A second irradiation was performed at the Compact Cyclotron of the Forshungszentrum in Karlsruhe (Germany) with 26 MeV protons with fluences up to 2×10^{15} n_{eq}/cm^2. The 50 μm thick epitaxial Si devices have been irradiated with 24 GeV/c protons up to 5×10^{15} n_{eq}/cm^2 and also with fast neutrons in the Ljubljana nuclear reactor up to 8×10^{15} n_{eq}/cm^2.

Pre-irradiation measurements

Pre-irradiation results of n-type diodes (SFZ, MCz) have shown a uniform resistivity and current density within the same wafer [2], while MCz p-type wafers have shown significant spread of the full depletion voltage (see Fig. 12) [3,4]. A microscopic study on the reasons of this full depletion voltage (V_{fd}) variations has been performed by low temperature Thermally Stimulated Currents on single pad diodes. The analysis has shown that this spread is mainly due to the activation of shallow levels related to thermal donors during the process [5].

Post-irradiation results

IV and CV measurements were performed at 20 °C, 0 °C and -3 °C keeping the first guard ring connected at ground. Annealing of radiation damage has been studied maintaining the devices at room temperature or heating them up to a temperature of 60 °C or 80 °C for known time intervals [6,7,8]. Microscopic investigation by Thermally Stimulated Current (TSC) measurements has been performed on a wide temperature range, starting from 4.2K to detect the shallow levels produced by traditional dopants (i.e. Phosphorous and Boron), Thermal Donors (TDs) and other defects which may be present in oxygen enriched Si [2]. The current related damage has been evaluated for all radiation sources and on n- and p-type materials. Measurements have shown good agreement with NIEL hypothesis [2] and the leakage current density increase rate (α) values are compatible with expectations: $<\alpha> \cong 4\ 10^{-17}$ A/cm [6] after 8 min at 80°C annealing.

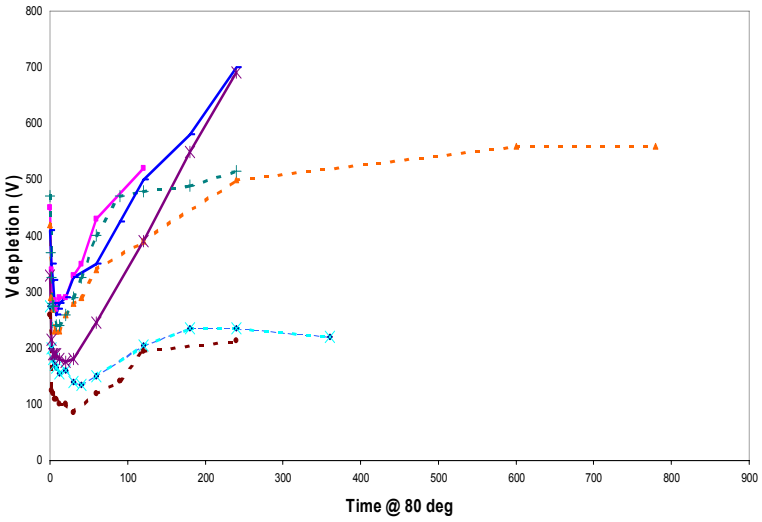

Figure 13: Bias voltage annealing curves for SFZ (full line) MCz(dashed line) irradiated with 26 MeV protons (see text).

An example of the change in full depletion voltage during annealing is shown in Fig. 13 for SFZ and MCz diodes of both n- and p-types irradiated with 26 MeV protons at two different fluences 6×10^{14} $n_{eq}/cm^2$and 8×10^{14} n_{eq}/cm^2. For both bulk types an improved reverse annealing behavior of MCz Si is observed with a clear saturation beyond 200 minutes at 80°C, while the V_{fd} values of SFZ materials still increase. If confirmed, such reduced reverse annealing growth of the full depletion voltage would represent a significant improvement of MCZ Si against SFZ in terms of radiation hardness during operational-maintenance run of SuperLHC.

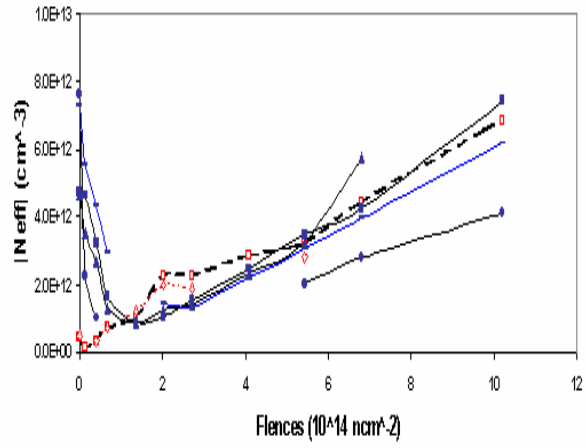

Figure 14: Effective doping concentration on SFZ (dashed lines) and MCz (full lines) as a function of fluence. Each line connects samples belonging to the same wafer.

N-type SFZ diodes were already type inverted at the lowest fluence investigated in this study and the measured V_{fd} values increase in the whole fluence range [6×10^{13} n_{eq}/cm^2 to 3×10^{15} n_{eq}/cm^2]. On the contrary, the V_{fd} values of the n-type MCz diodes show a minimum at 1.86×10^{14} n_{eq}/cm^2 with a small spread due to the different initial resistivity. At this minimum the full depletion voltage, and, hence, the effective doping concentration N_{eff} (see Fig. 14), is always significantly different from zero, suggesting that no space charge sign inversion (SCSI) occurred. However, the annealing curves of V_{fd} for diodes beyond this minimum (Fig. 13) show a behavior typical of an inverted SFZ device, with the beneficial annealing that leads towards a minimum [6,7,8]. For what concerns the V_{fd} *vs* Φ behaviour, epitaxial devices show similar results for proton irradiation and less pronounced effects for neutron irradiation [10].

A study of transient current at constant temperature measurements after trap priming [11] was performed to investigate if the SCSI is occurring in single pad detectors after irradiation with 24GeV/c and 26MeV protons in the fluence range 10^{14}-10^{15} cm^{-2} [12]. These studies proved that n-type SFZ Si irradiated with 24 GeV/c protons at a fluence of 2.04×10^{14} n_{eq}/cm^2 exhibits SCSI during the emission from the so called I defect [13],

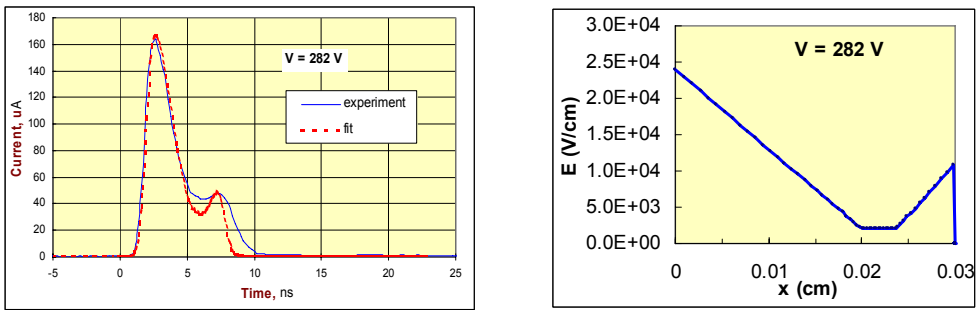

Figure 15: TCT profile showing the double peak effect and electric field in a n-type MCz Si diode irradiated with 1.54x10^{15} 1/cm^2 24 GeV protons.

demonstrating that at this fluence the SFZ under study is type-inverted. On the contrary inversion was not observed with this technique in n-MCz Si for a fluence up to 10^{15} n_{eq}/cm^2. According to preliminary simulation studies, it seems that the occurring of a minimum of depletion voltage without SCSI could be explained in terms of double junction effects [12].

To investigate more in detail the issue of the space charge sign inversion of n-type MCz Si the group of Ioffe St. Petersburg performed Transient Current Technique (TCT) analysis of three n-type MCz Si diodes irradiated by 24 GeV proton fluences of 5.1e14, 1.54e15 and 2.17e15 p/cm^2. Results have been presented and discussed in [12]. At low bias voltage the TCT signal from electron collection has a single peak shape for all samples. As the bias is increased, the response takes a double peak shape, originating from the electric field distribution typical of a double junction (significant electric field at both p^+ and n^+ sides) [14,15]. The electron current pulse response measured in the diode irradiated with 1.54x10^{15} p/cm^2 is shown in Fig. 15, left. The measured pulse shapes have been fitted according to the procedure described in [16] in order to determine the electric field distribution inside the sample (Fig. 15 right). The electric field profile seems to indicate that the dominant junction is still on the p^+ side, i.e. the sample is still not type inverted a this fluence. It is important to note that

all the samples studied by current transient techniques did not undergo annealing. A study of the evolution of the electric profile with annealing will be the subject of forthcoming works.

The SMART simulation activity of radiation damage in Silicon detectors also achieved significant results. The tool used to model radiation hardness is based on ISE-TCAD with discrete time and spatial solutions to transport equations. The damage modeling is performed considering activation energies, cross sections for majority and minority carriers and trap concentrations of the main defects observed by TSC and deep level transient spectroscopy (DLTS). Up to now, in p-type FZ Si, a three level model has been considered, with two acceptors at 0.42eV and 0.46eV plus a donor at 0.36eV as in [17]. Simulated results for CCE after fast hadrons

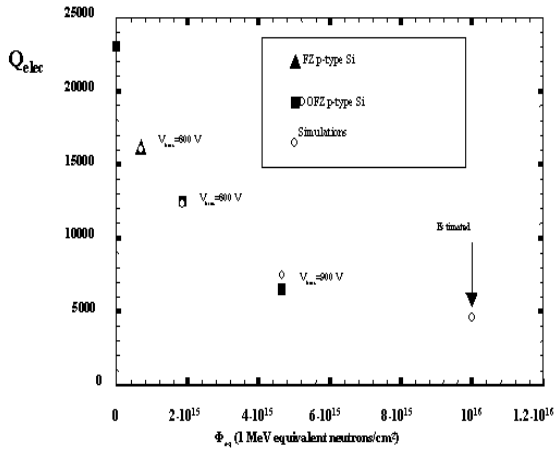

Figure 16: Simulation: Collected charge on p-type device from a m.i.p. particle as a function of the irradiation fluence

fluence of $10^{15} n_{eq}/cm^2$ well reproduce experimental data taken with detectors [18]. The prediction for the charge collected on a p-type device at the highest fluences foreseen at SLHC (see Fig. 16) show that the expected charge from a mip is below 5000 electrons.

References

[1] M. Bruzzi et al., *"Processing and first characterization of detectors made with high resistivity n- and p-type Czochralski silicon*" Nucl. Instr. and Meth. A 552 (2005) 20.
[2] RD50 Status report, CERN Dec. 2004.
[3] C. Piemonte *"Preliminary electrical characterization of n-on-p devices fabricated at ITC-irst"* presented at the 5th RD50 Workshop Available: http://rd50.web.cern.ch/rd50/.
[4] N. Zorzi et al. Workshop on the development of p-type Si detectors, Trento, February 2005.
[5] M. Bruzzi et al., *"The issue of doping disuniformity in p-type MCz Si detectors"* presented at the 7th rd50 Workshop, Oct. 2005, CERN, available: http://rd50.web.cern.ch/rd50/.
[6] G.Segneri et al, *"Radiation hardness of high resistivity n- and p-type magnetic Czochralski silicon"*, proceedings of the PSD07 conference, Nucl. Instr. and Meth. A (submitted for publication).
[7] A.Macchiolo et al, *"Characterization of micro-strip detectors made with high resistivity n- and p-type Czochralski silicon"*, proceedings of the PSD07 conference, Nucl. Instr. and Meth. A (submitted for publication).
[8] V.Radicci et al., *"Study of radiation damage induced by 24GeV/c and 26MeV protons on heavily irradiated MCz and FZ silicon detectors"*, presented at the 7th International Conference on Large Scale Applications and Radiation Hardness of Semiconductor Detectors, submitted for publication on Nucl. Instr. and Meth. A.
A. Messineo et al., *"Development of radiation hard Silicon detectors: the SMART project"*, presented at the 9th ICATPP Conference, submitted for publication on Nucl. Instr. and Meth. A.
[9] C.Piemonte *"TCAD simulations of isolation structures for n^+-on-p silicon microstrip detectors"* presented at the 7th RD50 Workshop. Available: http://rd50.web.cern.ch/rd50/.
[10] A. Candelori "*Semiconductor materials and detectors for future very high luminosity colliders"* NSREC 2005. Available: http://rd50.web.cern.ch/rd50/.
[11] D. Menichelli, M. Scaringella, M. Bruzzi, I. Pintilie, E. Fretwurst, Phys. Rev. B 70, 195209 (2004).
[12] M. Scaringella et al., presented at the 7th International Conference on Large Scale Applications and Radiation Hardness of Semiconductor Detectors, submitted for publication on Nucl. Instr. and Meth. A.
[13] I. Pintilie, E. Fretwurst, G. Lindstrom, and J. Stahl *"Second-order generation of point defects in gamma-irradiated float-zone silicon, an explanation for ''type inversion''"* Applied Phisics Letters Vol 82, n. 13 (2003).
[14] V. Eremin et al. Nucl. Instrum. Meth. A 1995
[15] V. Eremin et al. Nucl. Instrum. Meth. A
[16] E. Verbitskaya, *"Operation of heavily irradiated silicon detectors in non-depletion mode"*, NIM A, in press.
[17] M. Petasecca et al., *"Numerical simulation of radiation damage effects in p-type silicon detectors"* presented at the 6th RD50 Workshop. Available: http://rd50.web.cern.ch/rd50/.
[18] M. Petasecca, F. Moscatelli and G. U. Pignatel, "*Analysis and simulations of charge collection efficiency in silicon thin detectors"* Nucl. Instrum. and Meth. A 546 (2005) pp. 291-295.

5.4. Studies of n-type MCz, DOFZ and FZ detectors

The materials used in this study are n-type FZ (f2), DOFZ (d1), MCz (n320) processed by the Helsinki Institute of Physics (H.I.P.), and high resistivity n-type 15 kΩcm oxygenated FZ (W317) processed by the ST Microelectronics. The properties of investigated samples can be found in Table 3. All samples have an aluminum grid on the rear ohmic contact and an opening in the front aluminum for laser studies. The irradiations were performed at CERN PS with 24 GeV/c protons. Unless mentioned otherwise the diodes were annealed for 4 minutes at 80°C prior to the measurements.

Table 3. The active area of the dioedes was 0.25 cm^2.

Sample name	Silicon type	Manufacturer	Crystal orientation	ρ [kΩcm]	Processing	Oxygenation	Thickness [μm]	Initial V_{fd} [V]
f2	FZ	Okmetric Oyj	<1 00>	1	H.I.P	-	295 ± 2	235 ± 15
d1	DOFZ	Okmetric Oyj	<1 00>	1	H.I.P	75h at 1100°C	295 ± 2	269 ± 7
W317	DOFZ	Wacker	<1 1 1>	15	ST	60 h at 1200°C	300 ± 2	14 ± 2
n320	MCz	Okmetric Oyj	<1 00>	1	H.I.P	-	304 ± 2	309 ± 5

Effective doping concentration

The dependence of full depletion voltage on fluence for FZ and DOFZ is shown in Fig. 17. As expected the diodes undergo type inversion at relatively large fluences of ~1.5 10^{14} cm^{-2}, which shows a positive effect of smaller initial resistivity of the starting material. High resistivity samples (W317) invert at much smaller fluences. Contrary to the results obtained with the FZ and the DOFZ devices a less pronounced change in the depletion voltage of the MCz detectors is observed (Fig. 17). As will be shown by TCT measurements the space charge in these detectors doesn't change sign. The full depletion voltage determined from C-V (10 kHz, 20°C) coincides within reasonable margins with TCT measurements (Q-V method see [1]) for all samples. The full depletion voltage determined from I-V on the other side underestimates the one from C-V and Q-V up to factor of 2. The data on figures were fit with equation $V_{fd} = \left| V_o\left(1 - e^{-c\Phi}\right) + g_C\Phi \right|$, where V_o is the depletion voltage before irradiation, g_c is the net acceptor generation rate and Φ is the fluence. The complete donor removal was assumed. The results of the fits and detailed discussion can be found in [2].

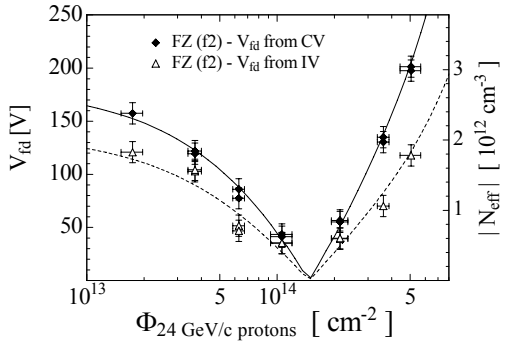

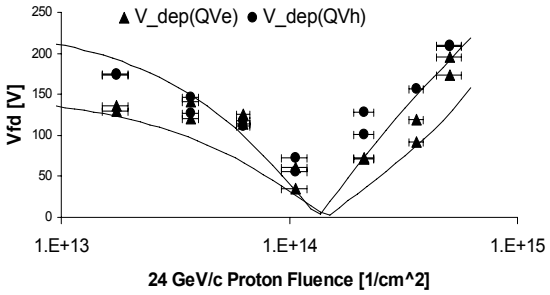

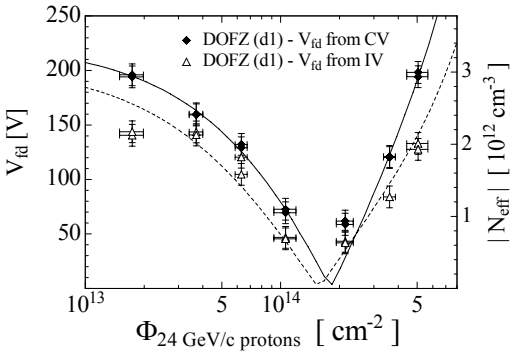

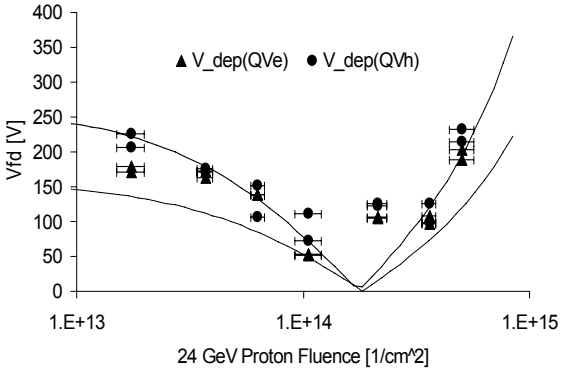

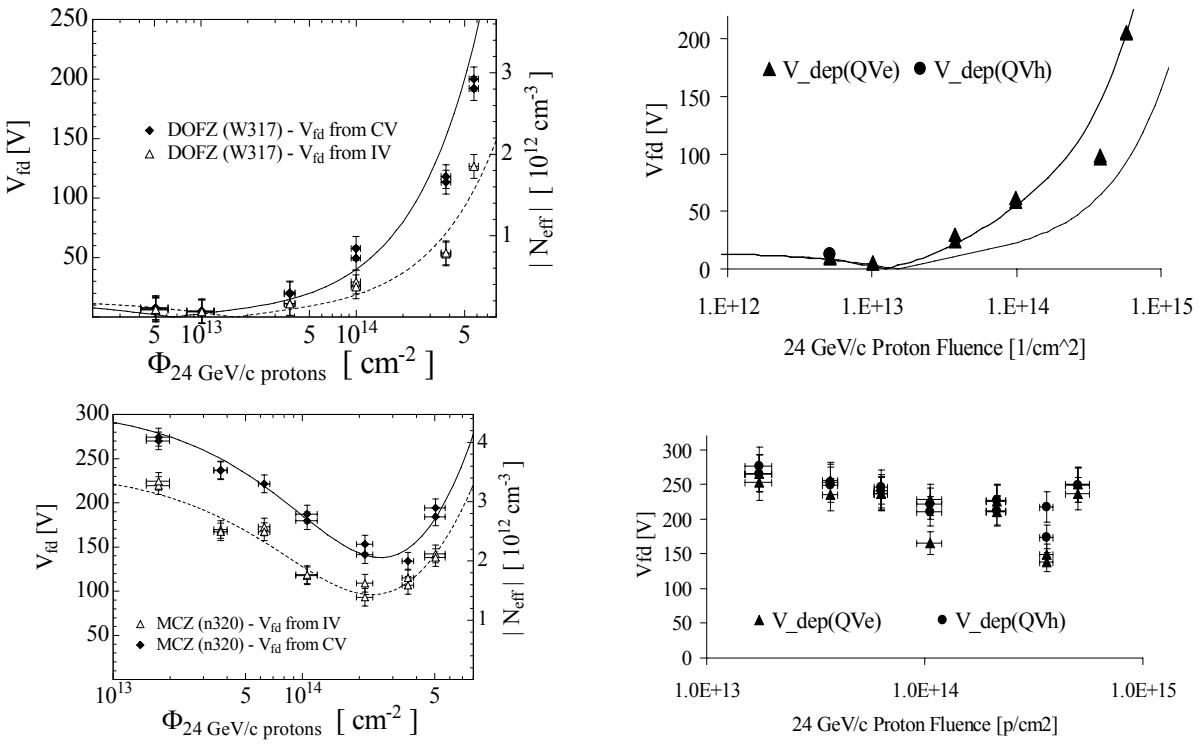

Figure 17: Depletion voltage of different detectors as function of proton fluence. Values obtained from CV (closed squares) and IV (open triangles) measurements are presented on the left and the corresponding depletion voltage extracted from the Charge-Voltage, QV, method using both electron (QVe) and hole injection (QVh) on the right.

Space charge sign

The shape of the induced current after illumination of either side of the diode with light of small penetration depth (red, green) reveals the sign and space charge profile (see also 1.1.3). In case of heavily irradiated samples

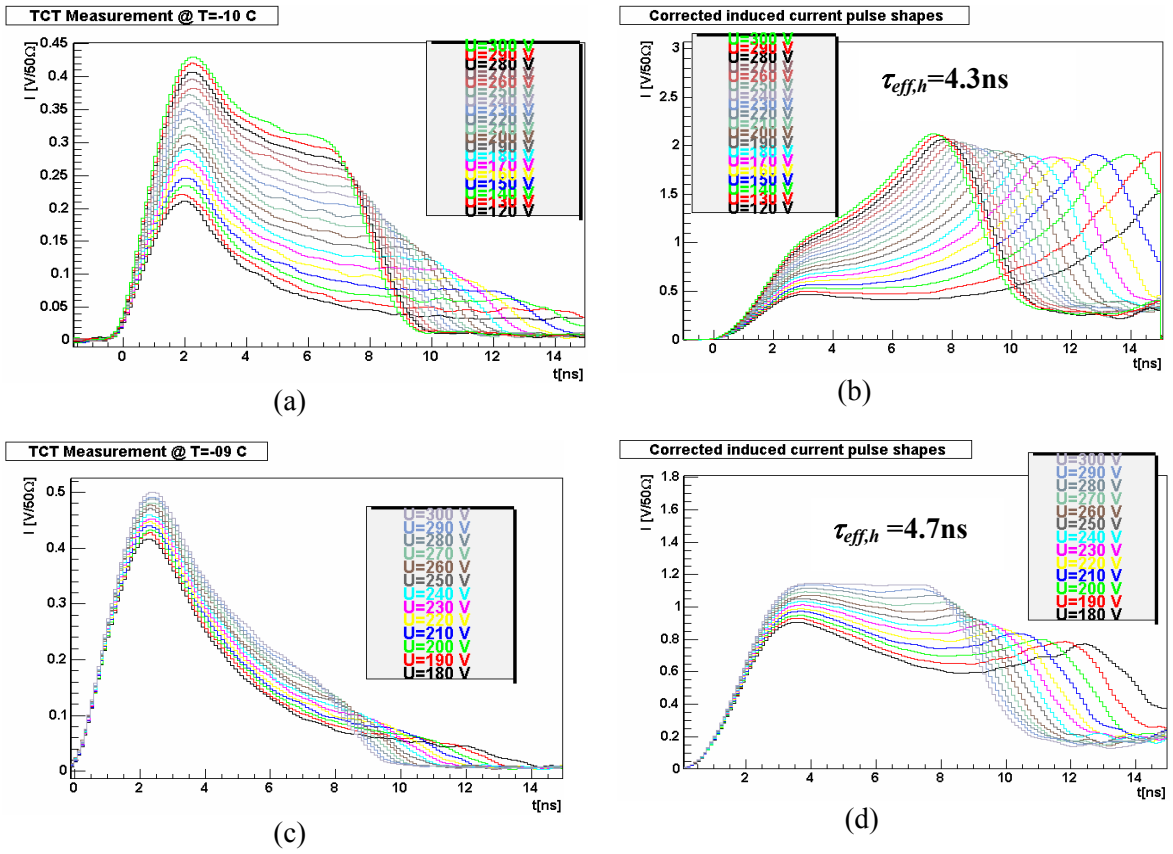

Figure 118: The induced current pulses at different voltages after hole injection for MCz detector (a) and Fz detector (c) . The pulse shapes corrected for trapping are shown in (b) for MCz and (d) for Fz. The measurements were taken at 10°C. Prior to the measurements detectors were annealed at RT until the end of beneficial annealing.

the determination of space charge is non-trivial as the effective dopant concentration can be non-homogenous and the pulses are also damped by the trapping. In is therefore necessary to correct induced current pulse shapes for trapping before any conclusion about the space charge can be made [3]. To determine the space charge of MCz and FZ detectors irradiated to $5x10^{14}$ p cm^{-2} the induced current pulses after hole injection were compared (see Fig. 18).

The uncorrected pulses in Fig. 18. would lead to conclusion that the space charge in both detectors is negative as the signal is highest at n^+ contact and decreases as the holes drift to the p^+ electrode. After corrected for trapping the pulses for MCz sample show a shape of a detector with positive space charge. On the other hand the pulse shape of Fz detectors still has the shape typical for the negative space charge - the main junction is at the back. The space charge of n type MCz sensors after irradiation therefore remains positive. This conclusion has been confirmed at different fluences by various groups [2,3,4] also from observation of the induced currents after electron injection.

Effective trapping times

The effective trapping times of electrons and holes were determined by using charge correction method ([5,6]). The effective trapping times τ_{eff} depend on fluence as $\frac{1}{\tau_{eff_{e,h}}} = \beta_{e,h}\Phi_{eq}$, where β is the effective trapping times damage constant. The $\beta_{e,h}$ for MCz detectors are shown in Fig. 7. [2]. the measurements agree with previously measured values gathered in the Table 4. This confirms the observation that effective trapping times damage constants don't depend on type of silicon.

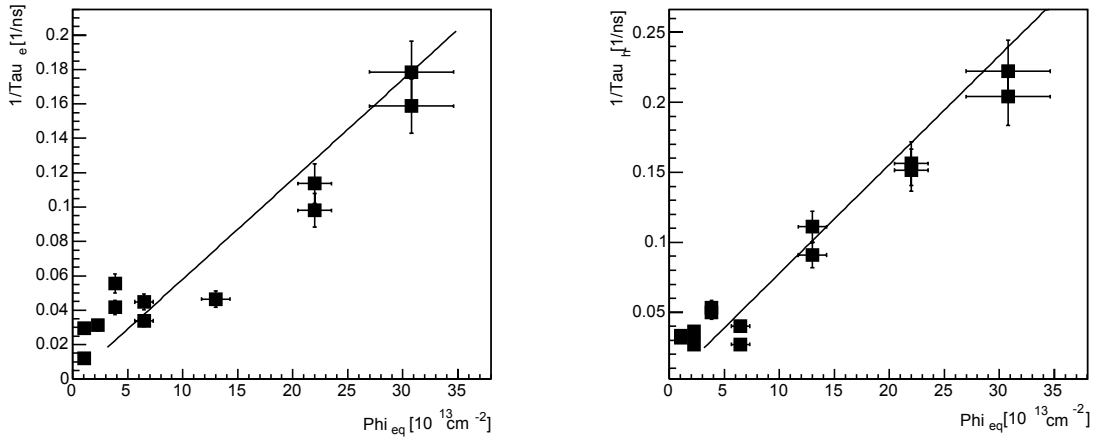

Figure 19: Trapping probability, $1/\tau_{e,h}$, as a function of fluence determined after electron (left) and hole (right) injection for MCz silicon.

Table 4: Comparison of β_e and β_h determined after 24 GeV/c proton irradiation. All values have been scaled to 5°C, for the temperature dependence of β (see section 1.4.3.1).

	β_e [10^{-16} cm^2/ns]	β_h [10^{-16} cm^2/ns]
CERN [2] (DOFZ,FZ,MCz)	5.48 ± 0.22	6.02 ± 0.29
Dortmund [7] (DOFZ)	5.08 ± 0.16	4.90 ± 0.16
Ljubljana (DOFZ and FZ [8], MCz [3])	5.34 ± 0.19	7.08 ± 0.18
Lancaster/Hamburg [5] (FZ)	5.32 ± 0.30	6.81 ± 0.29
Hamburg [9] (FZ, DOFZ and MCz)	5.07 ± 0.16	6.20 ± 0.54

Temperature dependence of effective trapping times

The temperature dependence of effective trapping times was found to be in agreement with previously measured values [8]. Effective trapping times scale with temperature as given by $\beta_{e,h}(T) = \beta_{e,h}(T_o)(T/T_o)^{\kappa_{e,h}}$, with κ_e= -0.88 ± 0.06 and κ_h= -1.55 ± 0.06 and T_0=*263* K.

Annealing of effective trapping times

The effective trapping times change with time after irradiations. The previous measurements on DOFZ and FZ material [7,8] have shown that the behavior can be parameterized by a simple model $\beta_{e,h}(t) = \beta_{o_{e,h}} \exp\left(\frac{-t}{\tau_{e,h}}\right) + \beta_{\infty_{e,h}}\left(1 - \exp\left(\frac{-t}{\tau_{e,h}}\right)\right)$ where β_0 and β_∞ represent the trapping time damage constant before and after annealing. The underlying model assumes the decay of defects responsible for trapping to new defects. Detectors were annealed at elevated temperatures of 80°C and measurements were taken between annealing steps at 20°C. Dependence of β_e and β_h on annealing time for MCz samples is shown in Fig. 20 [2]. The effective trapping time of electrons decreases the with time by about 40% while the effective trapping time of holes increases with time by roughly the same amount. This is in agreement with previously reported measurements [8] where annealing was performed at 60°C. The time constants were found to be of order of few hours at 80°C, which is only slightly less than what was found at 60°C. Clearly more annealing studies of trapping times are needed at different temperatures to be able to make a reliable prediction of trapping times evolution at Super LHC temperatures.

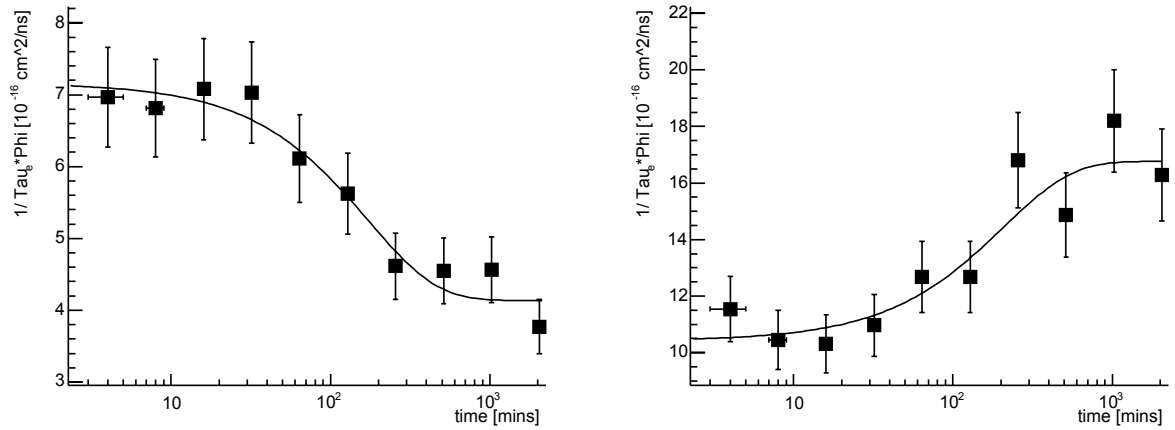

Figure 20 Trapping times for electrons (left) and holes (right) as a function of annealing time at 80°C for MCz samples [2].

Charge collection measurements of MCz and FZ samples with ^{90}Sr electrons

The fact that trapping times are equal for all materials is reflected also in the charge collection efficiency measured with ^{90}Sr electrons and LHC speed electronics (for details see [10]). The MCz and Fz samples irradiated to 10^{14} and $5x10^{14}$ p cm^{-2} were annealed at room temperature until the end of beneficial annealing. After that the measurements were performed at -10°C. The measured most probable charge as a function of voltage is shown in Fig. 21. The charge Q and CCE scale were calibrated with signals from 59.6 keV photons (^{241}Am) and ^{90}Sr electrons in a non-irradiated float zone detector.

The full depletion voltage of both heavily irradiated sensors is about the same. In spite of different electric field profiles (see section 1.4.2) almost the same dependence of collected charge on voltage can be observed. CCE of around 83% can be reached at bias voltages well over full depletion voltage. The dependence of

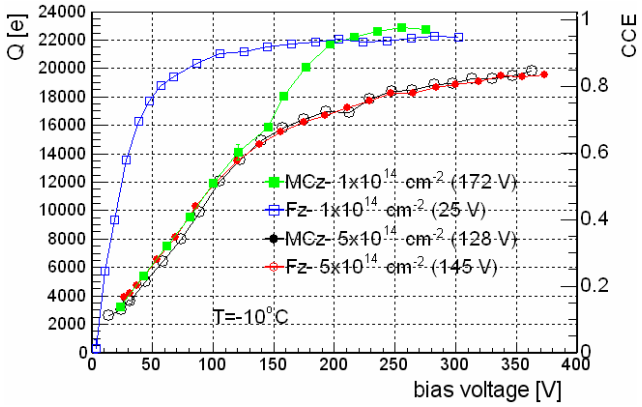

Figure 21: Charge collection measurement with MCz and Fz detectors. Full depletion voltages of the detectors are given in the brackets.

collected charge on voltage is different for both detectors irradiated to low fluence, due to difference in full depletion voltages. The CCE at large bias voltages is however almost the same.

References

[1] G. Kramberger, Doctoral thesis, Ljubljana 2001.
[2] A. G. Bates and Michael Moll, " A comparison between irradiated Magnetic Czochralski and Float Zone silicon detectors using the Transient Current Technique ", in press Nucl. Instr. And Meth.
[3] G. Karmberger, I. Mandić, "TCT measurements on MCz and Fz material", Presented at 4th RD50 workshop CERN, 2004.
[4] M. Scaringella et al., presented at the 7th International Conference on Large Scale Applications and Radiation Hardness of Semiconductor Detectors, submitted for publication on Nucl. Instr. and Meth. A
[5] T.J. Brodbeck et. al., Nucl.. Instr. Meth. A 455 (2000) 645.
[6] G. Kramberger et. al, Determination of effective trapping time of electrons and holes in irradiated silicon, Nucl. Instr. and Meth. A 476 (2002) 645-651.
[7] O. Krasel, PhD thesis, Charge Collection in Irradiated Silicon Sensors in the ATLAS Pixel Detector, Dortmund University, July 2004.
[8] G. Kramberger et al., Effective trapping time of electrons and holes in different silicon materials irradiated with neutrons, protons and pions, Nucl. Instr. and Meth. A 481 (2002) 297-305
[9] E. Fretwurst et al., Survey of Recent Radiation Damage Studies at Hamburg, 3rd RD50 Collaboration Workshop, 4th November 2003.
[10] Kramberger et al., "Charge collection properties of heavily irradiated epitaxial silicon detectors", Nucl. Instr. and Meth. A 554 (2005) 212-219.

5.5. Epitaxial-Si detectors

Several RD50 groups are involved in the research of detectors processed on epitaxial silicon grown on Cz substrate. These detectors were found to exhibit the superior radiation hardness in terms of N_{eff} [1].

Samples and Experimental Procedure

25, 50 and 75 µm thick epitaxial n-type layers with a nominal resistivity of 50 Ωcm were produced by ITME, using highly doped Cz-silicon substrates (0.01 Ωcm) and pad diodes (5 x 5 cm² active area) were processed by CiS. Recently detectors were processed on same wafers also by IRST and exhibit similar performance as the CiS ones. Depth profiles of resistivity and oxygen concentration are displayed in Fig. 22 and Fig. 23 respectively.

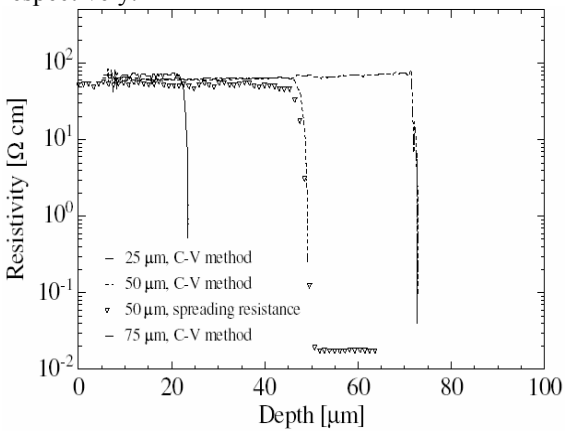

Figure 22: Resistivity depth profiles as measured by spreading resistance (symbols) and C/V methods (lines) for 25, 50 and 75 µm n-type epi diodes.

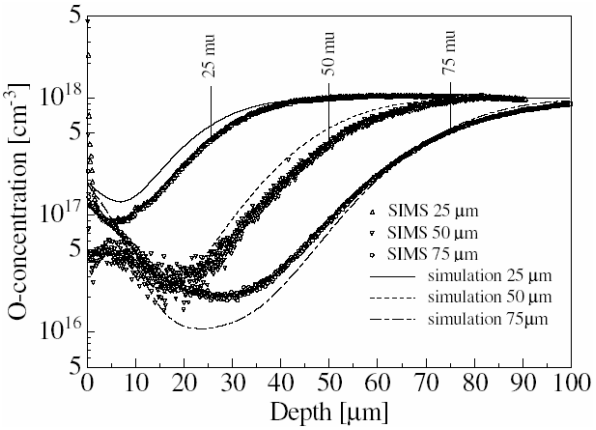

Figure 23: Oxygen concentration profiles measured with SIMS (symbols) in comparison with process simulation results (lines) in the investigated epi-Si diodes.

Oxygen is out diffusing from the Cz substrate mainly during the high temperature diode process steps as verified by comparison of SIMS results with process simulations [2, 3]. Average carbon concentration was also determined and was found to be lower by an order of magnitude than that of the oxygen. Irradiations had been performed at CERN-PS with 24 GeV/c protons as well with MeV neutrons from the research reactor of the Jozef Stefan Institute in Ljubljana. In both cases 1 MeV neutron equivalent fluences of up to 10^{16}cm^{-2} were reached. Irradiations were performed to fixed fluences and also according to so called CERN scenario.

Effective doping concentration

Stable damage (shallow donor generation)

A build up of positive space charge in epi diodes with increasing fluence was observed and can be seen in Fig. 24 [4]. Here the effective doping concentration after 10 min at 80°C, corresponding roughly to the end of the short term annealing, is plotted as function of the equivalent fluence for all three (25, 50 and 75 µm thick) n-type epi devices. Contrary to the damage effects for FZ silicon the effective doping concentration stays always positive and after crossing a slight minimum increases almost linearly with fluence. This holds for proton and neutron irradiated detectors (see Fig. 25 [4]) although the introduction rate of effective donors is smaller for the latter. The initial decrease in positive space charge with fluence is attributed to donor removal which is much faster for proton than for neutron irradiated detectors. The donor removal constant c was found comparable with the one in float zone detectors [6].

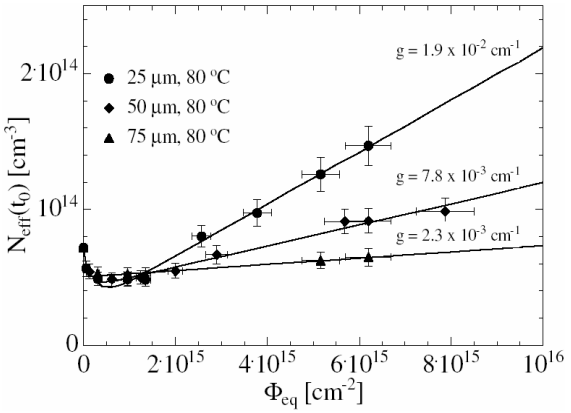

Figure24: Effective doping concentration, as measured after the end of beneficial annealing as function of fluence after 24 GeV/c proton irradiation. Solid lines represent fits according to a model description [5], slope values assigned to the curves represent the donor generation rates. C-V measurements were performed at 100 kHz.

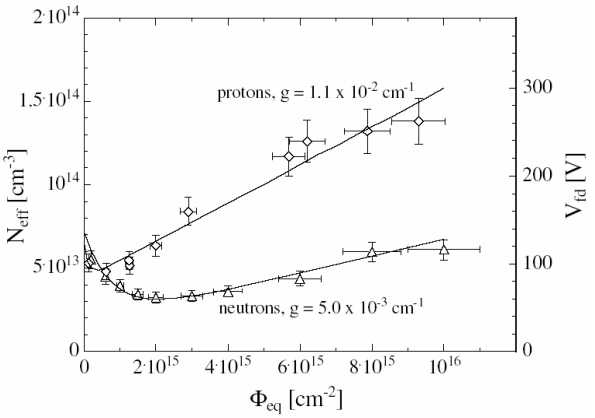

Figure 25: Comparison between donor generation in 50 µm epi-diodes after 24 GeV/c proton and reactor neutron irradiation, measured at the end of the beneficial annealing. Solid lines are fits using a model description [5]. Given slope values represent the donor generation rates

The introduction rate of positive space charge depends on detector thickness and is related to concentration of oxygen dimers in the epi-Si (see [7,8] for details). Oxygen dimers are produced during the high temperature process steps via out-diffusion from the Cz substrate. Because of the much smaller thickness it is plausible that the dimer concentration could be larger in thinner samples thus explaining difference in stable damage. Apart from this difference all other damage parameters are the same for detectors of different thicknesses [5].

Evolution of the effective dopant concentration with time

Typical annealing curves for the full depletion voltage V_{fd} respectively the effective doping concentration N_{eff} for an annealing temperature of 80°C are shown in Fig. 26 [5].

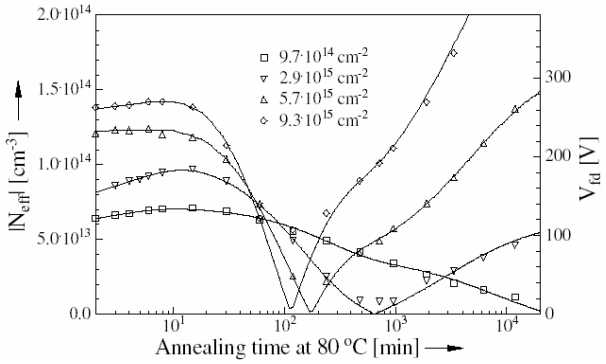

Figure 26: Examples of annealing function for 50 µm thick n-type epi diodes at 80°C after irradiation with different 1 MeV neutron equivalent fluences of 24 GeV/c protons. Lines represent model fits [5].

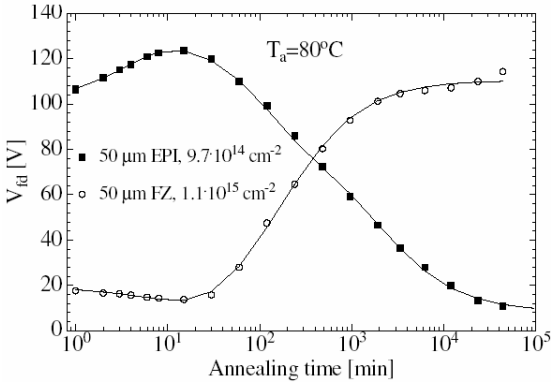

Figure 27: Comparison of full depletion voltage for thin epi and FZ diodes as function of annealing time at 80°C after $\Phi_{eq} \approx 10^{15}$ cm^{-2}.

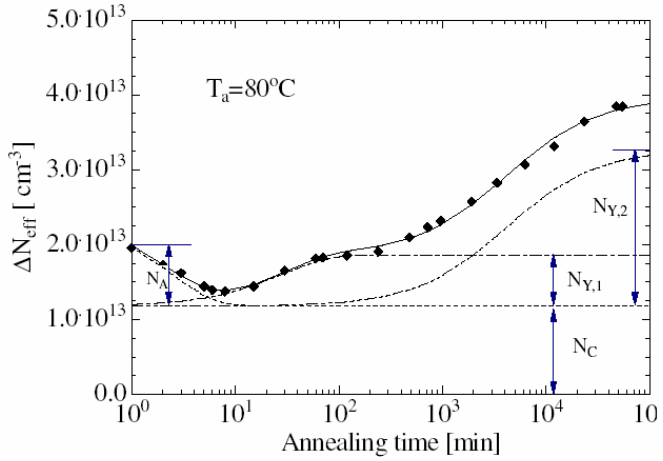

Figure 28: Different components of the annealing function for the change of the effective doping concentration in an epi-diode irradiated with Φ_{eq} = 3.1·10^{14} cm^{-2}.

The initial change of N_{eff} is probably attributed to acceptors annealing out within a short time after irradiation ("beneficial" annealing). A relative maximum of N_{eff} is observed at about 10 min. With increasing annealing time negatively charged acceptors are prevailing (similar to effects in FZ silicon) compensating the initial positive space charge and finally leading to type inversion. For an irradiation with Φeq = 9·10^{15} cm^{-2} type inversion occurs however only at about 100 min, which would correspond to a storage time of 500 days at room temperature [6]. A drastic example for the opposite annealing behavior is shown in Fig. 27.

The annealing curves were fitted with Hamburg model [6]. It turned out that a model assuming short term annealing part, stable damage (already discussed in previous paragraph) and two long term components fit the data very well as can be seen in Fig. 28 [5]. The damage parameters were extracted from the fits.

Initial ("beneficial") annealing

The initial annealing was found to be similar to the one in FZ material. The time constants for this process are comparable with the ones measured in the FZ material.

Long-term ("reverse") annealing

The late stage annealing is beneficial for epi-Si detectors as the effective acceptors compensate the stable positive space charge (see Fig. 27). The reverse annealing in epi-Si detectors consists of two components (Fig. 28). In the early stage (10 to 10^3 minutes at 80°C) a first-order process dominates while at much longer times the second-order process is responsible for creation of effective acceptors. The concentration of defects responsible for the first component was found to linearly increase with fluence (Fig. 29 [5]) and the introduction rate was extracted to be $g_{Y,1}$ = 2.9·10^{-2} cm^{-1} [5].

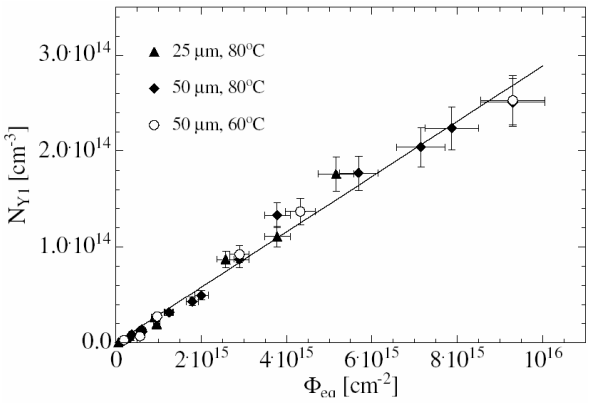

Figure 29: The first (fast) component of the reverse annealing as function of equivalent fluence. Note the universal behavior independent of epi-thickness and annealing temperature.

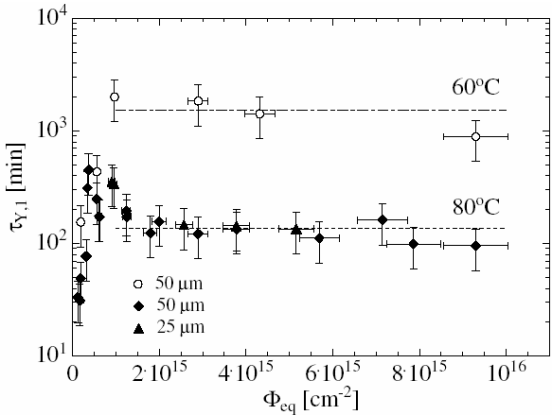

Figure 30: Time constants for the first reverse annealing component as function of equivalent fluence for temperatures at 60°C and 80°C.

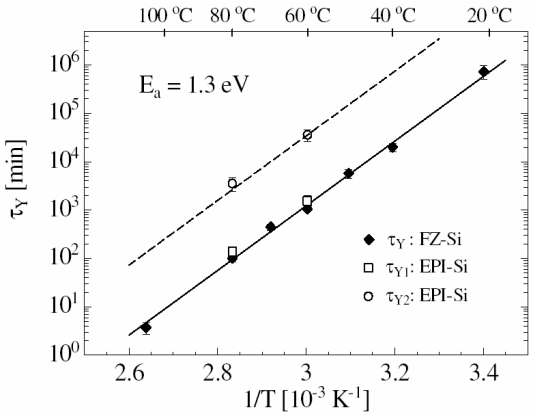

Figure 121: Reverse annealing time constant as function of temperature as reported in [8] for FZ diodes together with values measured here for epi devices.

In Fig. 30 the analyzed time constants responsible for the first reverse annealing component are displayed. Except for the lowest fluence values the time constants do not depend on the fluence, as to be expected for a first order process. The behavior at very low fluences might be due to the annealing of the vacancyphosphorus (VP) complex leading to an increase of positive space charge partly counteracting the growth of negative space charge. The difference of reaction time constants obtained from the 60°C and 80°C annealing functions indicates that the first order annealing process is governed by the same activation energy as in standard FZ detectors (E_a=1.3 eV [6]), an assumption well confirmed by the comparison shown in Fig. 31 [5].

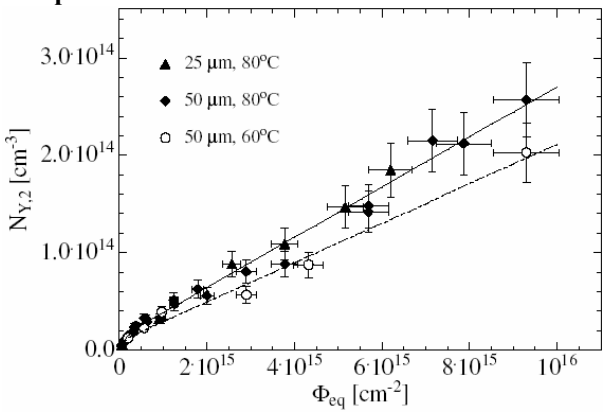

Figure 32: The second (long) reverse annealing amplitude as function of the equivalent fluence. The small differences between the 80°C and the 60°C annealing could be due to the experimental limitation.

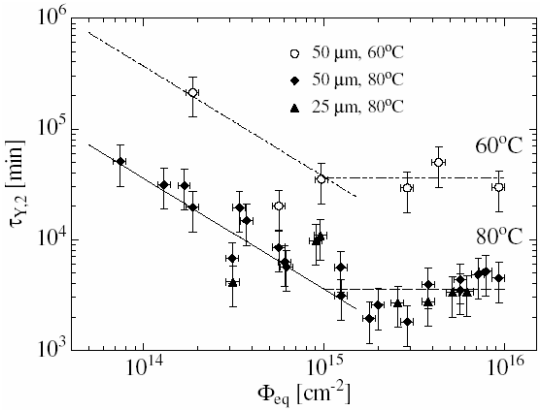

Figure 33: Time constant for the second reverse annealing component as function of equivalent fluence of the reverse annealing (depicted as N_{Y2} in section).

The long component of the reverse annealing contributes significantly to the effective doping concentration at time scales above 10^3 minutes at 80°C and 10^4 minutes at 60°C. As derived from Fig. 32 [5] apart from very low fluence values the corresponding annealing amplitude increases linearly with fluence. An introduction rate of g_{y2} = $2.6 \cdot 10^{-2}$ cm^{-1} for 80°C and a slightly lower one of $2.0 \cdot 10^{-2}$ cm^{-1} for 60°C was extracted [5]. The time constant depends linearly on the inverse of the defect concentration for fluence values below 10^{15} cm^{-2} (Fig. 33 [5]) as expected for second-order processes. The saturation effect at large fluences cannot be explained. The difference in the time constants derived from annealing at 60°C and 80°C shows that the activation energy is comparable to the one of the first component.

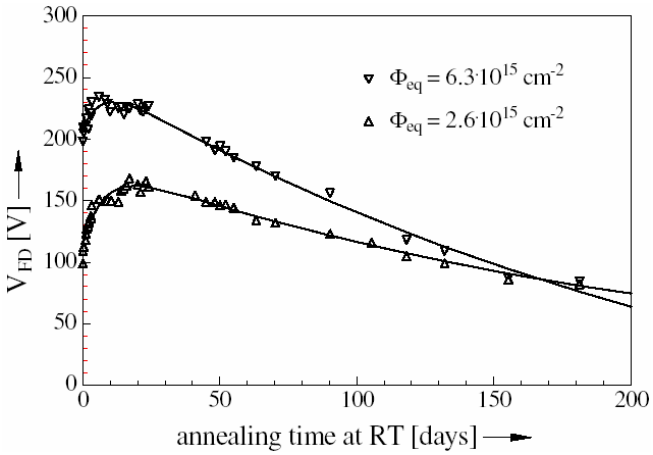

Figure 34: Room temperature annealing curves (20 – 23°C) for the full depletion voltage of 50 µm n-type epi diodes after 24 GeV/c proton irradiation with 2 different fluences. Symbols: experimental points, solid lines: fits according to a model description [4], see text.

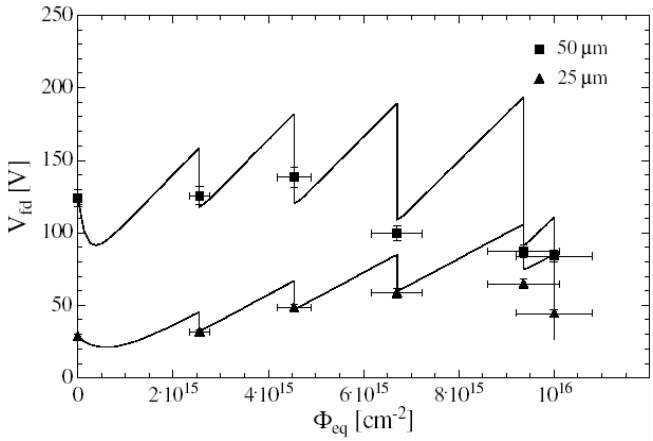

Figure 35: Results of successive irradiation with 24 GeV/c protons with steps of Φ_{eq} = $2.2 \cdot 10^{15}$ cm^{-2} followed by annealing for 50 min at 80°C. Symbols: experimental points, solid lines: simulations.

In addition to the annealing experiments at elevated tempertures, for a smaller number of samples room temperature annealing had also been carried out both after high fluence proton and neutron irradiation [9]. An example is shown in Fig. 34. In addition to the experimental data a fit had been performed, using the model description detailed in [4]. All important damage parameters are comparable with those obtained at elevated temepratures with exception of time constant which tends to be by around 4 times shorter. Evidently more annealing studies also at lower temperatures and in the time domain of interest here , i.e. equivalent to several 100 days at RT are necessary.

Simulation of SLHC scenario

In contrast to FZ silicon detectors which would always have to be stored at low temperatures in order to avoid an intolerable increase of the depletion voltage, in the case of epi-detectors such low temperature storage is not necessary. In addition keeping the detectors at room temperature during beam off periods could be very profitable because the increase of the depletion voltage as resulting from donor generation during the beam periods would be partly compensated by annealing induced acceptor generation. In order to prove this suggestion the following dedicated experiment had been performed [6]. Both 50 and 25 µm epi-diodes had been irradiated with 24 GeV/c proton fluence steps of $\Phi_{eq} = 2.2 \cdot 10^{15}$ cm^{-2}. After each damage step the diodes were annealed for 50 min at 80°C corresponding approximately to the 265 days beam off period at RT (using E_a=1.31 eV). On the other hand a simulation was used calculating the depletion voltage along the full irradiation and annealing cycles. Values extracted from a detailed parameterization fit of extensive annealing experiments at 60°C and 80°C had been employed. After each annealing step the depletion voltage had been measured followed by the next irradiation step. The meaured data of this experiment together with the simulations are given in Fig. 35 [6]. An excellent agreement was obtained both for the 25 µm as well as the 50 µm diodes.

Leakage current

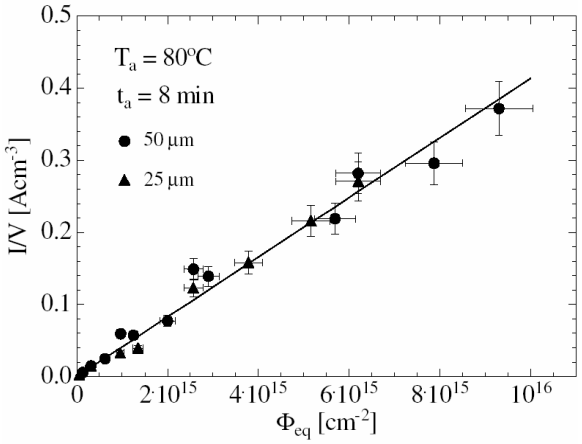

Figure 36: Reverse current per cm³ as function of equivalent fluence for 25 µm and 50 µm epi diodes, measured at the early annealing after end of short term annealing.

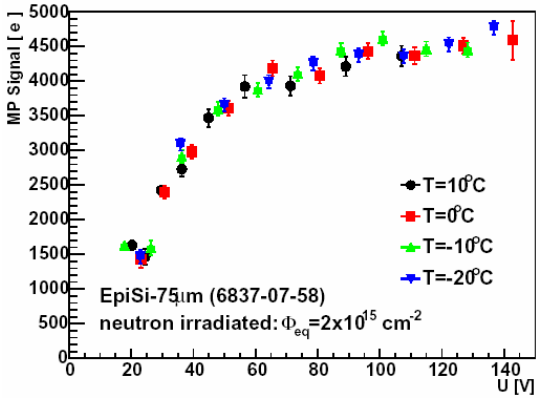

Figure 37: Dependence of signal on voltage at different temperatures. The detector was annealed for 2000 hours at 20°C prior to the measurement. Vfd of the detector was 66V.

Fig. 36 shows the results for the damage induced reverse current at the same annealing stage. The dependence on the fluence is almost identical to that known from FZ silicon devices. The extracted current related damage constant is $4.1 \cdot 10^{-17}$ A·cm^{-1} [5].

Charge collection properties

The charge collection measurements were performed on several samples irradiated with protons and neutrons up to $\Phi_{eq}=10^{16}$ cm^{-2} [10]. An example of the collected charge on voltage at different temperatures is shown in Fig. 37 for a 75 mm thick device irradiated with neutrons. Collected charge was found independent on operation temperature in the range from -20°C to +10°C, which is in agreement with expectations. The decrease of mobility with temperature is compensated by the decrease of effective trapping probabilities.

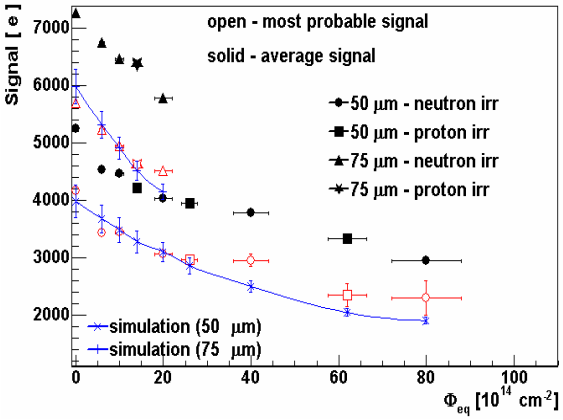

Figure 38: Collected charge for different epi-Si samples and the comparison with simulation (lines).

It was found that full depletion voltage determined from C/V agrees with the one determined from the Q/V [10] and that over-depleting the detectors doesn't improve much the signal. Average of the collected charge above the full depletion voltage as the function of fluence is shown in Fig. 38. To evaluate the effect of trapping the measured points were compared with simulation (details about it can be found in [13]). Below $\Phi_{eq}=2 \cdot 10^{15}$ cm^{-2} the simulation agrees nicely with measurements for both 50 and 75 µm diodes while at larger fluences underestimates the collected charge. Charge collection at $\Phi_{eq}>2 \cdot 10^{15}$cm^{-2} is strongly dependent on effective trapping times of electrons and holes and much less on electric field distribution. This leads to conclusion that effective trapping probability at very high fluences could be lower than extrapolated from measurements found in [12,13,14,15].

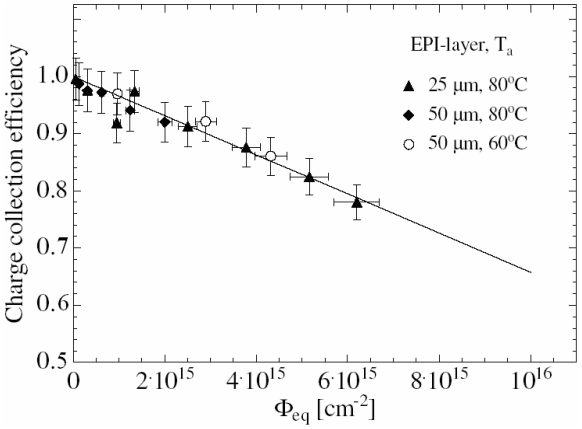

Figure 39: Charge collection efficiency as function of equivalent fluence after 24 GeV/c proton irradiation for 25 µm and 50 µm epi diodes as measured with 5.8 MeV α-particles. The solid line represents the linear fit to the measured points.

The charge collection measurements were performed also using collimated beem of 5.8 MeV α-particles with penetration depth of 24 µm [5]). The measurement points shown in Fig. 39 are obtained in the same way as for ^{90}Sr measurements [10] with bias voltage always kept sufficiently above the depletion voltage. Taking into account that in this case holes and electrons don't contribute equally to the induced charge for 50 µm thich detector, the measured CCE is compatible with the one obtained for electrons from ^{90}Sr.

Summary of Epi-Si measurements

Superior radiation hardness of Epi-Si in terms of N_{eff} has so far been demonstrated for both neutron and proton irradiated samples. Good reproducibility of results and the ability to successfully model the damage enable long term prediction of performance. The main difference between n-type epi-Si and FZ materials is generation of positive space charge in epi-Si, which doesn't anneal out i.e. stable damage. As the introduction rate of negative space charge, which appears during the late annealing stages, surpasses the introduction rate positive space charge it is possible to find an operation scenario where effective acceptors compensate donors. Effective doping concentration can thus be controlled in such a way that detectors could be fully depleted over entire period of SLHC. Measurements performed so far show that it will be possible to keep detectors at RT during the beam off period. Charge collection measurements using minimum ionizing electrons from ^{90}Sr source have been performed at equivalent fluences of ~10^{16} cm^{-2} and compared to simulations. Very good agreement was found for $\Phi_{eq}<2\cdot10^{15}$ cm^{-2} while at larger fluences more charge is measured than expected. Keeping detectors with n^+ read-out at room temperature could have additional advantage, because effective trapping probability for electrons anneals roughly by 40% [12,13,16].

In the near future p-type epi-Si detectors will be produced on p-type Cz substrate to investigate the radiation hardness of n^+-p epi-Si detectors, where major contribution to the signal comes from drift of electrons. Also detectors with higher initial resistivity and larger thickness will be fabricated.

References

[1] G. Kramberger et al., Nucl. Instr. and Meth. A 515 (2003) 665-670.
[2] A. Barcz, SIMS laboratory, Institute of Phhysics, Warsaw; private communication
[3] Li Long, Institute for Micro Sensors CiS, Erfurt, private communication
[4] G. Lindström, E. Fretwurst, F. Hönniger, G. Kramberger, M. Möller-Ivens, I. Pintilie and A. Schramm, "Epitaxial Silicon Detectors for Particle Tracking -Radiation Tolerance at Extreme Hadron Fluences", submitted for publication in Nucl. Instr. and Meth. A.
[5] G. Lindström, E. Fretwurst, F. Hönniger, G. Kramberger, M. Möller-Ivens, I. Pintilie. A. Schramm; "Radiation tolerance of epitaxial silicon detectors at very large proton fluences"; in press Nucl. Instr. and Meth. A.
[6] M. Moll. PhD thesis. University of Hamburg 1999; DESY THESIS-1999-040, December 1999
[7] I. Pintilie, M. Buda, E. Fretwurst, F. Hönniger, G. Lindström, J. Stahl; Radiation induced donor generation in epitaxial and Cz diodes. Accepted for publication in Nucl. Instr. a. Meth. A.
[8] I. Pintilie, M. Buda, E. Fretwurst, G. Lindström, J. Stahl; Stable radiation induced donor generation in silicon diodes, submitted for publication in Nucl. Instr. and Meth. A
[9] I. Dolenc et al.; "Room temperature annelaing of Epi-Si diodes"; presented at 7th RD50 Workshop, CERN 2005.
[10] G. Kramberger et al., Nucl. Instr. and Meth. A 554 (2005) 212-219.
[11] G. Kramberger et al., Nucl. Instr. and Meth. A 457 (2001) 550.
[12] G. Kramberger et al., Nucl. Instr. and Meth. A 481 (2002) 297-305
[13] A. G. Bates and Michael Moll, " A comparison between irradiated Magnetic Czochralski and Float Zone silicon detectors using the Transient Current Technique ", in press Nucl. Instr. And Meth.
[14] O. Krasel et al., IEEE Trans. NS 51(1) (2004) 3055.
[15] E. Fretwurst et al., Survey of Recent Radiation Damage Studies at Hamburg, 3rd RD50 Collaboration Workshop, 4th November 2003.
[16] T. Lari et al., Nucl. Instr. and Meth. A 518 (2004) 349.

6. New materials

6.1. Research activity on Silicon Carbide

Detector processing

Two types of detectors were manufactured on n-type 4H-SiC epitaxial layers grown earlier at the Institute of Crystal Growth of Berlin and on CREE epilayers. The diodes were processed in the framework of two sub-projects: 1) so-called Alenia project, Schottky diodes, and 2) Perugia University jointly with CNR-IMM, Bologna, p^+-n junction diodes.

Alenia Marconi Systems diodes [1-3]

Two batches of common RD50 samples with Schottky barriers and a guard ring were manufactured by Alenia Marconi Systems (AMS), Rome.

The first batch manufactured earlier and described in [1] was processed on epitaxial layers 4H-SiC grown by IKZ (Berlin) and CREE Research (USA). The thickness of the layers was measured by optical interferometry and was in the range 20 to 50 μm and about 50 μm for CREE and IKZ layers, respectively. The doping concentration was $(4\text{-}5)\cdot10^{14}$ cm^{-3}. Specific feature of processing is that in these samples Schottky barrier of the diodes was made as Ni_2Si contact. The back contact was obtained by a deposition of a multilayer Ti/Pt/Au onto the back side of the substrate. The biggest diameter of the sensitive region was 2.5 mm. Thick (5 μm) gold dots with a diameter of 60 μm were deposited on the diode and guard ring dots for wire bonding.

The second batch was manufactured by AMS in 2005 on 2" CREE grown 4H-SiC layers with similar parameters: thickness of 50 μm and doping concentration of $5\cdot10^{14}$ cm^{-3}. The procedure is described in [2, 3]. Photomasks were developed in Torino. The layout of the cells with multiplicity of 4 diodes per cell and the diode are presented in Figs. 1 and 2, respectively. The ohmic contact was made on the whole back of the substrate (C-face) by the deposition of the multilayer Ti/Pt/Au (30/30/150 nm) followed by the annealing at 1000°C in a N_2/H_2 atmosphere. Schottky barrier was made by sequential evaporation of Ni and Au, each film of 100 nm. Electrical contacts with bonding pads air-bridge were electroplated with Au, 3μm thick. The device diameter are: 2.5 – 3.0 – 5.0 mm. The diodes were processed as common RD50 samples and are available for community.

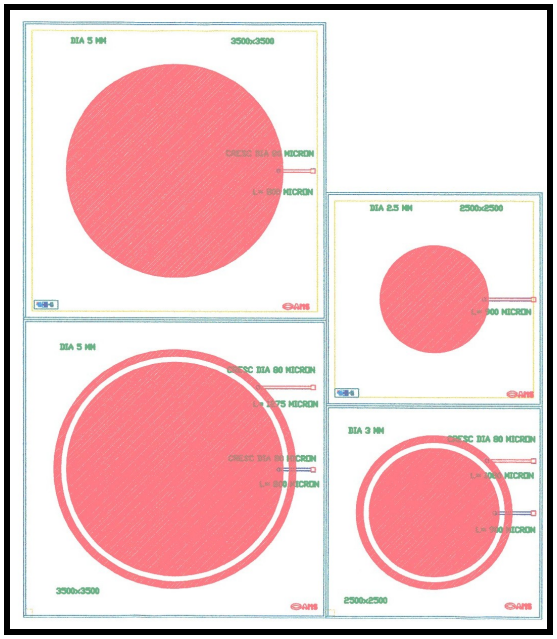

Fig 1. Layout of a cell with SiC diodes processed with photomask set of Torino group.

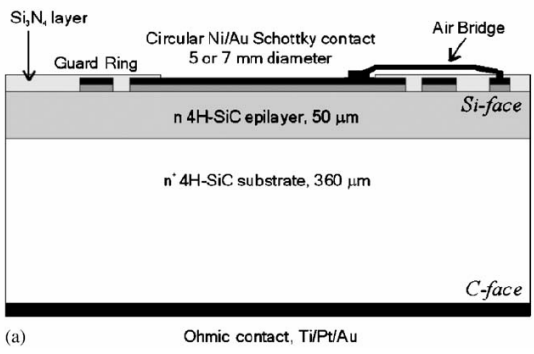

Fig. 2. Design of SiC diodes processed by AMS

Perugia diodes [4, 6, 7]

In a previous work [4] a collected charge on p^+n junction SiC diodes was reported of the order of 1700 e^-. In the literature [5] the maximum collected charge reported so far for SiC detectors is of the order of 2200 e^-. Recently [1] radiation hardness of SiC Schottky diodes has been analysed after 24 GeV/c proton irradiation. These diodes had been tested with β particles and a charge collection efficiency (CCE) of the order of 30% has been achieved after a fluence of $1.4 \cdot 10^{16}$ p/cm^2. Moreover, a technological process based on only Schottky barriers is unsuitable for the realization of complex radiation detectors featuring an integrated electronic readout on board of the detector chip. In the latter case, p-n junctions are needed for building electronic switches like MOSFETs or JFETs.

The new SiC p^+-n junction diodes have been processed in March 2005 and the first results on their study were presented at 6th and 7th RD50 collaboration workshops [6, 7]. The diodes were manufactured on epitaxial layers 4H-SiC grown by IKZ (Berlin). Parameters of the wafer are specified below:

Wafer IKZ N41-32, 2" n-type 4H-SiC Si face
Doping: wafer: $5 \cdot 10^{18}$ cm^{-3}
buffer layer (5 μm): $1 \cdot 10^{16}$ cm^{-3}
nominal epilayer (55 μm): $1.6\text{-}2.1 \cdot 10^{14}$ cm^{-3}

A mask set for processing p^+-n junction diodes was designed and fabricated in 2004 [4]. Two different chips are included, called SiCPOS 1 and SiCPOS 2. The main difference is the density of diodes: the number of chips SiCPOS 1 is greater than SiCPOS 2. The SiCPOS chip with a set of p^+/n junction diodes is presented in Fig. 3. The p-n diode structure (Fig. 4) made at CNR-IMM (Bologna, Italy) is based on a 0.45 μm deep, $N_A = 4 \cdot 10^{19}$ cm^{-3} doped p^+ emitter, ion implanted in the n-type epilayer. The annealing for the electrical activation of the implanted Al was done in an inductive furnace at 1600°C for 30 min. The diameters of the diodes are 200 μm to 1000 μm and the area is in the range 0.0028 to 0.0078 cm^2. All diodes featured 200 μm wide junction terminal extensions featuring a doping $N_A = 4 \cdot 10^{17}$ cm^{-3}. Schottky diodes with a diameter of 400 μm have also been incorporated in the design. A metal scheme composed of Al-1%Si(350nm)/Ti(80nm) was deposited on the front and Ni was deposited on the back. The metal contacts were alloyed in Ar ambient at 1000°C for 2 min. A "virgin" quarter of the SiCPOS wafer is dedicated to the RD50 community.

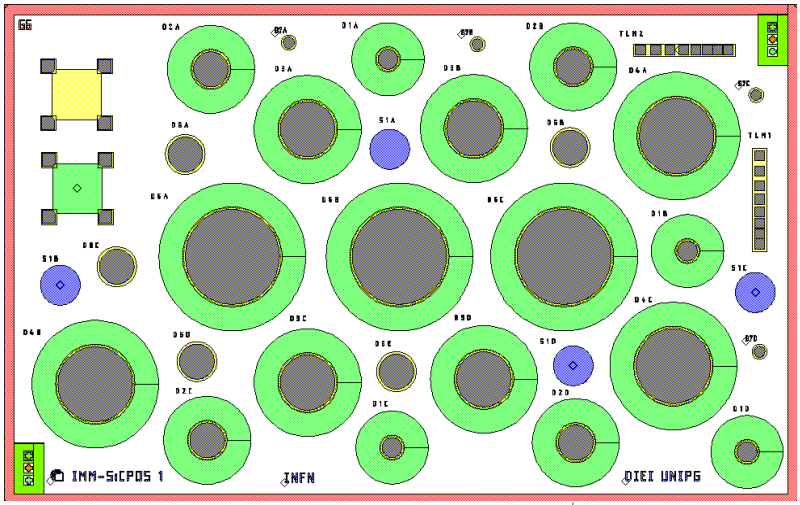

Fig. 3. Topology of the SiCPOS chips with a set of p^+/n junction diodes

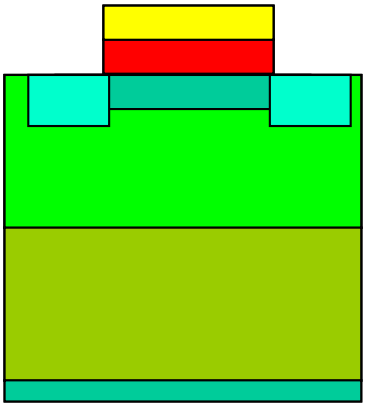

Fig. 4. Design of SiC diodes processed by CNR-IMM of Bologna

Characteristics of as-processed SiC detectors

Alenia detectors

SiC diodes from batch 1 were studied in 2004-2005 and some data were presented in RD50 Annual Report 2004 [8]. Ref. [1] represents the results of the systematic studies of the diodes before and after irradiation. The parameters of the diodes from batch 1 processed on IKZ and CREE SiC epilayers are specified in Table 1 [1]. The detectors were characterized by C-V measurements and the measurements of the CCE with α-particles ^{241}Am (E_α = 5.5 MeV) and MIPs from a ^{90}Sr source. In the latter case the shaping time of the amplifier was 2.4 μs and equivalent noise charge (ENC) was 280 e^-.

C-V characteristic of the diode plotted as C^{-2} vs. V is linear and gives the mean effective doping concentration $N_{eff} = (4\text{-}5)\cdot 10^{14}$ cm^{-3}. In the CCE measurements with MIPs the maximal reverse bias is limited by the increase of the current (presumably due to surface effects) and reduction of S/N ratio. β charge collection measurements yield a collected electron equivalent charge of (1400±200) e^- at V = 200 V. The Charge Collection Distance *CCD* that is defined as: *CCD* = *CCE* x (*active thickness*) was estimated from the data on the CCE with MIPs with the assumption on the value of *N* = 55 e/h pairs/μm. For different diodes the *CCD* of the carriers is 16-18 μm and of about 25 μm for 100 V and 200 V, respectively. Comparison of the *CCD* to the corresponding depletion depth of 16 μm (100 V) and 23 μm (200 V) shows that CCE equals to 100%.

Table 1. List of investigated samples from batch 1 processed by Alenia with the corresponding fluences [1].

Batch	Sample	Schottky contact	Manufacturer	Active thickness (μm)	N_{eff} (cm^{-3})	Irradiation
SiC038105	# G1	Au	CREE	24.5	5.5×10^{14}	1.4×10^{16} p/cm^2
IKZ N31-39	# 08	Ni_2Si	IKZ	51	5.0×10^{14}	No
R0501-04	# 86	Ni_2Si	CREE	45	$4.0 \pm 0.4 \times 10^{14}$	No
R0501-04	# 88	Ni_2Si	CREE	45	$4.0 \pm 0.4 \times 10^{14}$	No
IKZ N31-39	# 32	Ni_2Si	IKZ	50	5.0×10^{14}	3.0×10^{15} n/cm^2
R0501-04	# 21	Ni_2Si	CREE	45	$4.0 \pm 0.4 \times 10^{14}$	3.0×10^{15} n/cm^2
IKZ N31-39	# 55	Ni_2Si	IKZ	50	5.0×10^{14}	7.0×10^{15} n/cm^2
R0501-04	# 32	Ni_2Si	CREE	39	$4.0 \pm 0.4 \times 10^{14}$	7.0×10^{15} n/cm^2

Characterization of the SiC diodes from batch 2 was carried out by I-C and C-V measurements [3] and the results are presented in Figs. 5-6. A criteria for reverse current was chosen as 10 nA at V<100 V that gives the yield of accepted diodes of 60% and 44% for small (2.5-3 mm) and large (5 mm) samples, respectively, and the current density within 30 nA/cm^2. The forward current vs. voltage curves plotted in semilog scale were linear. Effective doping concentration $N_{eff} = N_D - N_A$ defined from C-V curves was in the range $(0.5\text{-}2.0)\cdot 10^{15}$ cm^{-3}.

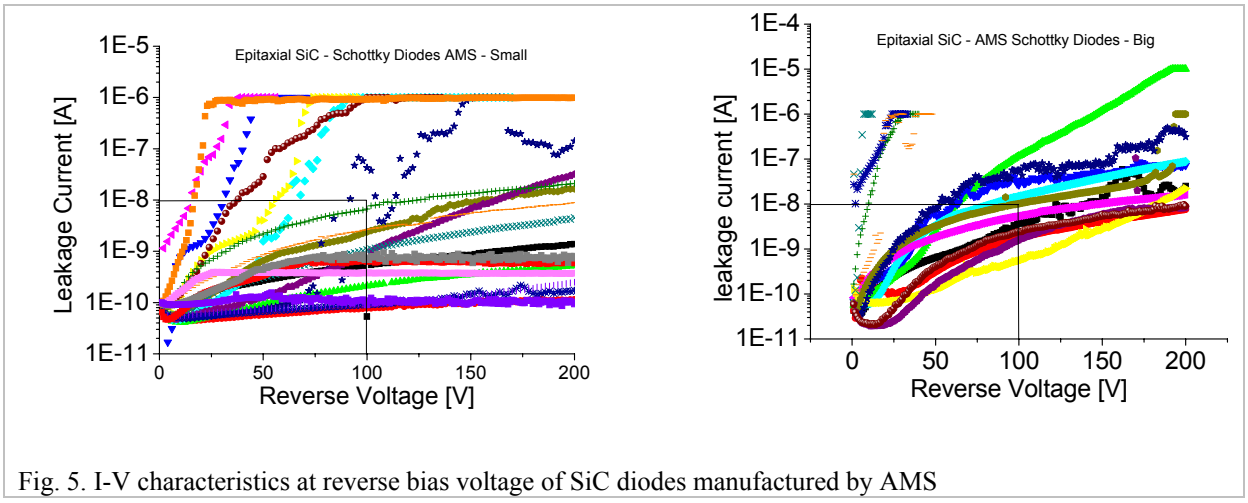

Fig. 5. I-V characteristics at reverse bias voltage of SiC diodes manufactured by AMS

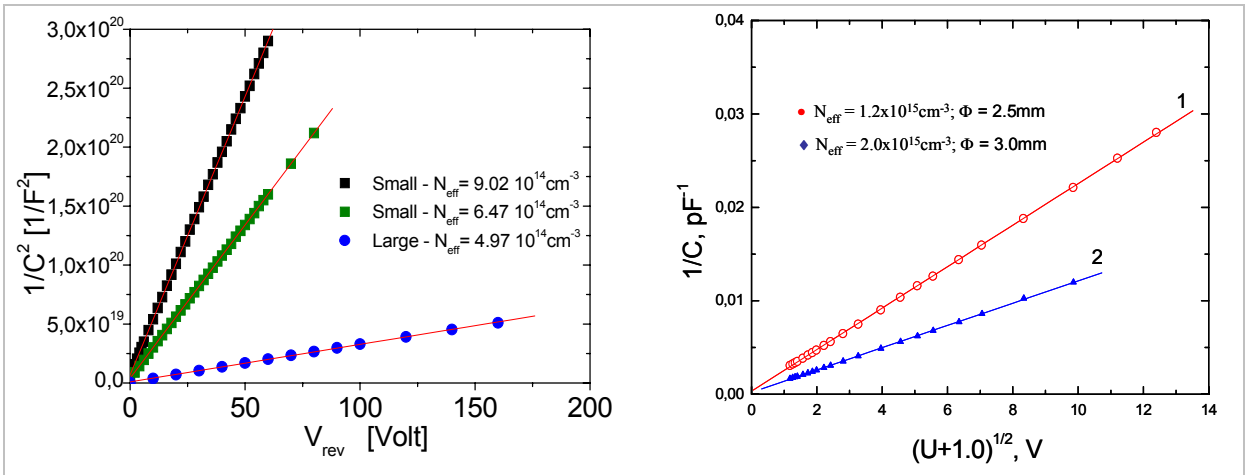

Fig. 6. C-V characteristics of AMS diodes measured at INFN (left) and Ioffe Institute (right, diodes ## C1 (1) and B2 (2))

Initial data on the charge collection efficiency the diodes from batch 2 (common RD50 samples) are obtained at the Ioffe Institute. The study is performed in the framework of sub-project "Radiation hardness of SiC-films to high fluences of 8 MeV protons". As-processed diodes reached Ioffe without preliminary test and therefore I-V and C-V measurements were initially carried out. Standard instrumentation was applied for the method of pulse-height analysis to determine the detector characteristics: CCE, energy resolution (*FWHM*) and character of the detector noise. Amplitude spectra from the α-particles ^{244}Cm with the impinging particle energy of 5.4 MeV were analyzed within a total channel number of 4000. The measurements were carried out in the air.

α-particle spectra of the diodes with the best characteristics (## B2 and C1 with diameters of 3.0 mm and 2.5 mm, correspondingly) are shown in Fig.7. The doping concentration is $4.1 \cdot 10^{15}$ cm^{-3} and $1.2 \cdot 10^{15}$ cm^{-3} for the diodes B2 and C1, respectively (Fig. 6, right). An essential distinction between the two samples was also observed in α-particle spectra. The other samples showed instability and increased noise at low bias voltage that does not allow application of high enough bias. An increased width of spectra of the diode # B2 is observed that is presumably related to the non-uniformity of the carrier lifetime over the SiC epilayer within this specimen.

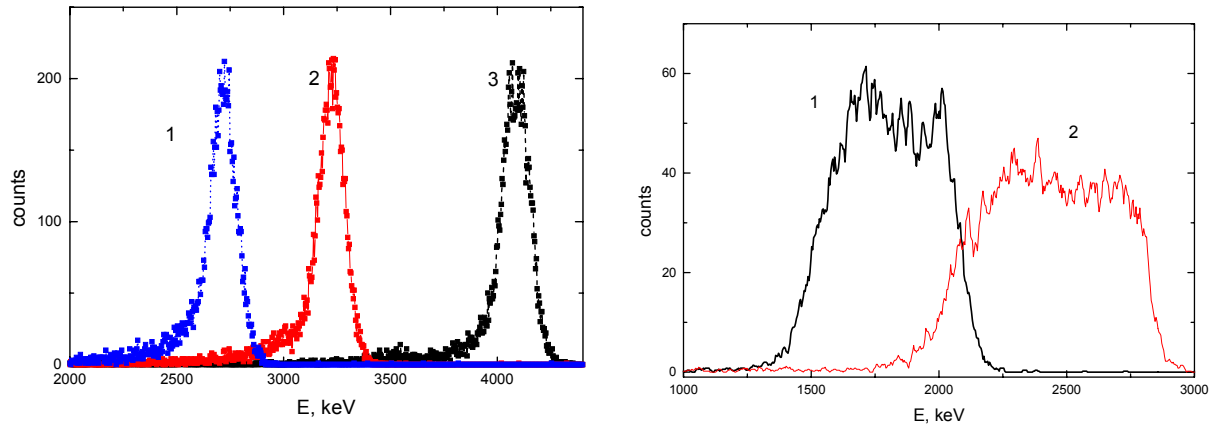

Fig. 7. α - particle spectra for Alenia diodes:
Left: # C1: 1 – 5 V; 2 – 20 V, 3 – 70 V; Right: #B2: 1 – 6 V, 2 – 50 V.

The approach for evaluation of the diffusion length L_D in detectors from epitaxial SiC films has been developed and described in [9]. The approach is based on charge collection data received from α-spectra analysis. In the method the diffusion length values in range 0.5-50 μm are suggested. Accordingly, the minimal value of a corresponding carrier lifetime is of about ns. The diode structure operated at the reverse bias is considered. Injection is carried out by α-particles of natural decay in a

mode of single-particle count. The nuclear spectroscopy technique measures the value of the nonequilibrium charge that diffuses in the base region towards the electric field region.

Calculations of the charge losses λ due to carrier diffusion were carried out as a function of a parameter ($R - W$), which is a penetration length of α-particle track with a range R inside the base region [10]. The obtained equation is:

$$\lambda(R-W) = \frac{\int_0^{R-W} g(x-W)\left[1-\exp\left(-\frac{x-W}{L_D}\right)\right]d(x-W)}{\int_0^{R} g(x)dx}$$

where $g(x)$ is the distribution of the energy loss of α-particles in ionization (Bragg ionization curve). The function has power-character: $lg\lambda = k + lg(R\text{-}W)$ and gives the relation between the diffusion length and the degree of an exponent and numerical factor.

Diffusion length of holes for the diode C1 was defined by comparison of the calculated charge loss with the variable parameter $R - W$ to the charge loss received in the experiment (Fig. 8). The experimental data are close to the dependence calculated with the assumption of L_D of 10 μm. Fitting of the experimental data gives L_D of 6.3 μm.

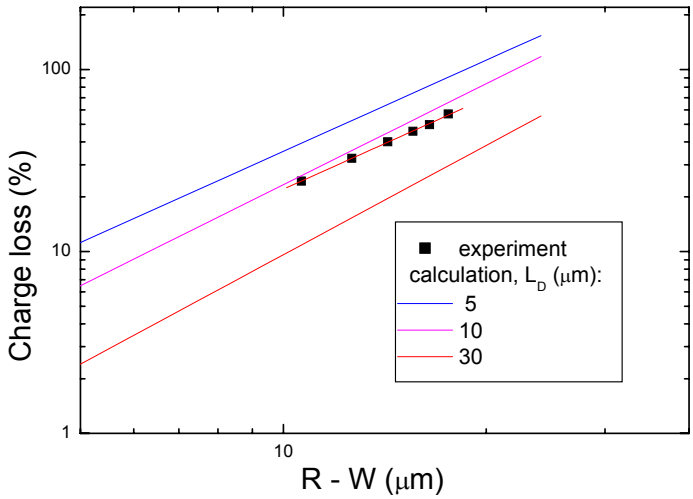

Fig. 8. Definition of diffusion length of holes for the diode # C1 from batch 2 processed by Alenia by adjustment of the experimental data on the charge loss to the calculated values [9].

Perugia detectors

Figs. 9 and 10 show the forward I-V characteristic and the ideality factor of as-processed p^+-n junction diodes as a function of the forward voltage for a typical good sample.

At reverse bias voltage the diode breakdown voltages were above 1000 V, which is the maximal bias voltage that could be applied. At 1000 V the leakage current was of the order of 1 nA for all the measured diodes (Fig. 11), independently of the diode area. Fig. 12 shows the reciprocal of the square capacitance $1/C^2$ versus reverse voltage acquired for a typical p^+n diode. The punch through depletion voltage is near 220-250 V for all diodes, even if a simple evaluation of this figure is difficult since the doping concentration is not constant as a function of the thickness of the depleted region. The average net doping concentration N_{eff}, extracted from Fig. 12, is $1.5 \cdot 10^{14}$ cm^{-3}, in agreement with the nominal value. The smooth decrease of the capacitance after the full depletion could be associated with the depletion of the buffer layer grown between the bulk and the epilayer. The buffer layer thickness is 3 μm with nominal donor doping $N_D = 1 \cdot 10^{16}$ cm^{-3}.

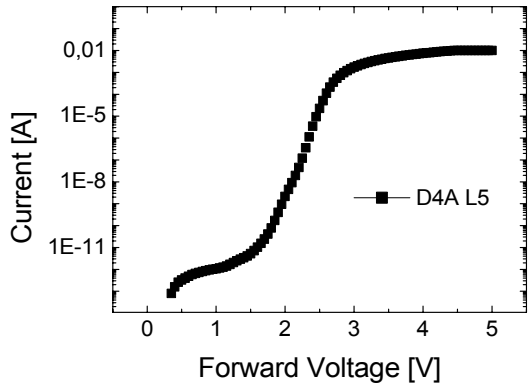

Fig. 9. Typical forward Current-Voltage characteristic

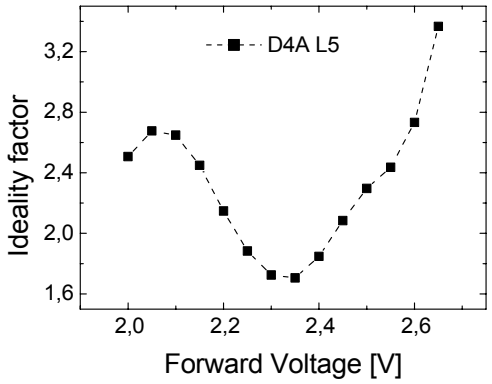

Fig. 10. Typical ideality factor as a function of the forward voltage

The charge collection efficiency to MIPs has been investigated by a ^{90}Sr β source. The equivalent noise charge of the measuring set-up is linearly proportional to the capacitance of the detector and is given by $ENC = 200e^- + 4.6e^-/pF$. The pulse height spectrum giving the charge response measured by the SiC detectors when exposed to ^{90}Sr β source was measured as a function of the reverse voltage in the range 0-605 V. At each bias point the signal was stable and reproducible, showing the absence of polarisation effects. This indicates that trapping/detrapping effects onto deep levels are negligible, due to the high crystalline quality of the material.

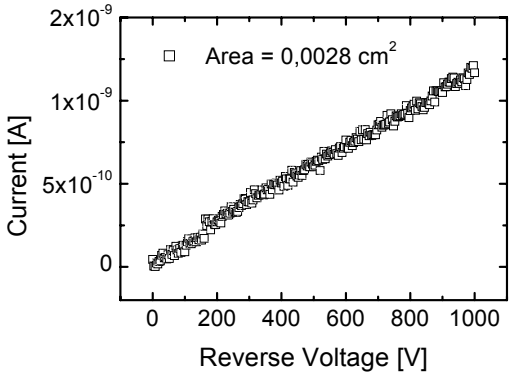

Fig. 11. Reverse current measured at room temperature

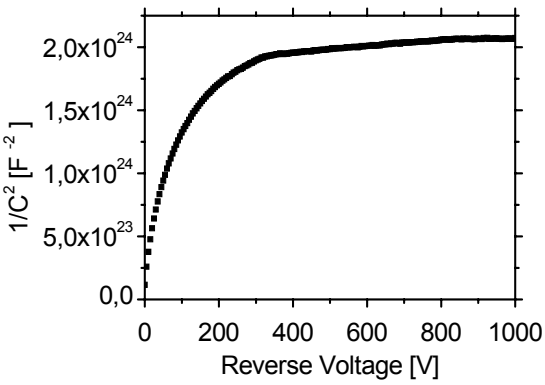

Fig. 12. 1/C2 versus reverse voltage acquired for a typical p+n junction SiC diode

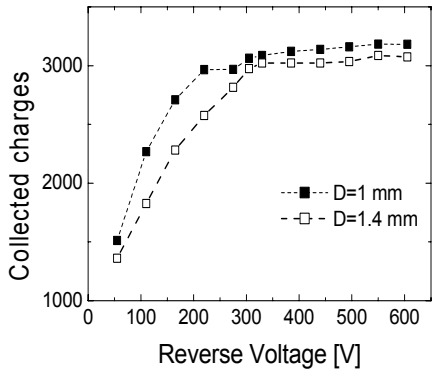

Fig. 13. Collected charges as a function of the applied reverse voltage for two p+n diodes featuring diameters of 1 and 1.4 mm

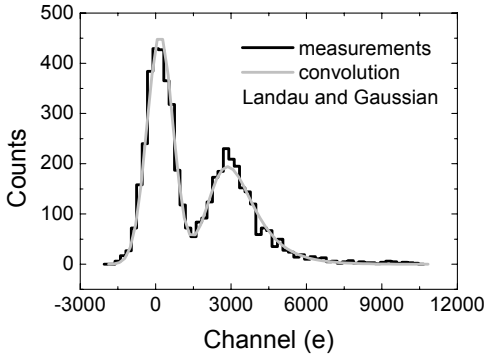

Fig. 14. Convolution of the signal and the pedestal at 330 V. The signal and the pedestal are well separated and deconvolution is easily accomplished

Fig. 13 shows the collected charge as a function of the applied reverse voltage for two diodes with a diameter *D* of 1 mm and 1.4 mm, respectively. As expected, the asymptotic values of collected

charge are approximately the same for the two diodes within an experimental error of about 100 e^-. On the other hand, a larger efficiency of a smaller diode in the case of low applied voltage can be attributed to a greater relative weight of the collection volume of the p^- junction terminal extension in the case of a smaller diode. In fact, this volume is the same for the two diodes, while the collection volume of the depleted region associated with the p^+ emitter increases as the diode diameter increases. At 220 V the collected charge is 2970 e^- for a smaller diode and saturates at 3150 e^- near 350 V. To our knowledge, this is the highest collected charge reported so far for SiC detectors. At bias voltages over than 100 V the spectrum was found to consist of two clearly separated peaks (Fig. 14). The peak on the left, called pedestal, is due to false events enlarged by noise contribution, and is well fitted by a Gaussian distribution. The peak on the right is the detector signal and is well fitted by a Landau distribution convoluted with the former Gaussian. Fig. 15 shows the Landau part of the pulse height spectrum at different voltages for the diode with a diameter of 1 mm. Around 250 V the signal saturates, in agreement with the C-V results. Under the hypothesis that the source produces 55 e/h pairs/μm, 58 μm of active region is obtained, in good agreement with the nominal thickness of the epilayer and of the buffer layer.

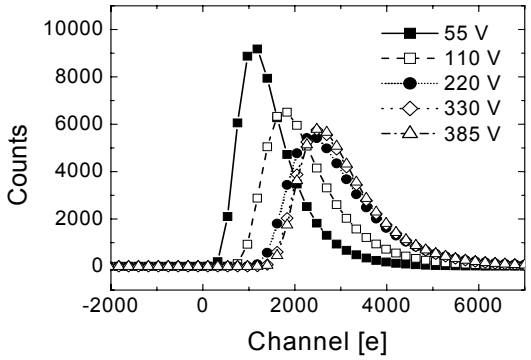

Fig. 15. Pulse height spectrum of the collected charge signal at different voltages for the diode with $D = 1$ mm. At 250 V the signal saturates

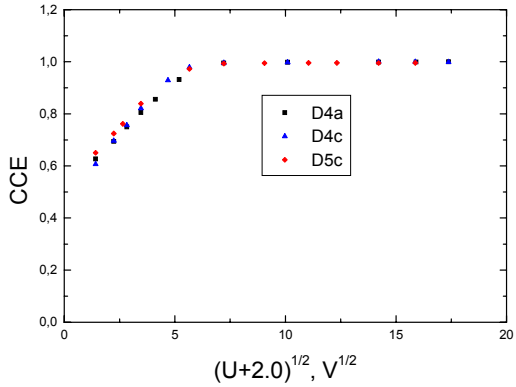

Fig. 16. CCE versus reverse bias for three p+-n diodes from the chip M6 manufactured by Perugia.

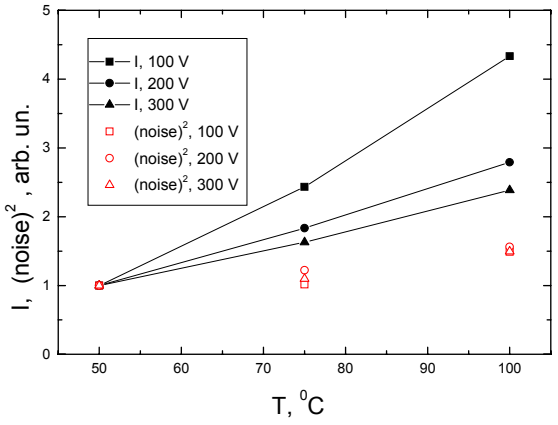

Fig. 17. Dependence of the relative changes of the reverse current and noise on temperature.

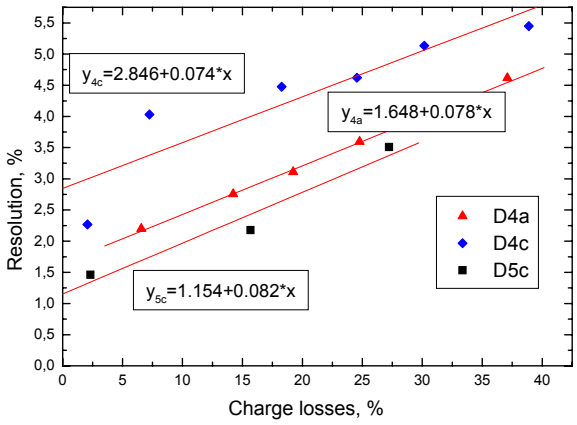

Fig. 18. Experimental dependences of FWHM on the charge losses and their linear fits for detectors from the chip M6.

The other set of the measurements of the p^+-n junction SiC diodes dedicated from Perugia was performed at the Ioffe Institute on the chip M6. Experimental results are presented in Figs. 16-18. The diameter of the studied detectors is 0.8 mm (D4) and 1.0 mm (D5). CCE in the sensitive region of the structure measured by α-particles vs. the reverse bias voltage is depicted in Fig. 16. Maximal reverse bias is 300 V. CCE equals to 1 at V ≈ 60 V. Linear growth of the dependences at V < 60 V shows the CCE increase due to the increase of W ($W \sim V^{0.5}$). The diffusion lengths are respectively: D4A - 14 μm, D4C - 12.8 μm, and D5C - 15.4 μm.

The low noise level ensures high energy resolution of the detectors. In Fig. 17 the dependences of the reverse current and a square of the noise on temperature for the diode # D5C are presented. Linear increase of a square of the noise with a current is specific for shot noise. In the studied diodes the detector noise is practically constant at these temperatures. At the same time the increase of the current in the experimental curves is significant. Therefore the current is controlled by the growth of the leakage rather than by the bulk generation current.

The charge losses originate from the incomplete charge transfer due to carrier diffusion. According to [11] the dependence of the energy resolution (*FWHM*) is proportional to the charge loss λ: $FWHM = k \times \lambda$. The slope of dependence characterizes non-uniformity of the bulk properties of the SiC epilayer with respect to the collection of the carriers generated within the individual tracks of α-particles. In Fig. 18 the experimental data on *FWHM* vs. λ and the linear fits are presented. The values of k derived from the fits are of about 0.10 that indicates a high uniformity of the SiC epilayer bulk. The best experimental value of *FWHM* is 1.5% that is in agreement with earlier results [5].

Results on the evaluation of the theoretical limit of the energy resolution of SiC detectors for ions [11] and on radiation hard devices based on SiC [12] have been presented at the International Conference on Silicon Carbide and Related Materials (ICSCRM 2005). The main contribution to *FWHM* arises from elastic scattering events of impinging particles with the atoms of crystal lattice.

Characteristics of irradiated detectors [1, 7]

Alenia detectors

The investigation of Alenia diodes processed in batch 1 on the epitaxial layers 4H-SiC grown by IKZ and CREE started in 2004 and some results for the diodes from batch 1 were described in [8]. The diodes were irradiated by increasing fluence of 1 MeV neutrons at TRIGA Nuclear Reactor, Ljubljana. The diode # G1 manufactured as Schottky diode with Au contact on the epilayer grown by CREE was irradiated by 24 GeV/c protons with a fluence F_p of $1.4 \cdot 10^{16}$ cm^{-2} at CERN PS (Table 1).

The capacitance of the diodes irradiated by a fluence beyond 10^{15} cm^{-2} was constant for any radiation and corresponded to the geometrical dimensions of the diodes that is the evidence that SiC becomes compensated and the resistivity is close to intrinsic.

The charge collection measurements with α-particles have been performed over a wide range of irradiation than that presented in Table 1. The CCE and collected charge (in e^-) vs. bias voltage ranging up to 800 V of the diodes processed on CREE epilayer and irradiated by neutrons are shown in Fig. 19. A strong decrease in the CCE is observed at a fluence level of ~10^{15} cm^{-2}.

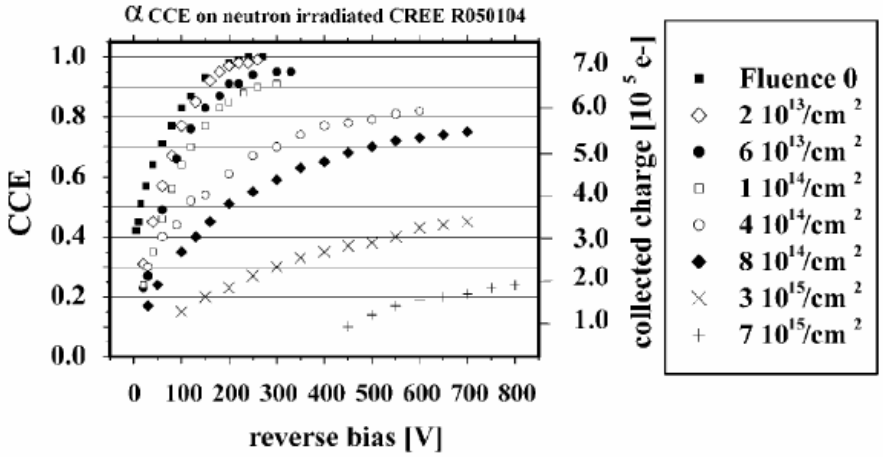

Fig. 19. α-particles CCE and collected charge vs. bias voltage curves of the diodes from batch 1 processed on CREE epilayers irradiated by neutrons.

Charge collection distance in irradiated diodes has been defined from β MIP charge collection measurements. In the diode # G1 irradiated by F_p of $1.4 \cdot 10^{16}$ cm^{-2} this parameter is reduced from 25

μm to about 30% (~ 7 μm) at the highest voltage of 800 V (Fig. 20). The bulk of SiC epilayer is intrinsic and the response is of the same order for both bias polarities (Fig. 21). The results on *CCD* presented in Fig. 22 demonstrate two features: 1) similar degradation of the *CCD* occurs in irradiation by equivalent fluence of neutrons and protons; 2) at the same fluence and bias voltage the *CCD* defined from α-particle data is larger than that from MIPs. This may be related to an enhanced hole trapping in charge collection that prevails over electron trapping.

The main result of the recent studies of irradiated SiC detectors [1] is that even at the highest irradiation fluence ($1.4 \cdot 10^{16}$ p/cm^2 and $7 \cdot 10^{15}$ n/cm^2) the diodes are still able to detect α and β particles. The CCE ranges from 25% to 30% (protons, *CCD* of 7 μm) and of about 18% (neutrons, *CCD* of 5 μm) at the highest reverse bias though the response is quite low (650 e^-). These values are smaller than those revealed in detectors from epitaxial Si with similar thickness. However they are received at room temperature while operational temperature for Si detectors irradiated at fluence beyond 10^{15} cm^{-2} is –10° to –20°C.

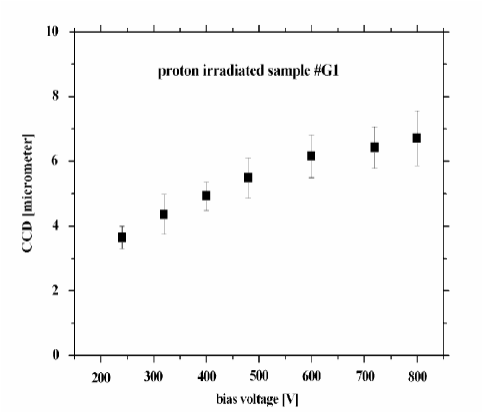

Fig. 20. β particle CCD curve of sample CREE # G1 irradiated at a fluence of $1.4 \cdot 10^{16}$ p/cm^2

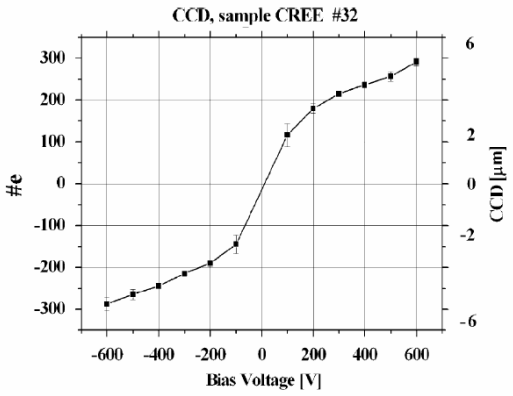

Fig. 21. β particle CCD curve of sample CREE # 32 irradiated at a fluence of $7 \cdot 10^{15}$ n/cm^2 at different bias polarities

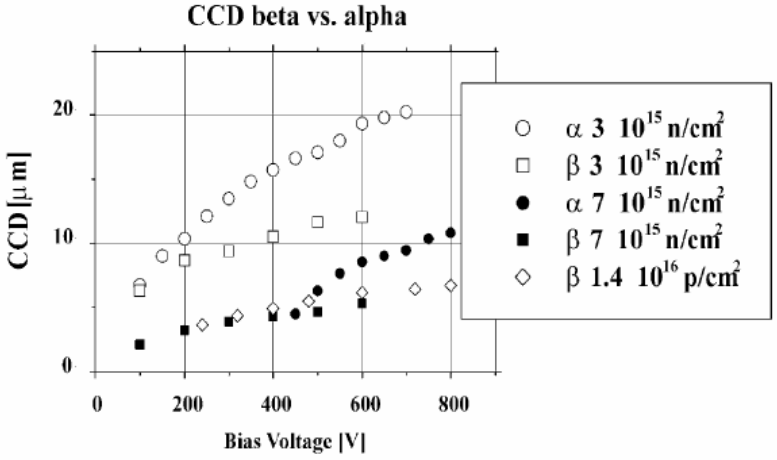

Fig. 22. β and α CCD curve of samples CREE irradiated at a fluence of $3 \cdot 10^{15}$ and $7 \cdot 10^{15}$ n/cm^2 and $1.4 \cdot 10^{16}$ p/cm^2.

Perugia detectors [7]

Radiation hardness of these devices is presently being tested considering 6 different fluences in the range 10^{14}-10^{16} 1 MeV neutrons/cm^2 (TRIGA reactor, Ljubljana). Fig. 23 show a comparison of I-V characteristics of the diodes with a diameter 1 mm at forward and reverse bias voltage, respectively, before and after irradiation by F_n of $3 \cdot 10^{14}$ n/cm^2 and after 7 days of RT annealing. After irradiation

by this fluence the bulk of SiC layer becomes intrinsic and capacitance if independent on fluence. The reverse current density vs. F_n is presented in Fig. 24. Reduction of current and current density is observed after irradiation up to the highest fluence of 10^{16} n/cm^2.

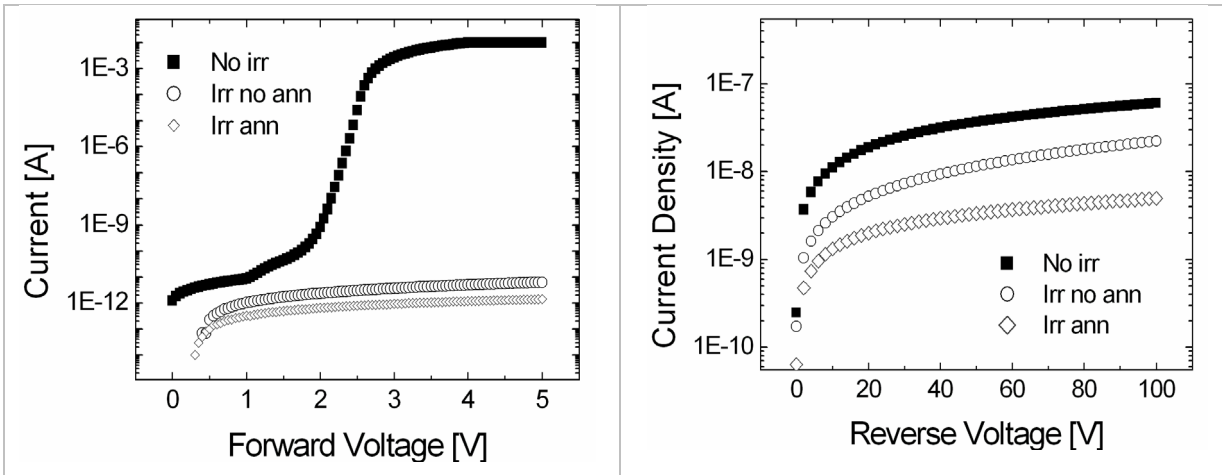

Fig. 23. I-V characteristics of the diode irradiated by $3 \cdot 10^{14}$ n/cm^2 at forward and reverse bias voltage

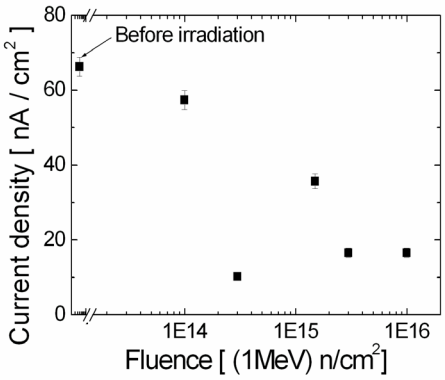

Fig. 24. Dependence of reverse current density on neutron fluence

The dependences of the collected charge on voltage ranging up to 1000 V for SiC detectors irradiated by F_n of $1 \cdot 10^{14}$ n/cm^2 and $1.5 \cdot 10^{15}$ n/cm^2 are presented in Fig. 25. The asymptotic values of the charge are 2800 e^- and 800 e^- (CCE of 90% and 26%, respectively). The total dependence of the collected charge on fluence is shown in Fig. 26. The collected charge stays high up to few 10^{14} n/cm^2 and decreases sharply after a fluence of 10^{15} n/cm^2. After irradiation by $1 \cdot 10^{16}$ n/cm^2 the collected charge is only 130 e^-. This result shows that SiC detectors do not show enhanced radiation hardness in comparison to Si detectors.

Future plans on SiC detectors

The effects of radiation damage on the leakage current, effective doping concentration and charge collection as a function of the fluence of 1 MeV neutrons and 24 GeV/c protons will be further analyzed and presented. In accordance with the work program of SiC sub-project started in 2005, in 2006 we plan to irradiate SiC diodes dedicated by collaboration by 8 MeV protons with the fluence ranging from 10^{14} cm^{-2} up to 10^{15} cm^{-2}. The work program includes also identification of radiation induced defects and search for the possibility to neutralize these defects. The study implies annealing treatment to verify the possibility for recovery of radiation damage. This systematic analysis will allow final conclusion on radiation hardness of SiC p^+-n devices.

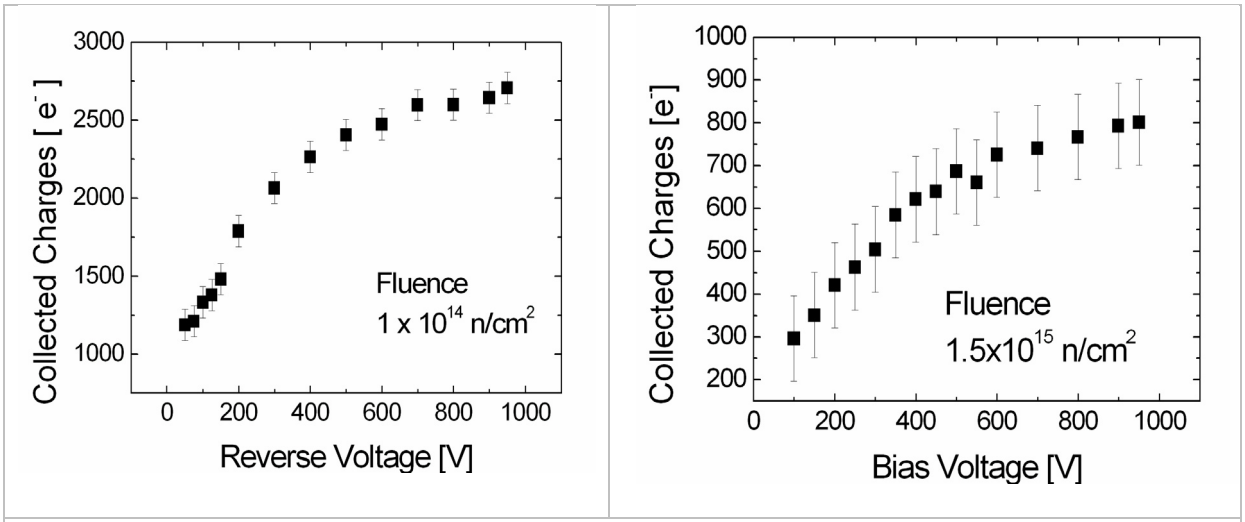

Fig. 25. Dependences of the collected charge on voltage for neutron irradiated SiC detectors

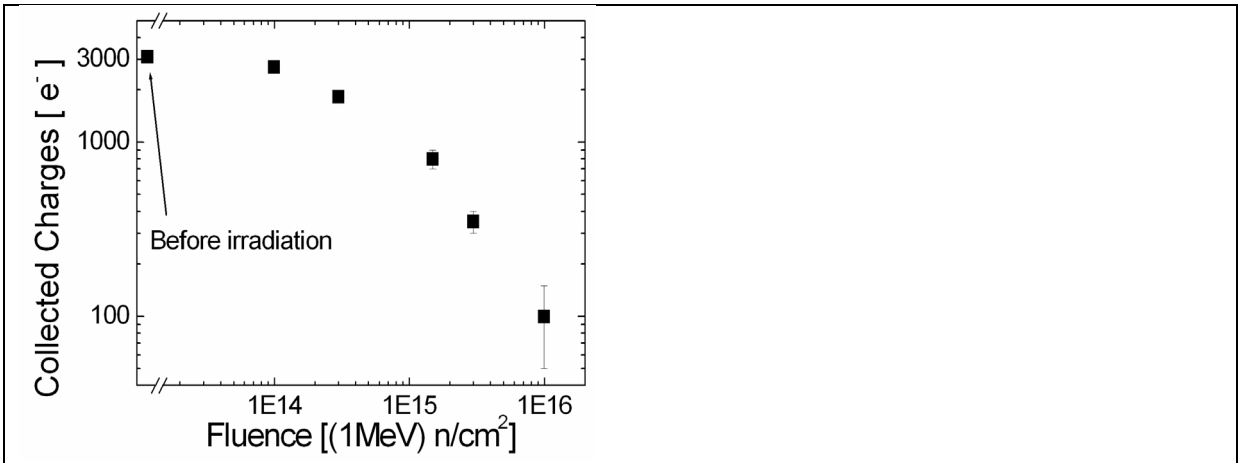

Fig. 26. Dependence of the charge collected in the bulk of SiC detectors on neutron fluence

References for Section 7.1 (SiC activities)

1. S. Sciortino at al., Nucl. Instr. And Meth., A552 (2005) 138-145, pres. 5RESMDD, Oct 10-12, 2004, Florence
2. C. Manfredotti et al., Nucl. Instr. And Meth., A552 (2005) 131-137
3. M. Bruzzi et al., "The SiC common structures project", pres. 7th RD50 workshop, Nov 14-16, 2005, CERN, Geneva
4. F. Moscatelli et al. Nucl. Instr. and Methods A 546 (2005) 218-221
5. F. Nava et al., IEEE Trans. Nucl.Sci., vol. 51, pp. 238–244, 2004
6. F. Moscatelli et al., "First characterizations of a minimum ionizing particle detector based on p^+n junction SiC diode", pres. 6th RD50 workshop, June 2-4, 2005, Helsinki
7. F. Moscatelli et al., "Radiation hardness of minimum ionising particles detectors based on SiC p^+-n junctions", pres. 7th RD50 workshop, Nov 14-16, 2005, CERN, Geneva
8. RD50 Status Report 2004, CERN-LHCC-2004-031 and LHCC-RD-005
9. N. B. Strokan et al., "Measurements of diffusion lengths of a micron range by techniques of nuclear spectrometry", to be published in "Semiconductors".
10. N. B. Strokan. Technical Physics Letters, Vol. 24 (1998) 186.
11. R. Yakimova et al., "The limit of SiC detector energy resolution in ions spectrometry", pres. Internat. Conf. on Silicon Carbide and Related Materials ICSCRM 2005, Sept 18-23, 2005, Pittsburgh, USA (to be publ. Mater. Sci. Forum)

12. E. Kalinina, A. Strel'chuk, A. Lebedev, N. Strokan, A. Ivanov, G. Kholuyanov, "Radiation Hard Devices Based on SiC", pres. Internat. Conf. on Silicon Carbide and Related Materials ICSCRM 2005, Sept 18-23, 2005, Pittsburgh, USA (to be publ. Mater. Sci. Forum)

6.2. Research activity on Gallium Nitride

GaN attracted an attention for the ionizing radiation detectors taking into account the main properties of material: the big density (2.7 times larger than Si), the wide bandgap and high enough carrier mobility. The comparison of the main parameters and properties of GaN and other semiconductors was presented in a review paper of P.Sellin and J.Vaitkus [1]. An extraction of the main parameters is presented in Table 2.

Table 2. Main parameters of semiconductors developed for radiation hard detectors

Property	Diamond	Si	4H- SiC	GaN
Z	6	14	14/6	31/7
Density [g/cm^3]	3.5	2.3	3.2	6.2
Dielectric constant	5.5	11.9	10.1	9
Breakdown voltage, [MV/cm]	10	0.5	4	2
E_g [eV]	5.5	1.12	3.3	3.39
μ_e [cm^2/Vs]	1800-2200	1450	800-1000	1000-1250
μ_h [cm^2/Vs]	1200-1600	450	50-115	30-850
e-h pair creation [eV]	13	3.6	7.8	8.9
Displacement energy [eV]	43	13-20	21.8	Ga 19±2; N 10
Saturated electron drift velocity (cm/s)	2.7x10^7	1.0x10^7	2.0x10^7	2.2x10^7

Therefore when a search for a semi-insulating material was successful a test of the material as an ionizing radiation detector was performed and a test of radiation hardness was started.

The first stage of the research - the offhand experiments demonstrated promising properties of GaN for radiation hard detectors [2-4]. In the material irradiation CERN (24 GeV protons), Imperial College (X-rays) and Ljubljana (reactor neutrons) participated. In the case of the particle irradiation the highest irradiation up to $1 \cdot 10^{16}$ cm^{-2} was reached. The following GaN epi-layers MOCVD grown on sapphire were investigated:

- Tokushima University and Nitride, Ltd. – Japan – SI-GaN layer ~2-2.5 μm,
- Lumilog, Ltd., - France - 12 μm, and
- HVPE-grown thick (~500 μm) layers (Lumilog, Ltd.)

The first preliminary data obtained for the films with a thickness of 2.5 μm by the joint attempts of Glasgow U and Vilnius U groups are presented in Table 3 [5].

Table 3. First data obtained on 2.5 μm thick films.

Sample irradiation /fluence	CCE, % /@ bias, V	I_{10V}, nA cm^{-2} /character	τ_{fast}, μs
Non-irradiated	95 / 30	0.06 /barrier	0.1-0.5
600 MRad X-rays	100 / 26	5.50 /barrier	0.08
Neutrons/ 5 10^{14} cm^{-2},	77 / 28	0.35 /resist.	0.015
10^{15} cm^{-2},	10 / 30	0.65 /barrier	0.02
10^{16} cm^{-2}.	5 / 16	0.23 /resist.	
Protons / 10^{16} cm^{-2}.	13.6 / 30	0.40 /barrier	<0.01

In the 12 μm thickness sample the direct measurement of charge collection efficiency (CCE) gave rather good result: CCE of ~26 % was observed in proton irradiated up to fluence 10^{16} cm^{-2} sample (presented at 5th RD50 Workshop, June 2-4, 2005).

The second stage of research was more systematic analysis of radiation hardness of GaN, especially semi-insulating GaN. The contributions of Glasgow U, Surrey U (UK) and Vilnius U groups creates the results of this GaN research line. The epilayers were investigated in more detail and a significant role of defect layer at the substrate was established [6, 7, and presentations at 5th and 6th RD50 Workshops]. It is important to point out that at highest irradiation fluences the resistivity of SI-GaN (initial - 10^9 Ω·cm) decreased, but it was bigger than $4 \cdot 10^6$ Ω·cm that shows the possibility to use this material as photoconductor type radiation detector.

The third stage of this research corresponds to the attempts to understand the peculiarities of material properties and the reasons for limitation of CCE [8], non-linearities of I-V dependence etc.

Peculiarities of material properties are shown by a comparison of luminescence spectra of thin and thick GaN layers presented in Fig. 27. The dependence of the luminescence spectra on the crystal quality was demonstrated also in [9-12].

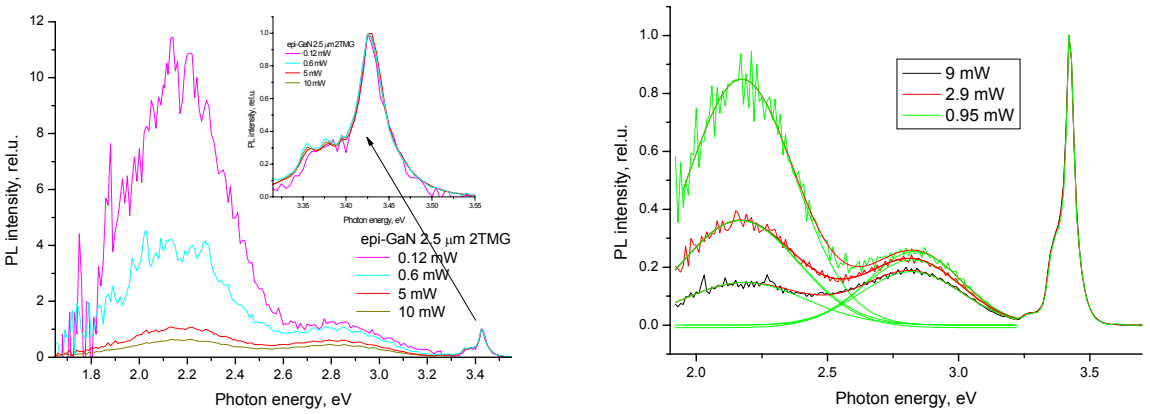

Fig. 27. Photoluminescence spectra in 2,5μm (left) and 12 μm (right) thickness samples at different intensity of excitation (spectra normalised at exciton peak wavelength).

The coincidence of a shape of excitonic band at any excitation levels shows the independence of local level filling on the excitonic recombination. The quality of crystal can be qualitative compared by a ratio of excitonic and deep level luminescence and by a shape of excitonic lines. The latter are shown in Fig. 28. A small shift to the higher energy of the excitonic line was observed in the thinner samples. A similar shift was also in the irradiated thick samples. It allows concluding that the defects are responsible for this effect.

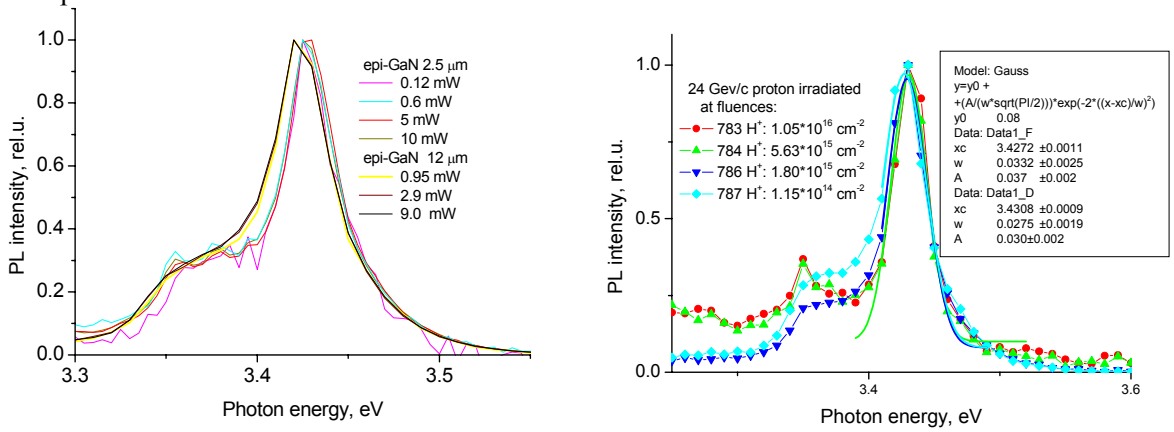

Fig. 28. The excitonic photoluminescence region (left – in thin and thick samples, right – in samples irradiated at different fluence by protons).

The first I-V and C-V measurements were performed on MOCVD grown thin and thick (12 micron) epitaxial GaN detectors. These measurements, as well as CCE dependences on the bias revealed some problematic questions. It was found that some of them are related to a specific structure of the sample that is given in Fig. 29. The character of conductivity time and bias dependence, a noise during photoconductivity and thermally stimulated current measurements, low value of the sample capacitance allowed to propose that all these problems are related to the contact between the rear contact (n*-GaN) of the investigated samples and the external measurement circuit (silver paint).

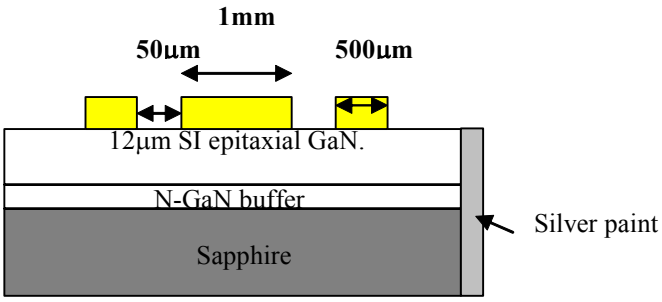

Fig. 29. Schematic of the sample cross-section

The highly doped layer conductivity was measured by van der Pauw method: thickness of layer 2 µm, electron mobility - 327 cm^2/Vs; Hall constant R - 4,2 cm^3/C, therefore the carrier concentration is $1{,}5 \cdot 10^{18}$ cm^{-3} with the accuracy of the measurement ~ 5% (plus an error of the layer thickness). The analysis of I-V and C-V dependencies showed that there is a serious contact problem: the used silver or other type conductive paints did not allow realizing the good contact. The sample capacitance was much smaller than an estimated geometric capacitance and the breakdowns that do not change the main sample properties were observed. This effect can be illustrated by a fragment of thermally stimulated current (TSC) dependence on temperature (Fig. 30): in a region where a high activation of conductivity is observed the switching of the current from a "higher" conductivity state to a "lower" conductivity did not change the activation energy that is mostly easy to explain by the bad contact of n*-GaN and electrode. Also, after a few temperature cycles this contact as usually became broken. In some samples the TSC was possible to measure and the data base has been started to collect.

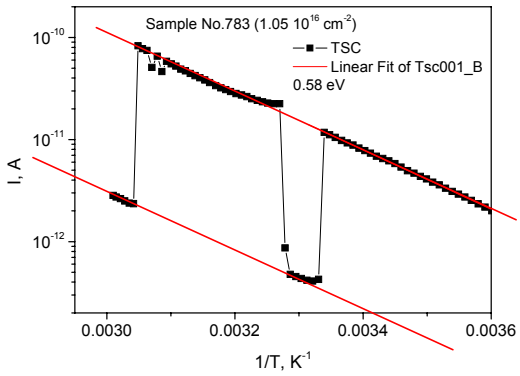

Fig. 30. A fragment of TSC vs. T curve. The red lines are parallel

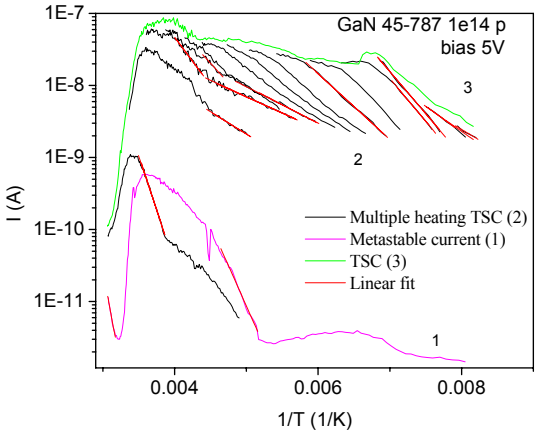

Fig. 31. TSC measured at different regimes

The bulk GaN samples had too high conductivity and only the space charge region can be used for the detector property analysis. The temperature dependence of conductivity and photoconductivity mainly depended on mobility of carriers [13-14]. In the SI-GaN crystals the overlap of influence of thermal stimulated excitation of traps and modulation of inter-crystallite barriers effects was observed and could be shortly illustrated by the TSC and multiple heating TSC presented in Fig.31. A set of activation energy was measured but the value of the trap energy will be found after evaluation of barrier effect (now three groups of traps can be recognized: ~140 meV, 230 meV, 600 meV. Long term memory is also shown: activation of similar levels that were filled up at room temperature and were occupied after keeping in the dark and cooling down to the low temperature (curve 1, Fig. 31).

The result of identification of an influence of the additional resistance between the rear contact and the electrode, and probably the distributed parameters of the buffer layer reduced the measured values of the CCE. Therefore it is proposed that the maximal CCE (~55%) in unirradiated detector with 12 μm thickness is also related to this contact problem. This experimental problem allows concluding that the previously measured values of CCE could be taken as a lower limit of the parameter.

The photoconductivity transient behavior demonstrated the decay characterized by the stretched exponent. This problematic result caused a necessity to improve the technology of contact preparation and the etching of SI-GaN to reach n*-GaN. We have attempted ICP etching some 2.5 micron epi GaN material. Fig. 32 presents a sample of the etched detector. The unexpected result was a measurement of a real thickness of the "thin" sample and the thickness was found to be 1.6-1.7 μm. This forces to re-evaluate the CCE in this series of samples and the corrected results are presented in Fig. 33. It shows that the true values of CCE are better than those presented in Table 1: the maximal CCE in the sample irradiated at $1\cdot 10^{16}$ cm^{-2} is 19 %. The improvement of 12 μm sample contact is planned for the future since the etching goes slower than predicted.

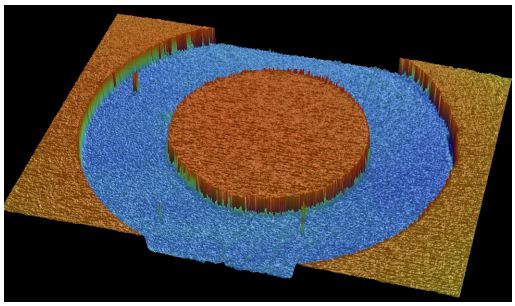

Fig. 32. The etched sample.

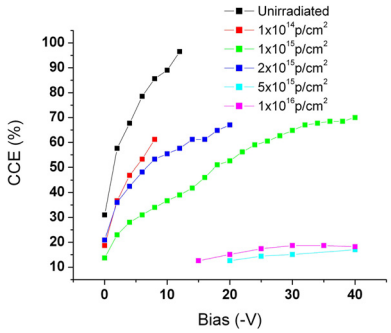

Fig. 33. The corrected CCE vs bias in the "thin" GaN samples.

Also these samples were irradiated by neutrons to get more reliable data on radiation hardness of GaN for neutron irradiation. The new series of 12 micron GaN, and ~2.5 μm 36-GaN and 45-GaN samples are irradiated by reactor neutrons in Ljubljana. Detectors have been irradiated to five neutron fluences of $1x10^{14}$ n/cm^2, $1x10^{15}$ n/cm^2, $2x10^{15}$ n/cm^2, $5x10^{15}$ n/cm^2 and $1x10^{16}$ n/cm^2. The results will be obtained in November since the samples are still too "hot" after irradiation.

All these results demonstrated two main problems to solve for improvement of device technology and correction the data related to the radiation hardness. The first problem is the development of the etching procedure of SI-GaN that enables to contact the high conductivity layer by plane but not by the edge. This problem is partly solved now but the thermally and mechanically strong contact technology is necessary to develop. The second problem is related to the improvement of epilayer structural properties namely reduction of the substrate induced defects.

Analysis of the current technology of the bulk GaN allows concluding that the SI-GaN growth on the high conductivity GaN now is not cost-competitive technology. Recently, innovations in metal-organic chemical vapor deposition (MOCVD) have enabled the growth of high-quality GaN layers on silicon. The process has been demonstrated on 4″ wafers and can be scaled to larger diameters. A high-quality epitaxial layer technology on a silicon substrate takes advantage of years of research into wafer fabrication equipment and processing techniques, which are routinely used in CMOS or BiCMOS integrated circuits. This GaN-on-silicon approach yields a low-cost, high-performance platform for RD50 application if the thick SI-GaN epi-layers will be grown. Now we have started the discussion with the companies that have this technology.

Conclusion: The GaN material still seems promising (earlier data show the lower limit of CCE) but the detector fabrication technology improvement is necessary and more correct parameter values are planned to be measured.

Nearest future Work plan

Now we are in discussion with the GaN layer growers (the mentioned above companies but also Aixtron is added and the Nitronex Ltd. is on the contact) about a possibility to grow thicker samples and to avoid the sapphire as the substrate. Hopefully the GaN on Si will be available for testing. The thick GaN growth limits a lack of financial resources.

HVPE GaN investigation can allow analysis of radiation hardness of the material that is not influenced by substrate misfit defects. The first alpha-particle data from HVPE-grown thick GaN which was obtained from Lumilog will be presented in November (Surrey U). The CCE has to be low in this material due to its high conductivity but it will work for the reference to the measurement after the sample irradiation. The Polish group will start to analyse the trap spectra in the available samples.

The improvement of detector fabrication technology is planned to be realized in the new clean room which will be soon operational in Glasgow U. The nearest steps are planned:

1. Etching the 12 μm GaN material to improve the contacting to the SI-GaN layer.

2. Using Gallium to contact with the buffer layer (GU and VU). If using Gallium is not effective, ICP etching the irradiated samples and placing a contact onto the buffer layer will be tested.

3. GU is ready to perform the measurements of I-Vs' and CCEs' of all the irradiated 12 micrometer thickness, 36GaN and 45GaN detectors that now are in CERN. Afterwards the samples will be sent to Vilnius for TSC, MWA and CPC measurements.

4. The different SI-GaN will be available from Aixtron Ltd., and attempt to get GaN-on-Si have started.

References for Section 7.2

1. P.J. Sellin and J. Vaitkus. "New materials for radiation hard semiconductor detectors". Nucl. Instr. and Meth. (to be published).
2. J.V.Vaitkus, W.Cunningham, M.Rahman, K.M.Smith, S.Sakai. Semi-insulating GaN and its first tests for radiation hardness as ionizing radiation detector / in UV Solid-State Light Emitters and Detectors, ed. by M.S. Shur and A. Zukauskas (Kluwer Academic Publishers, Dordrecht, 2004), pp. 279-286.
3. Rahman A., Al-Ajili A, Bates R, Blue A, Cunningham W, Doherty F, Glaser A, Haddad L, Horn A, Melone J, Mikuz A, Quinn T, Roy P, O'Shea V, Smith KM, Vaitkus J, Wright V. Super-radiation hard dectector technologies: 3-D and widegap detectors. IEEE Trans. Nucl. Sci. 51 (5): 2256-2261 Part 1, Oct 2004
4. P.J. Sellin et. al., Nucl. Instr. and Meth. A 531 (2004) 82–86.
5. J. Vaitkus J. et al., Phys. of Semicond., AIP Conf. Proc., V.772: 207-208, 2005.
6. Gaubas E, Kazlauskas K, Tomasiunas R, Vaitkus J, Zukauskas A. Appl. Phys. Lett. 84 (25): 5258-5260 (2004)
7. E. Gaubas, S. Juršenas, S. Miasojedovas, J. Vaitkus, and A. Žukauskas J. Appl. Phys., 96, No. 8 (2004), pp.4326-4333.
8. J. Grant et al., Nucl. Instr. and Meth. A546, Issues 1-2, p.p.213-217, 2005
9. E. Gaubas et al., „Photoluminescence and photoconductivity dynamics in semi-insulating epitaxial GaN layers". Acta Physica Polonica A, 107 (1): 215-219 Jan 2005
10. E. Gaubas, K. Kazlauskas, J.V. Vaitkus, A.Zukauskas, Phys. Stat. solidi C, 2005, vol. 2, no. 7, p. 2429-2432.
11. E. Gaubas et al., Nucl. Instr. and Meth. A 546 (2005) 247-251
12. E. Gaubas et al., Nucl. Instr. and Meth. A 552 (2005) 82-87.
13. V. Kazukauskas, J..V.Vaitkus, Opto-Electronics Review 12 (4) (2004) 399-403
14. V. Kazukauskas, V. Kalendra, J. V. Vaitkus, Acta Physica Polonica A, 107 (2): 340-345 Feb 2005

7. New Structures

7.1. Introduction

The major advances in the area of new structure developments over the past year have been in thin detectors and 3D detector fabrication. Better understanding of the charge collection properties of thin silicon detectors has been achieved with the use of Schokley-Read-Hall based models; while the first 3D detectors fabricated at ITC-irst have been realised and tested.

7.2. Thin Silicon detectors

The work of the Perugia group has concentrated on the electrical characterisation of silicon pad detectors realized on substrates with a thickness ranging from 20 to 300μm. In order to investigate the performance of these structures simulations have been carried out using the Schokley-Read-Hall, (SRH), statistics, implemented in the ISE-TCAD DESSIS device simulator. A three-level model has been developed to simulate the effects of the radiation fluence: the most important defects have been identified as the divacancy V_2 (acceptor) and the C_iO_i complex (donor) on account of their high introduction rates and relative proximity to mid-gap [1,2]. These defects play an important role in the simulation setup because they determine the macroscopic behaviour of radiation damaged detectors, in terms of type inversion and leakage current increase [3]. The formation of cluster defects is taken into account by assigning to the V_2O acceptor defect level an introduction rate higher than that reported from DLTS measurements (26 instead of 1.2). In the SRH statistics the recombination rate is determined by the ratio between the electron and hole cross-sections, (σ_n and σ_p), which, in turn, are related to the emission and capture coefficients of the charge carriers. In the simulations values of σ_p for the acceptors and σ_n for the donors from the literature were used [3], and the parameters σ_n and σ_p have been varied to fit the experimental data. The results are summarized in Table 1.

	V_2 Acceptor	V_2O Acceptor	C_iO_i Donor
E	E_c -0.42eV	E_c -0.55eV	E_v+0.36eV
σ_p	$8 \cdot 10^{-15}$cm^2	10^{-15} cm^2	10^{-16} cm^2
σ_n	10^{-16} cm^2	10^{-16} cm^2	10^{-15} cm^2
η	26 cm^{-1}	0.08 cm^{-1}	1 cm^{-1}

Table 1: Three level model parameters. The energy levels E are extracted from DLTS measurements [3], σn and σp are the cross section for electrons and holes, respectively, and η is the defect level introduction rate.

The V_2O defect (acceptor), located slightly above the mid-gap was shown to determine the fluence at which type inversion occurs, as reported in Fig.1. It can be seen that the energy of the V_2O defect as well as the introduction rate affects the inversion point. Fig.2 shows the difference in full depletion voltage that can be achieved with thinned devices for comparison with standard 300μm thick detectors. All simulations are performed assuming a high resistivity substrate, ($7x10^{11}$ cm^{-3} n-doped corresponding to 6kOhm-cm). All the structures are composed of a 40μm wide diode with a 6μm guard ring with a pad to guard separation of 15μm.

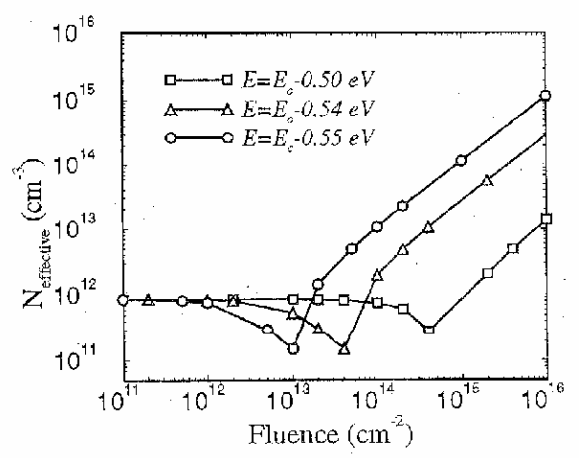

Fig.1: Effective doping concentration as a function of the fluence and as a function of the energy level of the V_2O acceptor defect.

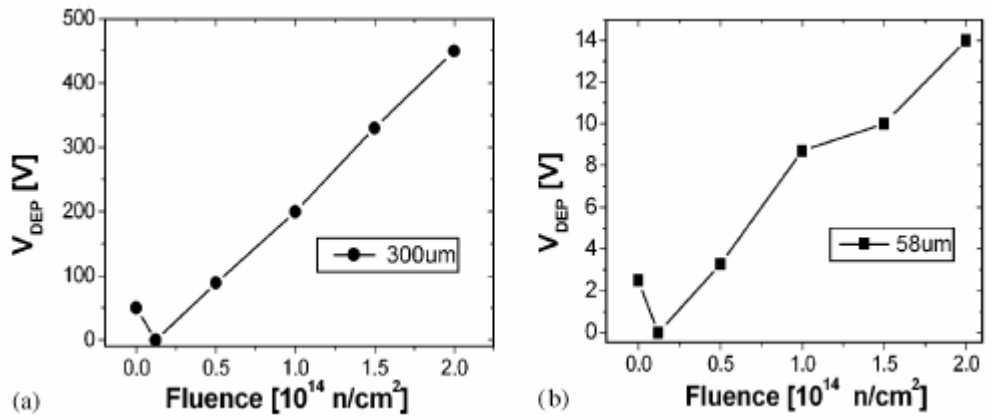

Fig.2: Comparison between full depletion voltage of thick (a) and thin (b) silicon detector [5].

The effect of the radiation damage on the charge collection efficiency, (CCE), of thin and thick silicon detectors has been also investigated. For each thickness, simulations were performed of the ionisation caused by the passage of a Minimum Ionizing Particle, (MIP), and the resultant induced current at the diode's electrode was calculated. The simulated collected charge from the 300μm thick diode, for fluencies up to $2 \cdot 10^{14}$ n/cm^2, is in agreement with the experimental data [5]; the simulation of thinner structures (50μm) shows a saturation of the number of e-h pairs collected at the diode's electrode.

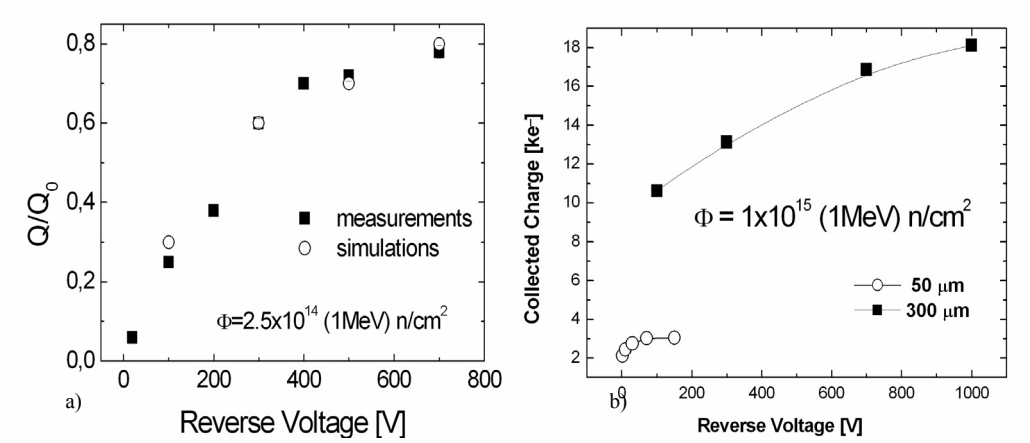

Fig.3: a) Comparison between the experimental [5] and simulated Charge Collection Efficiency for a thick detector at a fluence of $2 \cdot 10^{14}$ n/cm^2; b) Comparison between collected charge as function of the applied bias voltage and of the thickness of the detector.

Presently, the three level radiation damage model for n-type detector has been validated up to a fluence of $2.5 \cdot 10^{14}$n/cm^2. The comparison of data with experimental results obtained on n-type thinned pad diodes irradiated at higher fluencies is still a work in progress. In the mean time a new model for p-type substrates is under development. P-type silicon has been proposed as a suitable means to improve the long-term radiation hardness of silicon detectors [6].

7.3. 3D detectors

The majority of work in the area of 3D detectors over the past year has been to develop a fabrication effort in 3D detectors in a non-university institute. For this aim ITC-irst and CNM have worked together to produce their first 3D detectors. At present these are not full 3D devices as a simpler design was chosen for the first fabrication run to maximise yield. The University of Glasgow has developed a process to allow both n and p type doping of etched pores; however fabrication of significant numbers of devices was not possible to date due to the refurbishment of their engineering facilities.

7.3.1 3D-single column type

ITC-irst has developed a new 3D detector architecture aimed at simplifying the manufacturing process [7] in comparison to standard 3D detectors. The proposed device, in the following referred to as 3D-stc, features electrodes of one doping type only, e.g., n^+ columns in a p-type substrate, so that the column etching and doping are performed only once, resulting in a considerable process simplification.

Detector fabrication

The first batch of 3D-stc detectors has been fabricated on p-type, high-resistivity silicon FZ and Cz wafers, both with wafer orientation <100>. The FZ wafers were 500-μm thick with a nominal resistivity of 5kΩcm, whereas the Cz wafers were 300-μm thick with a nominal resistivity higher than 1.8 kΩcm. Detectors all have n-type columnar electrodes extending deep into the bulk, (down to 150 μm), but not extending all the way through it. A uniform p^+ layer provides the ohmic contact on the detector backside. A device cross section and an SEM micrograph of a structure is shown in Fig. 4a and in Fig. 4b, respectively.

The key points of processing, already reported in [8], are summarized in the following:

- Boron implantation is used to obtain the ohmic contact on the backside and the isolation between n^+ electrodes on the front-side;
- Circular pores with a diameter in the range 6 - 10 μm are etched by DRIE
- Column n^+ doping is performed by Phosphorus diffusion from a solid source.

All processing steps were carried out at ITC-irst, bar the pore etching which was performed at CNM in Barcelona by means of a DRIE machine.

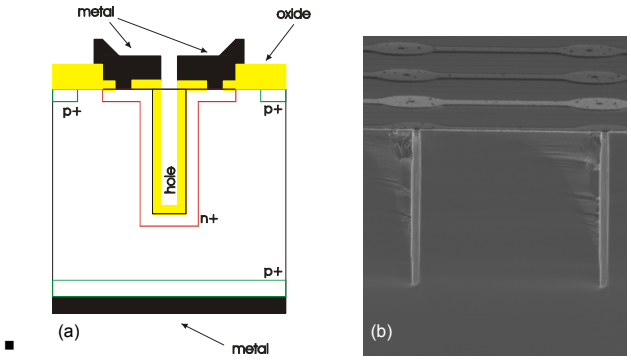

Fig. 4. (a) Schematic cross-section of one columnar electrode; (b) SEM cross-section of a 3D-stc structure.

Several detector layouts have been designed, differing by the following options:

- Two detector sizes have been considered, the first featuring an active area of 1 cm^2, and the second featuring an active area of 6 mm^2;
- Pore diameter: from 6 to 10 µm;
- Several pitches between pores have been considered, in the range 50 - 100 µm;
- Either p-stops or p-spray have been used for surface isolation;
- Either DC or AC coupling between strip diffusions and metal layers have been used. In the AC coupled detectors, strips are biased by punch-through at both edges from the inner guard ring, acting as a bias ring. The same effect can be exploited for test purposes on DC coupled detectors.

Experimental results

Planar test structures

Table 2 summarizes the main results obtained from planar test structures fabricated on the same wafer as the 3D-stc devices. All the performed measurements show that the DRIE step does not cause any detrimental effect on the substrate. Early breakdown is observed on wafers with p-spray, as expected from simulations [7]. Also the surface related parameters confirm the good quality of the fabrication process, with a slight difference between the wafers implementing the two surface isolation options as a result of the different thermal budgets characterizing the two process splits.

Table 2: Summary of the main results from planar test structures.

Parameter	Unit	Typical range	
		p-spray	p-stop
Substrate doping conc.	10^{12} cm^{-3}	1.6 – 2.3	
Depletion voltage	V	300 – 440	
Leakage current density	nA/cm^2	3.0 – 5.5	
Breakdown voltage	V	60 – 140	155 – 175
Field oxide thickness	nm	570 – 585	860 – 875
Field oxide charge density	10^{10} cm^{-2}	9.5 – 11.0	6.0 – 9.6
Surface generation velocity	cm/s	1.3 – 1.7	7.0 – 7.5

3D detectors and test structures

Capacitance-Voltage (C-V) and Current-Voltage (I-V) measurements have been performed on 3D detectors and test structures. From the capacitance values measured between columnar electrodes and substrate and between adjacent rows of columnar electrodes, we could infer the following information about the detector depletion:

- the lateral full depletion between columns is obtained at a very low voltage of only 5V for a pitch of 100µm;

- the vertical full depletion of the substrate region below the bottom of the columnar electrodes is estimated at voltages of about 200V.

These values are in good agreement with the substrate doping concentration extracted from planar test diodes. Nevertheless, it should be stressed that in 3D devices the analysis of C-V data is not straightforward, since the measured capacitances are largely affected by surface non idealities that are strongly dependent on the layout (e.g., the MOS-like effect of probe pads and metal interconnections). Thus, in order to extract accurate values, 3D numerical simulations are currently being carried out, enabling the discrimination between intrinsic column capacitances and parasitic capacitances. Leakage current measurements confirmed the good quality of the process. As an example, Fig. 5 shows the leakage current curves as a function of reverse bias for eight, 1-cm^2 large, AC-coupled detectors featuring p-stop and p-spray isolation and different combinations of column pitches and diameters. As can be seen, at low voltage, the leakage current is very good, its values corresponding to less than 1pA per column for all detectors. Note that for detectors with p-spray, the punch-through voltage is higher so that the columns are biased at a lower effective voltage. This effect, together with a reduced surface contribution, explains the leakage current difference observed in Fig.5.

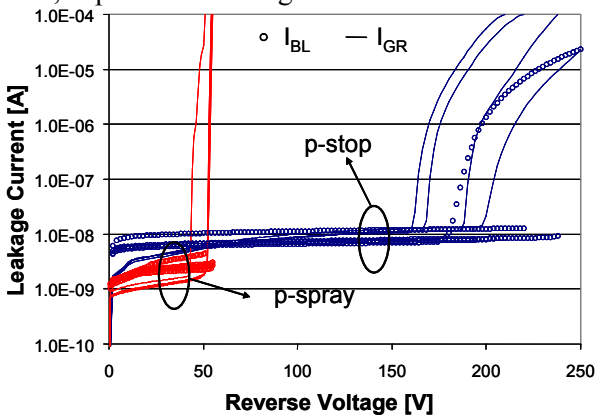

Fig. 5. Bias-line and guard-ring leakage currents vs. bias voltage in 8 AC coupled, 3D-stc detectors (4 with p-stop, 4 with p-spray).

At higher voltages, breakdown occurs on the guard-ring, and this can cause a sharp increase of the bias-line current too. For p-spray isolation the breakdown voltage is close to 50V, slightly lower than the value measured on planar diodes with p-spray; nevertheless, it should be mentioned that in planar diodes the presence of field-plates enhances the breakdown characteristics. For p-stop isolation, the breakdown voltage ranges from 150 to 200V, which are approximately the same values observed for planar diodes. The good agreement between breakdown voltages on 3D and planar structures suggests that breakdown is located at the surface. According to the simulations [7], the surface is indeed the most critical point for breakdown if the substrate doping is low, which is the case for the devices considered in this study, whereas column tips can be of concern at higher doping concentrations. Fig. 6 shows the distribution of the bias line leakage current measured at 40V (i.e., before breakdown) on 70 detectors: only a few detectors exhibit currents in excess of 50nA, evidence of the very good yield obtained with this process.

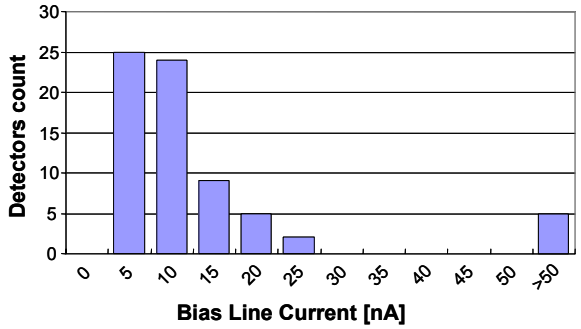

Fig. 6. Distribution of the bias-line leakage current measured at 40V on 70 3D-stc detectors with both p-stop and p-spray isolation.

7.4. Future work

Preliminary results from the detectors electrical characterization show the evidence of the very good yield obtained with this process and demonstrate the feasibility of this technological approach. A thorough analysis of device C-V characteristics with the aid of TCAD simulations is under way to gain deep insight into the depletion mechanisms characterizing these detectors.

Devices from these wafers have been distributed to the Glasgow and Freiburg groups for further electrical and change collection characterisation. Glasgow will test 3D pad detectors' response to irradiation by alpha, laser and MIPs. Freiburg will test strip detectors wire-bonded to ATLAS SCT readout electronics. Assuming that the devices work well as particle detectors then it is planned that the devices will be tested further with a micro-ion beam at Surrey University to map the charge collection efficiency as a function of position in the device.

Further development of pore formation has taken place. CNM have obtained pores with an aspect ratio of 23:1 with holes of diameter of 10um. Holes of 10um diameter and 230mu deep are shown in Fig 7. A new wafer run will be performed with deeper holes (230um) and thinner wafers (250um) so that the pores almost penetrate the full thickness of the device. These devices will be fully studied at collaborating institutes within the RD50 collaboration.

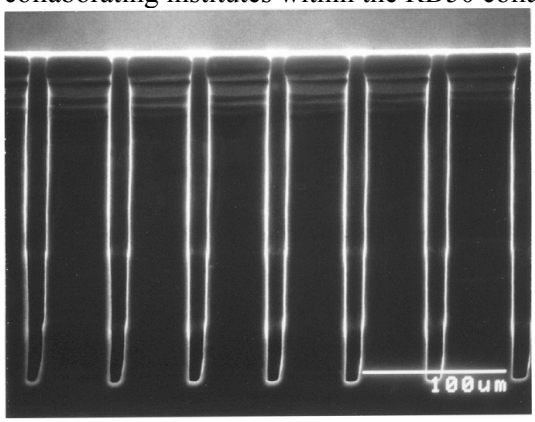

Fig. 7: Pores of 230um depth and 10um diameter fabricated at CNM

Glasgow will start device fabrication in the new year with the aim of developing full 3D detectors. Assuming that these devices will work successfully these will also be distributed to other RD50 institutes for full electrical and charge collection measurements.

A radiation hardness program will commence with the 3D detectors using the neutron source at Ljubljana once the devices are fully characterised before radiation. For a full radiation study more devices that those already produced at ITC-irst will be required. Therefore a further fabrication run will be required.

7.5. References

[1] S.J. Watts, Proc. of 1st ENDEASD Workshop, 1999
[2] Allport et al. NIMA 501 (2003) 146-152
[3] M. Moll - PhD Thesis, 1999
[4] M.Petasecca et al., IEEE TNS 51 (2004) 1759-1765
[5] M. Petasecca et al., NIMA 546 (2005) 291-295
[6] 5th RD50 Workshop, RESMDD 2004, Firenze Italy
[7] C. Piemonte et al. Nucl. Instr. Meth. A 541 (2005) 441
[8] S. Ronchin et al " Fabrication of 3D detectors with columnar electrodes of the same doping type" presented at PSD 07 Liverpool september 12 –16 2005 to appear in Nucl. Instr. Meth. A, 2006.

8. Full Detector Systems

The FDS research line of RD50 aims to test the properties of segmented detectors after heavy irradiation. The final goal is to test quantities like signal over noise (S/N) ratio and occupancy versus purity with simple but realistic systems (one detector coupled to one LHC-speed ASIC) in order to give indications on the performances of the devices after heavy irradiations.

8.1. Status of the investigation of p-type substrates

Annealing studies

The benefits of reading out silicon detectors from the segmented n-side are now well understood and widely accepted [1,2]. Also, the advantages of implementing the n-side read-out on p-type instead of n-type silicon substrates have already been discussed [3,4]. The charge collection efficiency after heavy irradiation (sLHC levels) has been measured up to 7.5×10^{15} cm^{-2} [3] (Fig. 2), while the noise has been proven to be constant with irradiation, when measured with LHC-speed electronics (Fig. 1).

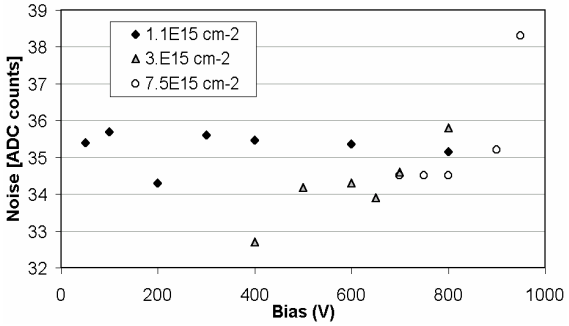

Fig. 1 Noise as a function of the applied voltage for the three different irradiation doses. The pre-irradiation value is about 35 ADC counts, similar to the value found after irradiation (G. Casse et al.)[3].

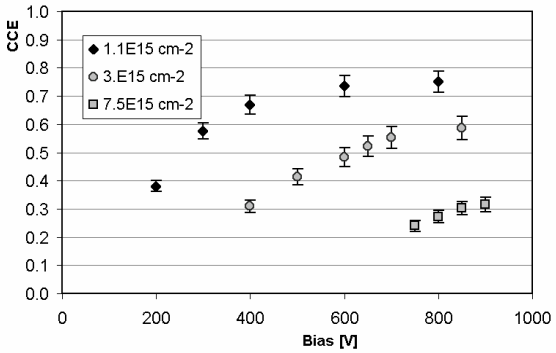

Fig. 2 Charge collection efficiency vs applied bias voltage, normalised to the pre-irradiation value, of n-in-p detectors after 1.1, 3 and 7.5 10^{15} p cm^{-2}. The detector irradiated to 3. 10^{15}

In order to qualify the p-type devices for high radiation environments, it is also necessary to address the question of the reverse annealing. To study the changes of the charge collection efficiency as a function of the applied reverse bias (CCE(V)), the same devices used to produce the results shown in Figures 1 and 2 were used. They are capacitively coupled, polysilicon biased, 1 cm long, 80μm pitch micro-strip detector processed on 280 μm thick, 2.8 kOhm cm p-type silicon wafers by the Centro Nacional de Microelectronica (Barcelona). The strip insulation method was p-spray. The measurements were performed at low temperature (-20^{o}C) and using the LHC-speed analogue SCT128a chip[5] based ^{106}Ru test-stand at Liverpool.

The changes of the full depletion voltage (V_{FD}) with time after irradiation are well known and accurately parameterised with n-type substrates [6,7]. They have been generally measured by mean of the Capacitance-Voltage characteristics (CV) after annealing stages at high temperature (60 or 80^{o}C) this latter temperature being favoured because it provides an acceleration factor of about 7400 times with respect to room temperature.

Monitoring the changes of the charge collection efficiency with time after irradiation is the most direct method to evaluate the parameters related to the actual operation of the detectors (signal and noise performance). The annealing studies were performed [8] with the miniature devices mentioned above and irradiated to 1.1, 3.5 and 7.5×10^{15} p cm^{-2}, and they were performed according the *standard* procedures: the detectors were submitted to several annealing steps of ~1 hour at +80^{o}C. Their charge collection properties were measured after each step. Figure 4, 5 and 6 show the collected charge for the annealing programme on the detector subjected to 1.1, 3.5 and 7.5×10^{15}p cm^{-2} respectively, both

as a function of the annealing time at high temperature and of the equivalent number of days at 20°C. The application of the high bias voltages proved difficult due to self-heating of the device even when kept at an environmental temperature of -20°C. In some cases, after the various annealing stages, some of the data were collected at different voltages.

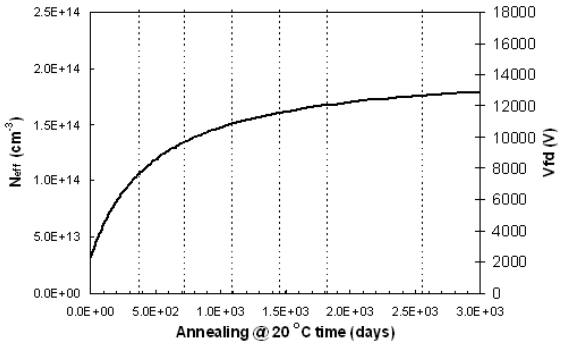

Figure 3. Changes (reverse annealing) of the space charge region (N_{eff}) and V_{FD} predicted by the annealing model presented in [6,7] and developed on the basis of CV measurements for a n-type detector irradiated to 7.5×10^{15} p cm^{-2}.

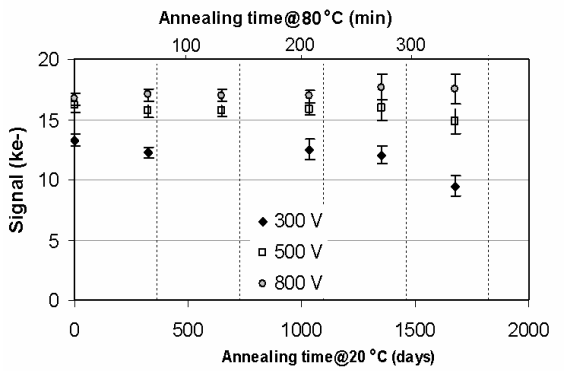

Figure 4. Changes of the collected mip signal as a function of time after irradiation (upper scale at 80 °C and lower scale 20°C equivalent) for a miniature micro-strip detector irradiated to 1.1×10^{15} protons cm^{-2} and biased at different voltages. The measurements were performed at -20°C (G. Casse).

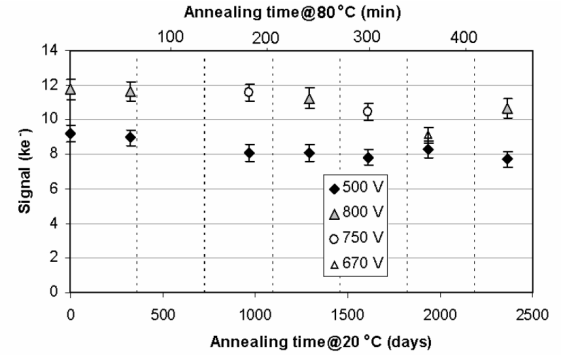

Figure 5. Changes of the collected mip signal as a function of time after irradiation (upper scale at 80 °C and lower scale 20°C equivalent) for a miniature micro-strip detector irradiated to 3.5×10^{15} protons cm^{-2} and biased at different voltages. The measurements were performed at -20°C (G. Casse).

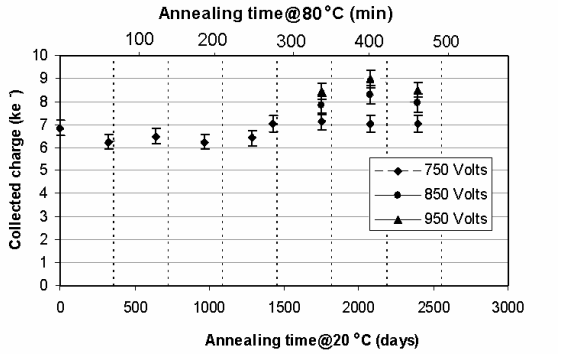

Figure 6. Changes of the collected mip signal as a function of time after irradiation (upper scale at 80 oC and lower scale 20oC equivalent) for a miniature micro-strip detector irradiated to 7.5×1015 protons cm-2 and biased at different voltages. The measurements were performed at -20oC (G. Casse).

Table 1, 2 and 3 show the ratio of the charge collected after different equivalent years (y_{EQ}) at room temperature to the one collected before reverse annealing at various voltages for the three irradiation fluences. It can be seen that for up to three years, no difference (above the uncertainty of the measurement) can be found even at the lower bias voltages for the different fluences. The charge collected at 300V after the lower dose shows a sensitive (30% loss) degradation only after 4 y_{EQ}, while at higher voltages the collected charge remains about constant up to the maximum time investigated.

Discussion

The results of the charge collection measurements do not support the accepted behaviour of the reverse annealing of the depletion voltage. The reverse annealing of n-type silicon has been extensively studied in term of changes of the full depletion voltage (V_{FD}) by mean of the capacitance-voltage (CV) method and an effective model well established ([6,7]). Figure 4 shows the prediction of the changes of V_{FD} with time after irradiation, for a device exposed to a proton fluence of 7.5×10^{15}

cm^{-2}. The V_{FD} goes from an initial value of ~2800V to more than 12000V after 7 shows the comparison of the mip signal measured before and after >$6y_{EQ}$ of annealing at the same applied voltage (750V) and no significant difference in the signal is observed. The model for the reverse annealing has been established with measurements on n-type bulk pad diodes, while the present CCE measurements are performed with p-bulk segmented devices. Nonetheless the apparent suppression of the reverse annealing is not likely to be due to the p-type material. It has been shown, for example, that with p-type diodes irradiated to much lower fluences, the changes of V_{FD} with time after irradiation, as measured with the CV method, follows a similar trend to the n-type material [9].

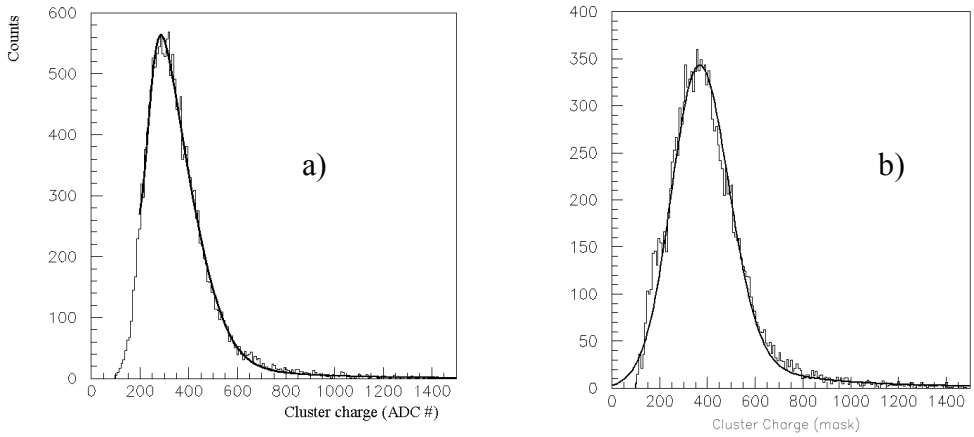

Figure 7. Comparison of the signal (measured with SCT128 40MHz analogue electronics) obtained with the p-type detector irradiated to 5 $x10^{15}cm^{-2}$: a) before reverse annealing b) after ~6.5 y_{EQ}.

If the reverse annealing suppression is not due to the material, the difference has to be ascribed to the measurement method. The description of the CCE property as extrapolated from the value of the V_{FD} with the CV method performed on simple pad diodes would lead to erroneous predictions. Part of the differences can arise from the segmented structure of the electrodes in micro-strip devices which leads to an electric field distribution substantially different from the simple pad devices. It has also been shown that the effective trapping of electrons (which predominantly contribute to the signal in the case of n-in-p segmented devices) anneals favorably with time [10]. This effect can partly compensate the variation of the effective space charge (and therefore V_{FD}) with time as measured from the CV technique.

Nonetheless, the concept of full depletion has to be reviewed, or abandoned after the evidence that in heavily irradiated detectors a relatively small free carrier concentration is found and an electric field appears in the whole thickness of the detector already at low bias voltages (so an electric-field free region implied by a non-depleted volume is not present in irradiated Si detectors) [11]. The so called double junction (presence of high electric field on both implant sides of the detector and of a weaker field in the intermediate region after heavy irradiation) has been argued for both from other measurements and from simulation studies [11,12,13,14,15]. An appropriate description of the charge collection properties and their change with time would require a realistic profiling of the electric field and a good estimate of the charge trapping characteristics of the irradiated silicon. Many efforts to this end are already taking place [10,13,15], as the importance of the electric field profile is being considered as crucial for a proper understanding by the high energy physics detector community.

Table 1. Ratio of the collected charge at different equivalent years at room temperature (y) to the charge collected before the start of reverse annealing at various bias voltages. Irradiation fluence $1.1\times10^{15}p\ cm^{-2}$.

Bias	1y	~ 3y	~ 4.5y
300 V	0.9	0.93	0.72
500 V	1.02	1.0	1.07
800 V	0.98	0.98	0.93

Table 2. Ratio of the collected charge at different equivalent years at room temperature (y) to the charge collected before the start of reverse annealing at various bias voltages. Irradiation fluence 3.5×10^{15}p cm^{-2}.

Bias	1y	~ 2.5y	~ 6.5y
500 V	0.98	0.9	0.87
800 V	0.98	0.94	0.88

Table 3. Ratio of the collected charge at different equivalent years at room temperature (y) to the charge collected before the start of reverse annealing at various bias voltages. Irradiation fluence 7.5×10^{15}p cm^{-2}.

Bias	1y	~ 2.5y	~ 6.7y
750 V	0.93	0.93	1.01

References for Section 8.1

[1] P.P. Allport, G. Casse, A. Greenall, "Radiation tolerance of oxygenated n-strip read-out detectors", *Nucl. Inst and Meth. A,* vol 513, pp.84-88, 2003

[2] ATLAS Inner Detector Technical Design Report, CERN/LHCC/97-16 and CERN/LHCC/97-17, 1997.

[3] G. Casse, P.P. Allport, S Marti i Garcia, M. Lozano, P.R. Turner , "*Performances of miniature microstrip detectors made on oxygen enriched p-type substrates after very high proton irradiation*", *Nucl. Inst and Meth. A,* vol 535,1/2, pp.362-365, 2004.

[4] G. Casse, P.P. Allport, T.J.V Bowcock, A. Greenall, M. Hanlon, J.N. Jackson, "First Results on the Charge Collection Properties of Segmented Detectors Made with P-type Bulk Silicon ", *Nucl. Inst and Meth. A,* vol 487, pp.465-470, 2002.

[5] F. Anghinolfi , W Dabrowski, E. Delagnes, J. Kaplon, U. Kotz, P. Jarron et al, "SCT A: A rad Hard BiCMOS Analog Readout ASIC for the ATLAS Semiconductor Tracker" *IEEE Trans. Nucl. Sci*. vol 44, pp 298-303, 1997.

[6] Michael Moll "Radiation Damage in Silicon Particle Detectors", *Dissertation zur Erlangung des Doktorgrades des Fachbereichs Physik de Universitat Hamburg,* 1999.

[7] G. Lindstroem et al., Nucl. Instr. and Meth. A 466 (2001) 308

[8] M. Lozano et al., 5th RD50 workshop, Florence, Italy, Oct. 2004.

[9] J. Härkönen et al., "Thermal donor generation in Czochralski silicon particle detectors", this conference.

[10] O. Krasel, *"Charge collection in irradiated silicon detectors: a study of the operation conditions of silicon sensors in the ATLAS pixel detector",* PhD thesis, University of Dortmund, Germany, 2004.

[11] G. Casse, M. Glaser, E. Grigoriev, "Study of evolution of active volume in irradiated silicon detectors" *Nucl. Inst and Meth. A,* vol 426, pp.94-98, 1999.

[12] V. Eremin, E. Verbitskaya, Z. Li, "Effect of radiation induced deep level traps on Si detector performance" *Nucl. Inst and Meth. A,* vol 476, pp.537-549, 2002.

[13] V. Chiochia et al., "Charge collection in irradiated pixel sensors: be am test measurements and simulation", this conference.

[14] G. Casse, P.P. Allport, S.F. Biagi, T.J.V Bowcock, A. Greenall, P.R. Turner, "Characterisation of an inhomogeneously irradiated microstrip detector using a fine spot infrared laser" *Nucl. Inst and Meth. A,* vol 512, pp.60-70, 2003.

[15] M. Swartz et al., "Updated double junction simulation of CMS pixel test beam data", 5th RD50 workshop, Helsinki, 2-4 June 2005, http://rd50.web.cern.ch/rd50/

8.2. p-type silicon detectors produced by the SMART network

The research actitvity of the SMART project [1], a collaboration of Italian research institutes funded by I.N.F.N., has been focused on the development of radiation hard silicon position sensitive detectors for the CERN Large Hadron Collider luminosity upgrade [2]. Electrical characterization of pad and micro-strip devices as well as study of microscopic defects on the bulk material has been carried out on **n**- and **p**-type 4" silicon wafers, grown with Standard Float Zone (SFZ), high resistivity Magnetic Czochralski (MCz) techniques. Produced devices have been irradiated at very high fluences with 24 GeV/c and 26 MeV protons (up to ~ 3 10^{15} 1 MeV neutrons equivalent cm^{-2} (n_{eq}/cm^2)) and with reactor neutrons (up to ~8 10^{15} n_{eq}/cm^2). Preliminary results of measurements before and after irradiations as well as material radiation hardness issues are discussed. In particular, this section

describes the most important results on microstrip detectors, while main results on pad structures are reported in the Pad Detector Characterization chapter.

Materials, processing and irradiation

Bare wafer materials with both n- and p-type bulk doping used in this study belong to the common RD50 procurement. MCz 4'' wafers were produced by Okmetic Ltd (Vantaa, Finland), few n-type epitaxial wafers (ρ = 50 Ωcm, EPI layer thickness = 50μm) grown at ITME, (Varsaw, Poland) have been also used. SFZ silicon wafers were also processed for performance comparison.

The wafer layout includes 66 test structures and 10 microstrip sensors of different geometries (see table 1). Processing has been performed by ITC-IRST (Trento, Italy) in two successive runs. The first run was dedicated to n-type (RUN-I) and the second one to p-type materials (RUN-II); they have been processed with the same mask-set, designed to be used with all the different silicon materials. For RUN-II the uniform p-spray technique [3] has been used to increase n^+ implants isolation with two different implantation doses, namely $3x10^{12}$ cm^{-2} (low p-spray) or $5x10^{12}$ cm^{-2} (high p-spray). Further details can be found in references [4,5,6].

μ-strip #	pitch (μm)	p+ width (μm)	Poly width (μm)	Metal width (μm)
S1	50	15	10	23
S2	50	20	15	28
S3	50	25	20	33
S4	50	15	10	19
S5	50	15	10	27
S6	100	15	10	23
S7	100	25	20	33
S8	100	35	30	43
S9	100	25	20	37
S10	100	25	20	41

Table 1: Geometrical parameters of microstrip detectors

The irradiation of devices has been performed with different particle beams. A first proton irradiation campaign was carried out at the CERN-SPS proton beam facility with 24 GeV/c protons with fluences up to 3×10^{15} n_{eq}/cm^2. A second irradiation was performed at the Compact Cyclotron of the Forshungszentrum in Karlsruhe (Germany) with 26 MeV protons with fluences up to 2×10^{15} n_{eq}/cm^2.

Pre-irradiation measurements

Pre-irradiation results of n-type devices (SFZ, MCz) have shown a uniform resistivity and current density within the same wafer and a good breakdown performance for all microstrip geometries [1,4,7]. MCz p-type wafers have shown local depletion voltage (V_{fd}) variations [5,7] due to thermal donors activation [8]. Moreover, low breakdown voltages on microstrip sensors processed in both SFZ and MCz material with high dose p-spray has been detected [7,9].

In order to quantify the contribution to the noise of a microstrip device assembled in a tracking detector unit, the pre-irradiation characterization includes interstrip capacitance (C_{int}) measurements[1]. For n-type material a typical behavior of C_{int} as a function of the bias voltage has been observed, with a saturation value in over-depletion condition ranging from 0.5 to 1.2 pF/cm (fig.1a), in agreement with the different device geometries.

On the other hand, the interstrip capacitance for p-type sensors shows a strong variation with bias voltage (fig.1b,c), starting from high values at low bias and slowly decreasing to a higher saturation value with respect to n-type sensors, while at the same time the interstrip resistance is increasing. Such behaviour is strongly influenced by the metal over-hang (Al strip wider than the n+ strip implant): the coupling between the Al strip and the p-spray layer causes an additional C_{int} contribution, that decreases as the bias voltage is increased. This effect has been checked by comparing the C_{int} measurements for sensors differing only by the metal overhang extension, see fig.1c (sensors s7, s9 and s10 have increasing metal overhang MO). The C_{int} saturation is faster in

[1] In all C_{int} measurements discussed here LCR terminals are connected to AC pads (metal-metal capacitance); in this configuration, high frequency measurements are appropriate: a 100 KHz value has been used for all measurements shown.

low p-spray sensors and for large pitches (fig.1b,c). A team of the Santa Cruz RD50 group is also studying the SMART microstrip sensors, getting similar results [10].

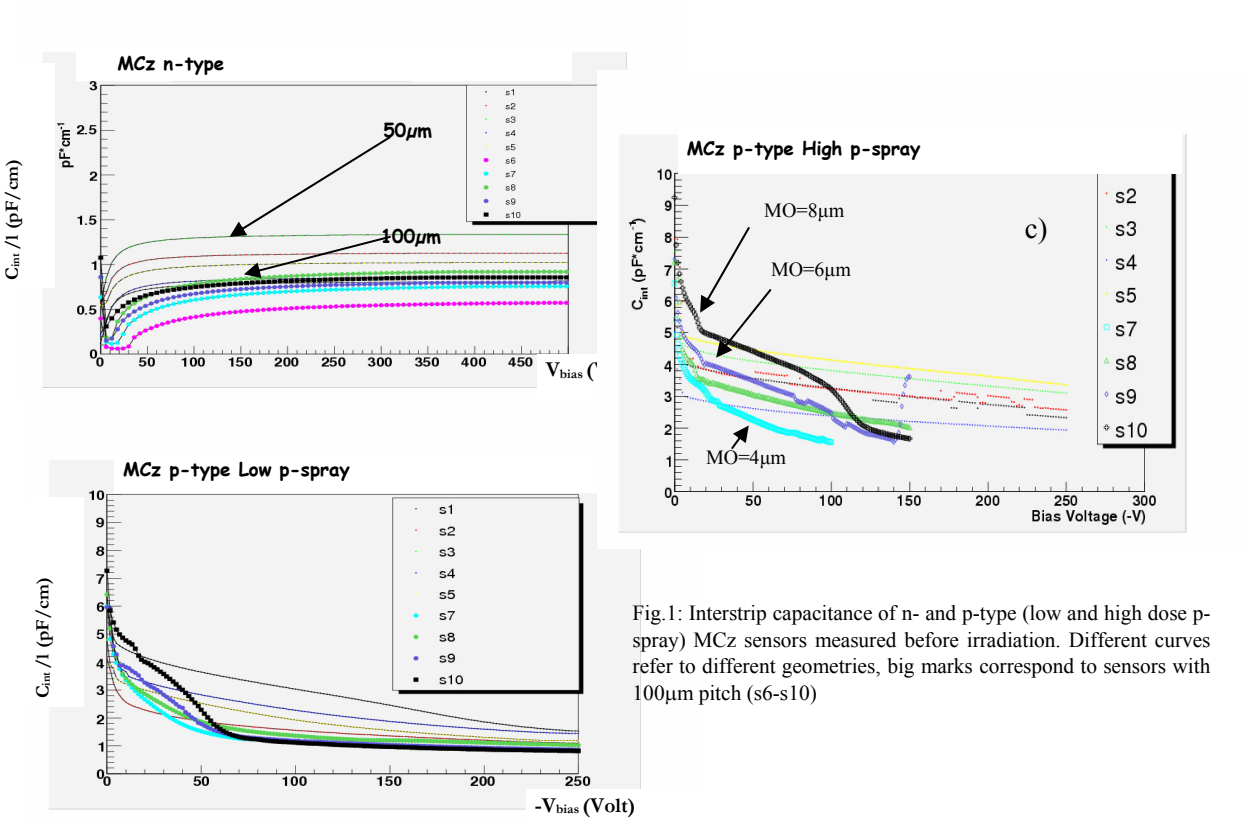

Fig.1: Interstrip capacitance of n- and p-type (low and high dose p-spray) MCz sensors measured before irradiation. Different curves refer to different geometries, big marks correspond to sensors with 100µm pitch (s6-s10)

The effect of the p-spray layer on the strip isolation and the relation between the p-spray dose, the MO and the interstrip capacitance are accurately described for different oxide charge densities by device simulations developed at IRST [11]; a good agreement with the experimental data is found.

The simulation results, confirmed by our observations, show that, depending on the oxide charge level, on the p-spray dose and on the MO value, isolation among n^+ strip implants and optimal interstrip capacitive coupling C_{int} can be reached, in several cases, only at high bias voltage. This behaviour must be carefully followed in irradiated detectors, where it could cause problems if partial depletion conditions were necessary.

Few micro-strip sensors have been assembled in detector units with the front-end electronics designed for the CMS silicon strip tracker and read-out with the standard DAQ system used for this experiment [12]. The detector performance has been studied with the analysis of the collected charge spectrum by electrons from ^{106}RU source, which are minimum ionizing particles. Preliminary measurements show that MCz and SFZ n-type detectors have similar performances: the average value of the charge collected on a 50 µm pitch detector is for both materials $\langle Q \rangle = 18.8 \pm 0.3$ (ADC Channels), suggesting that collection efficiency is also similar, and values of S/N ~19 have been measured for both detectors (see also [10]).

Post-irradiation results

All devices, diodes and mini sensors, have been fully characterized after irradiation (see also par. 1.3.3). The MCz and SFZ n-type microstrip detectors have shown good performances before and during the annealing treatment, with breakdown voltages well above their V_{fd} value (see fig.2); the leakage currents are proportional to the received fluence, as expected. The p-type detectors show an improved performance after irradiation: in the entire fluence range the breakdown voltages of the detectors with a low p-spray dose are fully comparable with the n-type sensors and are in excess of

600V, although the detectors with high dose p-spray recover completely (see fig. 3) only at irradiation fluences around $6x10^{14}$ 1-MeV n_{eq}/cm^2 [7,9].

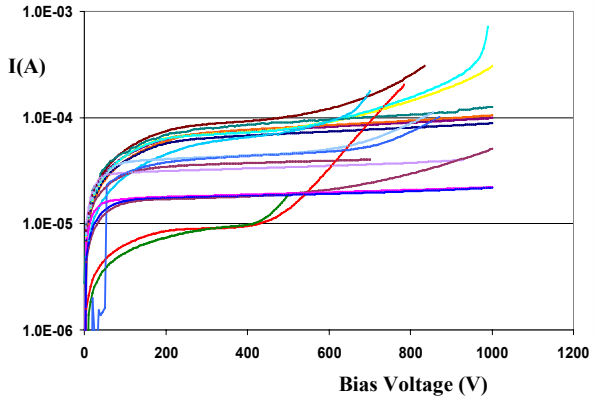

Fig. 2. IV curves of n-type microstrip sensor irradiated with 26 MeV protons from 6×10^{13} n_{eq}/cm^2 up to 2×10^{15} n_{eq}/cm^2

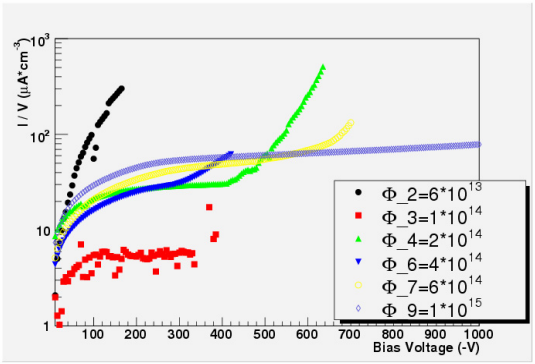

Fig. 3. Leakage Currents of high dose p-spray MCz p-type sensors irradiated with 26 MeV protons (fluences are expressed in n_{eq}/cm^2)

The MCz and the SFZ microstrip detectors have comparable performances[2] in terms of interstrip capacitance (C_{int}) after irradiation [7,9]. In fig. 4 the behaviour of sensors with different materials and technological production splittings is compared: within each plot, the same sensor geometry has been considered. For the n-type detectors C_{int} is not deteriorating significantly with the fluence, with the FZ devices following the classical <111> behavior [13]. The post-irradiation value for MCz sensors, after a sharp initial decrease with V_{bias}, is slightly higher and in the same range of the pre-irradiation values: 1.2-1.7 pF/cm for the detectors with a strip pitch of 50 μm and 0.5-1. pF/cm for the 100 μm pitch sensors. For what concerns p-type detectors, the same features observed before irradiation in the C_{int} *vs* V_{bias} curves are still present: interstrip capacitance decreases with V_{bias} towards a saturation value. The saturation is still faster for low p-spray isolation and for large pitches, with no differences between FZ and MCz substrates. It can be observed that the C_{int} behaviour for p-type devices improves with irradiation; in particular, low p-spray sensors become pretty comparable to n-type MCz irradiated sensors. The improvement of p-type microstrip sensor performances for what concerns breakdown voltage and interstrip capacitance is also nicely predicted by device simulation [11], where it is explained in terms of oxide charge density for different p-spray dose choices. In this respect, irradiation by γ from ^{60}Co at Santa Cruz [10] confirms that surface radiation damage (leading to oxide charge increase) has a strong influence on the C_{int} behaviour, as foreseen by simulations.

[2] It must be taken into account that all crystals but n-type FZ (which is <111>) are <100> oriented.

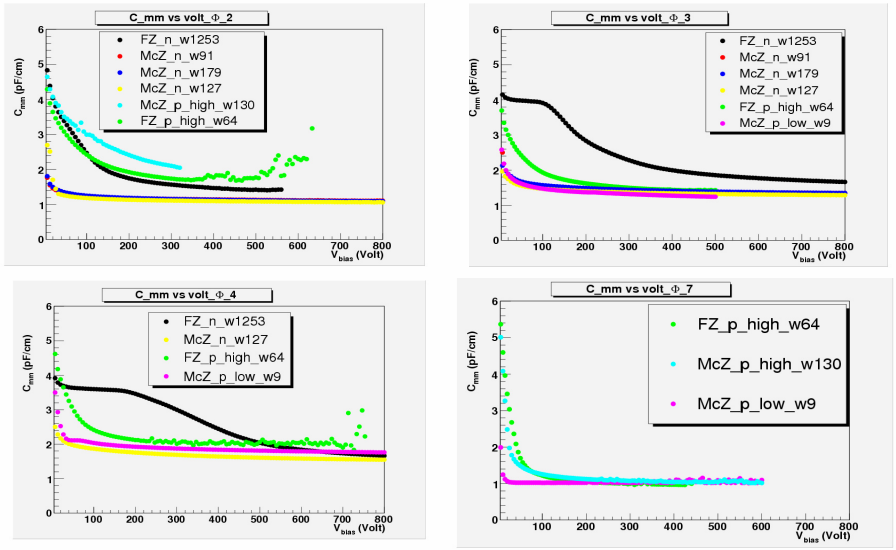

Figure 4. C_{int} *vs* V_{bias} for n- and p-type SFZ and MCz microstrip devices: a) Φ2 = $0.6x10^{14}$ n_{eq}/cm^2, sensor geom. S1; b) Φ3 = $1x10^{14}$ n_{eq}/cm^2, sensor geom. S2; c) Φ4 = $2x10^{14}$ n_{eq}/cm^2 , sensor geom. S3; d) Φ7 = $6x10^{14}$ n_{eq}/cm^2, sensor geom. S7.

References

[1] RD50 Status report, par. 8.6, CERN Dec. 2004.

[2] F.Gianotti et al., Eur. Phys. J. C 39 (2005), 293

[3] R. H. Richter et al., *"Strip detector design for ATLAS and HERA-B using two-dimensional device simulation"* Nucl. Instr. and Meth. A 377 (1996) 412.

[4] M. Bruzzi et al., *"Processing and first characterization of detectors made with high resistivity n- and p-type Czochralski silicon*" Nucl. Instr. and Meth. A 552 (2005) 20.

[5] C. Piemonte et al.,*"Preliminary electrical characterization of n-on-p devices fabricated at ITC-irst"* presented at the 5th RD50 Workshop. Available: http://rd50.web.cern.ch/rd50/.

[6] N. Zorzi et al., *"Characterization of n-on-p devices fabricated at ITC-irst",* presented at the 1st Workshop on the development of p-type Si detectors, Trento, February 2005. Available: http://rd50.web.cern.ch/rd50/

[7] A.Macchiolo et al, *"Characterization of micro-strip detectors made with high resistivity n- and p-type Czochralski silicon"*, proceedings of the PSD07 conference, Nucl. Instr. and Meth. A (submitted for publication).

[8] M. Bruzzi et al., *"The issue of doping disuniformity in p-type MCz Si detectors"* presented at the 7th RD50 Workshop, Oct. 2005, CERN. Available: http://rd50.web.cern.ch/rd50/.

[9] V.Radicci et al., *"Study of radiation damage induced by 24GeV/c and 26MeV protons on heavily irradiated MCz and FZ silicon detectors"*, presented at the 7th International Conference on Large Scale Applications and Radiation Hardness of Semiconductor Detectors, submitted for publication on Nucl. Instr. and Meth. A.
A. Messineo et al., *"Development of radiation hard Silicon detectors: the SMART project"*, presented at the 9th ICATPP Conference, submitted for publication on Nucl. Instr. and Meth. A.

[10] H. Sadrozinski et al., *"Signal-to-Noise ratio for silicon strip detectors and SiGe front-end electronics"* presented at the 7th RD50 Workshop. Available: http://rd50.web.cern.ch/rd50/.
H. Sadrozinski et al.,, *"Measurements on Short-Strip Silicon Detectors"* RD50 Status report 2005..

[11] C.Piemonte *"TCAD simulations of isolation structures for n^+-on-p silicon microstrip detectors"* presented at the 7th RD50 Workshop. Available: http://rd50.web.cern.ch/rd50/.

[12] CMS Tracker Technical Design Report, CERN/LHCC 98-6.

[13] G. Calefato et al., *"A comparison on radiation tolerance of 100 and 111 silicon substrates of microstrip detectors"* Nucl. Instr. and Meth. A 476 (2002) 744-750.

8.3. Frontend Readout ASIC in SiGe

This project is dedicated to the evaluation of integrated circuit technologies for the readout of the upgraded ATLAS ID, in particular the evaluation of new SiGe biCMOS technologies and the design of a prototype readout IC. The activity reported in the present section has been carried out mainly by the following RD50 members:

David E. Dorfan, Alexander A. Grillo, Jessica Metcalfe, Hartmut F.-W. Sadrozinski, Abraham Seiden and Ned Spencer from SCIPP, UC Santa Cruz, CA 95064 and Miguel Ullan CNM, Barcelona, Spain.

8.3.1 Detailed Results

Test structures of a SiGe biCMOS process were irradiated with protons to several fluences up to $1x10^{16}$ p/cm^2. Reasonable electrical performance was measured after irradiation demonstrating that the SiGe bipolar devices can be quite radiation hard. Several different SiGe fabrication processes are now being studied. A prototype, proof-of-principle, front-end circuit is now being designed to be ready for fabrication in fall 2005.

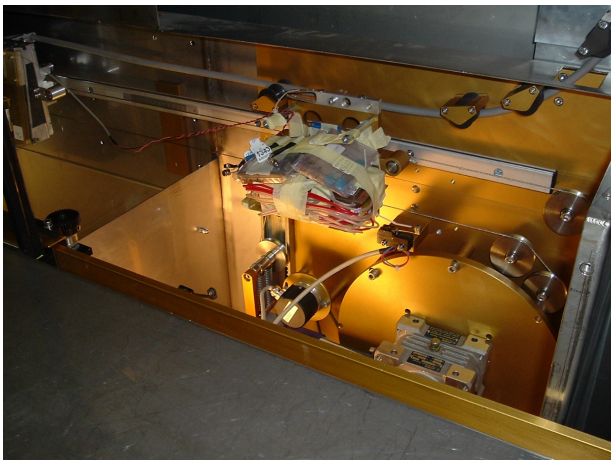

Figure 1: RD50 Shuttle for Irradiating Samples at the CERN PS

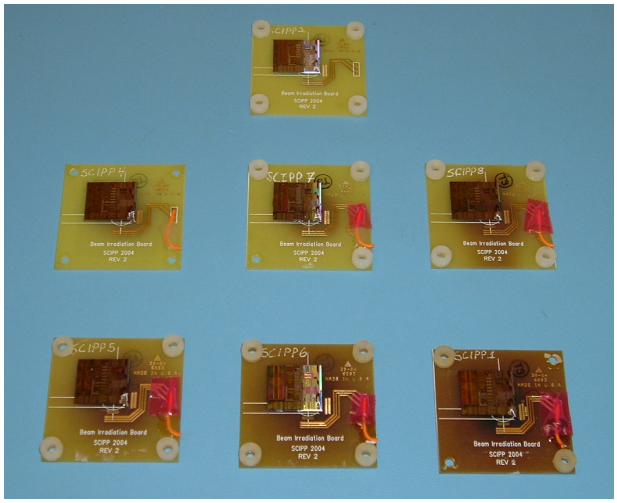

Figure 2: Test Structure Arrays on PCBs after Irradiations to Fluences of 0, $4x10^{13}$, $1x10^{14}$, $3.5x10^{14}$, $1x10^{15}$, $3.6x10^{15}$ and $1x10^{16}$.

Irradiation of Test Structures

The test structures were obtained from one of the commercial SiGe biCMOS (IBM 5HP) processes from collaborators at the Georgia Institute of Technology. Each set of test structures was a collection of several transistors and other components arrayed on a wafer chip. Several transistor sizes and some matched transistor pairs for testing were selected. The devices were characterized in Santa Cruz, then brought to CERN for irradiation with protons and then returned to Santa Cruz for re-testing after sufficient time for the activation to reach safe levels. The irradiations were carried out by our graduate student, Jessica Metcalfe, in the IRRAD1 [???] irradiation setup at the CERN PS in the fall of 2004.

The IRRAD1 shuttle system developed to move samples into the PS beam line is shown in Figure 1. The test structure arrays mounted on printed circuit boards for testing are shown in Figure 2 after they have been irradiated.

Irradiation Test Results

Figure 3 shows a typical Gummel plot of the performance of one transistor after i irradiation to $1.3x10^{15}$ p/cm^2. As expected the radiation damage manifests itself as an increase in the base leakage current which effectively decreases the DC current gain β, which is the ratio of collector current to base current. When the bias current is scaled by the transistor size we see in Figure 4 that β as a function of fluence is independent of transistor size. This figure also shows that the transistors are still operational after being irradiated to $1x10^{16}$ p/cm^2 although the performance at the highest fluence is marginal.

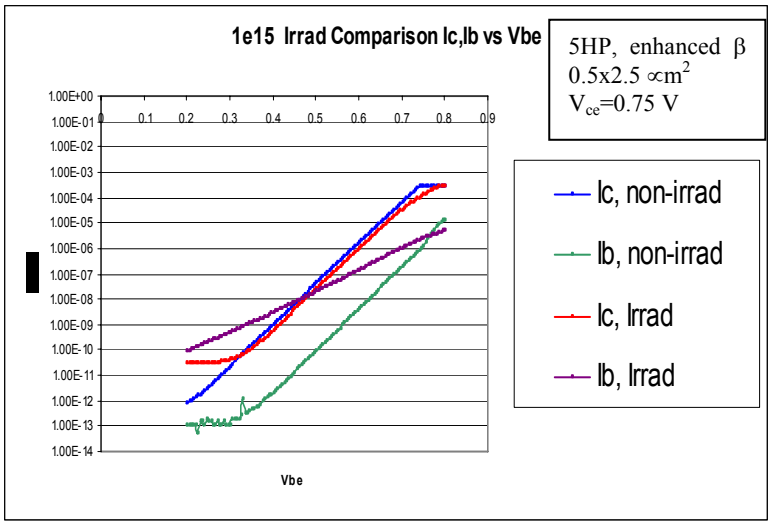

Figure 3: Gummel Plot for 0.5x2.5 mm^2 transistor irradiated to $1.3x10^{15}$ p/cm^2.

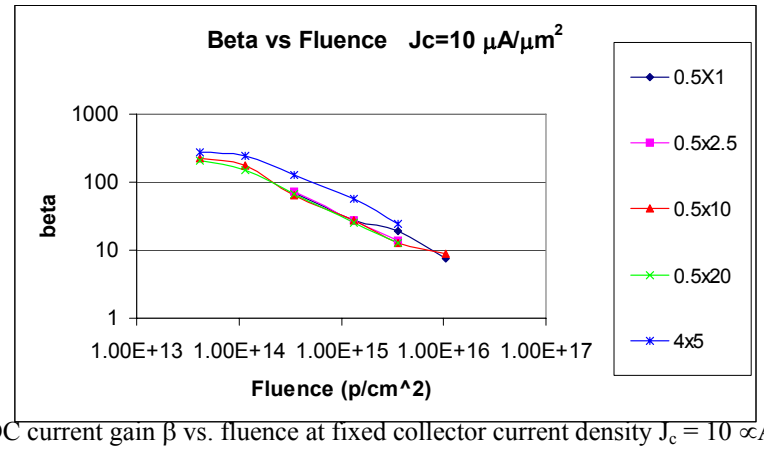

Figure 4: DC current gain β vs. fluence at fixed collector current density J_c = 10 ∝A/∝m^2.

After the post-irradiation testing was completed, annealing tests were performed to determine to what extent the damage can be repaired. Annealing at elevated temperature accelerates the repair thus emulating the effects of a longer time at normal operating temperatures. Figure 5 shows the resulting improvement of β for one transistor, which had been irradiated to 1x10^{15} p/cm^2. One can see from the plot a very marked improvement (.e.g. β increases from 15 to 51 at 10 ∝A of bias current) after full annealing. Part of our ongoing work is to determine how much of this annealing is to be expected during normal operation of the transistors over an extended period of time.

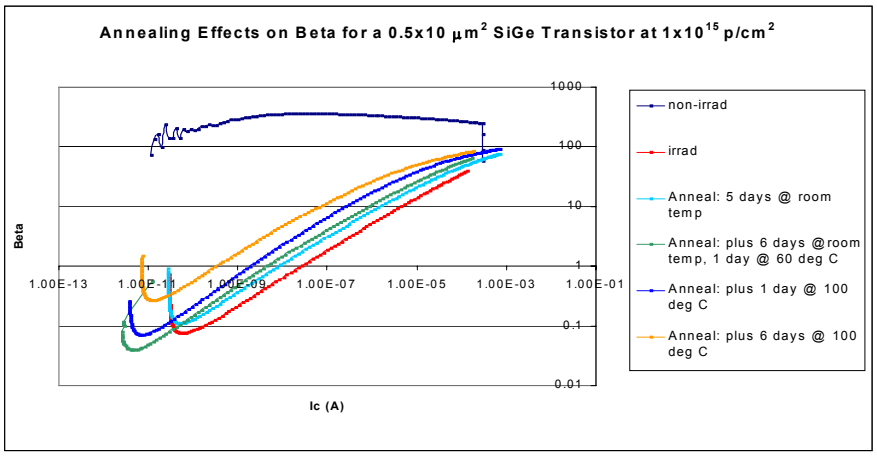

Figure 5: Annealing of radiation damage after 3x10^{15}p/cm^2: part of the β loss is restored.

The results up to a fluence of 3x10^{15} p/cm^2 look quite encouraging. The data point at 1x10^{16} p/cm^2 was taken as an exploratory measure just to see how rad-hard this technology is. The range of interest for mid and outer radii of the upgraded ATLAS Inner Tracker does not exceed 3x10^{15} p/cm^2 and is probably closer to 1x10^{15} p/cm^2 for the inner most radius of interest for non-pixel silicon detectors. It is envisioned that pixel detectors with solely CMOS, not biCMOS, electronic readout will occupy the inner most radii where the fluences exceed 3x10^{15} p/cm^2. The fact that these SiGe devices are still operational at 1x10^{16} p/cm^2 shows that there is some margin above the desired fluence.

Table 1: Bias Currents required to achieve β of 50 at fluence of $1.3x10^{15}$ p/cm^2

Fluence: 1.34E15		
β=50	Required Current	
Transistor Size μm^2	I_c irrad	I_c anneal
0.5x1	3.E-05	1.E-07
0.5x2.5	7.E-05	4.E-06
0.5x10	4.E-04	1.E-05
0.5x20		6.E-05
4x5	1.E-04	1.E-05

If one chooses a β of 50 as the minimum acceptable value for post-rad operation, one can estimate at what minimum bias current each different size transistor can operate and whether this will represent a significant power savings over CMOS. Table 1 shows that all of the various transistor sizes will operate at a fluence of $1x10^{15}$ p/cm^2 with very modest bias currents, less that 100 ∝A for the large transistor to be used as the first stage amplifier and a fraction of a micro-Amp for the smallest transistors to be used in the other shaping and comparator stages. Using more conservative estimates of currents of 50-150 ∝A for the large front-end transistor and 5 ∝A for the small transistors, a crude estimate for power consumption is 0.25 to 0.50 mW/channel which would be a factor of 3 to 4 lower than that achieved by a comparable CMOS circuit [1]. If this can be realized, it would represent a considerable power savings for the ATLAS Tracker and help the problem of providing services.

R&D Plan for Year 2006

We have determined that there are at least 25 fabrication facilities that make similar SiGe biCMOS integrated circuits [2]. Some have more than one generation. Since each of these processes differs in the details of the collector-base-emitter structure and in particular differs in the structure of the oxide isolation, it is possible that they have different levels of radiation tolerance. We believe that it is important to understand these differences and to judge a few of the available processes in order to best choose the appropriate process for a future upgrade. We have made arrangements to sample test structures from three vendors, IBM, IHP and STm. While UCSC will continue to work with IBM, Barcelona has received IHP test structures. In the Fall 2005, we expect test structures from STm, thanks to the collaboration of the CERN Microelectronics group and Pierre Jarron. We plan to do similar radiation studies with samples from all three vendors, in some cases with more than one of their generations. Our planning document "Uniform Testing for Technology Radiation Hardness Comparison" defines the following items:

- Type and sizes of devices to consider,
- a minimum set of measurements to be performed on the devices,
- the setup for these measurement and the environmental conditions (temperature, bias, …),
- conditions of the irradiations
- a set of figures of merit for the radiation damage to be extracted from the measurements

This will give us a better understanding of the sensitivities of radiation tolerance to device structure and process. We have made arrangements to irradiate samples with neutrons and gammas as well as protons. This will be accomplished in this second year. Eventually we will arrive at a set of criteria for the figures of merit in terms of usability for the s-LHC Front End Electronics.

We will update the technology files to reflect post-rad parameters of the one process, which appears to be a potential technology for a future upgraded tracker.

In order to advance our understanding of the true power savings beyond the level of calculated estimates, we will also design and fabricate a chip with a few channels of a front-end readout using one of the available processes that we are studying. Technology files from IHP have been obtained and design work has started. This may not be our final choice for optimum process but should be representative of the potential power savings. A full readout chip with a fully qualified SiGe biCMOS process will await future work after year 2 is completed.

References for Section 8.2

[1]J. Kaplon et al., "Fast CMOS Binary Front-End for Silicon Strip Detectors at LHC Experiments", 2004 IEEE NSS-MIC, Rome Oct 2004.
[2] http://isde.vanderbilt.edu/Content/muri/2005MURI/Cressler_MURI.ppt

8.4. Initial studies of commercial 0.13-μm CMOS devices

The feature size of the ASIC chips used to amplify and read-out the present LHC silicon detectors is 0.25 μm. New, smaller feature size are already available and will be the dominant technology by the time the sLHC devices will be commissioned. The proof of the radiation hardness of these very deep sub-micron CMOS technologies has to be proven. Here some results on the investigation of commercial 0.13μm CMOS devices are presented [1].

The devices used in this study were n- and p-channel MOSFETs manufactured by STMicroelectronics, Agrate Brianza, Italy in a commercial (non hardened) 0.13 μm CMOS technology. The gate oxide was oxynitride, its thickness 2.5 nm. The channel width (W) ranged from 10 μm down to 0.35 μm, the channel length (L) from 10 μm to 0.13 μm. The gate electrode was n-doped (p-doped) polysilicon for p-substrate (n-substrate). Ligthly Doped Drains (LDD) were used to reduce hot carrier effects. The LDD spacers were made of nitrided oxide. Shallow Trench Isolation (STI) was used to isolate one device from the other. The transistors were arranged in arrays of given channel width or length with common gate, source, and bulk terminals and separated drain contacts. Some arrays were provided with a protection diode at the common gate. In the following we will refer to n-channel devices built on p-type substrates as NMOSFETs, and to p-channel devices built on n-type substrates as PMOSFETs.

The 24-GeV proton irradiation was carried out at the CERN facilities in Geneva, Switzerland, on May 2004. Three different fluences were used, namely $2 \cdot 10^{15}$, $6 \cdot 10^{15}$, and 10^{16} p/cm^2. A total of more than 300 devices were measured, irradiated at the die level with all the terminals floating, and measured again after they cooled down to a safe level, at the beginning of 2005. Hence, about eight months elapsed between irradiation and post-irradiation measurements. The high fluence irradiation was unfeasible on packaged devices, since material activation would have prevented safe manual handling for several years. Before and after irradiation, the gate leakage (I_g-V_g), transfer (I_{ds}-V_{gs}) and output characteristics (I_{ds}-V_{ds}) of the MOSFETs were measured.

NMosfet

Fig. 1 shows the degradation of the gate leakage current in an array of n-channel MOSFETs with a total gate area of 210 μm^2 after 24-GeV proton irradiation with a fluence of 10^{16} protons/cm^2. After irradiation, the gate leakage curent almost doubles. As Fig. 2 shows, the increase in gate leakage is proportional to the proton fluence.

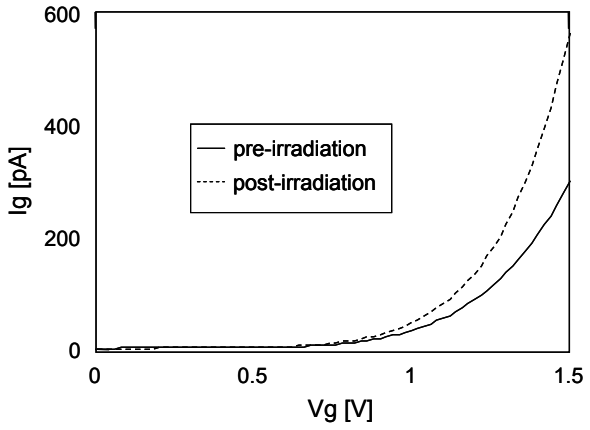

Fig. 1: Gate leakage current of an array of NMOSFETs (total gate area = 210μm^2) before and after 24-GeV proton irradiation with a fluence of 10^{16} p/cm^2.

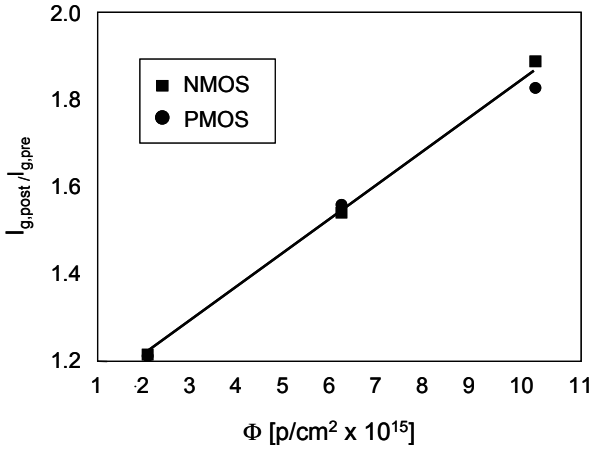

Fig. 2: Gate leakage increase as a function of the irradiation fluence for some arrays of NMOSFETs and PMOSFETs (total gate area = 210μm^2) irradiated with 24-GeV protons.

As can been seen from Fig. 3, where the I_{ds}-V_{ds} characteristics of two NMOSFETs with different aspect ratios, namely W/L = 10μm/1μm and W/L = 10μm/0.2μm, are plotted, the drain current is slightly reduced following proton irradiation. Fig. 4 displays the transconductance versus gate voltage for the same two devices of Fig. 3. Even though there is no shift in the curves, i.e no change in the threshold voltage, the transconductance peak is significantly decreased. Transconductance peak drops as large as 10% are observed after the highest fluence irradiation. Fig. 5 displays the I_{ds}-V_{gs} characteristics of the same two samples. A moderate increase (hundreds of pA) in the off-current, i.e. the drain current for V_{gs}=0, and at the same time a small increase in the subthreshold swing are present.

After showing the phenomena occurring after irradiation, we now analyze the dependence of the degradation on the proton fluence and device geometry.

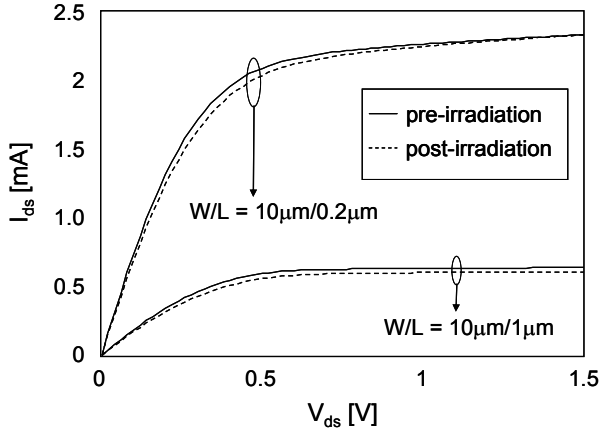

Fig. 3: I_{ds}-V_{ds} of two NMOSFETs with different aspect ratios, before and after 24-GeV proton irradiation with a fluence of 10^{16} p/cm^2.

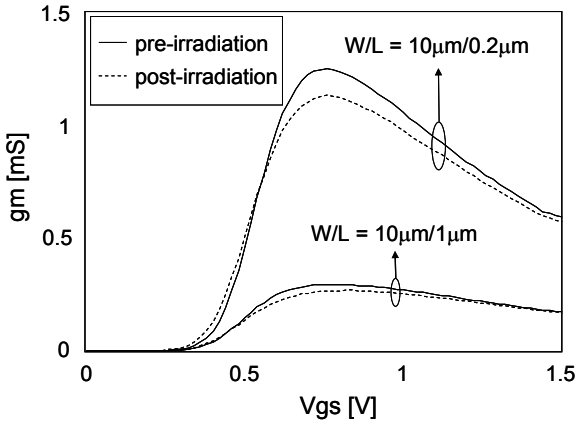

Fig. 4: Transconductance of two NMOSFETs with different aspect ratios, before and after 24-GeV proton irradiation with a fluence of 1016 p/cm2.

Fig. 5 presents the reduction in transconductance as a function of the channel length and irradiation fluence for samples with fixed W= 10 μm. As far as the channel length is concerned, no clear dependence emerges from our data. All the devices are affected in a similar measure by the irradiation. On the contrary, a rough proportionality is observed between the induced damage and the proton fluence.

PMosfet

Whereas the gate current degradation is quite similar, see again Fig. 2, significant differences appear in the behavior of the drain current of PMOSFETs as compared to NMOSFETs following high-energy proton irradiation.

Fig. 7 displays the degradation of the I_{ds}-V_{ds} for two p-channel MOSFETs with the same aspect ratios (W/L = 10μm/1μm and W/L = 10μm/0.2μm) as the two NMOSFETs of Fig. 3. A large reduction in the saturation drain current is observed (even 40% in some cases). Fig. 8 displays the degradation of the transconductance versus gate voltage for the same two PMOSFETs of Fig. 7.

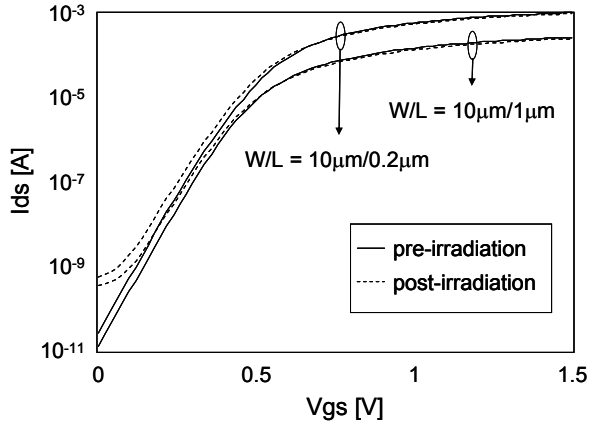

Fig. 5: Transfer characteristics of the same NMOSFETs of Fig.1, before and after 24-GeV proton irradiation with a fluence of 10^{16} p/cm^2.

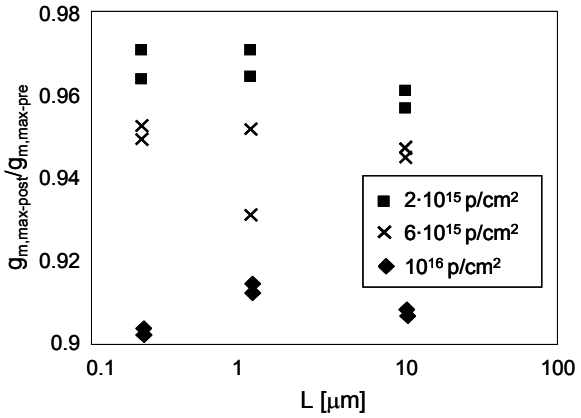

Fig. 6: Normalized transconductance degradation for several NMOSFETs with the same channel width (W=10μm) but with different channel lengths, after 24-GeV proton irradiation at three different fluences.

In this case, the transconductance peak not only decreases, as in the case of NMOSFETs, but also shifts leftward. The shift in the threshold voltage is particularly remarkable and can be as large as 150 mV after the highest fluence (10^{16} p/cm^2). The g_m peak drop is also larger (up to 18%) than in nMOS devices. Fig. 9 displays the I_{ds}-V_{gs} characteristics of the same two devices of Fig. 7: besides the already mentioned threshold voltage shift, it's interesting to observe that the subthreshold swing doesn't change appreciably following irradiation.

Again there is a modest increase (some pA) in the off-current although it is less pronounced than for NMOSFETs.

As done before with the NMOSFETs, we now present the dependence of the radiation induced changes on the proton fluence and device geometry. Figs. 10 and 11 show the dependence of the transconductance peak drop and threshold voltage shift, respectively, on the channel length and irradiation fluence for samples with fixed W = 10 μm. As far as the transconductance is concerned, short p-channel devices seem to suffer a higher degradation than long channel ones.

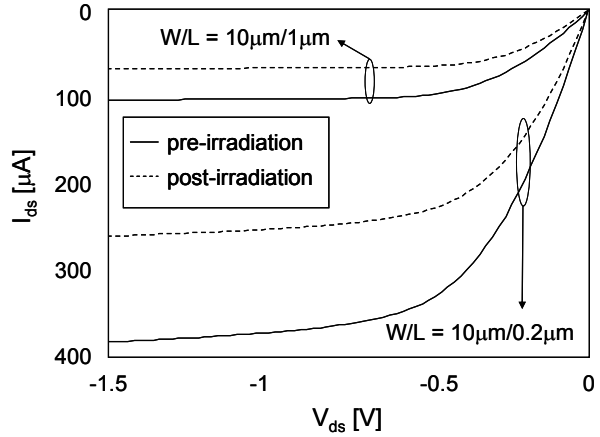

Fig. 7: I_{ds}-V_{ds} of two PMOSFETs with different aspect ratios, before and after 24-GeV proton irradiation with a fluence of 10^{16} p/cm^2.

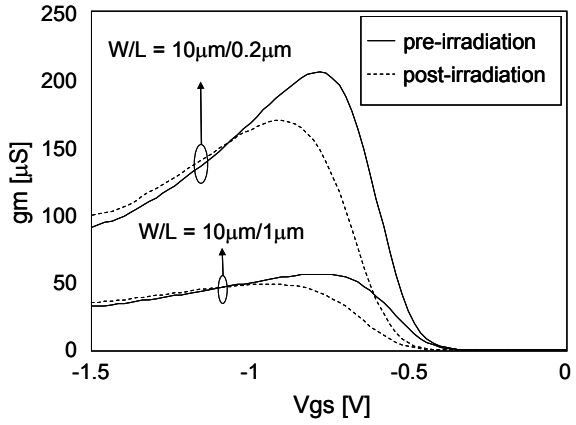

Fig. 8: Transconductance of three PMOSFETs with different aspect ratios before and after 24-GeV proton irradiation with a fluence of 10^{16} p/cm^2.

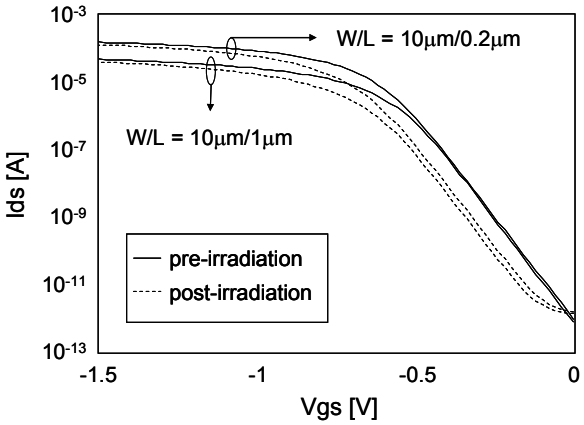

Fig. 9: Transfer characteristics of the same PMOSFETs of Fig. 4 before and after 24-GeV proton irradiation with a fluence of 10^{16} p/cm^2.

As for the threshold voltage, the situation is reversed: long-channel devices exhibit a larger shift. Again a rough proportionality is observed between the induced damage and the proton fluence.

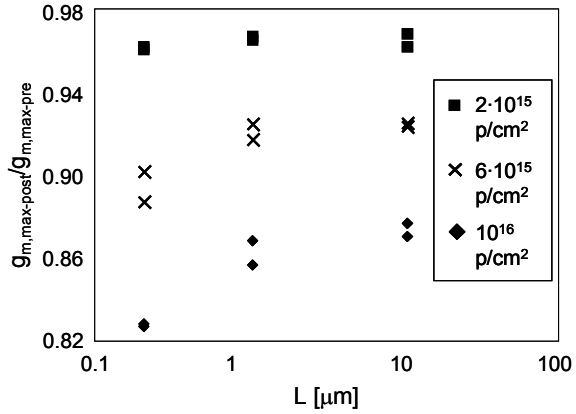

Fig. 10: Normalized transconductance degradation for several PMOSFETs with the same channel width (W=10μm) but with different channel lengths after 24-GeV proton irradiation at three different fluences.

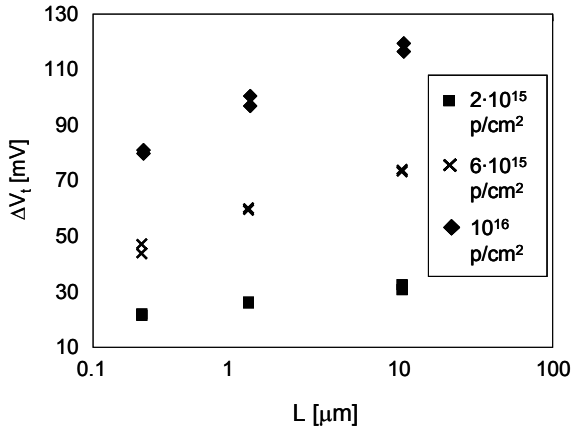

Fig. 11: Threshold voltage as a function of the channel length for PMOSFETs with the same channel width (W=10μm) at three different fluences.

Discussion

One first observation is that all the effects described in the previous section (gate leakage and off-current increase, threshold voltage shift, and transconductance drop) depend on the irradiation fluence and are found to increase with it in a roughly linear way, Figs. 2, 6, 10, and 11.

This stresses the fact that the observed phenomena are total dose effects. In the following subsections, we will examine these changes occurring following irradiation one by one, comparing n- and p-type devices.

Gate leakage

To start with, the increase in gate leakage current (Figs. 1 and 2) can be ascribed to the creation of defects inside the gate oxide, a phenomenon which has been observed after irradiation with low LET particles (gamma and X rays, electrons, and low LET ions) and is known in literature as radiation induced leakage current [8-10]. The radiation-induced defects in the gate oxide act as "stepping stones" for the carriers that tunnel through the gate oxide, thus reducing the thickness of the barrier and increasing the gate current through trap-assisted tunneling conduction.

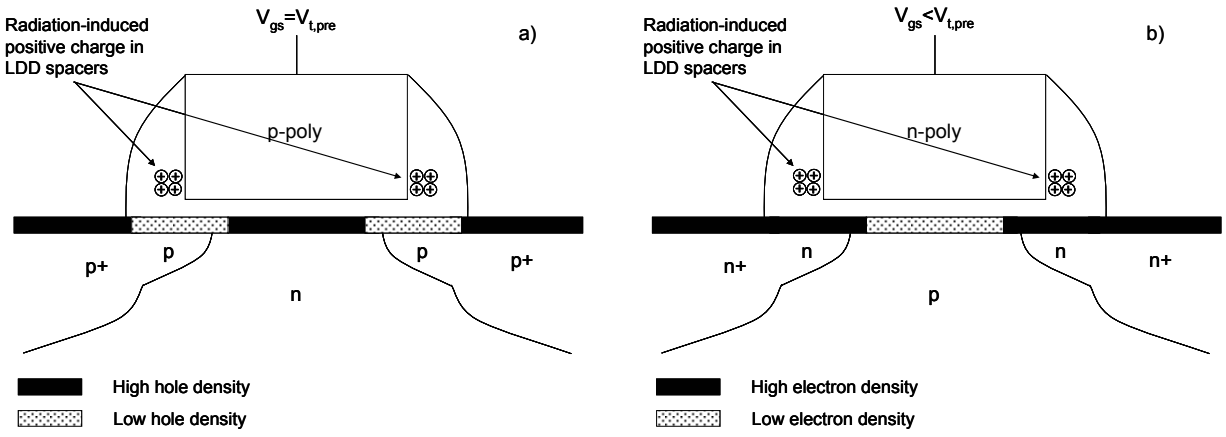

Fig. 12: Positive charge in the LDD spacers and its effect on the threshold voltage for PMOSFETs (a) and NMOSFETs (b).

Off-current

The first effect of importance concerning the drain current is the increase in off current. The excess current which is present after irradiation in the NMOSFETs (Fig. 5) flows between the source and drain terminals and is likely due to the build-up of positive charge in the STI [4-6]. This positive

charge causes the threshold voltage of the parasitic lateral transistors to decrease. Since the threshold of the "real" transistor is unaffected (Figs. 4 and 5) the net result is an increase in current for V_{gs}=0.

On the contrary, the excess current in the PMOSFETs (Fig. 9) flows between the drain and bulk terminals and is due to radiation induced defects in the drain p-n junction which enhance the reverse-bias current. This contribution is present also in the NMOSFETs, but it is negligible with respect to the parasitic transistors.

Threshold voltage

As far as the drain current of the devices after proton irradiation is concerned, one of the most striking feature is the difference between NMOS and PMOS devices. The large leftward shifts in the threshold voltage of PMOSFETs, Fig. 8, suggest the presence of positive charge somewhere in the proximity of the conducting channel. Yet, the same positive charge should cause a leftward shift of the transconductance peak in the NMOSFETs too, which, compare Figs. 4 and 8, does not take place at all, or at least not with comparable magnitude.

One possible explanation for this different behavior between NMOS and PMOS devices is that the threshold voltage is not altered "globally" by the irradiation, but only "locally" in some parts of the channel along its length, for instance only close to the drain and source regions. In this way, after irradiation, when an NMOSFET is turned on by raising the gate voltage, the conducting channel would form first for $V_{gs} < V_{t,pre}$ close to the drain and source diffusions, and only later for $V_{gs}=V_{t,pre}$ in the remaining part. Since no conduction is possible when only a part of the channel is present, no change in the threshold voltage of the whole device is observed, so that $V_{t,post} = V_{t,pre}$. On the contrary, the conducting channel of PMOSFETs would form first in the central part, far from the source and drain diffusions, for $V_{gs}=V_{t,pre}$. Yet, without a connection to the source and drain, the transistor would remain off until the channel forms also close to the source and drain extensions for $V_{gs} < V_{t,pre}$, hence $V_{t,post} < V_{t,pre}$.

Local changes in the threshold voltage, namely close to the drain, occur also during channel hot carrier stresses [11]. Whereas in the ohmic region the effects of a local change in V_t are indistinguishable from a global one, i.e. one that affects the whole gate area, in saturation one can tell if the change is local from the output resistance. If there's no decrease, then the V_t shift is global or, for accuracy's sake not localized to the terminal used as drain, otherwise it's localized there. No changes in the output resistance are present in our devices, see Fig. 7, but that's not because the shift is global, just because the damage is on both sides, i.e. both at the source and drain terminals.

As it's clear from the I_{ds}-V_{gs} curves in semi-log scale, Fig. 8, the threshold voltage shift in the PMOSFETs isn't due to a change in the subthreshold swing. This rules out the creation of interface states (or of any other defects that get charged and discharged with the gate voltage) as the reason for these shifts. So, it must be fixed charge.

As to the whereabouts of this fixed positive charge, it's unlikely that it is trapped in the gate oxide, because in that case the tunneling distance would be so short that it would be quickly neutralized. Given the fact that the shifts occur also in devices with large width (W=10μm), one can also exclude that the cause is the charge in the lateral isolation responsible for the increase in the off current.

Instead, a much more likely place are the spacers used for the implantation of LDDs. These are made of a thick oxide and therefore prone to charge trapping. Fig. 10 schematically depicts the location of the trapped positive charge and its effects on the inversion layer for both PMOS and NMOS devices. As seen in the figure, the spacers are located above the LDDs, which are regions with a relatively low doping. In the case of the NMOSFETs, these LDDs are n-type, and are brought into accumulation by the positive charge in the spacers. In this condition, the accumulation layer in the LDDs effectively screens the charge trapped in the spacers. Instead, the LDDs in the PMOSFETs are p-doped and the positive charge in the spacers tend to deplete them. Here, the screening is far less effective, being limited by the low doping, and the effect of the positive charge could be felt further than in NMOSFETs. So, there are two reasons why the NMOSFETs are less affected by positive charge in the LDD spacers than PMOSFETs: no global effect on the threshold voltage and more effective screening by the junctions.

Another interesting point is that, for the PMOSFETs, the threshold voltage shift increases with the channel length, Fig. 11. The reason is that in the unirradiated devices V_t increases for decreasing channel length (at least in the range we analyze here) as a consequence of the halo implantation .

Instead, after irradiation the threshold voltage is set by the behavior of the regions close to the source and drain and, therefore, it tends to become independent of the channel length. As a consequence, the shift is larger in the long channel devices.

According to the view we presented here, the shift in the threshold voltage depends heavily on the trapping characteristics of the spacer oxide. Since there is not a single recipe for spacer oxides (for example for the amount of nitridation), large variations can be expected from one technology to the other, resulting in very different responses to high-energy proton irradiation.

Transconductance

In general, the peak in the g_m-V_{gs} curves of a MOSFET occurs when the device enters the ohmic region, i.e. when V_{gs}-V_t=V_{ds}. In this region, the following relation holds [12]:

$$g_m = C_{ox}\frac{W}{L}\frac{\mu_0}{1+\vartheta_1(V_{gs}-V_t)}\cdot V_{ds} \qquad (1)$$

Where C_{ox} is the oxide capacitance per unit of area, μ_0 is the low field mobility, and ϑ_1 is the mobility attenuation. For high gate voltage, the transconductance is reduced because of the mobility degradation with the vertical field, which is accounted for by ϑ_1, and the series resistance, which reduces the effective V_{ds} [12]. So, there are two ways in which the irradiation can reduce the transconductance peak, either through the series resistance or through the mobility.

When the g_m peak occurs, the drain current is quite low, so the voltage drop in the series resistance should be negligible and then have no impact on the transconductance peak. Furthermore, we can rule out the series resistance as the culprit also on the account of the NMOSFETs. As discussed in the previous section, the positive charge in the spacers changes the distribution of the carriers inside the LDD regions. This has an impact on the series resistance of the devices. In particular, the series resistance of the NMOSFETs should be reduced due to the higher density of carriers in the LDDs, whereas the one of the PMOSFETs should be increased. Since the transconductance drops also in NMOSFETs, the series resistance is probably not involved.

So a reduction in mobility is the likely culprit for the observed degradation in the transconductance peak. The fact that the amount of the degradation depends on the channel length for the PMOSFETs, and in particular it decreases for increasing channel length, means that for PMOSFETs the mobility may be reduced more on the edges of the transistors, i.e. close to the drain and source regions, than in the center. On the contrary, there's no clear dependence on the channel length for the NMOSFETs, meaning the mobility is reduced all along the channel lentgh. Anyway, in both cases the degradation for the device with L=10μm, where edge effects should be negligible, is significant and of about the same amount in the two cases (compare Figs. 6 and 10), so there is a considerable contribution by the central part of the channel which seems to be independent of the substrate doping type.

As a result, we can split the reduction in mobility into two contributions, one independent of the channel length and present both in NMOSFETs and PMOSFETs, and the other of increasing importance for decreasing gate length and present only in PMOSFETs.

The first contribution can be related to the creation of interface traps in the gate oxide. This is probably true both for NMOSFETs and PMOSFETs, even though only in the first case there is direct evidence in the form of an increased subthreshold swing, Fig. 5. On the contrary, no or very little changes occur in the subthreshold region of PMOSFETs, but this can be explained by the fact that the behavior in the subthreshold region after irradiation is determined by the regions close to the drain and source, i.e. the last ones to turn on as we explained earlier, so it's less affected by defects in the central part of the channel.

The second mechanism which causes the additional degradation occurring in PMOSFETs may be attributed to the positive charge present in the LDD spacers. In fact, the electric field originating from it may increase the Coulomb scattering, thus reducing the mobility close to the source and drain. This contribution is not present in NMOSFETs because of the more effective screening of the positive charge by the LDD regions.

Impact on circuits

Before analyzing the impact of the degradation on actual circuits, we must make a couple of observations. Firstly, since the post-irradiation measurements were carried out eight months after exposure (due to safety reasons), it may be possible that some annealing took place in the elapsed time. Secondly, the devices were left floating during irradiation, which is probably not the worst case condition. As a result, the data we present here may somewhat underestimate the degradation occurring in devices operating in real circuits.

Furthermore, 24-GeV protons may provoke a variety of nuclear reactions with the emission of high-LET ions or neutrons which could give rise to an anomalous degradation in some devices from time to time. Some transistors may indeed deviate from the illustrated "typical" behavior (see for instance the two nominally identical samples with L=1mm of Fig. 6, one of which exhibits a larger-than-expected degradation).

Anyway, the good news is that the transistors remain fully operational even after irradiation at the highest fluence. The relatively bad news is that there are some issues related to the performance and power consumption of these devices after exposure to high energy protons that have to be considered. First of all, both the gate leakage and the off current increase after irradiation, meaning, for instance, that a circuit designed with this technology will tend to dissipate more static power as it is exposed to radiation. Anyway, the increase is quite modest and won't probably make much of a difference.

From the performance viewpoint, the PMOSFETs are strongly affected. In particular, the saturation drain current of the PMOSFETs seems to be the most critical parameter. As discussed before, the current can drop by as much as 40%, and this translates directly into a slow-down of the pull-up networks of a fully complementary digital CMOS design or in the reduction of the gain bandwidth product of an amplifier.

8.3.4 References for Section 8.3

[1] A. Candelori et al., Radecs 2005, Eight European Conference on Radiation and Its Effects on Components and Systems, Cap d'Agde, France, from 19 to 23 September 2005
[2] LHC website: http://public.web.cern.ch
[3] G. Anelli, M. Campbell, M. Delmastro, F. Faccio, S. Florian, A. Giraldo, E. Heijne, P. Jarron, K. Kloukinas, A. Marchioro, P. Moreira, W. Snoeys, "Radiation tolerant VLSI circuits in standard deep submicron CMOS technologies for the LHC experiments: practical design aspects", IEEE-TNS Vol. 46, pp. 1690-1696, 1999
[4] M. Turowski, A. Raman, R. D. Schrimpf, "Non uniform Total-Dose-Induced Charge distribution in Shallow-Trench Isolation Oxides", *IEEE Trans. Nucl. Sci*., Vol. 51, No. 6, pp. 3166-3171, 2004.
[5] F. T. Brady, J.D. Maimon,, M.J. Hurt, "A Scalable, Radiation Hardened Shallow Trench Isolation Oxides", *IEEE Trans. Nucl. Sci*., Vol. 46, No. 6, pp. 1836-1840, 1999.
[6] M. R. Shaneyfelt, P.E. Dodd, B.L. Draper, R.S. Flores, "Challenges in Hardening Technologies Using Shallow-Trench Isolation", *IEEE Trans. Nucl. Sci*., Vol. 45, No. 6, pp. 2583-2592, 1998.
[7] F. Gianotti et al., "Physics potential and experimental challenges of the LHC luminosity upgrade", hep-ph/0204087, April 2002.
[8] A. Scarpa, A. Paccagnella, F. Montera, G. Ghibaudo, G. Pananakakis, G. Ghidini, and P. G. Fuochi, "Ionizing Radiation Induced Leakage Current on Ultra-Thin Gate Oxides", IEEE Trans. Nucl. Sci., Vol. 44, No. 6, p. 1818-1825, Dec. 1997.
[9] M. Ceschia, A. Paccagnella, A. Cester, A. Scarpa, and G. Ghidini, "Radiation Induced Leakage Current and Stress Induced Leakage Current in Ultra-Thin Gate Oxides", IEEE Trans. on Nucl. Sci., vol. 45, No. 6, p.2375-2382, Dec. 1998.
[10] A. Cester, A. Paccagnella, "Radiation Effects and Soft Errors in Integrated Circuits And Electronic Devices", Vol. 34, pp. 279-290, 2004
[11] G. Groeseneken, R. Degraeve, T. Nigam, G. Van den bosch, H.E. Maes, "Hot carrier degradation and time-dependent dielectric breakdown in oxides", *Microelectronics Reliability*, vol. 49, pp. 27-40, 1999.
[12] G. Ghibaudo, "New method for the extraction of MOSFET parameters", *Electronics Letters*, vol. 24, p. 543, 1988

9. Resources

All participating institutes organize their own resources required for the research activities in their home laboratories. Integration in a CERN approved R&D project allows them to apply for national funding in terms of financial and manpower resources. The collaboration comprises several institutes, which have access to irradiation sources (reactors and accelerators, see [1]), as well as clean room and sensor processing facilities. A very wide range of highly specialized equipment for characterization of sensors and materials is also available (see [2]) .

9.1. Common Fund

RD50 has a Common Fund to which each institute contributes every year a certain amount. The Common Fund is used for project related investments, like processing of common test structures or purchasing of special material and equipment. Furthermore it is used to cover the organization of collaboration workshops, common irradiation runs, or other specific activities of common interest.

9.2. Lab space at CERN

The RD50 collaboration was temporarily using existing infrastructure and equipment at CERN in 2005 and requests to continue to do so in 2006. As a member of the collaboration, the section PH-DT2/SD can provide access to available lab space in building 14 (characterization of irradiated detectors), in building 28 (lab space for general work) and in the PH Departmental Silicon Facility (hall 186, clean space). The collaboration would like to keep the RD50 visitor office in barrack 591 and use the CERN infrastructure to organize one workshop at CERN in 2006.

9.3. Technical support at CERN

A low level of support from PH-DT2/SD (wire bonding and sensor mounting) may be profitable. The expected work volume for 2006 is estimated to be very limited.

[1] An extensive list of irradiation facilities open to RD50 can be found on the RD50 web page: http://www.cern.ch/rd50/
[2] R&D Proposal - DEVELOPMENT OF RADIATION HARD SEMICONDUCTORDEVICES FOR VERY HIGH LUMINOSITY COLLIDERS, LHCC 2002-003 / P6, 15.2.2002.